Exploring the therapeutic potential of protein tyrosine phosphatase inhibition in neuroblastoma

Elsa Irving

University College London

Great Ormond Street Institute of Child Health

A thesis submitted for the degree of Doctor of Philosophy

I, Elsa Irving, confirm that the work presented in this thesis is my own. Where information has been derived from other sources, I confirm that this has been indicated in the thesis.

Abstract

Neuroblastoma accounts for 15% of paediatric cancer deaths and there is an urgent need for improved therapeutic strategies. Phosphotyrosine signalling, regulated by the opposing actions of protein tyrosine kinases and protein tyrosine phosphatases (PTPs), is critical for virtually all aspects of cell behaviour, and is commonly perturbed in cancer. We have previously shown that pan-inhibition of PTPs using oxidovanadium induces cytotoxicity in a panel of neuroblastoma cell lines. We therefore hypothesise that there exist specific PTPs that promote tumour cell survival, and that their specific or pan-inhibition may be beneficial for the treatment of neuroblastoma.

Whilst promising preclinical data using vanadium-derived compounds in *in vitro* and *in vivo* models of cancer has been reported, clinical trials have been prevented in part due to concerns surrounding off-target tissue toxicity. I have taken several approaches to harness the cytotoxic properties of oxidovanadium, and PTP inhibition, with the aim to develop new therapeutic strategies for neuroblastoma. The tumour-promoting roles of specific PTPs were investigated using loss-of-function approaches including RNAi and CRISPR/Cas9 gene knockout. The dual specificity phosphatase CDC14B was identified as a potential candidate, although further validation studies need to be considered for this enzyme to be taken forward as a potential therapeutic target. In a parallel study, the first genome-wide transcriptomic analysis in neuroblastoma cells treated with oxidovanadium has revealed a potential role for cAMP signalling in bismaltolato oxidovanadium (BMOV)-induced cytotoxicity. This pathway and others that are affected by oxidovanadium may be a source of useful therapeutic targets for neuroblastoma in the future. Finally, I have shown for the first time that hydrophobic oxidovanadium can be packaged into liposomes and maintains its cytotoxicity when delivered to neuroblastoma cells. This presents a novel opportunity to deliver vanadium with potentially fewer safety concerns, whilst retaining its broad activity and high levels of anti-cancer efficacy.

Impact Statement

The aim of this project was to explore the potential of targeting protein tyrosine phosphatase (PTP) signalling for the treatment of neuroblastoma and to deliver new conceptual approaches and opportunities for future therapies. We believe that there is enormous therapeutic potential in targeting PTPs. These enzymes, along with their functional partners, protein tyrosine kinases, are responsible for the regulation of tyrosine phosphorylation, which is vital for proper cell function, and its deregulation is implicated in a broad spectrum of human diseases including cancer. PTPs are increasingly being positively implicated in tumourigenesis and cancer progression, and several have now been labelled as *bona fide* oncogenes in several tumour types including neuroblastoma. We therefore suggest that therapeutic inhibition of these, and other yet to be identified PTPs, will be useful in developing much needed improved therapeutic strategies for high-risk neuroblastoma. Here I present data indicating that targeting of specific pro-tumour PTPs, as well as pan-PTP inhibition using vanadium-derived compounds may be of benefit for neuroblastoma treatment.

I utilised genomic technologies including siRNA and shRNA-mediated gene knockdown, and CRISPR/Cas9-mediated gene deletion, to identify specific PTPs that are required for growth and/or survival of neuroblastoma cell lines. If confirmed *in vivo*, therapeutic targeting of these enzymes may have significant clinical impact.

Vanadium-derived compounds are considered broad-spectrum inhibitors of the entire PTP superfamily and have been of interest in disease research including cancer for many decades. Despite considerable research efforts reporting anti-cancer activity in *in vitro* and *in vivo* tumour models, and even human clinical trials in the diabetes setting, vanadium compounds have yet to achieve clinical approval, due in part to concerns regarding the safety of their use in humans. Here I attempted to deconvolute the mechanisms driving oxidovanadium cytotoxicity, using genome-wide transcriptomics. These data revealed a broad range of transcriptional changes, suggesting that several effector pathways likely contribute to the observed cytotoxicity. One such

pathway was identified as cAMP signalling, and early validation suggests that cAMP signalling is activated by oxidovanadium and may be involved in cytotoxicity. Targeting of this pathway and other oxidovanadium effectors may be useful in the treatment of neuroblastoma.

Both the targeting of specific pro-tumour PTPs and BMOV effectors are reductionist approaches to harness the cytotoxicity associated with oxidovanadium-mediated pan-PTP inhibition. An alternative approach is the therapeutic use of oxidovanadium itself. Here I present a novel hydrophobic oxidovanadium liposomal formulation that can be delivered to neuroblastoma cells in culture. This nanoparticle formulation may allow safer delivery of oxidovanadium to tumour cells *in vivo*, both by enhancing the efficiency of delivery and reducing off-target tissue toxicities. These formulations may be useful not only in the treatment of neuroblastoma but also in other cancers, as well as other diseases related to PTP signalling, namely diabetes, where vanadium-derived compounds have previously been trialled.

My research will therefore raise the profile of PTP signalling as a therapeutic target in the cancer field and will also promote new thinking about how to utilize the cytotoxic potential of oxidovanadium for cancer and other disease treatment.

Acknowledgements

I would first like to thank Andy Stoker. Your calming influence, patience, enthusiasm, and willingness to help is inspirational, and I truly couldn't have hoped for a better supervisor. I also owe a huge thank you to Vruti Patel. I am so glad that you joined the lab, your advice, and let's face it counselling, really has helped me through to the end! I am also very grateful for the help of many other scientists based at ICH. In particular, thank you to JP for his support and advice, Aris and Ruhina for synthesising my liposomes, and Simon and Mike for their help with HPLC.

I have made great friends during my time at ICH, who have supported me enormously. I'd especially like to thank all 'residents' of office W2.04 past and present. Amy, Vruti, Aara, Lisa, and Elliot, you are all fantastic people and you deserve medals for putting up with me during writing this thesis! Lucy, we've been in it together since day one, and we've done it! (And Amy you will too!). I hope I will be lucky enough to work with a group of people just as fun, driven, kind, and coffee and cake dependent again.

Most importantly, thank you to my amazing family and friends in London and further afield, who have supported me unconditionally. Catherine, you've been my cheer leader! Thank you for your pep talks over coffee and breakfast, you've kept me sane (ish!). I will be forever grateful to the Flahertys for welcoming me into their wonderful home and providing me with endless fun and distraction. I have been so lucky to come home to supportive family, lovely food and a comforting home every day. Owen, thank you for always telling me I can do this and for reminding me that 'No stress is best!'. 2018 has been a very challenging year but, thanks to you, also one of my best! Alice, you know me better than I know myself, and never fail to make me smile during meltdowns, however ridiculous they may seem! You and Dicken have been inspiring and encouraging me for my whole life, and this PhD has been no different. Finally, thank you to my parents. Mum and John, you have supported me in everything I have achieved, and have always told me I can do anything I put my mind to. I love you both, and if there is one thing I know, it is that this PhD would not have been possible without your love and support.

Table of contents

List of figures

List of tables

Abbreviations

2-AAF	2-acetylaminofluorence
AC	Adenylyl cyclase
ACP1	Acid phosphatase 1
ALK	Anaplastic lymphoma kinase
Amp	Amplified
ANOVA	Analysis of variance
ATP	Adenosine triphosphate
BEOV	Bisethylmaltolato oxidovanadium
BET	Bromodomain and extra-terminal domain
BMOV	Bismaltolato oxidovanadium
bpv(pic)	Picolinato-bis(peroxido) oxidovanadate
bpv-phen	Bisperoxo (1,10-phenanthroline) oxidovanadate (V)
BSA	Bovine serum albumin
BSO	Buthionine sulphoximine
cAMP	Cyclic adenosine monophosphate
CAR	Chimeric antigen receptor
CCK-8	Cell counting kit 8
CDC14B	Cell division cycle 14B
CDK	Cyclin-dependent kinase
cGMP	Cyclic guanosine monophosphate
CLL	Chronic lymphocytic leukaemia
CML	Chronic myeloid leukaemia
CMV	Cytomegalovirus
CRISPR	Clustered regularly interspaced short palindromic repeats
CTCL	Cutaneous T-cell lymphoma
DCTN1	Dynactin subunit 1
DDR	DNA damage repair
DEN	Diethylnitrosamine
DMBA	7,12-dimethylbenzlαanthracene
DMEM	Dulbecco's Modified Eagle Medium
DMH	1,2-dimethylhydrazine
DMSO	Dimethyl sulfoxide
DNA	Deoxyribonucleic acid
dNTPs	Deoxyribonucleotide triphosphates
DOPC	Dioleoyl phosphatidylcholine
DOTMA	1,2-di-O-octadecenyl-3-trimethylammonium propane
DOX	Doxycycline
DSB	Double stranded break
DSP	Dual-specificity phosphatase
EB	Elution buffer
ECL	Electrochemiluminescence
ECM	Extracellular matrix

EDTA	Ethylenediaminetetraacetic acid
EGFR	Epidermal growth factor receptor
EHNA	Erythro-9-(2-hydroxy-3-nonyl) adenine
EPR	Enhanced permeability and retention
ETOH	Ethanol
EYA	Eyes absent family
FACS	Fluorescence-activated cell sorting
FBS	Foetal bovine serum
FDA	Food and Drug Administration
FWD	Forward
GD2	Disialoganglioside 2
gDNA	Genomic deoxyribonucleic acid
GFP	Green fluorescent protein
GI	Gastrointestinal
GLMP	Glycosylated lysosomal membrane protein
GN	Ganglioneuroma
GNB	Ganglioneuroblastoma
gRNA	Guide ribonucleic acid
GSH	Glutathione
HCC	Hepatocellular carcinoma
HDR	Homology directed repair
HEPES	4-(2-hydroxyethyl)-1-piperazineethanesulfonic acid
HPLC	High performance liquid chromatography
HPR	Horseradish peroxidase
HSCT	Haematopoietic stem cell transplantation
IARC	International Agency for Research on Cancer
IF	Immunofluorescence
indels	Insertions and deletions
INRG	International Neuroblastoma Risk Group
INRGSS	International Neuroblastoma Risk Group Staging System
INSS	International Neuroblastoma Staging System
IPA	Ingenuity Pathway Analysis
IR	Ionising radiation
KIF11	Kinesin family member 11
LB	Luria-Bertani
LC	Laryngeal carcinoma
LMW-PTP	Low molecular weight protein tyrosine phosphatase
MAPK	Mitogen-activated protein kinase
MCB	Monochlorobimane
MEM	Minimum Essential Medium
metvan	Bis(4,7-dimethyl-1,10-phenanthroline)sulfatooxidovanadium
MNU	1-methyl-1-nitrosourea
mRNA	Messenger RNA
MTMR12	Myotubularin related protein 12

NA	Non-amplified
NAC	N-acetyl L-cysteine
NCBI	National Center for Biotechnology Information
NES	Nuclear export signal
NHEJ	Non-homologous end joining
NMR	Nuclear magnetic resonance
NRF2	Nuclear factor-like 2
NSCLC	Non-small cell lung cancer
NSG	NOD scid gamma
NTS	Nuclear targeting sequence
P/S	Penicillin/Streptomycin
PAM	Protospacer adjacent motif
PBS	Phosphate buffered saline
PCA	Principle component analysis
PCR	Polymerase chain reaction
PDE	Phosphodiesterase
PDE2A	Phosphodiesterase 2A
PEG	Polyethylene glycol
PFA	Paraformaldehyde
phen	1,10-phenanthroline
PKA	Protein kinase A
PLL	Poly-L-lysine
PTEN	Phosphatase and tensin homolog
PTK	Protein tyrosine kinase
PTP	Protein tyrosine phosphatase
PTPRN	Protein tyrosine phosphatase receptor type N
PVDF	Polyvinyldifluoride
qPCR	Quantitative polymerase chain reaction
REV	Reverse
RIN^{e}	RNA integrity number
RISC	RNA-induced silencing
RNAi	RNA interference
RNAseq	Ribonucleic acid sequencing
ROS	Reactive oxygen species
rpm	Revolutions per minute
RPMI	Roswell Park Memorial Institute
RTK	Receptor tyrosine kinase
rtTA	Reverse tetracycline-controlled transactivator
SCR	Scrambled
SD	Standard deviation
SDS-PAGE	Sodium dodecyl sulfate–polyacrylamide gel electrophoresis
shRNA	Short hairpin RNA
siRNA	Small interfering RNA
SSG	Sodium stibogluconate

STR	Short-tandem repeat
T7E1	T7 endonuclease 1
TBS/T	Tris buffered saline/Tween-20
TCGA	The Cancer Genome Atlas
TET-On	Tetracycline-on
TRE	Tetracycline response element
TUBGCP6	Tubulin gamma complex associated protein 6
UT	Untreated
V10	Decavanadate

Chapter 1. Introduction

1.1. Neuroblastoma

1.1.1. Incidence and clinical presentation

Cancer remains a leading cause of death in young people as well as adults. Behind accidents, assault and intentional self-harm, cancer is the biggest killer of children aged between 1 and 19 in the US (Hamilton et al., 2013). Neuroblastoma is the most common extra-cranial solid tumour in children and accounts for around 15% of all paediatric cancer related deaths (Miller et al., 1995). In 2010, there were 10.7 cases of neuroblastoma per million children aged 1-14 in the US (Louis et al., 2015), and in the UK, approximately 100 children are diagnosed with neuroblastoma each year, most of whom are under 5. In fact, 90% of patients are diagnosed before they reach 10 years old (London et al., 2005). Although much less frequent, neuroblastoma can also develop in older children, teenagers and adults. The median age of diagnosis is 19 months, and in most cases, children whose tumours present at a younger age will have a more favourable prognosis compared with children diagnosed at 18 months or older (London et al., 2005, Whittle et al., 2017) (**Figure 1.1A**). Neuroblastoma is a very intriguing tumour type, in that some patients present with tumours that spontaneously regress, requiring only careful observation and no further treatment (Brodeur and Bagatell, 2014). Children with high-risk disease however, are subjected to aggressive multimodal therapy, and survival for this group remains below 50% (Whittle et al., 2017, Park et al., 2013) (**Figure 1.1B**). This clearly highlights the need for novel therapeutic strategies in the treatment of this devastating disease.

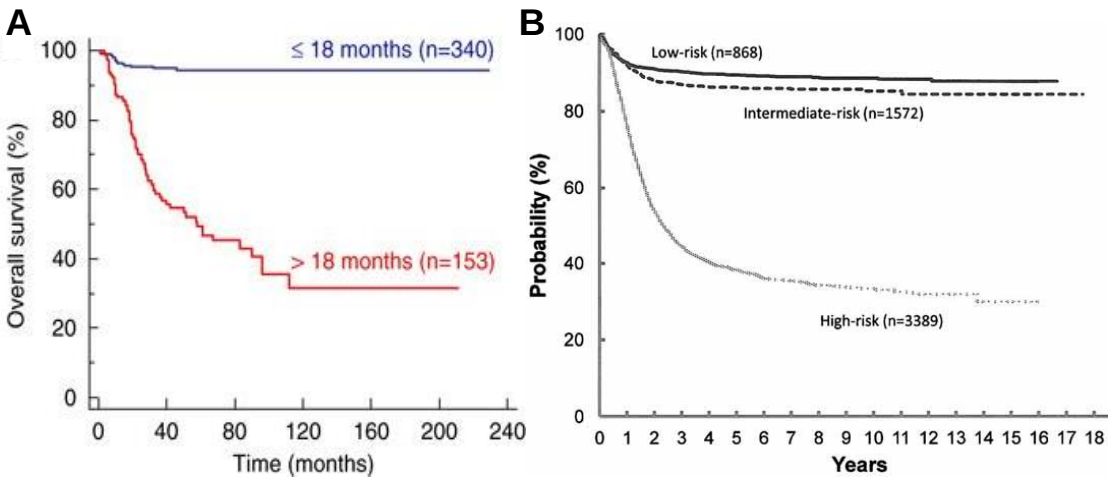

Figure 1.1 – Prognosis for neuroblastoma patients
***A** - Kaplan-Meier plot showing probability of overall survival based on age at diagnosis. Taken from Janoueix-Lerosey et al. (2010). **B** - Kaplan-Meier plot showing probability of event-free survival for neuroblastoma patients categorised as low, intermediate or high risk based on clinical and biological factors. Taken from Park et al. (2013).*

Neuroblastoma is an embryonic cancer with tumours arising throughout the developing sympathetic nervous system in tissues of neural crest origin, predominantly in the adrenal medulla (Maris, 2010). Normal mammalian development involves migration of neural crest cell precursors from the dorsal neural tube to various locations, these cells then differentiate into the tissues and organs of the sympathetic nervous system (Bronner, 2012, Jiang et al., 2011). Neuroblastoma is thought to arise due to defects in this migration, maturation or differentiation (Hoehner et al., 1996, Whittle et al., 2017). Tumours arise throughout the sympathetic nervous system, in particular in the adrenal medulla and paraspinal ganglia. They are most commonly reported in the adrenal gland, but are also found in tissues in the neck, chest, pelvis and abdomen (Matthay et al., 2016, Whittle et al., 2017). Due to the range of primary as well as metastatic tumour sites, neuroblastoma patients present diverse pathological features (**Figure 1.2**). When primary tumours arise in the upper chest or neck, Horner's syndrome can occur, characterised by miosis (constricted pupil), ptosis (droopy eyelid) and anhydrosis (decreased sweating), whereas tumours within the spine can compress the spinal cord causing paralysis (Maris, 2010). Neuroblastoma tumour cells can also both infiltrate local organ structures, and metastasise to distant tissues such as lymph node, bone marrow and liver (DuBois et al., 1999).

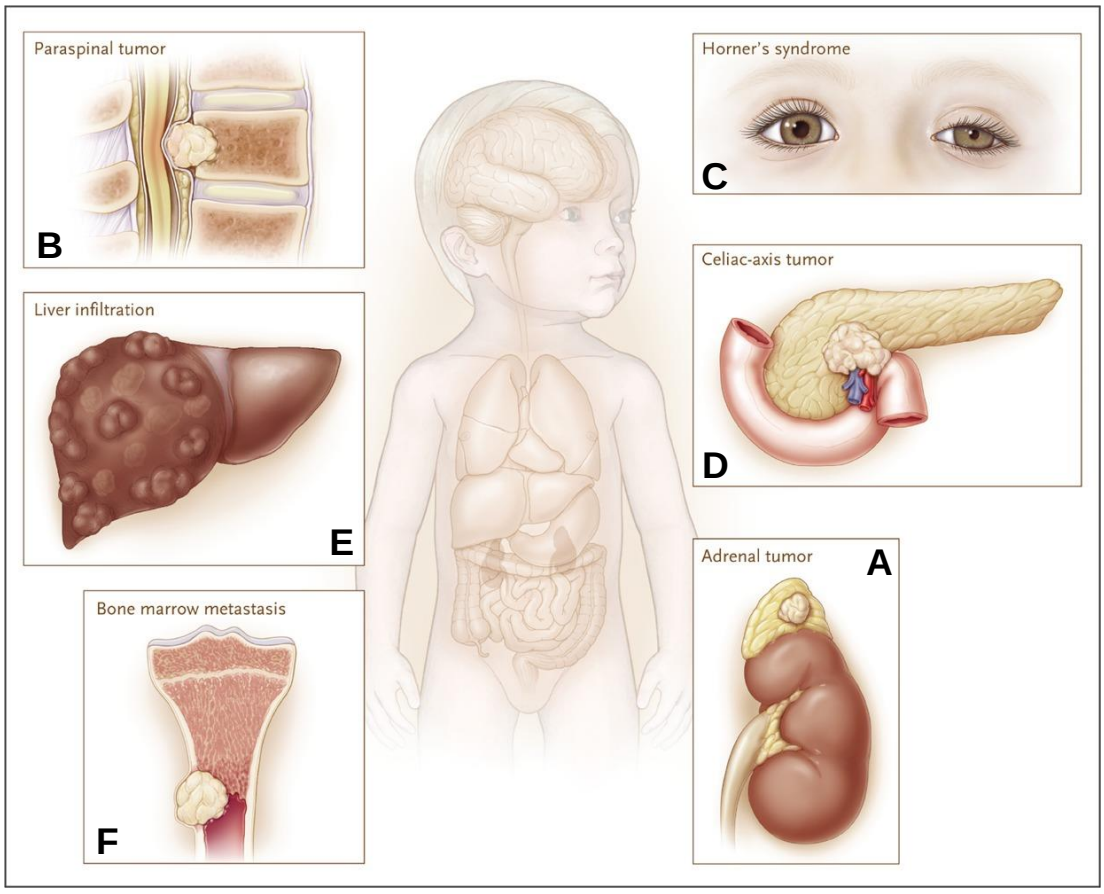

Figure 1.2 – Clinical presentation of neuroblastoma
*Neuroblastoma tumours occur most commonly in the adrenal gland (**A**), but may also arise in tissues throughout the sympathetic nervous systems, thus are associated with many pathological features. Primary tumours within the spine can cause spinal cord compression and in some cases paralysis (**B**), whereas tumours arising in the neck or upper chest are associated with Horner's syndrome (**C**). Tumours may infiltrate into local organ structures such as the celiac-axis (**D**), or metastasise to other tissues such as the liver (**E**) or bone marrow (**F**). Taken from Maris (2010).*

1.1.2. Disease classification and treatment

Upon diagnosis, neuroblastoma patients are classified based on various properties of their disease. This stratification allows patients to be directed towards appropriate therapy and gives an indication of their likely prognosis. Tumour staging is an important element in this stratification. Until recently, the International Neuroblastoma Staging System (INSS) was used to group neuroblastoma tumours into stages. This system was implemented in 1986, and revised in 1993 (Brodeur et al., 1988, Brodeur et al., 1993), and was partly based on the degree of tumour resection during surgery. Thus, this system did not allow tumour staging prior to treatment initiation. There were also some issues with standardisation across clinical groups, for example in lymph node

sampling (Whittle et al., 2017, Tolbert and Matthay, 2018, Monclair et al., 2009). More recently, the International Neuroblastoma Risk Group (INRG) set about creating new staging and risk classification systems for neuroblastoma (Monclair et al., 2009, Cohn et al., 2009). In the INRG Staging System (INRGSS) (**Table 1.1**), tumours are classified based on image-defined risk factors and age of diagnosis, which are predictive of prognosis. As this classification is based on imaging rather than surgical sampling, tumours can be classified before treatment begins (Tolbert and Matthay, 2018).

Table 1.1 – International Neuroblastoma Risk Group Staging System (INRGSS)
In this system, neuroblastoma cases are assigned to stage L1, L2, M or M3 based on image-defined tumour location and degree of metastasis, as well as patient age. Modified from Monclair et al. (2009)

Stage	Description
L1	Localised tumour not involving vital structures as defined by the list of image-defined risk factors and confined to one body compartment
L2	Locoregional tumour with presence of one or more image-defined risk factor
M	Distant metastatic disease (except stage MS)
MS	Metastatic disease in children younger than 18 months with metastases confined to skin, liver and/or bone marrow

The INRG then used this new tumour staging system, together with biological features that had been correlated with patient outcomes, to create risk stratifications (Cohn et al., 2009). They used a large cohort of 8000 patients from North America, Europe and Japan and looked for correlation between a longlist of potential risk factors and event-free and overall survival. From this analysis, they created a shortlist of factors that would be used to classify patients into risk groups. These risk factors include INRG tumour stage, age at diagnosis, tumour histology, degree of tumour differentiation, *MYCN* amplification, 11q chromosomal aberration and DNA ploidy (Cohn et al., 2009, Whittle et al., 2017, Tolbert and Matthay, 2018). According to this risk stratification system, patients can be classified as very low risk, low risk, intermediate risk and high risk (**Figure 1.3**), which are associated with >85%, 75-85%, 50-75% and <50% 5 year event-free survival respectively (Cohn et al., 2009).

INRG Stage	Age (months)	Histologic Category	Grade of Tumor Differentiation	*MYCN*	11q Aberration	Ploidy	Pretreatment Risk Group
L1/L2		GN maturing; GNB intermixed					A Very low
L1		Any, except GN maturing or GNB intermixed		NA			B Very low
				Amp			K High
L2	< 18	Any, except GN maturing or GNB intermixed		NA	No		D Low
					Yes		G Intermediate
	≥ 18	GNB nodular; neuroblastoma	Differentiating	NA	No		E Low
					Yes		H Intermediate
			Poorly differentiated or undifferentiated	NA			
				Amp			N High
M	< 18			NA		Hyperdiploid	F Low
	< 12			NA		Diploid	I Intermediate
	12 to < 18			NA		Diploid	J Intermediate
	< 18			Amp			O High
	≥ 18						P High
MS	< 18			NA	No		C Very low
					Yes		Q High
				Amp			R High

Figure 1.3 - International Neuroblastoma Risk Group (INRG) pre-treatment classification scheme
Patient risk group (right hand column) is determined based on INRG tumour stage, age at diagnosis, and various biological factors. GN = ganglioneuroma, GNB = ganglioneuroblastoma, Amp = amplified, NA = non-amplified. Taken from Cohn et al. (2009).

These kinds of classifications are very important in the treatment of neuroblastoma. On the one hand, they allow effective identification of very high-risk patients and allocation of appropriately aggressive therapy. However, on the other hand, they also allow for the intensity of treatment to be reduced for much lower risk patients. This can be considered equally as important, since the therapies that are used to treat neuroblastoma are often very invasive and are associated with significant life-long health complications, particularly critical for patients undergoing treatment at such young ages.

As discussed above, neuroblastoma is a highly heterogeneous disease, thus treatment can be extremely challenging and involves many different approaches depending on tumour stage and the risk associated with a patient's disease. Currently, treatment for neuroblastoma ranges from observation and in some cases surgery to remove primary tumours for low-risk patients, to aggressive multimodal therapy lasting 18 months or longer and involving significant hospital stays for high-risk patients (Tolbert and Matthay, 2018) (**Figure 1.4**). This multimodal therapy involves a combination of chemotherapy, surgery, stem cell transplantation, radiotherapy, as well as

ongoing maintenance therapy, including anti-GD2 targeted immunotherapy and retinoid treatment (Louis et al., 2015, Tolbert and Matthay, 2018). Maintenance therapy aims to treat residual disease, minimising the risk of disease reoccurrence. For example, treatment with retinoids such as isotretinoin, is thought to force tumour cells to differentiate, hopefully leading to reduced proliferation (de Thé, 2018). Although new treatments are constantly in development, and overall survival of high-risk patients has increased from 29% to 50% over the last 20 years, very little progress has been made in the last 10 years (Pinto et al., 2015). Thus, clearly there is still a significant need for novel therapies to treat high-risk patient groups.

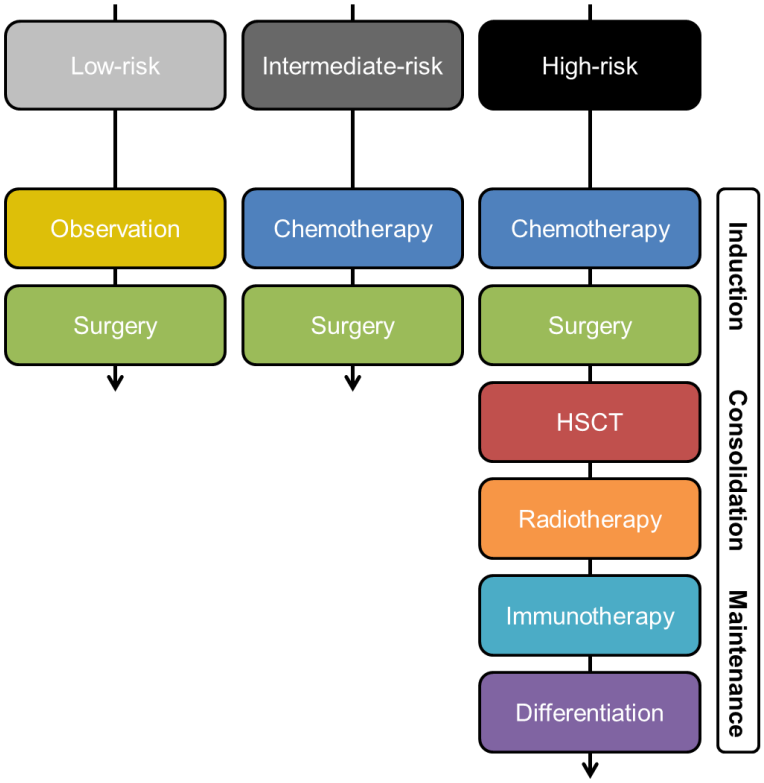

Figure 1.4 – Neuroblastoma treatment based on risk stratification
Summary of therapeutic strategies used to treat neuroblastoma patients in each risk group. HSCT = Haematopoietic stem cell transplantation. Modified from Tolbert and Matthay (2018).

1.1.3. MYCN amplification

The high degree of heterogeneity between neuroblastoma tumours indicates that there are a complex range of genetic or epigenetic aberrations that drive this disease. Although for most neuroblastoma tumours these genetic drivers are not well understood, there are some genetic markers that have been correlated with disease progression and prognosis. Chromosomal aberrations

such as losses at chromosome 1p and 11q, and overall ploidy correlate with poor prognosis and these are included in the INRG risk classification scheme (Brodeur, 2003, Attiyeh et al., 2005, Cohn et al., 2009) (**Figure 1.3**). *MYCN* amplification occurs in 22% of neuroblastoma patients and is the most robust genetic marker available for patient stratification (Brodeur, 2003, Cohn and Tweddle, 2004). MYCN is a transcription factor with a basic helix-loop-helix domain, and has been described as a proto-oncogene (Adhikary and Eilers, 2005). Specifically in neuroblastoma, amplification of *MYCN* is associated with advanced disease and correlates with unfavourable prognosis (Schwab et al., 1983, Brodeur et al., 1984, Seeger et al., 1985) (**Figure 1.5**). *MYCN* amplification drives tumourigenesis and cancer progression in a variety of ways, including by inhibiting cell cycle arrest (Bell et al., 2006), and enhancing proliferation (Schweigerer et al., 1990), genomic instability (Sugihara et al., 2004), angiogenesis (Fotsis et al., 1999), therapeutic resistance (Veas-Perez de Tudela et al., 2010), tumour cell motility and invasiveness (Goodman et al., 1997), and evading immune responses (Song et al., 2007). In fact MYCN activity can be related to almost all of Weinberg's Hallmarks of Cancer (Huang and Weiss, 2013, Hanahan and Weinberg, 2011). Moreover, Weiss et al. (1997) showed that over expression of *MYCN* in mice neuroectoderm caused formation of neuroblastoma-like tumours.

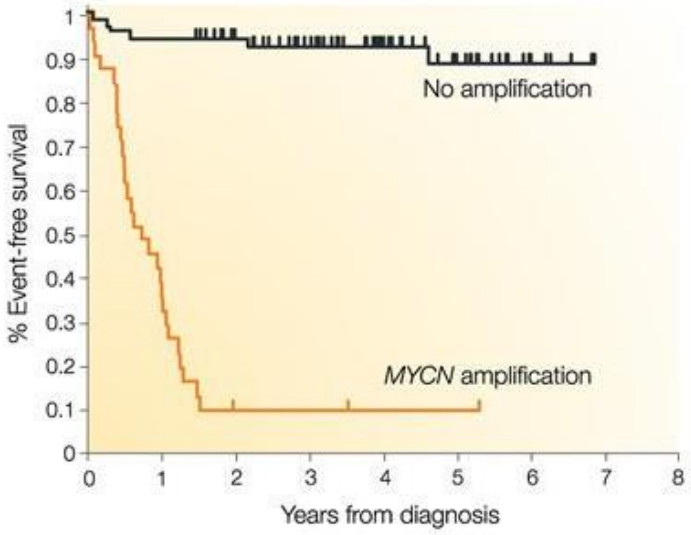

Figure 1.5 – MYCN amplification correlates with poorer prognosis
Kaplan-Meier plot showing 3-year event-free survival for infants under 1 years old with metastatic neuroblastoma, grouped based on MYCN amplification. 93% of non-MYCN amplified patients had 3 years event free survival, compared to 10% with MYCN amplification. Taken from Brodeur (2003).

Given this strong correlation between the amplification of *MYCN* and poor prognosis, it is an obvious choice for therapeutic targeting. MYCN has long been regarded as 'undruggable' due in part to challenges in targeting protein-DNA interactions. Thus, efforts have largely been focussed on indirect targeting of MYCN, for example by identifying and targeting critical MYCN substrates, or enzymes that regulate *MYCN* expression and protein stability (Barone et al., 2013, Bayliss et al., 2017). For example, Aurora A kinase is known to indirectly stabilise the MYCN protein by preventing its degradation, and there has been interest in targeting this kinase in neuroblastoma, including clinical trials using the small molecule inhibitor alisertib (Otto et al., 2009, Greengard, 2018, Richards et al., 2016, Mossé et al., 2012, DuBois et al., 2016). Similarly, the bromodomain and extra-terminal domain (BET) protein family is involved in regulating *MYCN* transcription, and BET inhibitors have shown anti-cancer effects in preclinical neuroblastoma studies (Puissant et al., 2013, Shi and Vakoc, 2014).

1.1.4. Driver mutations

Targeted therapy is currently the focus of a large proportion of cancer research efforts, and involves the targeting of molecules that act as drivers of specific tumours. It is generally hoped that these will allow effective cancer treatment with fewer side effects compared to conventional cancer therapies. In order to develop targeted therapies, the proteins that drive tumourigenesis or tumour progression often following over- or under-expression or genetic alteration, must be identified. As has been discussed, MYCN is the most robust neuroblastoma driver to be described so far. In most cases, *MYCN* amplifications, rather than mutations within the gene itself, are present in neuroblastoma. In fact the overall mutation frequency in neuroblastoma is relatively low compared to adult solid tumours and to date very few mutations in cancer genes have been described. This includes both oncogenic or pro-tumour drivers as well as tumour suppressor genes. Phosphatase and tensin homolog (PTEN) and p53 are very commonly mutated tumour suppressor genes in cancer. Mutations in neither are commonly reported in neuroblastoma cell lines or primary tumours, although p53 is often mutated or otherwise suppressed in relapsed disease (Izycka-Swieszewska et al., 2010, Muñoz et

al., 2004, Moritake et al., 2001, Tweddle et al., 2003, Carr et al., 2006). Pugh et al. (2013) studied the genome and transcriptome of 240 cases of neuroblastoma and found an exonic mutation frequency of just 0.6 per Mb. Furthermore, they noted very few genes that were frequently mutated across the tumour panel. Nonetheless, *ALK*, *PTPN11*, *ATRX*, *MYCN* and *NRAS* where identified as genes with a significant frequency of recurrent somatic mutations in neuroblastoma (Pugh et al., 2013).

Activating mutations or amplifications in anaplastic lymphoma kinase (*ALK*) are present in around 14% of high-risk neuroblastoma tumours, and over half of hereditary cases, which represent 1-2% of all neuroblastoma patients (Shojaei-Brosseau et al., 2004). These mutations correlate with poorer prognosis and commonly occur in parallel with *MYCN* amplification (Mosse et al., 2008, Janoueix-Lerosey et al., 2008, Trigg and Turner, 2018, De Brouwer et al., 2010). Under normal conditions, *ALK* is predominantly expressed in developing neural tissue making it an attractive therapeutic target, as fewer off-target tissue toxicities would be predicted (Barone et al., 2013). There has been some reported success in targeting ALK in neuroblastoma, most notably by using the small molecule inhibitor crizotinib, although both innate and acquired drug resistance is likely to be a problem (Sekimizu et al., 2018, Bresler et al., 2011, Mossé et al., 2013). The ATRX protein is involved in regulating telomere length, and loss-of-function mutations in this gene are associated with neuroblastoma in older children and adolescents (Cheung et al., 2012). NRAS, as well as other components of the RAS-MAPK pathway, has been heavily implicated in virtually all types of cancer, and has been the focus of a great deal of therapeutic targeting (Santarpia et al., 2012). Mutations in the RAS-MAPK pathway are rare in primary neuroblastoma; however, it has been reported that almost 80% of relapsed tumours have mutations in this pathway (Eleveld et al., 2015). Therefore, there has been interest in targeting RAS-MAPK pathway components in relapsed neuroblastoma (Greengard, 2018). Related to this, somatic mutations in *PTPN11* were reported in 2.9% of neuroblastomas (Pugh et al., 2013). The *PTPN11* gene encodes SHP2, a protein tyrosine phosphatase (PTP) that is involved in RAS-MAPK signalling and has been implicated in various cancers, including neuroblastoma

(Bentires-Alj et al., 2004). There is ongoing interest in targeting SHP2 and several small molecule inhibitors are currently in development (Zeng et al., 2014, Zhang et al., 2016, Chen et al., 2016, Sun et al., 2018b). The role of this PTP and others in neuroblastoma and cancer more broadly will be discussed in more detail later (**Section 1.2.3.**).

Given that survival for high-risk neuroblastoma remains stubbornly below 50%, there is a clear requirement for improved therapeutic strategies. Small molecule inhibitors of specific molecular targets are not currently part of any approved treatment plans for neuroblastoma, although several molecules are currently in clinical trials including ALK and Aurora A kinase inhibitors (Greengard, 2018). The continued identification and validation of specific molecular drivers of this disease, including the genetic aberrations described above and others, will be required for the development of successful targeted therapies. These will allow children to be treated with specific interventions designed explicitly to target the drivers and dependencies of their disease, hopefully resulting in improved outcomes.

1.2. Phosphotyrosine signalling

1.2.1. Reversible phosphorylation

The survival of multicellular organisms relies on their ability to respond to internal and external stimuli. This is dependent on biochemical signalling that allows communication between and within cells. Reversible phosphorylation of tyrosine residues is one mechanism by which cells are able to transmit signals, and it is involved in virtually all aspects of cell behaviour. This addition and removal of phosphate groups from tyrosine residues is catalysed by two classes of enzymes, the protein tyrosine kinases (PTKs) for phosphorylation and the protein tyrosine phosphatases (PTPs) for dephosphorylation (**Figure 1.6**). Given its pivotal role in cell signalling, it is unsurprising that tyrosine phosphorylation is under very tight regulation. Disruption to normal PTK and PTP signalling, brought about by mutations in relevant signalling molecules, results in abnormal proliferation, survival, motility, differentiation and metabolism, underlying the pathogenesis of a range of human diseases

including cancer (Tonks, 2006). Specific PTKs and PTPs are therefore attractive drug targets and have gained much attention across several therapeutic areas.

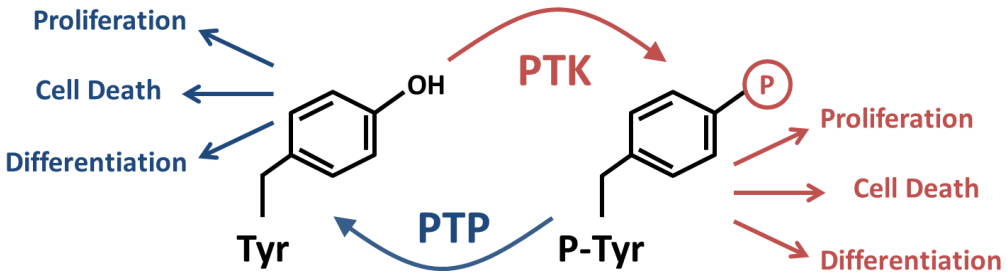

Figure 1.6 – Reversible tyrosine phosphorylation
Addition and removal of phosphate groups to/from tyrosine residues is catalysed by protein tyrosine kinases (PTKs) and protein tyrosine phosphatases (PTPs) respectively. Both phosphorylation and dephosphorylation have impacts on downstream signaling, leading to numerous cell fates including proliferation, cell death and differentiation.

1.2.2. Oncogenic PTKs

As alluded to above, phosphotyrosine signalling has a significant role in cell signalling pathways related to cancer (Hunter, 1998). Tyrosine kinases, as well as serine/threonine kinases, often act to promote cell survival, proliferation and migration. Therefore, their overexpression or over-activation is in many cases associated with tumourigenesis (Montor et al., 2018). Many specific oncogenic kinases have been described and these have accounted for a significant proportion of drug discovery and development research efforts. Indeed, over the last 30 years the kinase family has proven to be a rich source of druggable targets (Wu et al., 2016b). Second to G-protein-coupled receptors, kinases are the most targeted protein family in cancer. There are currently 37 FDA approved kinases inhibitors, at least 27 of which target tyrosine kinases, and around 150 more in clinical trials (Bhullar et al., 2018).

The majority of human PTKs are receptor tyrosine kinases (RTKs) (Robinson et al., 2000). These are tyrosine kinases with a membrane-spanning domain and an extracellular ligand-binding region, as well as an intracellular kinase domain (Hubbard, 1999). In many cases, RTKs are activated by extracellular growth factors and function to regulate cell survival, proliferation, migration, cell-cycle progression, and metabolism (Hubbard, 1999, Hubbard and Miller,

2007, Zwick et al., 2001). As with PTKs more broadly, RTKs are very commonly overexpressed or mutated in cancer, and many are classified as oncogenic (Blume-Jensen and Hunter, 2001). For example, the epidermal growth factor receptor (EGFR) is differentially expressed or mutated in various cancers including lung, breast, head and neck, and gastrointestinal (Montor et al., 2018). In fact it has been estimated that up to 30% of solid tumours may possess gain-of-function mutations in EGFR (Wykosky et al., 2011, Salomon et al., 1995). Ligand binding causes dimerisation of EGFR, leading to receptor autophosphorylation on multiple tyrosine residues (Heldin, 1995). These phosphotyrosine residues serve as recruitment domains for adapter and scaffolding proteins containing SH2 domains, which facilitate the activation of EGFR targets such as RAS, itself a very important oncogene. Ras activation leads to the initiation of multiple downstream signalling pathways including the MAPK cascade and the PI3K/AKT axis, which function in proliferation, survival and motility (Hubbard and Miller, 2007, Tabernero, 2007). Therapeutic inhibition of EGFR is being used with some success in cancers driven by these signalling pathways. In many cases this involves the use of small molecule EGFR inhibitors such as gefitinib, erlotinib or osimertinib, or the EGFR targeted monoclonal antibody cetuximab (Dassonville et al., 2007, Wykosky et al., 2011, Seshacharyulu et al., 2012). There are many other examples of oncogenic tyrosine kinases that are being successfully targeted in the treatment of a range of tumour types (**Table 1.2**), clearly demonstrating the pivotal role that phosphotyrosine signalling plays in cancer initiation and progression (Bhullar et al., 2018).

Table 1.2 – FDA approved kinase inhibitors
Small molecule kinase inhibitors approved by the FDA for use in cancer, many of which target protein tyrosine kinases (PTKs). Note, ALK inhibitors are not yet approved specifically for neuroblastoma but are in clinical trials. Adjusted from Bhullar et al. (2018).

Target	Kinase classification	Inhibitor
ALK	Tyrosine	Crizotinib, Ceritinib, Alectinib, Brigatinib
BCR-ABL	Tyrosine	Bosutinib, Dasatinib, Imatinib, Nilotinib, Ponatinib
BRAF	Serine/Threonine	Vemurafenib, Dabrafenib
BTK	Tyrosine	Ibrutinib
CDK	Serine/Threonine	Palbociclib, Sorafenib, Ribociclib
c-Met	Tyrosine	Crizotinib, Cabozantinib
EGFR family	Tyrosine	Gefitinib, Erlotinib, Lapatinib, Vandetanib, Afatinib, Osimertinib

Table 1.2 continued

JAK	Tyrosine	Ruxolitinib, Tofacitinib
MEK1/2	Dual specificity	Trametinib
PDGFR α/β	Tyrosine	Axitinib, Gefitinib, Imatinib, Lenvatinib, Nintedanib, Pazopanib, Regorafenib, Sorafenib, Sunitinib
RET	Tyrosine	Vandetanib
Src	Tyrosine	Bosutinib, Dasatinib, Ponatinib, Vandetanib
VEGFR	Tyrosine	Axitinib, Lenvatinib, Nintedanib, Regorafenib, Pazopanib, Sorafenib, Sunitinib

1.2.3. Oncogenic PTPs

Historically, and as has been described above, kinases have been regarded as the active drivers of phosphotyrosine signalling. PTPs were formally discovered in the late 1980s, and were originally thought of as housekeeping enzymes that serve to negatively regulate kinase signalling. As such, it has been presumed that PTPs play largely tumour suppressive roles in cancer, dampening down signalling produced by oncogenic kinases, thus protecting cells from tumourigenesis and tumour progression (Wang et al., 2004, Motiwala and Jacob, 2006, Laczmanska and Sasiadek, 2011). Indeed several tumour suppressive PTPs have been described, for example PTEN. PTEN is a dual specificity PTP (DSP) that preferentially dephosphorylates phosphoinositides and negatively regulates PI3K/AKT signalling. It is one of the most commonly mutated tumour suppressor genes and loss-of-function is associated with many human malignancies (Hollander et al., 2011, Song et al., 2012). However, it is now clear that this model of oncogenic kinases versus tumour suppressive phosphatases is over simplistic. We now know that PTPs are also active signalling molecules under tight regulation. They can sustain cancer phenotypes by facilitating pro-cancer signalling, and when disrupted they too can act as oncoproteins that drive tumourigenesis (He et al., 2014, Elson, 2018). In a study by MacKeigan et al. (2005), HeLa cells were transfected with siRNAs to knockdown every member of the phosphatase family. Apoptosis was triggered following knockdown of almost a third of all phosphatases (regulatory and catalytic subunits of serine/threonine phosphatases, PTPs and DSPs), including a significant proportion of PTPs and DSPs. This demonstrates that specific PTPs may be essential for survival

in these tumour cells and are therefore interesting candidate therapeutic targets.

The human PTP superfamily, or 'PTPome', consists of 107 genes, based on experimentally validated PTPs and proteins with domains homologous to known PTP catalytic domains. However, of these only 81 dephosphorylate phosphotyrosine, whilst the remaining 26 dephosphorylate inositol phospholipids, carbohydrates or mRNA, or are catalytically inactive (Alonso et al., 2004). In general, PTPs are characterised by the presence of active site cysteine residues, which act as critical nucleophiles during catalysis (Guan and Dixon, 1991). Specifically, the catalytic loop of PTP domains contain a CXXXXXR motif, where C is the catalytic cysteine residue, which transiently accepts the phosphate group, forming an enzyme intermediate that is stabilised by the arginine residue (R). X can be any amino acid (Alonso et al., 2016). The PTP superfamily can be divided into four sub-families based on active site amino acid sequence and substrate specificity (**Figure 1.7**) (Kim and Ryu, 2012, Alonso et al., 2016). Briefly, class I PTPs include the classical PTPs and DSPs. Classical PTPs, both receptor and non-receptor, exclusively dephosphorylate phosphotyrosine and have highly conserved sequence and structure at the active site. DSPs have much lower sequence homology, allowing them to accommodate a wider range of substrates including phosphoserine, phosphothreonine, phospholipids, and phosphorylated carbohydrates and mRNA. LMW-PTP (or ACP1) was originally the sole member of class II, which differs from class I as catalytic cysteine and aspartic acid residues are much further apart. Ssu72 has been recently added to class II, and unlike ACP1, it can dephosphorylate phosphoserine as well as phosphotyrosine (Xiang et al., 2010). Class III contains CDC25A, B and C, which dephosphorylate cyclin-dependent kinases (CDKs) on tyrosine and threonine residues leading to their activation, thus are involved in cell cycle regulation (Boutros et al., 2007). Unlike other PTPs, class III PTPs have a catalytic rhodenese-like domain (Fauman et al., 1998). Finally, class IV PTPs include the eyes absent (EYA) family, which use aspartic acid rather than cysteine as the catalytic nucleophile (Kim and Ryu, 2012, Rayapureddi et al., 2003). EYA PTPs are transcription factors, but also dephosphorylate both

tyrosine and threonine residues likely using distinct catalytic domains (Alonso et al., 2016, Patterson et al., 2009, Jung et al., 2010). Oncogenic or tumour-promoting roles, and/or high tumour expression has now been described for specific PTPs across these sub-families (Elson, 2018, Pulido and Hooft van Huijsduijnen, 2008). At least 19 PTPs have now been implicated in the initiation or maintenance of cancer phenotypes including sustained proliferation, evading apoptosis, increased migration and invasion, angiogenesis and suppression of the immune response (MacKeigan et al., 2005, Bollu et al., 2017). Therefore, interest in therapeutically targeting PTPs has grown over the last decade. These oncogene-like roles of PTPs in specific tumours have been expertly reviewed elsewhere (Elson, 2018, Frankson et al., 2017, Bollu et al., 2017, Labbé et al., 2012), however below are some examples of PTPs that display oncogenic behaviour. It should be noted that, although not the focus of this thesis, serine/ threonine phosphatases also play important roles in cancer (MacKeigan et al., 2005). For example, PPM1D/Wip1 has been labelled as a proto-oncogene and is overexpressed, amplified and mutated in various cancers, correlating with poor prognosis, and has been the subject of recent drug development efforts (Oghabi Bakhshaiesh et al., 2017, Kleiblova et al., 2013).

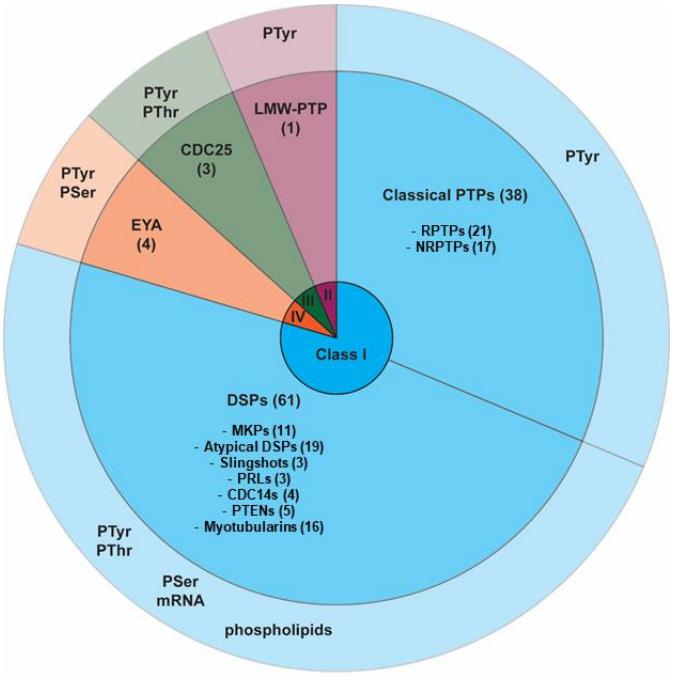

Figure 1.7 - Protein tyrosine phosphatase (PTP) superfamily
PTPs can be divided into 4 classes (detailed in inner rings), with differing substrate specificities (outer ring). Note: Substrate specificities include those for entire classes, every member of each class is not necessarily able to dephosphorylate all of these substrates. 81 family members are able to dephosphorylate phospho-tyrosine. Taken from Irving and Stoker (2017).

PTPN11, encoding the non-receptor classical PTP SHP2, was the first PTP gene to be labelled as a proto-oncogene (Chan and Feng, 2007). SHP2 activity is required for full activation of the Ras-ERK pathway, as well as other signalling cascades that are implicated in cancer such as PI3K/AKT, JAK/STAT and JNK (Huang et al., 2014, Frankson et al., 2017). Gain-of-function mutations in *PTPN11* have been reported in up to 50% of patients with Noonan syndrome, a developmental disorder associated with an increased risk of cancer (Tartaglia et al., 2001). Indeed, gain-of-function mutations have also been reported in several leukaemias and in some solid tumours, including neuroblastoma (Chan and Feng, 2007, Bentires-Alj et al., 2004). Most strikingly, 34% of all juvenile myelomonocytic leukaemia patients are reported to have activating mutations in *PTPN11* (Tartaglia et al., 2003). Overexpression of SHP2 has also been reported in a number of human malignancies including amongst others, breast cancer, leukaemia and thyroid cancer (Zhou et al., 2008, Xu et al., 2005, Hu et al., 2015). Furthermore, there is evidence to suggest that SHP2 overexpression or over-activation may actively drive cancer phenotypes. For example, in breast cancer cell lines shRNA-mediated inhibition of SHP2 reversed epithelial-to-mesenchymal transition and reduced migration and invasion (Zhou and Agazie, 2008). Given its well described oncogenic role, SHP2 is a target of high interest for therapeutic intervention in cancer. The allosteric SHP2 inhibitor SHP099 inhibits proliferation of RTK-driven tumour cells *in vitro* and *in vivo* (Chen et al., 2016, Sun et al., 2018b). Furthermore, sodium stibogluconate (SSG) inhibits SHP2 as well as SHP1, and is being used in early clinical trials for advanced solid tumours including melanoma (Bollu et al., 2017).

PTP1B is another example of a non-receptor classical PTP that has been described as an oncogene (Lessard et al., 2010, Elson, 2018). *PTP1B* is overexpressed in some breast tumours, which has been correlated with poor prognosis in particular in oestrogen receptor-positive tumours (Liu et al., 2016). Inhibition of PTP1B using small molecules or genetic ablation reduced tumour burden in mouse models of HER/Neu mutant breast cancer. Furthermore, overexpression of *PTP1B* was sufficient to drive breast tumourigenesis in mice (Julien et al., 2007). Overexpression of *PTP1B* has also been correlated with

poorer prognosis in various other cancer types, for example gastric, colorectal, liver and non-small cell lung cancer (NSCLC) (Wang et al., 2015, Hoekstra et al., 2016, Tai et al., 2016, Liu et al., 2015a). PTP1B was the first PTP to be recognised as an interesting therapeutic target, although this was for diabetes and obesity given PTP1B's role in insulin sensitivity (Elchebly et al., 1999, Gum et al., 2003). Several PTP1B inhibitors are now in development. The most promising of these is trodusquemine (MSI-1436), which is in clinical trials for type II diabetes as well as metastatic breast cancer (Bollu et al., 2017, Krishnan et al., 2014, Thompson et al., 2017).

Oncogenic roles for non-classical PTPs have also been described, for example PRL3 (Campbell and Zhang, 2014). The PRL family, also known as the PTP4A family, are dual specificity tyrosine and serine/threonine phosphatases with largely unknown biological functions (Bessette et al., 2008). However, cancer-promoting roles have been described for these PTPs, in particular PRL3, which is upregulated in advanced tumours, correlating with poor prognosis (Wei et al., 2018). PRL3 is upregulated in colorectal cancers, in particular metastases in the liver and lungs, and reduced expression impairs tumour cell motility and colony formation *in vitro* and *in vivo* (Saha et al., 2001, Kato et al., 2004). *PRL3* is also expressed at high levels and correlates with poor prognosis in breast tumours (Radke et al., 2006, Wang et al., 2006), as well as gastric cancers, where its expression is reported to correlate with lymph node metastasis (Miskad et al., 2004, Miskad et al., 2007, Li et al., 2007). *PRL3* under- and overexpression studies have been performed *in vitro* and *in vivo* in many tumour types, for example breast, lung, colorectal, gastric, ovarian and melanoma (Wei et al., 2018, Bessette et al., 2008). These studies reported increased motility, migration, invasion and proliferation when *PRL3* was over expressed, and reductions in these metastatic properties when gene expression was silenced. Given its pro-tumour role, it is unsurprising that there have been attempts to develop PRL3 inhibitors. JMS-053 is a thienopyridone derivative that has shown promising anti-cancer efficacy in ovarian cancer models (McQueeney et al., 2018). JMS-053 is a potent allosteric inhibitor of PRL3, however it also inhibits the other PRL family members and to date no specific PRL3 inhibitors have been described.

These are just a few examples of PTPs that have been positively implicated in tumourigenesis and progression, and for which therapeutic targeting is in development. This demonstrates that in specific contexts PTPs can drive tumourigenesis and cancer progression (Elson, 2018, Frankson et al., 2017). PTPs, like PTKs, are therefore a very valuable source of therapeutic targets for cancer.

1.2.4. Phosphotyrosine signalling in neuroblastoma

Above I have described the pivotal role that phosphotyrosine signalling plays both in normal physiology and in the pathology of cancer. Most notably, both PTKs and PTPs can act as oncogenic drivers of cancer. This role of phosphotyrosine signalling is relevant to all human cancers, including of central relevance to this project, neuroblastoma. ALK is an RTK and is the most commonly mutated gene in high-risk neuroblastoma (Trigg and Turner, 2018, Pugh et al., 2013). As discussed previously (**Section 1.1.4.**) gain-of-function mutations occur in inherited and sporadic neuroblastoma, and correlate with poorer prognosis (Shojaei-Brosseau et al., 2004, Ogawa et al., 2011, Trigg and Turner, 2018). The fact that *ALK* is only physiologically expressed in the developing nervous system, and at much lower levels in some adult brain tissues, points to a role in neuronal development and perhaps explains its involvement in developmental tumours such as neuroblastoma (Iwahara et al., 1997, Vernersson et al., 2006). ALK mutations in neuroblastoma almost always result in constitutive activation of the kinase domain. Chen et al. (2008) provided functional evidence that these activating ALK mutations are oncogenic drivers of neuroblastoma when they reported that overexpression of mutant ALK led to tumourigenesis *in vitro* and *in vivo*. Additionally, knockdown of *ALK* expression in ALK-mutant neuroblastoma cell lines led to reduced proliferation (Chen et al., 2008). Activating mutations in ALK can occur alongside *MYCN* amplification in neuroblastoma (Mosse et al., 2008, George et al., 2008). In this context, ALK-induced pro-survival signals may counteract MYCN-associated apoptosis, further propagating tumour progression (Zhu et al., 2012). As mentioned previously, clinical trials using ALK inhibitors such as crizotinib and ceritinib in neuroblastoma patients are ongoing and are producing some promising results, although therapeutic

resistance is a significant problem (Trigg and Turner, 2018). ALK is one of the very few well described molecular drivers of neuroblastoma, clearly pointing to an important role for phosphotyrosine signalling in neuroblastoma pathogenesis.

As well as PTKs, specific PTPs, both classical and non-classical, also have pro-tumour roles in neuroblastoma. *PTPN11*, encoding SHP2, is a *bona fide* oncogene in many tumour types (Chan and Feng, 2007, Matozaki et al., 2009) (**Section 1.2.3.**). Gain-of-function mutations have been reported in neuroblastoma, where *PTPN11* is in fact the third most commonly mutated gene (Bentires-Alj et al., 2004, Pugh et al., 2013). Zhang et al. (2017) provided evidence that activating mutations in SHP2 may co-operate with *MYCN* amplification to drive neuroblastomagenesis. They expressed SHP2 with activating mutations in a zebrafish model of MYCN-overexpressing neuroblastoma and found increased formation and penetrance of neuroblastoma-like tumours (Zhang et al., 2017). The dual specificity phosphatase 26 (DUSP26) is overexpressed in neuroblastoma, where it has been suggested to promote tumour growth by inhibiting p53 signalling (Shang et al., 2010, Shi et al., 2015). DUSP26 inhibition using shRNA or the small molecule inhibitor NSC-87877 reduced growth and increased apoptosis via activation of p53 in neuroblastoma models *in vitro* and *in vivo* (Shi et al., 2015). ShRNA data from our own laboratory have so far not supported an oncogenic role for DUSP26 in neuroblastoma cell lines, although further validation may be required (A. Cichon and A. Stoker, unpublished). PTPN2 is expressed at high levels in some tumour cells, and its down-regulation has been reported to reduce lymphomagenesis (Elson, 2018, Young et al., 2009). Mitra et al. (2011) showed that PTPN2 overexpression prevents forskolin-induced neurite outgrowth in neuroblastoma cells, perhaps suggesting that inhibition of PTPN2 may promote differentiation in these cells.

1.2.5. Therapeutic targeting of oncogenic PTPs

A number of developmental small molecule PTP inhibitors have been mentioned above, however designing small molecules to inhibit specific PTPs is challenging and there are currently no FDA approved PTP inhibitors. Many

drug development efforts have aimed to design compounds that target enzyme active sites, competing with substrates for binding. In the case of PTPs, this requires the development of phosphotyrosine mimetics. As has been discussed, PTPs and in particular classical PTPs have highly conserved active sites (Alonso et al., 2016, Tonks, 2013). Therefore, achieving a high level of PTP enzyme specificity using competitive inhibitors is difficult. Specificity is particularly important when considering targeting pro-tumour PTPs in cancer, as some PTPs have been described as tumour suppressors, thus their off-target inhibition may promote further tumour progression (Wang et al., 2004, Motiwala and Jacob, 2006, Laczmanska and Sasiadek, 2011). The development of competitive PTP inhibitors has also been hindered by the polar nature of phosphotyrosine. Compounds that mimic phosphotyrosine and bind to PTP active sites are also likely to be polar, and as such will struggle to cross plasma membranes (He et al., 2014). Lack of specificity and bioavailability has therefore impeded the development of potent, specific competitive PTP inhibitors. Drug development efforts have thus been shifted towards allosteric inhibitors, which have binding sites distinct from the substrate-binding region and alter protein confirmation upon binding to prevent catalysis, as well as dual-binding inhibitors that bind to both the catalytic site and a specific, neighbouring region (Stanford and Bottini, 2017, Lazo et al., 2018, Zhang, 2017, He et al., 2011). Indeed, the aforementioned SHP2 inhibitor SHP099, the PRL3 inhibitor JMS-053, and the PTP1B inhibitor trodusquemine are all allosteric inhibitors (Chen et al., 2016, Sun et al., 2018b, McQueeney et al., 2018, Krishnan et al., 2014). However, given that these allosteric sites are less well-defined compared to active sites, developing these inhibitors remains challenging.

The difficulty in chemically targeting PTPs, together with the fact that PTPs were initially thought of as negative regulators of tumourigenesis, has caused the development of specific PTP inhibitors to lag behind kinase inhibitors. There are therefore very few specific small molecule PTP inhibitors available for preclinical target validation studies (Stanford and Bottini, 2017, Lazo et al., 2018). This has somewhat forced the field to consider the use of non-specific pan-PTP inhibitors, the clearest examples of which are vanadium-derived

compounds (Gordon, 1991, Huyer et al., 1997, Peters et al., 2003). Our group have previously reported that treating subsets of neuroblastoma cell lines with the oxidovanadium derivative bismaltolato oxidovanadium (BMOV) induces anti-cancer phenotypes including cytotoxicity and differentiation (Clark et al., 2013, Clark et al., 2015). This net response to vanadium compounds provides support for the hypothesis that there exist oncogenic or tumour-promoting PTPs that are important for neuroblastoma cell survival and potentially therefore tumourigenesis and tumour progression.

1.3. Vanadium

1.3.1. Vanadium as a metallotherapeutic

A Swedish chemist named Nils Gabriel Sefström discovered the group 5d transition metal vanadium in 1830. Vanadium is present ubiquitously in nature, found in soil, water, air and living organisms. In fact, it is the 18th most abundant chemical element in the Earth's crust (Rehder, 2012). Vanadium is an essential micronutrient in lower organisms, and although this has yet to be confirmed in humans, vanadium is very likely to play a regulatory role in human cells (Schroeder et al., 1963, French and Jones, 1993, Harland and Harden-Williams, 1994). There has also been great interest over many decades in the use of vanadium-derived compounds as pharmacological agents to treat human disease, most notably diabetes and cancer (Barrio and Etcheverry, 2010, Evangelou, 2002, Rehder, 2012, Rehder, 2013, Thompson and Orvig, 2006). Active research into the use of these compounds as metallotherapeutics is ongoing, with over 1200 publications regarding vanadium and cancer or diabetes since 2000 (PubMed.). As will be discussed below, expansive preclinical studies have and continue to provide promising data for the therapeutic use of vanadium compounds, and phase I and II clinical trials have been completed in the diabetes setting (Thompson and Orvig, 2006, Thompson et al., 2009). Despite this, an approved vanadium-derived drug has yet to reach the market, due in part to concerns regarding off-target toxicities that will be discussed below.

1.3.2. Vanadium as a pan-PTP inhibitor

In nature vanadium exists in a number of oxidation states from –III to +V, but in biological solutions the majority is in the form of tetravalent vanadyl cations (IV) or pentavalent vanadate ions (V) (Nechay, 1984). Orthovanadate has a tetra-coordinated structure with the vanadate ion at the centre, and an overall negative charge. These features are shared with phosphate groups, including those on phosphorylated PTP substrates (**Figure 1.8A**). This similarity in 3D shape and charge allows orthovanadate to bind to PTP active sites, stabilised by a complex network of hydrogen bonds, and to mimic the trigonal bipyramidal transition state that occurs during PTP-mediated phosphoryl transfer reactions (**Figure 1.8B**) (Simons, 1979, Peters et al., 2003, Crans et al., 2004, Brandão et al., 2010). The ability of vanadate to mimic phosphate and bind to PTP active sites renders it a broad specificity, competitive and reversible PTP inhibitor (Crans et al., 2004, Huyer et al., 1997, Swarup et al., 1982, Heneberg, 2009). As has been stated previously, PTPs share a highly conserved catalytic domain, in particular in the substrate-binding region at the active site (Alonso et al., 2016, Tonks, 2013). It is therefore reasonable to assume that vanadium-derived compounds can inhibit all members of the PTP superfamily, although perhaps not with equal potency. Indeed, vanadium salts are commonly used as PTP inhibitors to preserve the phosphorylation status of proteins following extraction from cells prior to immuno detection (Gordon, 1991). Reports of vanadate inhibition of family members from across the PTP superfamily can be found in the literature. For example, Scrivens et al. (2003) showed that several human PTPs were inhibited by orthovanadate, including DSPs from class I and class III, and both receptor and non-receptor class I classical PTPs. Similarly, Peters et al. (2003) showed that BMOV inhibited class II LMW-PTP, as well as both receptor and non-receptor classical class I PTPs, with IC50 values between 26 nM and 201 nM, and Ki values of 0.79 µM and 0.9 µM for human LMW-PTP and PTP1B respectively. Vanadium has not been reported to reversibly inhibit serine/threonine phosphatases in this way. Serine/threonine phosphatases have distinct catalytic mechanisms compared to PTPs, therefore vanadate binding cannot mimic the transition state occurring during phosphoryl transfer reactions for these enzymes (Shi, 2009,

Barford et al., 1998). Importantly, it is not simply that vanadate resembles phosphate that enables it to reversibly inhibit PTPs, but, crucially, that it mimics the bipyramidal transition state.

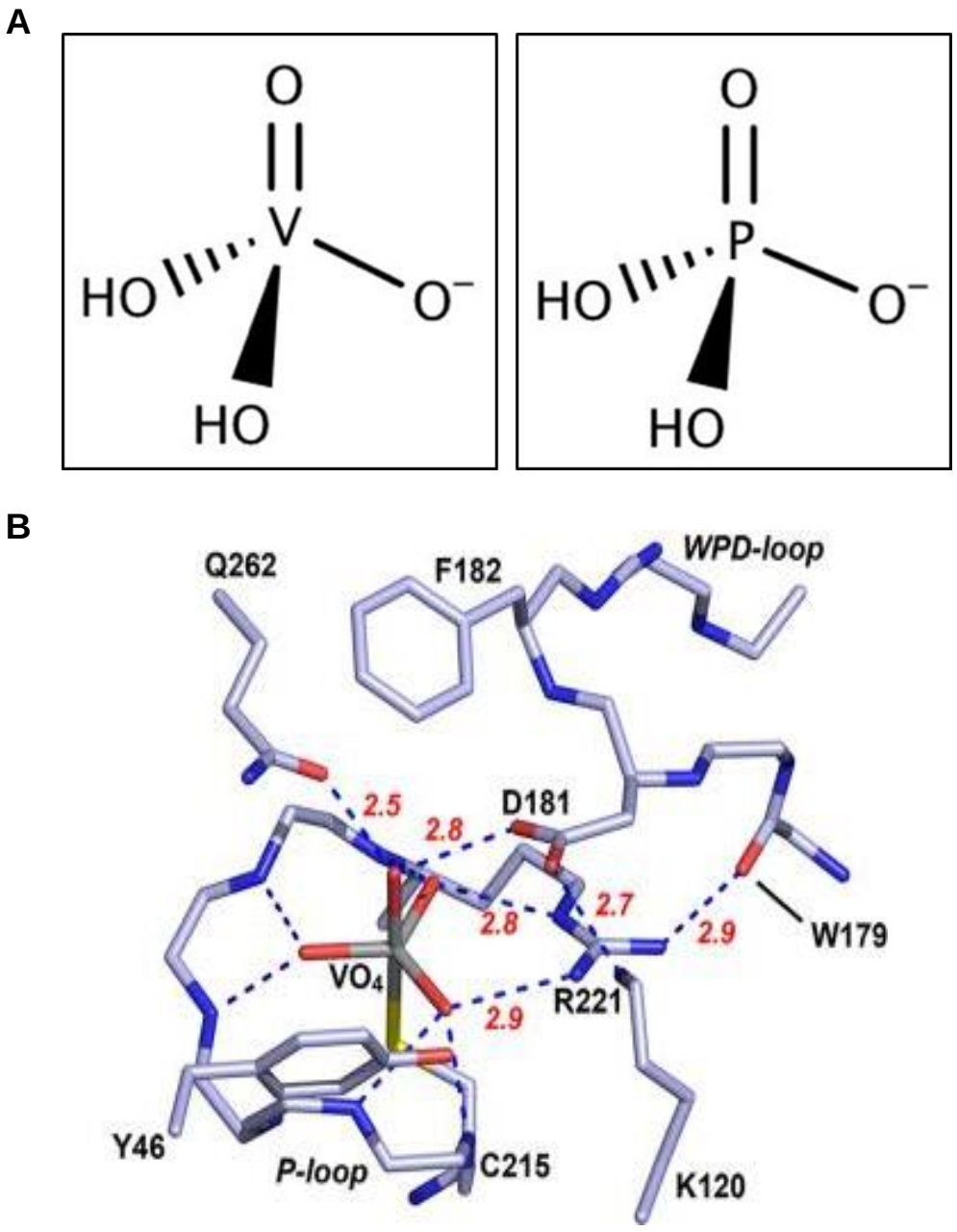

Figure 1.8 – Vanadate resembles phosphate
A *- Orthovanadate (left) and phosphate (right) both have a tetra-coordinated structure and overall negative charge.* ***B*** *– Crystal structure showing the trigonal bipyramidal transition state complex between PTP1B and orthovanadate. Hydrogen bond lengths (red) are in Å. Taken from Brandão et al. (2010).*

Some specific vanadium-derived compounds, namely peroxidovanadium complexes, are able to inhibit PTPs via a distinct and sometimes irreversible mechanism (Bevan et al., 1995, Huyer et al., 1997, Scrivens et al., 2003, Evangelou, 2002, Heneberg, 2009). These compounds can oxidise cysteine residues in the PTP active site, which are critical for catalysis, therefore rendering enzymes catalytically inactive (Ostman et al., 2011, Barford, 2004). This was confirmed in a study by Peters et al. (2003) where human LMW-PTP and PTP1B were treated with the peroxidovanadium compound bisperoxo (1,10-phenanthroline) oxidovanadate (V) (bpv-phen). Following treatment with bpv-phen, shifts in mass spectra were observed that were consistent with active site cysteine oxidation; this was not observed for an alternative oxidovanadium compound, BMOV (Peters et al., 2003). The vanadium ion can also indirectly contribute to PTP inhibition by oxidation of active site cysteine residues. In the cell, there is interconversion between the vanadyl (IV) and vanadate (V) redox states of the vanadium ion. This interconversion occurs via Fenton-like reactions and generates reactive oxygen species (ROS) (Sakurai et al., 1980, Nechay, 1984). As with peroxidovanadium compounds, ROS can oxidise active site cysteine residues, causing enzyme inactivation (Groen et al., 2005, Barford, 2004, Salmeen et al., 2003). Vanadium-derived compounds can therefore be considered broad-spectrum PTP inhibitors, both via competitive active site binding and in some cases active site cysteine oxidation. This activity is likely related to the therapeutic potential of these compounds in cancer models as will be further discussed in **Section 1.3.6**.

1.3.3. Oxidovanadium compounds

Over several decades, the nature of the vanadium-derived compounds that have been investigated as therapeutic agents, has evolved. Early studies focussed on the use of simple, inorganic vanadium salts, whereas later studies have used more bulky and complex compounds, for example those shown in **Figure 1.9**. In the majority of cases, these complexes contain a single vanadium ion co-ordinated by organic ligands of varying complexity, and included but are not limited to maltolato vanadium compounds, vanadocenes, and peroxidovanadium complexes (Rehder, 2012). Vanadium oligomers have also been developed, most notably decavanadates (**Figure 1.9D**). Distinct

intracellular responses have been described for decavanadates compared to monomeric vanadium complexes, namely a unique oxidative stress response and an allosteric ATPase inhibition mechanism (Tiago et al., 2007, Fraqueza et al., 2012, Soares et al., 2007b, Soares et al., 2007c). Importantly however, in biological systems treated with decavanadate, monomeric vanadate is released, likely causing a degree of PTP inhibition (Aureliano and Crans, 2009, Aureliano and Gandara, 2005, Aureliano, 2016). One factor that has contributed to the increased use of bulky oxidovanadium complexes with organic ligands seems to be their improved bioavailability *in vivo* compared to vanadate (Thompson and Orvig, 2006, Thompson et al., 2009, McNeill et al., 1992). However, increasing evidence from detailed speciation studies now suggests that these larger oxidovanadium complexes (e.g. BMOV – **Figure 1.9A**) are often subjected to a complex range of ligand exchange events in the gut, circulation and/or within target cells, ultimately releasing un-complexed vanadate, which is in fact the PTP-inhibiting moiety (Caravan et al., 1995, Levina et al., 2014, Levina and Lay, 2017, Scior et al., 2016) (**Figure 1.10**). Support for this hypothesis comes from a study by Peters et al. (2003). They reported first that NMR shifts indicating active site changes were identical when LMW-PTP was treated with either BMOV or sodium orthovanadate. This suggests that the same moiety, uncomplexed vanadate, was responsible for active site changes, and therefore PTP inhibition, in both cases. Secondly, from analysis of BMOV soaked PTP1B crystals, they concluded that the vanadate ion, but not intact BMOV, was consistent with the observed electron density at the active site. If uncomplexed vanadium is really the active PTP-inhibiting moiety within these vanadium complexes, one could question the benefit of the continued development of complex oxidovanadium structures. However, these alternative vanadium co-ordination complexes may still improve anti-disease efficacy via optimised vanadate bioavailability and targeting. Indeed, vanadate accumulation in various tissues has been reported to be 2-3 times higher following BMOV treatment compared to vanadyl sulphate (Setyawati et al., 1998).

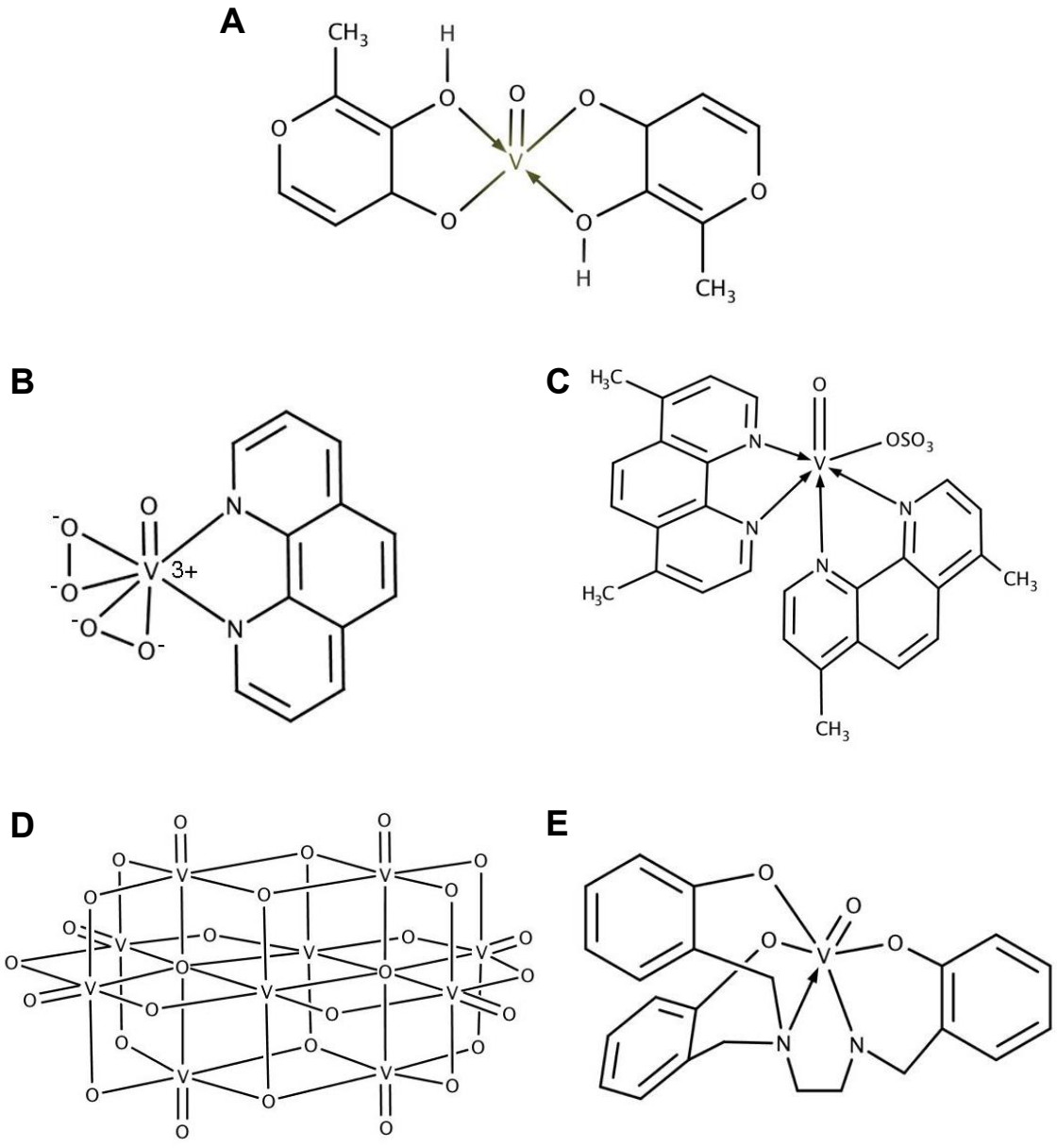

Figure 1.9 – Oxidovanadium derivatives
A *– Bismaltolato oxidovanadium (BMOV).* ***B*** *- Bisperoxo(1,10-phenanthroline)oxidovanadate(V) (bpv-phen).* ***C*** *- Bis(4,7-dimethyl-1,10-phenanthroline)sulfatooxidovanadium(IV) (Metvan).* ***D*** *- Decavanadate (V10).* ***E*** *- Vanadium(V) oxo phenolato complex (Reytman 2016). Modified from Irving and Stoker (2017).*

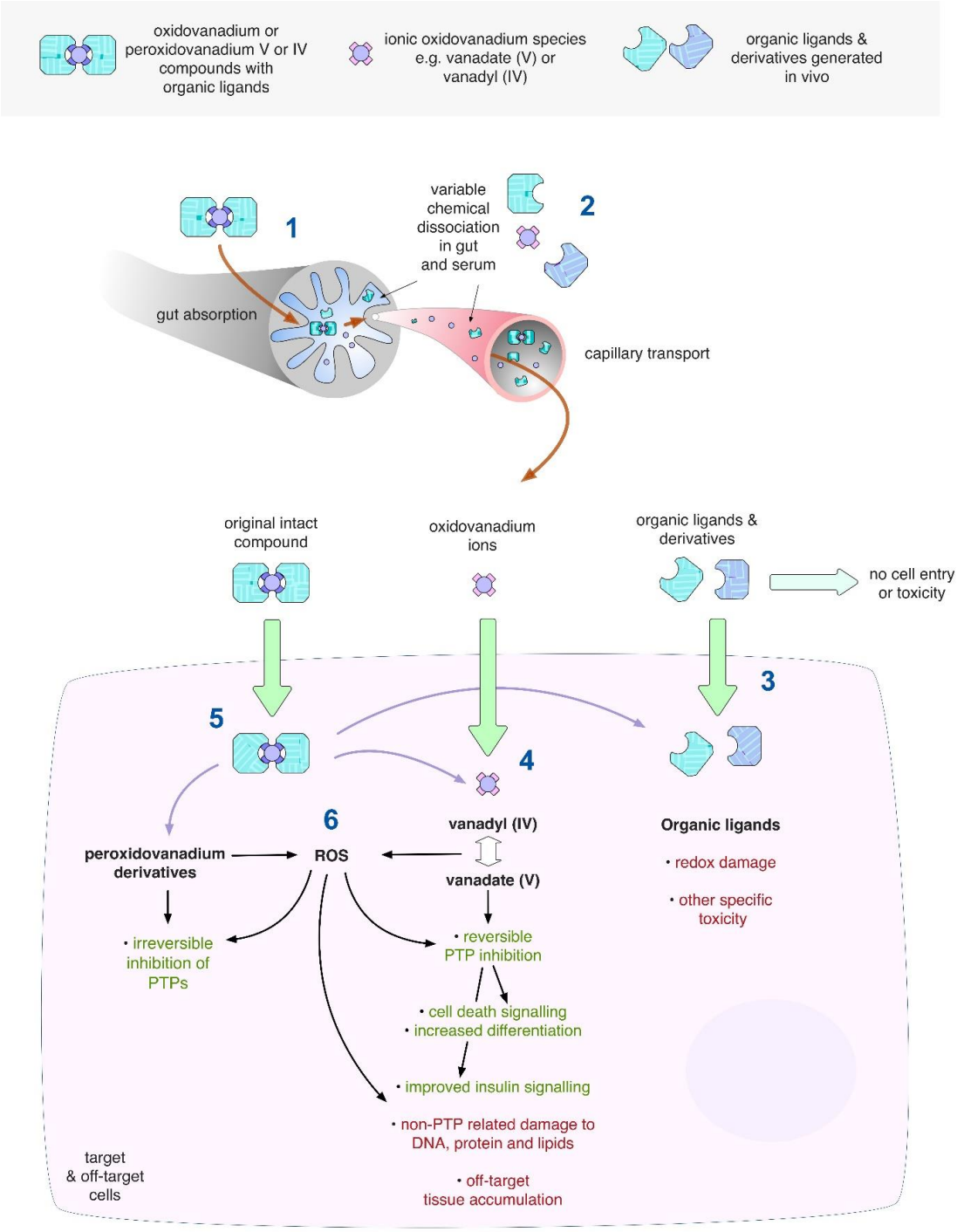

Figure 1.10 – Ingestion, chemical dissociation and cellular targeting of generic oxidovanadium complexes

Oxidovanadium complexes with organic ligands are readily absorbed through the gut wall [(1)], but then can rapidly dissociate in the gut or bloodstream to release vanadate and ligand molecules [(2)]. Both can be taken up by the cell, and when ligands do enter the cell, they can have significant cytotoxic effects [(3)]. Intracellular vanadate has a range of effects including PTP inhibition [(4)]. Some oxidovanadium compounds may be more stable and reach the cell intact, although they too are thought to dissociate ultimately within the cell [(5)]. Oxidovanadium compounds, in particular peroxidovanadium, can produce ROS directly or indirectly, and this may contribute to PTP inhibition and other non-specific cytotoxicity [(6)]. The cells described could be within on-target or off-target tissues. Modified from Irving and Stoker (2017).

1.3.4. Ligand toxicity

As has been discussed above, oxidovanadium complexes with organic ligands often dissociate in biological solutions, including culture media during *in vitro* experiments and in circulation *in vivo* (Levina and Lay, 2017) (**Figure 1.10**). This dissociation releases vanadate, the active moiety for PTP inhibition, as well as ligand derivatives. Whilst the development of these complexes has led to improved bioavailability of vanadate (Setyawati et al., 1998), there is a danger of losing sight of the potential cellular actions of the organic ligands themselves. These ligands may enter cells independently or be released from more stable oxidovanadium complexes within cells, but either way their effect on cell viability may be significant. Importantly, the cells affected by this ligand toxicity may be on-target, for example tumour cells, or off-target, therefore potentially resulting in adverse effects.

An example of an oxidovanadium complex that utilises cytotoxic ligands is bis(4,7-dimethyl-1,10-phenanthroline)sulfatooxidovanadium(IV) (Metvan) (**Figure 1.9C**). Metvan has been used in a number of preclinical studies using cancer cell lines and *in vivo* models, where it has shown anti-cancer efficacy in the nanomolar and low micromolar range. Specifically, it has been reported that treatment with metvan leads to ROS-associated apoptosis and loss of invasive properties (Narla et al., 2001, D'Cruz and Uckun, 2002). However, it has also been shown that the 1,10-phenanthroline (phen) ligands used to co-ordinate vanadate in metvan are also cytotoxic (Coyle et al., 2004). The phen ligands alone generated a similar toxicity profile compared to metvan using leukaemia and lung cancer cell lines (Dong et al., 2000, Le et al., 2017). Furthermore, it has recently been shown that like other oxidovanadium complexes, metvan dissociates in biological solutions to release vanadium and free phen ligands (Le et al., 2017, Sanna et al., 2017). Phen ligands can then be efficiently taken up by cells partially by complexing with copper and iron. In the cell, they induce ROS production pushing cells into oxidative catastrophe and ultimately cell death (Le et al., 2017). This systemic toxicity associated with phen ligands has also been demonstrated *in vivo* (Li et al., 2004, Le et al., 2017). Therefore, in the case of metvan and perhaps some other oxidovanadium derivatives, vanadium may be largely acting as the carrier for

cytotoxic ligands, rather than the other way around. These particular ligands are therefore unlikely to be suitable for therapeutic applications directed solely at PTP inhibition.

As will be discussed, a wide range of oxidovanadium compounds have been used in preclinical studies of human diseases, in particular cancer. In many cases the effects of organic ligands have not been considered and free ligand effects may well contribute to some of the differences in observed efficacy (Levina and Lay, 2017). It should be noted that some oxidovanadium compounds with much higher stability have been used in preclinical studies. For example, Reytman et al. (2016) described a six-fold octahedral oxidovanadium complex with pentadentate phenotlato ligands (**Figure 1.9E**), which displayed very high anti-cancer efficacy *in vitro* and *in vivo*. They reported that this complex is highly stable in biological solutions, and remains intact until it is delivered to the cell (Reytman et al., 2016). Similarly, the anti-cancer pyridinone ligated oxidovanadium complexes described by Rozzo et al. (2017) have high stability and do not dissociate before uptake into target cells. It is not yet clear whether these complexes dissociate once inside the cell, and therefore whether PTP inhibition by vanadium is required for their anti-cancer efficacy.

This discussion highlights the importance of considering the biological activity of all components of oxidovanadium complexes before prematurely assigning phenotypes as vanadium- or PTP-induced responses. This is important when reviewing the wide range of preclinical data that suggest anti-cancer activities of various oxidovanadium complexes in *in vitro* and *in vivo* tumour models (described in **Section 1.3.6.**).

1.3.5. Vanadium in diabetes

Vanadium-derived compounds are of interest for this thesis due to their ability to inhibit PTPs, some of which may be oncogenic drivers of neuroblastoma. The anti-cancer efficacy of various vanadium derivatives has been well reported and will be discussed in **Section 1.3.6.** However, interest in vanadium as a metallotherapeutic originated within the diabetes field, and research surrounding the use of vanadium as an insulin mimetic is ongoing, due in part

to its ability to inhibit PTPs, in particular PTP1B (Poucheret et al., 1998, Thompson et al., 2009, Treviño et al., 2018). Whilst this activity of vanadium is somewhat distinct from its potential in cancer therapy, many studies, both preclinical and clinical, have been carried out in this setting, and much can be learnt from them regarding toxicity and bioavailability.

The first reported case of therapeutic vanadium use in humans was as far back as 1899, when Lyonnet and colleagues treated 60 patients with sodium metavanadate. Three of these patients were diabetic, two of whom displayed a modest reduction in blood glucose following treatment. No adverse effects were reported for diabetic or healthy patients (Thompson and Orvig, 2006). Despite displaying promising results during later preclinical *in vivo* testing, interest in vanadium dwindled when insulin was discovered in 1922 and quickly became the primary therapeutic used to treat diabetes (Banting et al., 1922). During the 1950's and 1960's, clinical trials were carried out using vanadium to reduce cholesterol, as reduced cholesterol had been observed in vanadium workers, but clinical efficacy was disappointing. Importantly, however, side effects were limited to nausea, abdominal pain, pharyngitis and anorexia, suggesting a reasonable tolerance for vanadium compounds in humans (Somerville and Davies, 1962). Towards the end of the 20th century, studies in rat models of diabetes began to show the specific activity of vanadium ions in mimicking/enhancing insulin signalling (Heyliger et al., 1985, Meyerovitch et al., 1987, Brichard, 1995, Blondel et al., 1989). This led to renewed interest in the use of vanadium-derived compounds in replacing invasive insulin injections. Insulin signalling is critical for the proper regulation of blood glucose and energy storage. Abnormal insulin signalling is characteristic of diabetes, where insulin cannot be produced (type 1 diabetes) or cells do not respond to it correctly (type 2 diabetes). Several PTPs are involved in insulin signalling, in particular PTP1B, which is able to dephosphorylate and inhibit the insulin receptor (Seely et al., 1996, Salmeen et al., 2000). It is thought that vanadium is able to improve diabetic symptoms by inhibiting these PTPs, therefore enhancing signalling throughout the insulin signalling network (Mehdi et al., 2006). Indeed, it has been shown that vanadate can inhibit PTP1B *in vitro* and *in vivo*, and X-ray diffraction and NMR spectroscopic techniques have revealed

vanadate coordinated within the PTP1B active site following treatment with vanadium compounds (Huyer et al., 1997, Mohammad et al., 2002, Treviño et al., 2018). Importantly, identical structures are observed following treatment with vanadyl sulphate or BMOV, again suggesting that oxidovanadium complexes dissociate in biological solutions to release active PTP-inhibiting vanadate (Sánchez-Lombardo et al., 2015, Treviño et al., 2018).

With an increasing bank of preclinical data supporting vanadium-based diabetes therapeutics, randomised clinical trials were carried out in the 1990's and into the 2000's. The early trials used simple, inorganic vanadium compounds including vanadium sulphate and ammonium metavanadate (Goldfine et al., 1995, Goldfine et al., 2000, Cohen et al., 1995, Halberstam et al., 1996, Boden et al., 1996, Cusi et al., 2001). Doses of up to 100 mg vanadium per day were tolerated in these trails with minor gastrointestinal (GI) distress reported as the main adverse response. However, high variability between patient responses was reported, and in general therapeutic efficacy for diabetic patients was low (Thompson and Orvig, 2006, Smith et al., 2008). These outcomes highlighted the need for vanadium complexes with organic ligands that would allow fine-tuning of the vanadium response. It was thought that good vanadium ligands would prevent premature degradation of the complex during digestion, allowing sufficient time for absorption into the bloodstream, and minimising toxicity such as GI distress. Vanadium complexes would ideally ultimately dissociate, releasing vanadate and an inert ligand that would not be toxic itself. Two such oxidovanadium complexes were introduced and dominated this field. These were BMOV, and its ethylmaltol analogue bisethylmaltolato oxidovanadium (BEOV). In 2000 Medeval Ltd (Manchester, UK) performed phase I BEOV dose escalation trials using between 25 and 90 mg. The trial results confirmed that BEOV had three times higher bioavailability compared to vanadyl sulphate, with increased absorbance into the bloodstream achieving plasma concentrations up to 170 ng/ml (492.75 nM), and increased half-life. Evidence of tissue accumulation was reported, although liver and kidney functions were not affected. GI function was also normal, and no other adverse effects were reported (Thompson and Orvig, 2006). A phase IIa clinical trial using seven type 2

diabetic patients was subsequently completed by Akesis Pharmaceuticals, Inc. (La Jolla, CA). Patients were treated with 20 mg BEOV once daily for 28 days, and reduced glucose levels with no major adverse effects were reported (Thompson et al., 2009). These trials were unfortunately abandoned partly because BEOV came off patent in 2011 (Thompson and Orvig, 2006, Crans, 2015).

Despite these apparently positive results regarding vanadium-derived compounds as insulin mimetics, it has been stated that based on current clinical trial data, the use of vanadium to treat diabetes could not be recommended since efficacy was too variable (Smith et al., 2008). Furthermore, given that the treatment of diabetes requires very long-term dosing, there are significant safety concerns in particular regarding tissue accumulation. These have not been addressed by the current clinical trials, which have only used short-term dosing schedules. Thus, a longer term safety study with a focus on cumulative vanadium toxicity will be required if vanadium-based therapy for diabetes is to progress any further (Setyawati et al., 1998, Domingo, 2000, Domingo and Gómez, 2016).

1.3.6. Vanadium in cancer

Vanadium has long been of interest in cancer biology, with the first reports of its anti-cancer activity dating back to 1965 (Kieler et al., 1965). Since then many studies have described the potential for therapeutic vanadium-based compounds in preventing the onset of tumourigenesis and for the treatment of cancer (Evangelou, 2002, Bishayee et al., 2010). Several intracellular consequences of vanadium treatment have been described that may be relevant to the mechanisms that drive vanadium-induced anti-cancer activity, including pan-PTP inhibition (**Figure 1.11**). Given their very broad activity, not least in inhibiting all members of the PTP superfamily, it is unsurprising that vanadium compounds are able to inhibit cancer initiation and progression by acting against several of Weinberg's hallmarks of cancer. For example, inducing apoptosis and other cell death pathways, reducing proliferation, and inhibiting migration and metastasis (Hanahan and Weinberg, 2011). The most successful cancer therapies are likely to be those that target multiple aspects

of tumour biology, therefore vanadium-derived compounds could be very promising multifunctional therapeutic candidates. **Table 1.3** and **Table 1.4** (modified from my own review on this subject (Irving and Stoker, 2017)) summarise several studies where anti-cancer properties of a variety of vanadium compounds are reported *in vitro* and *in vivo*. In these studies the net effect of treatment with vanadium-derived compounds, and therefore pan-PTP inhibition, is anti-cancer, suggesting that oncogene-like roles for PTPs may be dominant over tumour suppressive ones.

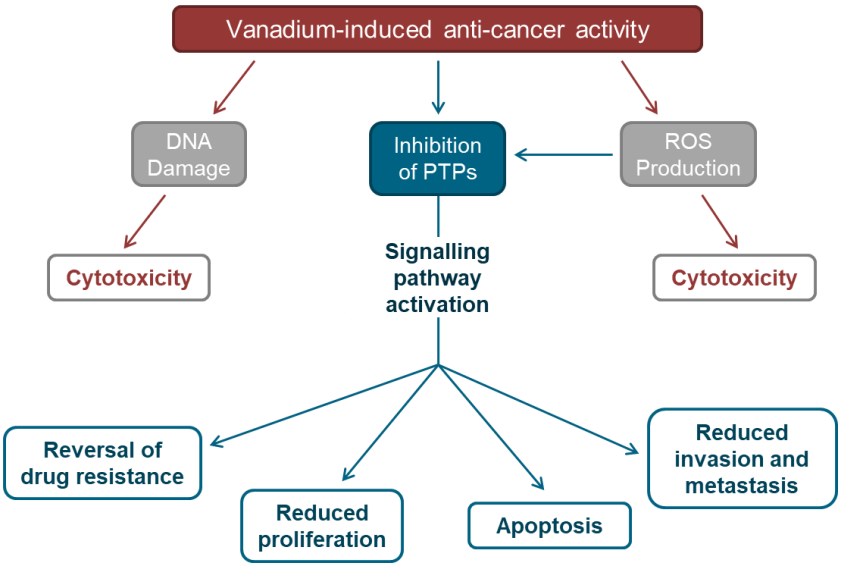

Figure 1.11 – Anti-cancer activities associated with vanadium-derived compounds
Vanadium-derived compounds have multiple anti-cancer effects in tumour cells, some of which are outlined here. Cytotoxicity can arise as a result of DNA damage, or increased production of reactive oxygen species (ROS). PTP inhibition by the vanadate ion itself or indirectly via ROS leads to altered signal transduction down multiple pathways contributing to reversal of drug resistance, reduced proliferation, increased apoptosis and reduced invasion and metastasis. Based on Evangelou (2002).

Table 1.3 - Anti-cancer activities of vanadium in animal cancer models
Table summarising some published anti-cancer activities of various vanadium-derived compounds in animal models of cancer. Examples are grouped by tumour type (coloured white or grey to differentiate). The table details disease model, vanadium compound, dose administered, route of administration, tumour effects, and any proposed mechanism of action. DEN, diethylnitrosamine; 2-AAF, 2-acetylaminofluorence; DMH, 1,2-dimethylhydrazine; MNU, 1-methyl-1-nitrosourea; DMBA, 7,12-dimethylbenzlαanthracene. Modified from Irving and Stoker (2017).

Model	Compound	Effect	Proposed Mechanism
DEN rat liver model (Bishayee et al., 1999, Chakraborty et al., 2006a, Chakraborty et al., 2006b, Chakraborty et al., 2006c, Chakraborty et al., 2007c, Chakraborty et al., 2007a)	Ammonium metavanadate *(0.5 ppm/ 4.27 µM in drinking water)*	Chemopreventative – reduced proliferation and premalignant nodule incidence	Reduced DNA damage Increased expression of drug metabolising enzymes

Table 1.3 continued

2-AAF rat liver model (Chakraborty et al., 2003, Chakraborty et al., 2005, Chakraborty et al., 2007b)	Ammonium monovanadate/ ammonium metavanadate *(0.5 ppm/ 4.27 µM in drinking water)*	Chemopreventative – reduced tumour incidence, reduced proliferation and increased apoptosis	Reduced DNA damage Increased expression of drug metabolising enzymes Induction of p53
Orthotopic Hepatocellular carcinoma mouse model (Wu et al., 2014)	Sodium orthovanadate *(10-20 mg/kg)*	Reduced cell proliferation and tumour volume	
DMH rat colon model (Samanta et al., 2008b, Samanta et al., 2008a)	Vanadium *(0.5 ppm/ 4.27 µM in drinking water)*	Chemopreventative – reduced proliferation, increased apoptosis	Reduced DNA damage Induction of p53
DMH rat colon model (Kanna et al., 2004)	Ammonium monovanadate *(0.5 ppm/ 4.27 µM in drinking water)*	Chemopreventative – reduced tumour incidence	Reduced DNA damage
MNU rat mammary model (Thompson et al., 1984)	Vanadyl sulphate *(25 ppm in feed)*	Chemopreventative – reduced tumour incidence and increase survival	
DMBA rat mammary model (Sankar Ray et al., 2004, Ray et al., 2005, Sankar Ray et al., 2005, Ray et al., 2007)	Ammonium monovanadate / ammonium metavanadate *(0.5 ppm/ 4.27 µM in drinking water)*	Chemopreventative - reduced tumour incidence and size. Reduced proliferation and increased apoptosis	Reduced DNA damage Induction of p53
DMBA rat mammary model (Manna et al., 2011)	Ammonium monovanadate *(0.5 ppm/ 4.27 µM in drinking water)*	Chemopreventative – reduced tumour incidence, reduced proliferation and increased apoptosis	Reduced DNA damage Induction of p53
DMBA rat mammary model (Bishayee et al., 2000)	Ammonium monovanadate *(0.5 ppm/ 4.27 µM in drinking water)*	Chemopreventative – reduced tumour incidence	Increased expression of drug metabolising enzymes
MDA-MB-231 mouse breast cancer xenograft model (D'Cruz and Uckun, 2002, Narla et al., 2001)	Metvan *(10 mg/kg intraperitoneal)*	Reduced tumour progression and increased apoptosis	Induction of oxidative damage
DA3 mouse breast cancer xenograft model (Scrivens et al., 2003)	Bisperoxidovanadium compounds *(20 mg/kg intraperitoneal)*	Reduced tumour growth	CDC25A inhibition leading to cell cycle arrest and apoptosis
U87 mouse glioblastoma xenograft model (D'Cruz and Uckun, 2002, Narla et al., 2001)	Metvan *(10 mg/kg intraperitoneal)*	Reduced tumour progression and increased apoptosis	Induction of oxidative damage
L1210 injected mice (leukaemia) (Köpf-Maier et al., 1981)	Vanadocene dichloride *(10 – 130 mg/kg)*	Increased life span	

Table 1.4 - Anti-cancer activities of vanadium in cancer cell lines
A summary of some published anti-cancer activities of various vanadium-derived compounds in cancer cell lines. The table details tumour type, vanadium compound, dose administered, cellular effects, and any proposed mechanism of action. Modified from Irving and Stoker (2017).

Tumour Cell Type	Compound	Effect	Proposed Mechanism
Cervical (Nair et al., 2014)	Nicotinoyl hydrazine vanadium complexes *(50-100 μM)*	Increased apoptosis	p53 induction
Hepatocellular carcinoma (HCC) (Wu et al., 2014)	Sodium orthovanadate *(15-30 μM)*	Decreased Proliferation G2/M arrest Increased Apoptosis	
Osteosarcoma (Leon et al., 2013, Leon et al., 2014)	Oxidovanadium flavonoid complexes *(10-100 μM)*	Increased apoptosis DNA damage Cell cycle arrest	ROS production DNA strand breaks
Osteosarcoma (Molinuevo et al., 2008)	Vanadium (IV) complexes *(2.5-5 μM)*	Reduced cell adhesion and migration Reduced colony formation	Reduced actin polymerisation via suppressed PKA activity
Malignant melanoma (Rozzo et al., 2017)	Pyridinone ligated oxidovanadium complexes *(1 -100 μM)*	Reduced proliferation Increased apoptosis Cell cycle arrest	
Lung and Melanoma (Strianese et al., 2013)	Pyridoxylideneiminato vanadium *(50 μM)*	Increased apoptosis	ROS production
Lung and breast (Petanidis et al., 2016)	Vanadium(V)-peroxido-betaine *(25-50 μM)*	Reduced migration Increased cell death	Reduced TGFβ-mediated epithelial–mesenchymal transition
Lung and Breast (Petanidis et al., 2013)	Vanadium-peroxido-betaine *(100-400 μM)*	Increased apoptosis DNA damage	ROS production Reduced HRAS and MMP2 expression
Breast (Ray et al., 2007)	Ammonium monovanadate *(100-250 μM)*	Apoptosis and cell cycle arrest	
Breast (Navara et al., 2001)	Vanadocene dichloride *(10 – 20 μM)*	Reduced proliferation G2/M arrest	
Glioma (Ajeawung et al., 2013)	Picolinato-bis(peroxido) oxidovanadate (V) (Bpv(pic)) *(5-20 μM)*	Reduced proliferation S phase and G2/M accumulation Increased apoptosis Reduced migration and invasion	Inhibition of PTP expression and activity
Rhabdomyosarcoma (Dąbroś et al., 2011)	BMOV and vanadium salts *(10-40 μM)*	Growth inhibition	
Chronic myeloid leukaemia (CML) (Meshkini and Yazdanparast, 2010)	VO-salen *(6-32 μM)*	Proliferation inhibition G2/M arrest Chemosensitisation to taxol	
Neuroblastoma (Clark et al., 2013, Clark et al., 2015)	BMOV *(10 μM)*	Cytotoxicity Differentiation	PTP inhibition
Testicular (Ghosh et al., 2000)	Vanadocene dichloride *(100 μM)*	Apoptosis	

Table 1.4 continued

Prostate (Liu et al., 2012)	Vanadate *(25-100 µM)*	G2/M arrest Growth inhibition	ROS-mediated CDC25C degradation
Ovarian and Prostate (Scalese et al., 2017)	Heteroleptic Schiff base vanadium complexes *(1 -150 µM)*	Cytotoxicity	Disrupted mitotic spindle formation
Pancreas (Kowalski et al., 2017)	Phenanthroline/quinolone ligated vanadium *(1 -100 µM)*	Increased apoptosis and necroptosis G2/M arrest	ROS production
Pancreas (Wu et al., 2016a)	Bis(acetylacetonato)-oxidovanadium(IV) *(1-400 µM)*	Reduced proliferation G2/M arrest	ROS production ERK pathway activation
Colorectal (Sinha et al., 2017)	Schiff base vanadium complex *(20 µg/ml)*	Increased apoptosis G2/M arrest	Glutathione depletion ROS production DNA damage

Many *in vivo* studies have described chemoprevention using vanadium-supplemented drinking water in chemically-induced models of breast, colon and liver cancer (Ray et al., 2007, Chakraborty et al., 2006b, Samanta et al., 2008b, Ray et al., 2005). In most cases, these studies concluded that reduced tumour incidence was due to up-regulation of drug metabolising enzymes, protection from DNA damage, and induction of the p53 response (Bishayee et al., 2010) (**Table 1.3**). Additionally, it has been shown that vanadium-derived compounds can inhibit tumour growth and progression using xenograft models of breast cancer, hepatocellular carcinoma, glioblastoma and leukaemia (Scrivens et al., 2003, D'Cruz and Uckun, 2002, Wu et al., 2014, Köpf-Maier et al., 1981). The mechanisms driving these anti-cancer activities are not fully described. However, some studies explicitly implicate vanadate-induced PTP inhibition, and oxidative damage, which itself may contribute to PTP inhibition (Scrivens et al., 2003, D'Cruz and Uckun, 2002, Narla et al., 2001).

A plethora of studies using cell culture tumour models for various cancers have corroborated the anti-cancer activity of vanadium, and in some cases have begun to identify vanadium effectors (**Table 1.4**). The wide range of vanadium-induced cellular effects and proposed mechanisms highlights that vanadium can inhibit multiple cancer phenotypes due to its broad activity. This includes inhibition of PTPs, directly or as a consequence of ROS production, thus affecting several key cancer related signalling pathways. In many of the studies detailed in **Table 1.4**, reduced proliferation and increased apoptosis is

reported following treatment with various vanadium compounds. In a study published by Ajeawung et al. (2013), bis(peroxido)oxidovanadate (V) (Bpv(pic)) was able to reduce proliferation, induce apoptosis, and inhibit migration in paediatric glioma cells, by inhibiting the activity and expression of specific PTPs involved in these processes. Wu et al. (2016a) reported reduced proliferation caused by G2/M cell cycle arrest in pancreatic cells treated with bis(acetylacetonato)-oxidovanadium(IV). They concluded that these effects were dependent on ROS-mediated ERK pathway activation. In contrast, as will be described in more detail in **Chapter 4**, previous publications from our group have shown that BMOV induces cytotoxicity and/or differentiation in neuroblastoma cell lines, most likely driven at least in part by PTP inhibition, rather than by increased ROS. This oxidovanadium-induced cytotoxicity could be greatly enhanced by combining BMOV with the glutathione suppressor buthionine sulphoximine (BSO) (Clark et al., 2013, Clark et al., 2015). Vanadium has also been shown to reduce the metastatic potential of cancer cells. For example, a vanadium(V)-peroxido-betaine complex was shown to inhibit TGFβ-mediated epithelial-mesenchymal transition, thus reducing tumour cell migration (Petanidis et al., 2016).

Clearly there is a large bank of preclinical data that supports anti-cancer activities of vanadium-based compounds (Evangelou, 2002, Crans et al., 2018). Many of these studies have not explored the cellular mechanisms driving these activities, and in particular do not implicate PTP inhibition explicitly. However, given the expansive role that PTPs play in intracellular signalling pathways related to cancer, it is likely that many of these effects are in fact driven by PTP inhibition, both directly by competitive inhibition by vanadate, and via ROS-driven active site cysteine oxidation.

1.3.7. Non-PTP-directed vanadium activity

Vanadium compounds also have intracellular activities distinct from PTP-inhibition that may contribute to their anti-cancer efficacy. As discussed in **Section 1.3.4.**, the ligand molecules used to coordinate vanadium may affect cancer phenotypes (Levina and Lay, 2017). However, vanadium itself is also associated with non-PTP related activities (**Figure 1.11**), these may be

beneficial in cancer treatment, but they may also be a source of off-target toxicity *in vivo*.

Vanadate is able to inhibit PTPs in part by mimicking phosphate and competing for enzyme active site binding. Thus, vanadate can also interact with and inhibit other phosphate-binding molecules such as ATPases, including ABC transporters (Cantley et al., 1977). The mechanism of this inhibition is likely to be distinct to that of PTPs, as vanadate has been shown to trap an ATPase enzyme intermediate that occurs after ATP binding and hydrolysis (Smith and Rayment, 1996, Sharma and Davidson, 2000, Pezza et al., 2002, Collauto et al., 2017). However, ATPases are nonetheless a class of off-target vanadate effectors that may contribute to anti-cancer efficacy. Inhibition of ABC transporters has in particular been implicated in vanadium-induced reversal of drug resistance (Evangelou, 2002). ABC transporters couple ATP hydrolysis to the movement of molecules across membranes against concentration gradients (Dahl et al., 2004, Martin et al., 2000). For example, P-glycoprotein has been shown to efflux drug molecules, and is reported to be upregulated as a mechanism of drug resistance (Eckford and Sharom, 2009, Sharom, 2011). Vanadate may inhibit P-glycoprotein by trapping an enzyme intermediate and preventing ADP release, which in turn alters enzyme conformation in such a way that prevents further substrate binding, thus reducing drug resistance (Loo and Clarke, 2002, Urbatsch et al., 1995, Shepard et al., 1998, Lugo and Sharom, 2014). Similarly, decavanadate also inhibits ATPases, such as actin-stimulated myosin ATPase and sarcoplasmic reticulum Ca^{2+} ATPase, through a distinct, allosteric, non-competitive mechanism with a binding site distinct from the ATP-binding pocket (Aureliano, 2016, Tiago et al., 2007, Fraqueza et al., 2012). Decavanadate also accumulates in the mitochondria and induces mitochondrial effects that have not been described for monomeric vanadate. These include altered mitochondrial antioxidant enzyme activities, and mitochondrial membrane depolarisation, perhaps by acting on complex III cytochrome *b* (Aureliano, 2016, Soares et al., 2007b, Soares et al., 2007c). Although some of these effects appear to be specific to decavanadate, they cannot be entirely discounted with respect to monomeric vanadium compounds since some

conversion from monomeric to polymeric vanadium species likely occurs within cells (Aureliano and Crans, 2009, Willsky et al., 1984).

As discussed previously, intracellular conversion between redox states of the vanadium ion leads to the generation of ROS (Nechay, 1984). One key consequence of these ROS is inhibition of PTPs by oxidation of active site cysteine residues (Ostman et al., 2011). However, ROS may also contribute to the cell death described in some of the *in vitro* anti-cancer studies via mechanisms that are distinct from PTP inhibition. ROS are produced within cells continuously and play important roles by acting as second messengers during signal transduction (Finkel, 2000, Herrlich and Böhmer, 2000, Gulati et al., 2001). However, at high concentrations, ROS can cause direct damage to DNA as well as other macromolecules such as lipids and proteins (Trachootham et al., 2008). ROS production, leading to p53 activation assed using a p53 luciferase reporter (PG13) and ultimately apoptosis was shown in mouse epidermal cells treated with vanadium salts (Huang et al., 2000a). Cancer cells often exist in a state of sub-lethal oxidative stress, thus even small increases in ROS may have dramatic effects on tumour cell viability (Halliwell, 2007, Engel and Evens, 2006). Indeed, this 'Achilles Heel' of tumour cells has been exploited by some conventional chemotherapies that induce oxidative stress, as well as some novel redox regulating molecules such as the glutathione inhibitor BSO (Huang et al., 2000b, Engel and Evens, 2006, Liou and Storz, 2010, Raj et al., 2011). ROS-induced cytotoxicity is thus likely to contribute to the anti-cancer efficacy of certain vanadium compounds in some tumour types. Some vanadium compounds, in particular vanadocenes, can also directly complex with DNA, causing DNA damage and inhibition of RNA and DNA synthesis, likely contributing to their anti-cancer activity (Harding and Mokdsi, 2000, Köpf-Maier et al., 1983). Whilst oxidative stress as well as other vanadium effects described above may be relevant to tumour cell cytotoxicity induced by some vanadium-derived compounds, we and others suggest that PTP-inhibition is responsible for at least some of this cytotoxicity (Clark et al., 2013, Clark et al., 2015, Evangelou, 2002, Rehder, 2012). In particular given the vital role that this enzyme family plays in cancer cell signalling.

1.3.8. Vanadium toxicity

When administered orally, vanadium is absorbed from the GI tract into the bloodstream. Once in the bloodstream, many vanadium compounds undergo ligand exchange reactions that transfer the vanadium ion to other species including metabolites such as lactate and citrate, and proteins, predominantly transferrin (Rehder, 2012, Rehder, 2013). Vanadium can then enter cells of various tissues from the bloodstream via multiple routes depending on its ligation and therefore redox state. These include passive diffusion for vanadate, active transport through anion channels for vanadyl, and possibly endocytosis when bound to transferrin (Yang et al., 2003, Levina and Lay, 2017, Korbecki et al., 2015). Unabsorbed vanadium exits the body in faeces, whereas absorbed vanadium is eventually cleared in urine and from hair and skin loss. A study using ^{48}V radiolabelled vanadium tracers in rats showed that vanadium accumulates differentially in specific tissues with a relative abundance as follows; bone > kidney, liver > blood > muscle > brain (Setyawati et al., 1998, Dąbroś et al., 2011). A small proportion of ingested vanadium accumulates in these tissues for long periods of time (Thompson and Orvig, 2006, Domingo, 2000). Long-term accumulation occurs in particular in bone, where vanadate can replace phosphate in the hydroxyapatite lattice of bone mineral, however it is not yet clear whether this has an effect on bone quality (Fukui et al., 1999, Facchini et al., 2006). Nonetheless, this tissue accumulation presents a potential safety concern in administering oxidovanadium as a therapeutic. This is potentially a more significant concern in the diabetes field, where patients would be treated with vanadium over very long periods, but perhaps less of an issue for the short-term treatment of cancer patients.

The International Agency for Research on Cancer (IARC) has not classified vanadium as a carcinogen; however, there have been a small number of reports of vanadium-induced tumourigenesis, potentially due to increased production of ROS (Evangelou, 2002). A study by Ress et al. (2003) reported increased alveolar/bronchiolar neoplasms in rodents associated with long-term exposure to airborne vanadium pentoxide. This study involved two years of exposure to vanadium pentoxide, so again is perhaps not applicable to

short-term vanadium treatment (Ress et al., 2003). Generally, however, very few adverse effects have been reported in preclinical animal models and only GI distress, weight loss and anorexia in human clinical trials (Thompson and Orvig, 2006, Thompson et al., 2009). Systemic toxicities associated with vanadium itself, as well as ligand molecules used in more complex oxidovanadium complexes, have nevertheless been a major factor discouraging the systemic use of vanadium-based compounds in humans so far.

1.4. Project aims

Based on the critical and seemingly ubiquitous role that phosphotyrosine signalling plays in the initiation and progression of human cancer, and in particular the growing number of PTPs that are being implicated as drivers of tumourigenesis, we hypothesised that there are specific PTPs that promote growth and survival in neuroblastoma. Targeting PTPs would therefore represent an attractive therapeutic avenue for the treatment of neuroblastoma (**Figure 1.12**). Three such enzymes, SHP2, DUSP26 and PTPN2, have already been highlighted (Zhang, 2017, Shi et al., 2015, Mitra et al., 2011). We have therefore sought to identify further examples of PTPs that may be useful therapeutic targets for neuroblastoma, using genomic approaches (**Chapter 3**). Furthermore, vanadium is a pan-inhibitor of PTPs (Gordon, 1991) and as discussed above, the anti-cancer efficacy of vanadium-derived compounds has been demonstrated *in vitro* and *in vivo* for many tumour types (**Table 1.3 and Table 1.4**). Our group have previously reported that the oxidovanadium derivative BMOV induces cytotoxicity and/or differentiation in neuroblastoma cell lines (Clark et al., 2013, Clark et al., 2015). Pan-inhibition of PTPs using oxidovanadium derivatives is therefore a candidate therapeutic strategy for neuroblastoma. However, there are significant concerns regarding the safety of vanadium use in man, including the effects of ligands, non-PTP inhibiting functions of vanadium, and tissue accumulation. In **Chapter 4** and **Chapter 5** of this project I have attempted to better harness oxidovanadium efficacy by circumventing the concerns regarding off-target toxicities. First, transcriptomics was used to begin to characterise the molecular pathways that

drive oxidovanadium activity in neuroblastoma cells (**Chapter 4**). We hoped this may lead to the identification of critical BMOV effector molecules or pathways, PTP-related or not, that could themselves be targeted therapeutically, potentially with fewer safety concerns. We also asked how the BMOV-induced transcriptional response was altered when BMOV was combined with BSO-mediated glutathione blockage, which enhances BMOV-induced cytotoxicity (Clark et al., 2015). Second, I have explored the potential of nanoparticle delivery of oxidovanadium (**Chapter 5**). A hydrophobic complex of oxidovanadium was packaged into liposomes and delivered to neuroblastoma cells. As will be discussed, this liposomal delivery may allow more efficient and safer delivery of vanadate to tumour cells *in vivo*.

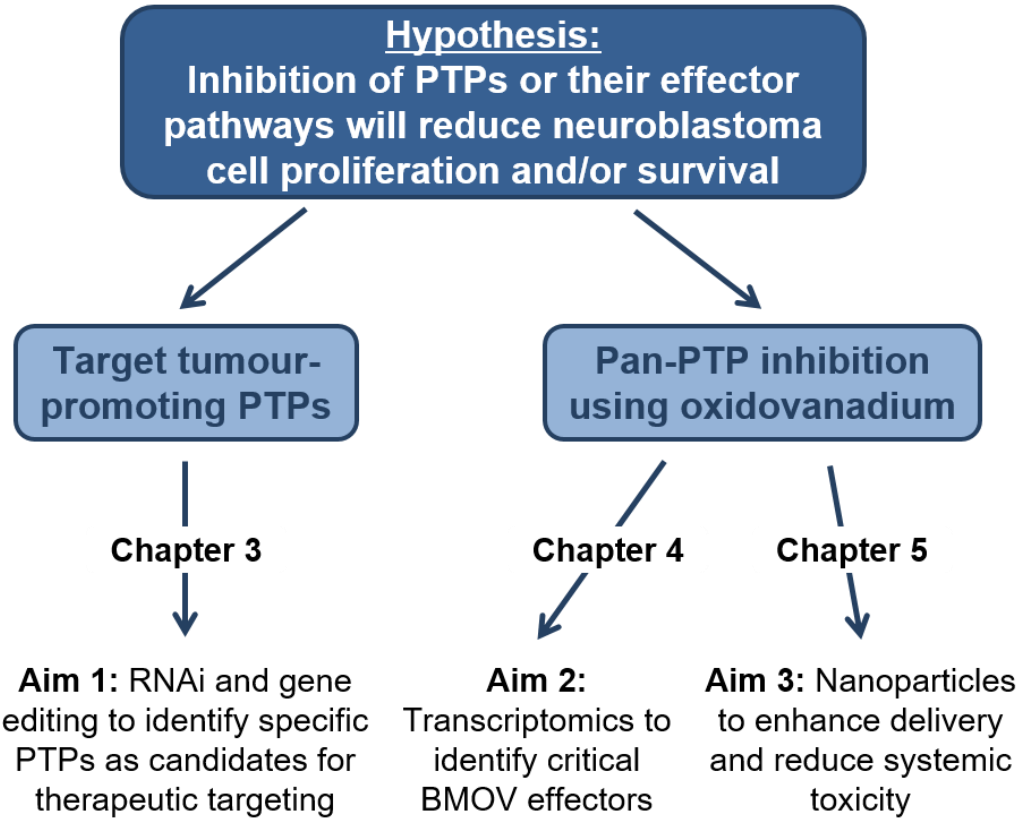

Figure 1.12 – Project aims
We hypothesise that there are PTPs that promote cell growth and survival in neuroblastoma, and that their direct or indirect targeting may be a useful therapeutic strategy. ***Chapter 3*** *describes the use of RNAi and gene editing to identify specific PTPs that are required for neuroblastoma cell survival, revealing potential therapeutic targets.* ***Chapters 4*** *and* ***5*** *address the use of oxidovanadium for pan-PTP inhibition in neuroblastoma. In* ***Chapter 4*** *transcriptomics was used to characterise the potential mechanisms that drive BMOV-induced cytotoxicity, in particular in combination with glutathione suppression. Whilst in* ***Chapter 5*** *I describe the first use of nanotechnology for the cellular delivery of a hydrophobic oxidovanadium compound using liposomes.*

Chapter 2. Materials & Methods

2.1. Cell culture

2.1.1. Cell lines

A range of established, patient-derived cell lines were used throughout this project, including those from neuroblastoma and non-neuroblastoma tissues (**Table 2.1**). Cells were sent to AATC for short-tandem repeat (STR) profiling to authenticate their identity. The neuroblastoma cell lines have diverse genetic makeup (**Table 2.2**), morphologies and growth rates and were used in an attempt to represent the highly heterogeneous nature of neuroblastoma tumours (Thiele, 1998). All cell lines were grown as monolayer cultures, maintained at 37°C and 5% CO_2. Cells were cultured under distinct media as listed in **Table 2.1.**, media components are outlined below.

Table 2.1 – Cell lines and culture conditions
Details of cell lines used in this project, including culture medium.

Cell line	Brief description	Culture medium
IMR32	Neuroblastoma – abdominal mass	RPMI
KELLY	Neuroblastoma	RPMI
LAN5	Neuroblastoma – bone marrow metastasis	RPMI
SK-N-SH	Neuroblastoma – bone marrow metastasis	MEM
SK-N-AS	Neuroblastoma – bone marrow metastasis	RPMI
SK-N-DZ	Neuroblastoma – bone marrow metastasis	RPMI
SK-N-BE(2)	Neuroblastoma – bone marrow metastasis	MEM
LAN1	Neuroblastoma – bone marrow metastasis	RPMI
HEK-293T	Human embryonic kidney + SV40 large T antigen	MEM
COS7	Monkey kidney - fibroblast-like + SV40 large T antigen	RPMI
MEFs	Mouse embryonic fibroblasts	MEM
IMCD3	Mouse kidney + SV40 large T antigen	MEM
Res259	Paediatric low-grade glioma	DMEM/F12
Res186	Paediatric low-grade glioma	DMEM/F12
SF188	Paediatric glioblastoma	DMEM/F12

Roswell Park Memorial Institute (**RPMI**) 1640 + GlutaMAX^{TM} (Gibco):

- 10% foetal bovine serum (FBS) (Gibco)
- 100 U/ml penicillin and 100 µg/ml streptomycin (1% v/v P/S - Invitrogen, California, USA)
- 25 mM HEPES (4-(2-hydroxyethyl)-1-piperazineethanesulfonic acid), pH 7 (Sigma-Aldrich, Dorset, UK)

Eagle's Minimum Essential Medium Eagle (**MEM**) (Gibco):

- 10% FBS
- 1% P/S
- 2 mM L-glutamine (Invitrogen, California, USA)

Dulbecco's Modified Eagle Medium/ Nutrient Mixture F-12 (**DMEM/F12**) + GlutaMAXTM (Gibco):

- 10% FBS
- 1% P/S
- 25 mM HEPES, pH 7

For the inducible CRISPR/Cas9 work (**Section 3.2.5.**), cells were cultured in RPMI 1640 + GlutaMAX^{TM} (Gibco), supplemented with 10% tetracycline-free FBS (Takara, Japan) and 25 mM HEPES, pH7.

Table 2.2 – Neuroblastoma cell line genetic information
Common cytogenetic abnormalities, including deletions in chromosomes 1 and 11, as well as MYCN amplification status for established neuroblastoma cell lines used in this project. See Thiele (1998) for further details.

Cell line	MYCN amplified	1p36 deletion	11q deletion
IMR32	Yes	Yes	Yes
KELLY	Yes	Yes	Yes
LAN5	Yes	Yes	No
SK-N-SH	No	No	Yes
SK-N-AS	No	Yes	Yes
SK-N-DZ	Yes	No	Yes
SK-N-BE(2)	Yes	Yes	Yes
LAN1	Yes	Yes	-

2.1.2. Cell passage

Cells were routinely passaged upon reaching 70-90% confluency. Briefly, cells were washed with PBS (phosphate buffered saline, Gibco) and detached by incubation in trypsin-EDTA (Sigma-Aldrich, Dorset, UK). Once detached, cells were resuspended in culture medium and centrifuged at 1000 rpm for 5 minutes. Cell pellets were resuspended in fresh medium, and re-plated at low density. When seeding into multiwell plates (Corning® Costar® TC-Treated multiple well plates and Nunc™ MicroWell™ 96-Well microplates) for experiments, cell number was calculated by pipetting 10 µl cell suspension into a haemocytometer (Bright-Line™ Hemacytometer) and counting cells in the central field of view (10^{-4} mm^3).

2.1.3. Chemical treatment

Throughout this project, cells were treated with various chemicals, including small molecule inhibitors and antibiotics (**Table 2.3**). Generally, and unless stated otherwise, cells were seeded into multiwell plates and treated the following day.

Table 2.3 – Chemicals
Details of chemicals used in this project, including source, stock solutions and storage, and working concentrations. BMOV, bis(maltolato)oxovanadium(IV); BSO, L-Buthionine-(S,R)-sulfoximine; dH_2O, distilled water; ETOH, ethanol; DMSO, dimethyl sulfoxide.

Chemical	Source	Stock solution	Working concentration
BMOV	ORGANICA Feinchemie GmbH Wolfen, Germany	10 mM in dH_2O (made fresh)	0.1 - 80 µM
BSO	ACROS Organics, Belgium	10 mM in dH_2O (made fresh)	10 – 400 µM
AL1	Dr. Ari Lehtonen, University of Turku, Finland	10 mM in ETOH (made fresh)	0.15 - 10 µM
AL2	Dr. Ari Lehtonen, University of Turku, Finland	1 mM in ETOH (made fresh)	0.15 - 10 µM
AL3	Dr. Ari Lehtonen, University of Turku, Finland	0.5 mM in ETOH (made fresh)	0.1 - 10 µM
AL4	Dr. Ari Lehtonen, University of Turku, Finland	1 mM in ETOH (made fresh)	0.15 - 10 µM
L1	Dr. Ari Lehtonen, University of Turku, Finland	1 mM in ETOH (made fresh)	5 - 10 µM
L2	Dr. Ari Lehtonen, University of Turku, Finland	1 mM in ETOH (made fresh)	5 - 10 µM
L3	Dr. Ari Lehtonen, University of Turku, Finland	0.5 mM in ETOH (made fresh)	5 µM
L4	Dr. Ari Lehtonen, University of Turku, Finland	1 mM in ETOH (made fresh)	5 - 10 µM
M1	Dr. Ari Lehtonen, University of Turku, Finland	2.5 mM in ETOH (made fresh)	10 µM
M2	Dr. Ari Lehtonen, University of Turku, Finland	5 mM in ETOH (made fresh)	10 µM
MK-2206	Cayman Chemical, Michigan, USA	20 mM in DMSO (-20ºC)	0.6 – 20 µM
U0126	Cell Guidance Systems, Cambridge, UK	20 mM in DMSO (-20ºC)	0.6 – 20 µM
U0124	Merck Millipore, Massachusetts, USA	20 mM in DMSO (-20ºC)	0.6 – 20 µM
Forskolin	Cell Guidance Systems, Cambridge, UK	100 mM in DMSO (-20ºC)	100 µM
Puromycin	Gibco™	1 mg/ml in dH_2O (-20ºC)	1 µg/ml
Doxycycline	Sigma-Aldrich, Dorset, UK	1 mg/ml in dH_2O (-20ºC)	1 µg/ml

2.1.4. Clonal expansion

Single cell clonal expansion was used to isolate new cell populations from mixed populations. Cells were counted and seeded into 96-well tissue culture plates at 1 cell in 100 µl media per well. After an initial growth period of 2 weeks, each well was assessed for cell growth and replenished with fresh media or transferred into larger well plates accordingly. Gradually single cell-derived cultures were expanded up to t75 flasks, at which point stocks were frozen down in normal culture medium with 10% DMSO.

During the CRISPR/Cas9 experiments (**Section 3.2.4.**), clonal expansion was carried out following fluorescence-activated cell sorting (FACS). For this, cells were trypsinised, centrifuged at 1000 rpm for 5 minutes, and then resuspended in OptiMEM (Gibco). Cells were then sorted for green fluorescence and GFP-positive cells were seeded in 96-well plates at one cell per well using a MoFlo XDP Sorter. Cells were seeded in 50% fresh media: 50% conditioned media (conditioned in 70% confluent cells for 48 hours, then filtered through a 0.22 µm syringe filter) to aid recovery. After sorting, 96-well plates were centrifuged at 200 xg for 1 minute to encourage cells to adhere to the bottom of the wells, then returned to normal incubation. As above, single cell cultures were closely monitored and transferred into larger wells as they became confluent.

2.2. Cell-based assays

2.2.1. Plasmid transfection

For overexpression of CDC14B and CRISPR/Cas9 machinery plasmids, transfection into mammalian cells was achieved using lipofection. Cells were seeded into multiwell plates and transfected the following day using Lipofectamine 2000 (Invitrogen, California, USA). Lipofectamine 2000 and plasmid DNA were diluted in OptiMEM (Gibco) and incubated at room temperature for 10 minutes, before dropwise delivery to cells. For small scale 96-well assays, 0.4 µl Lipofectamine 2000 and 100 ng plasmid DNA were used per well. For larger scale assays, cells were seeded into 12 well plates and transfected with 3 µl Lipofectamine 2000 and 1 µg plasmid DNA.

2.2.2. SiRNA-mediated gene knockdown

ON-TARGETplus siRNAs (small interfering RNAs) (Dharmacon, Colorado, USA) were used to knockdown specific gene expression. For PTP genes, 4 individual siRNAs were obtained per gene, and for RNAseq target genes, a pool of 4 siRNAs was used to target each gene (**Table 2.4**). Using a pool of 4 distinct siRNAs reduces the possibility of observing off-target gene knockdown events. A Dharmacon non-targeting siRNA pool (scrambled – SCR) was used as a negative control, and a KIF11-targeting siRNA was used as a positive control (Invitrogen - 5'-UUCAGUUCUUACCAGUGUUGAUGGG). KIF11 knockdown halts cells in the final stages of mitosis, resulting in distinctive round cells (Eschenbrenner et al., 2011). All siRNAs were resuspended in siRNA buffer (60 mM KCl, 6 mM HEPES-pH 7.5, 200 µM $MgCl_2$ - Dharmacon, Colorado, USA) and stored in aliquots at -20°C to prevent excessive freeze-thaw cycling.

For gene knockdown, cells were seeded into 96-well plates and transfected in triplicate with siRNAs the following day by lipofection using Lipofectamine RNAiMAX (Invitrogen, California, USA). Lipofectamine RNAiMAX and siRNAs were diluted in OptiMEM (Gibco) and incubated at room temperature for 5 minutes before dropwise delivery to cells. In early cell viability experiments, 6 pmol siRNA and 0.3 µl Lipofectamine RNAiMAX were used per well. However, it was later found that much less siRNA (0.5 pmol per well) could be used to achieve the same on-target knockdown, with potentially fewer off-target events. For larger scale experiments where cells were seeded into 12 well plates, 20 pmol siRNA and 3 µl Lipofectamine RNAiMAX were used per well.

Table 2.4 – ON-TARGETplus siRNA sequences
ON-TARGETplus siRNA obtained from Dharmacon (Colorado, USA). Four siRNAs are listed for each target gene, these were ordered as pools for all genes except PTPRN, CDC14B, MTMR12, ACP1, which were ordered as individual oligos.

siRNA	Sequence (5' – 3')	siRNA	Sequence (5' – 3')
PTPRN_06	GCCCACGGCUGUCUAUUUG	**TUBGCP6_17**	ACAUAUACGUCUGCGGAAA
PTPRN_07	GUAAAUGUUGGAGCUGAUA	**TUBGCP6_18**	GAAGGGACGCUUUCGACAA
PTPRN_08	GGACAGGUCUGGCUUGGCA	**TUBGCP6_19**	GGGAGAAACGUUCCGUACA
PTPRN_09	CAACAAGCAGGGCUGGUGA	**TUBGCP6_20**	UCAGAGACGCUUAUGGCGA
CDC14B_10	GCUACAUCAUGAAGCAUUA	**TLCD1_09**	GGGUAUUUCAUCCACGAUA
CDC14B_11	CGAAAUCAAUGGAGUGACA	**TLCD1_10**	CCCAUUUCUUCUUGCGUUA

Table 2.4 continued

CDC14B_12	GUACAUUAUUUCAGCAUAG	**TLCD1_11**	GCUAUUUGCUCGUUUGCUU
CDC14B_13	GUUGAUGACAUUUCCAUAA	**TLCD1_12**	CUACCGGGUUAACAAGUAU
MTMR12_09	CUAAACUGCUUAAACGAUU	**ANKRD39_17**	GUAGAUUUGGUGUGGCUAA
MTMR12_10	GGUCAUGGCAUACCAAUAU	**ANKRD39_18**	AGGCCAUCCGGGACCGAAA
MTMR12_11	CAAGAACCAUACCGUAAUG	**ANKRD39_19**	CCAGGGUGGUGGAUGACGA
MTMR12_12	GCCCAGCGCUACCUACGUU	**ANKRD39_20**	CUGGACAGAUGAUCAUAUU
ACP1_05	GGAUGAAAGCAAUCUGAGA	**SEPW1_09**	CGUUUAUUGUGGCGCUUGA
ACP1_06	GGAAUGACUCUGACUUUGA	**SEPW1_10**	ACUCUAAGAAGAAAGGCGA
ACP1_07	GGAAACUUGUAACCGAUCA	**SEPW1_11**	CGCCUUGGCUCAGGGCUAA
ACP1_08	UGAACUACUUGGGAGCUAU	**SEPW1_12**	CCACCGGGUUCUUUGAAGU
LPCAT3_09	GGGUUCUGCAGUCGGGUUU	**LYSMD1_17**	GGUAAGGGAACCUCAGUAA
LPCAT3_10	CCACCGGCAACUACGAUAU	**LYSMD1_18**	GGAUGAGGCAAUCGGUGAU
LPCAT3_11	GACAAAUGGCUUAAGGUGU	**LYSMD1_19**	CUGCAUAUUUAUUUGCGAU
LPCAT3_12	CUACUUUGACGGAGGGAAA	**LYSMD1_20**	GAGACCUGUUCAAUGGUUU
PTGES2_09	GGCUCAUGCUCAACGAGAA	**COX20_09**	GAGCAUAGAAGUCAAUGUA
PTGES2_10	GAGAUGAAGUGGCGGCAGU	**COX20_10**	UGUUACAUAUAGUGGACUU
PTGES2_11	CAGAGGGAAGGCAGCGGAA	**COX20_11**	GGGAAGUAUGCAGGGUUUA
PTGES2_12	GCUCAGGGAUGUUAGGGAC	**COX20_12**	CCUUGUAGUAGUAAGUAUA
DCTN1_05	CUGGAGCGCUGUAUCGUAA	**MRPL30_17**	GGAGAAGUAAGAAUUGUAA
DCTN1_06	GAAGAUCGAGAGACAGUUA	**MRPL30_18**	CAAUAUCCAUCCUGUCGUA
DCTN1_07	GCUCAUGCCUCGUCUCAUU	**MRPL30_19**	GAGAACAUGUCUAACACGU
DCTN1_08	CGAGCUCACUACUGACUUA	**MRPL30_20**	GUACAGAUUGGAUUCGUCA
SGSH_06	ACAAGGACCUCCGUCAUUA	**EMG1_17**	AGGGAAGACAUAUGAGCUA
SGSH_07	CCGCAUGGACCAAGGAGUU	**EMG1_18**	AAACAAGAUCGGAGGCCGU
SGSH_08	GAAUUAAGCUGCUCGUCCG	**EMG1_19**	CCUCAUGGUUCAACUUUUA
SGSH_09	GCACAGGCAUCAUCGGGAA	**EMG1_20**	GUUGAAGAAUGGACGGGAC
TMEM240_17	GGAACAUGGUACACGUGAA	**SHPK_05**	GAAAUAUCGCCCAGAGUUC
TMEM240_18	GCGCGAACACCAUGAUCUU	**SHPK_06**	GAGCAGGAUGUGAGUAGAA
TMEM240_19	UGACGGACAGUGUGACCAA	**SHPK_07**	GAAGAAUCCACUGUGUAUU
TMEM240_20	UCGCGUGCUUGAUGGACAU	**SHPK_08**	GCCGAAGUCUCAUCUCAGU
ITFG2_18	UCAGCCAGGUUGUGCGUAU	**CCDC61_14**	UGAAGCAGCAGCAGCGGAA
ITFG2_19	CAAACAAGGCCACGGCACU	**CCDC61_15**	CGACUGGACAUGCGGUCAU
ITFG2_20	UACCAAAGCAGCCGGGUCA	**CCDC61_16**	AGCUCAACUCCAAGCGCUA
ITFG2_21	ACGAGACACUAAUCGGAGA	**CCDC61_18**	CGAAAUAGACGCACGCCUG
GLMP_17	GGACAGGGCUAUUGAUAAG	**CALHM2_17**	GCGUCUACUUGUACCGUGA
GLMP_18	GUACCAGUCCAUAAAUUAA	**CALHM2_18**	GGAACUACCUGUACGGGCU
GLMP_19	GCACCAACGUGUCCGAUAC	**CALHM2_19**	ACAAGUGGGCCCAGGGUCU
GLMP_20	GCCUGAUGGUGCUCCCUAA	**CALHM2_20**	UCGCAGAGAACUUCCGCUU
FAXDC2_09	GUAGAGGGAAGGUCGGCUU	**LRRC75B_25**	CCAGAAAUCCAGUGUAAAU
FAXDC2_10	AGAAAGAACAGAUACGGUU	**LRRC75B_26**	CGACACAGGACGUGCAACA
FAXDC2_11	CAGGAGUUAGCUUAAGAAA	**LRRC75B_27**	CAUGAUAGUGGGCGAUGAA
FAXDC2_12	GGUCUCAAUUCAUGACAUA	**LRRC75B_28**	CGGACAAGAUCUGCCGACA
SARS2_09	CAGAGACAAACACGGGACA	**PDE2A_05**	GGAAAGUCCGGGAGGCUAU
SARS2_17	CCUGGAAAUUGGCGAGAAA	**PDE2A_06**	CGACGGCCUUCUCCAUCUA
SARS2_18	GGAACCUCCUGUACGAGUA	**PDE2A_07**	CCCAUUCUCUCCUAUACAA
SARS2_19	ACUUCCGGGUCCUGGAUAU	**PDE2A_08**	GGCCAUGGUUCAGCAAGUU

IL17RC_05	CUACGCACCUGCAGACAGA	**Scrambled_01**	UGGUUUACAUGUCGACUAA
IL17RC_06	UCAGGACGCUACCCACUGC	**Scrambled_02**	UGGUUUACAUGUUGUGUGA
IL17RC_07	GUACGAAUCUGGUCCUAUA	**Scrambled_03**	UGGUUUACAUGUUUUCUGA
IL17RC_08	GACCGCAGAUCAUUACCUU	**Scrambled_04**	UGGUUUACAUGUUUUCCUA
G6PC3_05	GGAAAUGGCCAGAAGAUAG	**GAPDH_01**	GUCAACGGAUUUGGUCGUA
G6PC3_06	GCACCAGCCUCAUCUAUUG		
G6PC3_07	ACACUGGGCCUGGAUCUUU		
G6PC3_08	GCGGUUGGCUUGUCGCGAA		

2.2.3. CDC14B rescue co-transfections

The CDC14B siRNA rescue experiments involved co-transfecting siRNAs with CDC14B expression plasmid DNA (**Section 2.6.1.**), both in small and large-scale experiments. In both cases, cells were transfected using Lipofectamine 2000 (Invitrogen, California, USA) 24 hours after seeding. For 96-well assays, 0.4 µl Lipofectamine 2000, 100 ng plasmid DNA and 1 pmol siRNA were diluted in OptiMEM (Gibco) and incubated at room temperature for 10 minutes before being added dropwise to cells. For larger scale experiments, cells were seeded into 12 well plates and transfected with 3 µl Lipofectamine 2000, 1 µg plasmid DNA and 20 pmol siRNA. Co-transfection was confirmed using a GFP reporter plasmid and KIF11-targeting siRNA, which resulted in rounded up green fluorescent cells.

2.2.4. Monochlorobimane (MCB) assay

The cell permeable dye monochlorobimane (MCB) can be used to measure levels of reduced glutathione in live cells (Durand and Olive, 1983, Fernández-Checa and Kaplowitz, 1990). For this assay, cells were seeded into black-walled 96-well plates (Corning® Costar® TC-Treated 96-well assay plates) and treated with chemicals the following day in triplicate. At the end point of the assay, all media was removed and 100 µl 50 µM MCB (Sigma-Aldrich, Dorset, UK) diluted in PBS was added to each well. Fluorescence was read immediately and after 75 minutes using a FLUOstar OPTIMA plate reader (BMG LabTech, UK) (absorbance 360 nm and emission 460 nm). MCB binds with high affinity to reduced glutathione, and once bound emits blue fluorescence. Therefore, the change in fluorescence between the initial and final readings could be used as a measure of the relative levels of reduced glutathione in cells following chemical treatment.

2.2.5. Neurite length assay

Neuritogenesis is associated with cellular differentiation, where increased neurite length is characteristic of differentiated cells (da Silva and Dotti, 2002). In this project, neurite length was used as a measure of differentiation in SK-N-SH neuroblastoma cells, as these cells have neurite like extensions that can be measured. For neurite length assays, SK-N-SH cells were seeded at low density (5000 cells per well) into 12 well plates and treated with various chemicals the next day. Following 5 to 6 days of chemical treatment, phase-contrast microscopy was performed to capture representative images of cells. Images were then randomised to blind analysis. The length of the neurites in each image was measured using the NeuronJ plugin on ImageJ (Meijering et al., 2004) (**Figure 2.1**). Neurites were only measured when they were at least as long as the diameter of the cell body, and branches were discounted. Ten fields of view were captured per well per chemical treatment. The average neurite length per field of view, and subsequently per treatment was recorded.

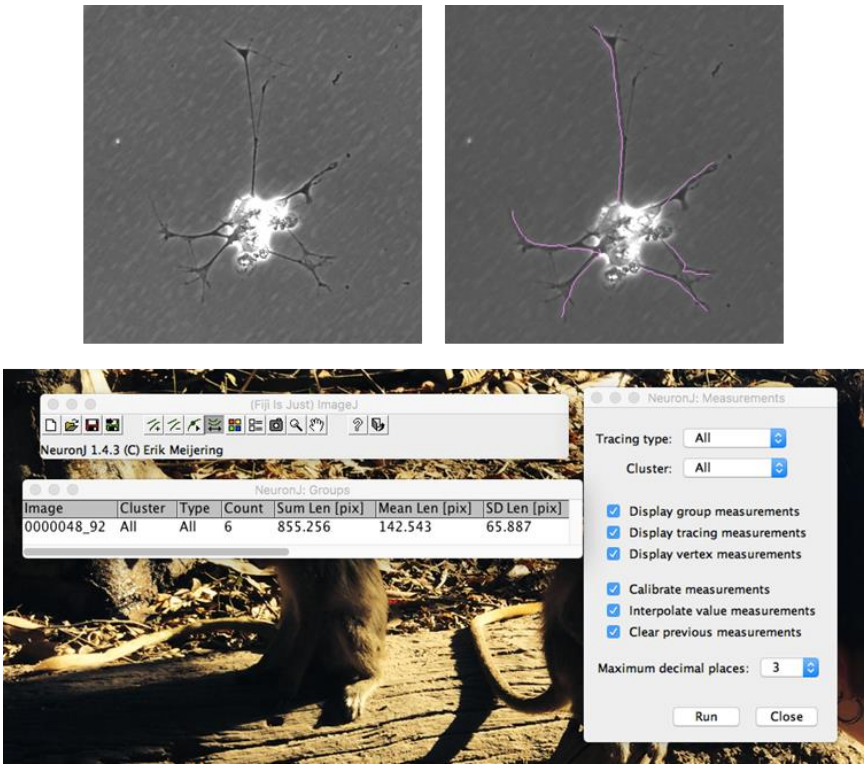

Figure 2.1 – Neurite length assay
Phase-contrast microscopy images were captured following chemical treatment and imported into ImageJ. The NeuronJ plugin (Meijering et al., 2004) was used to trace neurites and to quantify their length. Mean average neurite length in pixels was recorded.

2.2.6. Microscopy

All phase-contrast and fluorescence microscopy on tissue culture plastic was performed using an Olympus IX71 inverted microscope with a Hamamatsu Orca R2 monochrome camera. Immunofluorescence (IF) microscopy using cells on glass coverslips was performed using a Leica upright manual 3 colour fluorescence microscope with a Coolsnap camera. Image analysis was carried out using ImageJ (Schneider et al., 2012, Schindelin et al., 2015) and Fiji (Schindelin et al., 2012).

2.3. Cell viability assays

2.3.1. Cell counting kit 8 (CCK8)

The CCK-8 reagent (Sigma-Aldrich, Dorset, UK) contains WST-8, which is a tetrazolium salt that is reduced by dehydrogenases to produce formazan (Ishiyama et al., 1993). Formazan absorbs light at 460 nm, thus absorbance at 460 nm is directly proportional to cell density when the CCK-8 reagent is added to cells in culture. For CCK-8 cell viability assays, cells were seeded into 96-well plates and treated with various chemicals the following day in triplicate. After 3 to 6 days, final cell density was assessed by adding CCK-8 reagent diluted in culture medium to a final concentration of 10%. Plates were returned to the incubator for approximately 3 hours, after which absorbance at 460 nm was measured using a FLUOstar OPTIMA plate reader (BMG LabTech, UK).

2.3.2. Resazurin

Resazurin (R&D Systems, Minnesota, USA) is a redox-sensitive dye that changes from blue and non-fluorescent to pink and highly fluorescent when reduced to resorufin by reductases such as intracellular dehydrogenases, similar to CCK-8 (O'Brien et al., 2000). This florescent signal can be quantified as a relative measure of aerobic respiration and therefore cell viability. As for the CCK-8 assay, cells were seeded and treated in 96-well plates in triplicate. Cell density was quantified after 3 to 6 days by adding resazurin diluted in culture medium to a final concentration of 15 µg/ml (0.15 mg/ml stock solution

in PBS). Plates were returned to the incubator for around 4 hours until a colour change from blue to pink in wells with high cell density could be observed. Fluorescence was measured using 540 nm excitation and 590 nm emission wavelengths on a FLUOstar OPTIMA plate reader (BMG LabTech, UK).

2.3.3. ATPlite 1 step

The ATPlite 1step reagent (PerkinElmer, Massachusetts, USA) quantifies relative ATP abundance by coupling ATP to luciferase luminescence. Relative ATP levels are reflective of live cells; therefore, this assay can be used as a measure of cell viability (Cree and Andreotti, 1997). For this assay, cells were seeded into white walled 96-well cell culture plates (Grenier Bio-One, Austria) to prevent crossover of luminescent signal between wells. Various chemical treatments were added the following day in triplicate and cells were cultured for a further 3 to 6 days, after which reconstituted ATPlite was added to culture medium at a ratio of 1:1. Luminescence was immediately measured using a FLUOstar OPTIMA plate reader (BMG LabTech, UK).

2.3.4. Crystal violet staining

Crystal violet staining was performed in various well sizes. Where 96-well plates were used, triplicates were performed for each condition. At the end point of experiments, media was removed and cells were fixed in 4% paraformaldehyde (PFA) at room temperature for 10 minutes. Cells were then stained with crystal violet (1% crystal violet; 15% methanol) for 1 hour at room temperature, washed in distilled water, and air dried overnight. Photos of the stained wells were then taken. Where cell density was quantified, crystal violet stain was solubilised in 20% acetic acid (v/v) by shaking at room temperature for several hours, and absorbance at 595nm was measured using a FLUOstar OPTIMA plate reader (BMG LabTech, UK).

2.3.5. Nuclei counting

In this assay, Hoechst 33342 (Cayman Chemical, Michigan, USA) was used to fluorescently label nuclei (Latt and Stetten, 1976), which were then counted as a measure of cell number following chemical treatment. Cells were seeded

into 96-well plates and treated with various chemicals the following day in triplicate. After 3 to 6 days of chemical treatment, half of the total media volume was removed and replaced with fresh media containing 2 µg/ml Hoechst 33342 (final concentration 1 µg/ml). Plates were returned to the incubator for at least 30 minutes, before imaging for blue fluorescence. The ImageJ 'find maxima' tool was used with a tolerance of 2 to count the nuclei in each image (**Figure 2.2**). Low-power images were taken in the centre of each well and the average nuclei count across the triplicate was recorded for each condition.

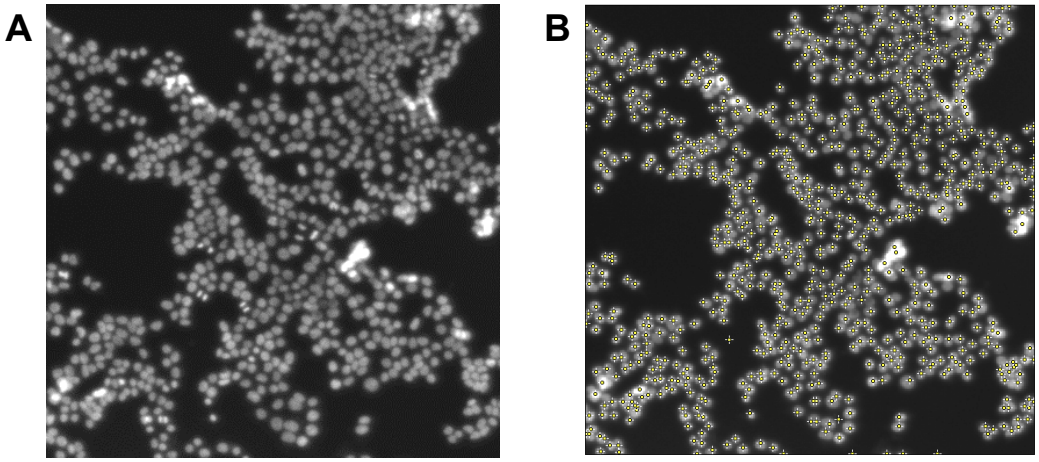

Figure 2.2 – Nuclei counting assay
A *- Cells were stained with 1 µg/ml Hoechst 33342 and low-power blue fluorescence microscopy images were taken.* ***B*** *- The find maxima tool on ImageJ with a tolerance of 2 was used to count nuclei, marking each counted nuclei with a yellow cross.*

2.4. Protein assays

2.4.1. Protein extraction

For protein extraction, monolayer cells were lysed in 50 mM Tris-base, pH 7.6; 150 mM NaCl; 1% Triton X-100; 0.02% sodium azide. 1 mM protease inhibitor cocktail (Roche, Switzerland) was added to prevent protein degradation, as well as 1 mM sodium orthovanadate and 25 mM sodium fluoride to preserve protein phosphorylation status. Cells were lysed on ice for 30 minutes, prior to centrifugation at 14,000 rpm for 15 minutes at 4°C to remove cell debris. Protein lysates were stores at -20ºC.

2.4.2. Bradford assay

Protein concentration was quantified using the Bradford reagent (Bio-Rad, California, USA). 2 µl lysate was mixed with 200 µl Bradford reagent (previously diluted 1:4 in distilled water) in a 96-well plate. Absorbance at 595 nm was measured using a FLUOstar OTIMA plate reader (BMG LabTech, UK). Known concentrations of bovine serum albumin (BSA) (from a 2 mg/ml stock solution - Bio-Rad, California, USA) diluted in lysis buffer were also analysed to generate a standard curve, from which sample protein concentrations could be extrapolated.

2.4.3. Western blotting

Protein lysates were prepared for sodium dodecyl sulfate–polyacrylamide gel electrophoresis (SDS-PAGE) by dilution in lysis buffer according to Bradford assay results, such that 5-20 µg of protein would be loaded per well. Protein loading (µg) was kept constant for each set of samples per gel, but varied between experiments. 4X sample loading buffer (25 mM Tris-HCl, pH 6.8; 60% glycerol (v/v); 8% SDS (w/v); 10% (v/v) β mercaptoethanol) was added to samples, which were then heated to 100°C for 5 minutes.

1 mm thick acrylamide gels were used for gel electrophoresis of whole cell protein lysates. Gels were cast by hand using the Mini-PROTEAN Tetra Cell casting stand and clamps (Bio-Rad, California, USA). 10% acrylamide resolving gel was prepared and cast (10% acrylamide; 375 mM Tris-Base, pH 8.8; 1% SDS (w/v); 0.0075% (v/v) ammonium persulfate (APS); 0.0012% (v/v) tetramethylethylenediamine (TEMED)), followed by 5% acrylamide stacking gel (5% acrylamide; 125 mM Tris-Base, pH 6.8; 1% SDS; 0.01 (v/v) APS; 0.0012% (v/v) TEMED). Gels were assembled into Mini-PROTEAN Tetra cell tanks (Bio-Rad), which were filled with running buffer (25 mM Tris-base; 192 mM glycine; 0.1% (w/v) SDS). 10 - 30 µl protein lysate was loaded per well, along with 7 µl Precision Plus Protein Standards (Bio-Rad). Proteins were separated based on size using gel electrophoresis at constant current of 25 milliamps per gel.

Protein was then transferred onto polyvinyldifluoride (PDVF) (Immobilon - Merck Millipore, Massachusetts, USA) using a standard wet transfer protocol. 10X transfer buffer (25 mM Tris-base; 192 mM glycine) was diluted to 1X using 20% methanol (v/v) and distilled water. Membranes were pre-soaked for 5 minutes shaking in methanol followed by transfer buffer. Transfer stacks were assembled using three pieces of transfer buffer-soaked chromatography paper, pre-soaked PDVF membrane, the SDS-PAGE gel, and more chromatography paper. Transfer stacks were placed between transfer buffer-soaked sponges in Mini Gel Holder Cassettes (Bio-Rad), and into a Mini Trans-Blot tank (Bio-Rad). Transfer was performed at constant 100V for 1 hour, after which membranes were fixed by soaking again in methanol for 1 minute. Membranes were then blocked in 10% (w/v) non-fat milk powder (Marvel) dissolved in Tris buffered saline (50 mM Tris-base, pH 7.4; 150 mM NaCl) with 0.1% (v/v) Tween-20 (TBS/T).

For immunoblotting, primary antibodies were diluted in blocking buffer with 0.05% (w/v) sodium azide (**Table 2.5**). Membranes were incubated in primary antibodies overnight at 4ºC with gentle agitation, after which they were washed in TBS/T three times for 10 minutes shaking at room temperature. Horseradish peroxidase (HPR)-conjugated secondary antibodies were used, including anti-rabbit and anti-mouse raised in goat, and anti-goat raised in rabbit (Agilent, Dako, California, USA). Secondary antibodies were diluted 1 in 10,000 in blocking buffer with no sodium azide. Membranes were incubated in secondary antibodies for 1 hour at room temperature with gentle agitation. Washes in TBS/T were then repeated. Protein-bound antibodies were detected using electrochemiluminescence (ECL) and autoradiography. Pierce™ ECL Plus western blotting substrate (Thermo Fisher Scientific, Massachusetts, USA) was added to membranes and incubated at room temperature for 5 minutes under dark conditions. Light produced as a product of HPR activity was detected using X-ray film (Amersham Hyperfilm, GE Healthcare) and a Xograph Compact X4 X-ray developer (Xograph Healthcare).

Where membranes were stripped of antibodies for re-probing, they were washed three times on a shaker in distilled water for 10 minutes. Followed by

stationary incubation in 0.2 M NaOH at 37ºC for 20 minutes and then shaking at room temperature for a further 20 minutes. After three further washes in TBS/T, membranes were blocked in 10% milk and probed with antibodies as described above.

In some cases western blot signals were quantified by measuring band intensity using ImageJ. Band intensity was measured for each lane, and normalised to the maximum intensity for each antibody. Next, phosphorylated protein signals were normalised to total protein signals. Finally values for chemical-treated samples were normalised to untreated control values. Mean averages from triplicate experiments were reported.

Table 2.5 – Primary antibodies
Details of primary antibodies, including antigen, clonality (including clone ID), host, supplier (including catalogue number) and dilution used for western blotting. CST; cell signalling technology.

Antigen	Clonality	Host	Supplier	Dilution
FLAG	Monoclonal – M2	Mouse	Sigma-Aldrich– F3165	1:10000
CDC14B	Polyclonal	Rabbit	Life Technologies - 348900	1:1000
β-actin	Monoclonal – 8H10D10	Mouse	CST3700	1:10000
GAPDH	Monoclonal – 14C10	Rabbit	CST2118	1:10000
Cas9	Monoclonal – EPR18991	Rabbit	Abcam – Ab189380	1:5000
GFP	Polyclonal	Goat	Abcam – Ab6662	1:5000
Phospho-AKT (Ser473)	Monoclonal – D9E	Rabbit	CST4060	1:1000
AKT	Polyclonal	Rabbit	CST9272	1:2000
Phospho-ERK (Thr202/Tyr204)	Monoclonal – E10	Mouse	CST9106	1:1000
ERK	Polyclonal	Rabbit	CST9102	1:1000

2.4.4. Immunofluorescence (IF) microscopy

For IF microscopy, cells were seeded onto 13 mm glass coverslips placed in 24 well tissue culture plates. Coverslips were pre-treated by rinsing for 30 minutes in concentrated nitric acid, then 30 minutes in distilled water, and finally 30 minutes in methanol. Coverslips were then air dried and baked at 150ºC for 4 hours before coating with poly-L-lysine (PLL). 40 µg PLL diluted in 90 µl distilled water was used to completely cover each coverslip and

incubated at room temperature for 1 hour, after which coverslips were left to air dry. Cells were then seeded onto coverslips and transfected with plasmid DNA the following day. At the end point of the experiments, cells were fixed using 0.5 ml 4% PFA per well incubated at room temperature for 20 minutes.

For immunodetection of FLAG-tagged proteins, coverslips were blocked with 1% (w/v) BSA/ 0.05% Triton X-100 (v/v)/ PBS shaking at room temperature for 15 minutes. Anti-FLAG primary antibody (**Table 2.5**) was diluted 1 in 1000 in 3% (w/v) BSA/ 0.05% Triton X-100 (v/v)/ PBS and added to coverslips for 1 hour at room temperature. Coverslips were washed in 0.1% (w/v) BSA/ 0.05% Triton X-100 (v/v)/ PBS three times for 10 minutes shaking at room temperature. Alexa Fluor® fluorescently labelled secondary antibodies from Life Technologies (California, USA) were used, specifically Alexa Fluor® 568 goat anti-mouse. Secondary antibody was diluted 1 in 500 in 3% (w/v) BSA/ 0.05% Triton X-100 (v/v)/ PBS and added to coverslips for 1 hour at room temperature under dark conditions, after which wash steps were repeated. Coverslips were then mounted onto glass slides using VECTASHIELD Hardset Antifade Mounting Medium with DAPI (Vector Laboratories, Peterborough, UK). Once the mount had set, cells were imaged using fluorescent microscopy to visualise antibody-labelled proteins.

2.5. RNA assays

2.5.1. RNA extraction

For RNA extraction, cells were lysed in 100 µl Trizol (Ambion, Life Technologies, California, USA) per cm^2 growth area and RNA was extracted using the Direct-zol™ RNA MiniPrep kit (Zymo Research, California, USA). Ethanol was added to each Trizol sample in a ratio of 1:1 before loading into Zymo-Spin IIC Columns, and centrifugation at 12,000 xg for 1 minute. Samples were then treated with an in-column DNase 1 digestion (Zymo Research, California, USA). For DNase 1 digestion, 5 units DNase1, mixed with DNase reaction buffer and RNA wash buffer, were applied to each column and incubated at room temperature for 15 minutes. Columns were washed with 400 µl Direct-zol RNA PreWash buffer, and 700 µl RNA wash buffer, and RNA

was eluted in 30 µl RNase/DNase free water. RNA concentrations were quantified by absorbance at 260nm using a NanoDrop ND-1000 spectrophotometer.

In later experiments the miRNeasy easy kit (QIAGEN, Germany) was used for RNA extraction. Monolayer cells from 12 well tissue culture plates were lysed in 700 µl QIAzol and 140 µl chloroform was added. Samples were centrifuged at 12,000 xg for 15 minutes at 4°C, and the upper, clear aqueous phase containing RNA was isolated. 525 µl ethanol was added to each RNA sample before loading into the QIAGEN spin columns, and centrifugation at 12,000 xg for 15 seconds. Again on-column DNase1 digestion (RNase-Free DNase set - QIAGEN, Germany) was performed at room temperature for 15 minutes. Columns were then washed with 700 µl RTW buffer, and 700 µl RPE buffer and RNA was eluted in 35 µl RNase/DNase water. RNA concentrations were quantified by absorbance at 260nm using a NanoDrop ND-1000 spectrophotometer.

2.5.2. cDNA synthesis

RNA was reverse-transcribed to produce cDNA using the Transcriptor First Strand cDNA Synthesis kit (Roche, Switzerland). Reactions were assembled using 1 µg template RNA, 60 µM random hexamer primers, 1X reverse transcriptase reaction buffer, 20 units RNase inhibitor, 1 mM dNTPs (per nucleotide), and 10 units reverse transcriptase enzyme. Thermocycling using the following program was then performed to generate cDNA; 25°C for 10 minutes, 55°C for 30 minutes, 85°C for 5 minutes.

2.5.3. Quantitative real time PCR (qPCR)

Primers were designed to amplify target genes during qPCR in order to assess relative gene expression (**Table 2.6**). Primers were designed using NCBI Primer BLAST (www.ncbi.nlm.nih.gov/tools/primer-blast), adhering to the following guidelines:

- Should cross exon-exon boundaries
- Amplicon length <200bp

- Melting temperature between 57ºC and 63ºC, optimally 60ºC with less than 3ºC difference between forward and reverse primers
- GC content of 50-60%, and ideally ending with a G or C
- No long stretches of repeat nucleotides
- Low self-complementarity

For qPCR, cDNAs were diluted 1 in 10 in MilliQ distilled water, and 2 µl was added to 0.5 µM forward and reverse primers, and 5 µl iTaq Universal SYBR Green supermix (Bio-Rad, California, USA) in a 96-well plate (Low-profile 96-well skirted plates, Bio-Rad). Plates were sealed (Microseal 'B' adhesive sealing films – Bio-Rad) and qPCR was performed using the CFX96 Real-Time system (Bio-Rad) and the following program; 95°C for 5 minutes, 40 cycles of 95°C for 15 seconds and 60°C for 1 minute, melt curve analysis (65ºC to 95ºC – 0.5ºC/5 seconds). Size analysis of qPCR products using gel electrophoresis, as well as melt curve analysis, confirmed primer specificity. Relative gene expression was calculated using the Livak method, commonly known as the 'Delta Delta CT' method (Livak and Schmittgen, 2001). CT refers to the cycle number at which SYBR green fluorescence crosses a threshold. First delta CT (ΔCt) is calculated by subtracting the CT value for a reference gene (in this case GAPDH) from that of the target gene. Delta delta CT (ΔΔCt) is next calculated by subtracting ΔCT for the internal control (untreated cells) from those of the experimental conditions. Finally, the relative fold change in gene expression is calculated using $2^{-\Delta\Delta Ct}$.

Table 2.6 – qPCR primer sequences
Forward and reverse primer sequences used for qPCR. Primers obtained from Sigma-Aldrich, Dorset, UK.

Target Gene	Forward (5' – 3')	Reverse (5' – 3')
CDC14B	CAAACCAACCTCTGGCTGGA	TCACTGTACGGTTCGGGTTC
ACP1	TGATCGGTTACAAGTTTCCTGA	AACAGGCTACCAAGTCCGTG
PTPRN	AAGGGTGCAGGAAGAAATCCG	CGGCCCCTCCATTGTTTTCT
MTMR12	GATCGACGAGAGACACCACA	GGAAACAAAGACGAGAGGCG
DCTN1	GCGAGCAGATCTATGGGACC	GCTCTGCATCATACTCCCCC
PDE2A	TACGAGAAAGATCGCGGAGC	CGGTCCATCATCTCCATCGG
GLMP	TTCAAGGCCACCCCATGAAC	GAAAAGGCCTGGACCCTGAAG
TUBGCP6	ACCCTTGTGGTGACAGGTTC	CTCGGTGGGACCTTAATAGCC
GAPDH	ATGACATCAAGAAGGTGGC	CATACCAGGAAATGAGCTTG

2.5.4. RNA sequencing (RNAseq)

For RNAseq, IMR32 and KELLY cells were seeded in triplicate into 6 well plates and treated with 10 µM BMOV/BSO the following day (each replicate was seeded and treated separately, on different days). After 24 hours chemical treatment, cells were harvested in 500 µl Trizol (Ambion – Life Technologies). RNA was extracted using the Direct-zol^{TM} RNA MiniPrep kit (Zymo Research, California, USA) as described in **Section 2.5.1.**, and sent to Tony Brooks (UCL Genomics) for quality assessment, sequencing and initial data analysis. The following method was used by Tony Brooks. The Agilent 2200 TapeStation system utilising high throughput electrophoretic RNA separation was used to measure RNA quantity and integrity. RNA integrity numbers (RIN^{e}) were calculated as a measure of degradation (Schroeder et al., 2006). Very high RIN^{e} numbers were reported, ranging from 9.6 to 10 (on a scale of 1 to 10), indicating high quality, intact RNA. The Kapa Stranded mRNA-Seq Sample preparation kit (Kapa BIOSYSTEMS - KK8400) was used according to manufacturer's instructions to create and amplify cDNA libraries for each RNA sample. Briefly, mRNA was isolated from total RNA samples by pulling down poly-adenylated transcripts using magnetic Oligo dT beads. Chemical fragmentation was used to fragment purified mRNA, which was subsequently primed using random hexamers. First strand cDNA was synthesised using reverse transcriptase and Actinomycin D. The second cDNA strand was synthesised and tagged by using dUTP rather than dTTP. Double stranded cDNA was then adenylated at the 3' ends to allow ligation to sequencing adapters that had thymine overhangs. Successfully ligated cDNA was enriched using a limited-cycle high-fidelity PCR reaction, where only the first strand containing dTTP is amplified to allow strand specific sequencing. Samples were sequenced using the NextSeq 500 instrument (Illumina, California, USA), using a 43 base pair paired end run. An average library size of 21,429,695 was achieved per sample, ranging from 18,318,299 to 23,232,389. Data analysis was carried out using the Illumina BaseSpace platform. First, sequencing data was converted to fastq files using bcl2fastq Conversion Software v2.17 and aligned to the UCSC human genome 19 reference genome using STAR on the BaseSpace RNA-Seq alignment app

v1.1.0. Reads per transcript counts were generated using the Python package HTSeq (Anders et al., 2015) and differential gene expression was calculated using the DESeq2 algorithm (Love et al., 2014).

Similar transcriptomic data was collected in a previous RNAseq experiment performed in the laboratory prior to me joining (A. Di Florio and A. Stoker, unpublished). In this experiment, LAN5 and SK-N-SH cells were treated with 10 µM BMOV for 24 hours before RNA extraction, cDNA synthesis, next generation sequencing and data analysis. The pipeline was very similar to that described above, also carried out by Tony Brooks. Samples were processed using Illumina's TruSeq RNA sample prep kit version 2 (Illumina, California, USA – RS-122-2001) according to manufacturer's instructions, which uses a very similar principle to that of the Kapa Stranded mRNA-Seq Sample preparation kit described above. Sequencing was again performed using the NextSeq500 (Illumina) using a 43 base pair paired end run. Data analysis involved the use of Illumina bcl2fastq conversion software v2 to create fastq files, and TopHat2 (Kim et al., 2013) for alignment to the UCSC human genome 19 reference genome. As above, HTSeq and DESeq2 were used estimate transcript abundance and calculate differential expression respectively.

2.5.5. Ingenuity Pathway Analysis

Ingenuity Pathway Analysis (IPA), produced and maintained by QIAGEN (Germany), was used for network analysis of RNAseq data in this project. During this analysis, experimental data is correlated with gene expression changes known to be related to specific signalling networks, upstream regulators, and biological functions. IPA utilises the Ingenuity Knowledge Base, a repository of biological interactions and functional annotations curated and reviewed for accuracy by PhD scientists. Right-tailed Fisher's exact tests are used to generate p values associated with each correlation, indicating the likelihood that the correlation between experimental data and a specific pathway or upstream regulator is due to chance alone. For the analysis presented in this thesis, gene lists for each chemical comparison within each cell line were filtered for significance ($p<0.05$) and log2FC (>0.3 or <-0.3) prior

to import into the software. The network analysis generated was used to generate hypotheses regarding signalling pathways and molecules that were affected by chemical treatment, and therefore could be important in intracellular chemical function. These hypotheses must then be experimentally validated.

2.6. DNA assays

2.6.1. CDC14B overexpression

Wild-type CDC14B and siRNA-resistant mutant CDC14B expression plasmids (based on pcDNA3.1-C-(k)DYK) were obtained from GenScript. These encode the full exonic sequence from the longest human isoform of CDC14B, isoform 2. The siRNA-resistant mutant plasmid has four silent point mutations in the CDC14B_12 siRNA-binding region, which confer resistance to siRNA-mediated knockdown (**Figure 2.3**). The plasmids were transformed into competent E. coli for amplification and DNA was extracted using alkaline lysis (as described in **Sections 2.6.5.** and **2.6.6.**). The entire cDNA sequences were obtained by Sanger sequencing (Source BioScience, Nottingham, UK) to ensure there were no extraneous base pair changes. The following Source BioScience sequencing primers were used for this; T7 forward 5'-TAATACGACTCACTATAGGG, bGH reverse 5'-TAGAAGGCACAGTCGAGG.

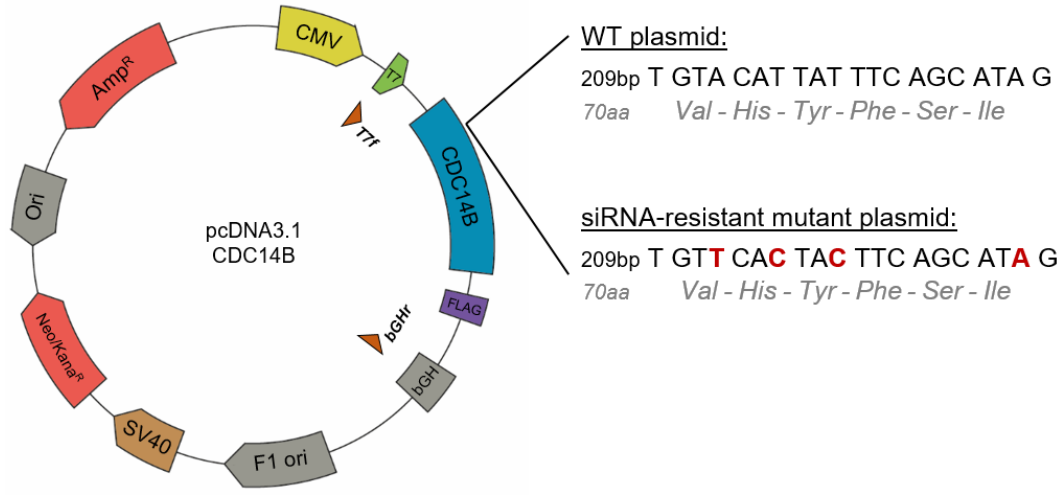

Figure 2.3 – CDC14B overexpression vectors
CDC14B wild-type and siRNA-resistant overexpression vectors based on the pcDNA3.1-C-(k)DYK backbone were obtained from GenScript. Four single nucleotide mutations (shown in red) were introduced within the CDC14B_12 siRNA binding region to confer resistance, these did not affect the amino acid sequence. T7 forward and bGH reverse sequencing primers were used during Sanger sequencing to confirm sequences.

2.6.2. EGFP-CDC14B constructs

GFP-tagged CDC14B overexpression constructs were generated using the wild-type and siRNA-resistant mutant constructs from the GenScript plasmids described above. A PCR reaction using Phusion® high-fidelity DNA polymerase (Thermo Fisher Scientific, Massachusetts, USA) was used to amplify the *CDC14B* gene constructs from these plasmids, whilst adding restriction sites that could be used to clone them in frame into a pEGFP-N2 reporter plasmid (**Figure 2.4**). Primers were designed that annealed to the 5' and 3' ends of the *CDC14B* gene and added HindIII and BamHI restriction site respectively (primers ordered from Sigma-Aldrich, Dorset, UK). PCR reactions were assembled in high-fidelity buffer (Thermo Fisher Scientific, Massachusetts, USA) using 10 ng wild-type or siRNA-resistant CDC14B plasmid DNA, 1 U Phusion polymerase, cloning primers to a final concentration of 1 µM and 0.25 mM dNTPs (Promega, Wisconsin, USA). PCR was performed using 40 cycles of 98ºC for 10 seconds, 68ºC for 30 seconds and 72ºC for 30 seconds with a final extension step at 72ºC for 10 minutes. PCR products were purified using QIAquick PCR purification kit (QIAGEN, Germany) according to manufacturer's instructions, which uses silica-membrane-based purification.

Both the GFP vector (5 µg) and the PCR amplified CDC14B constructs were digested with BamHI and HindIII (Promega). Double digest reactions were assembled in buffer E (Promega), using 50 U of each of BamHI and HindIII and BSA at a final concentration of 0.1 mg/ml. Digestion was carried out at 37ºC for 4 hours. Digested GFP and CDC14B constructs were separated by gel electrophoresis at 130V using a 0.7% agarose/TAE buffer (40 mM Tris base, 20 mM acetic acid, 1 mM EDTA, pH 8) gel. Digested products were cut out of agarose gels utilising ethidium bromine fluorescence, and purified by silica-membrane-based purification using the QIAquick gel extraction kit (QIAGEN, Germany).

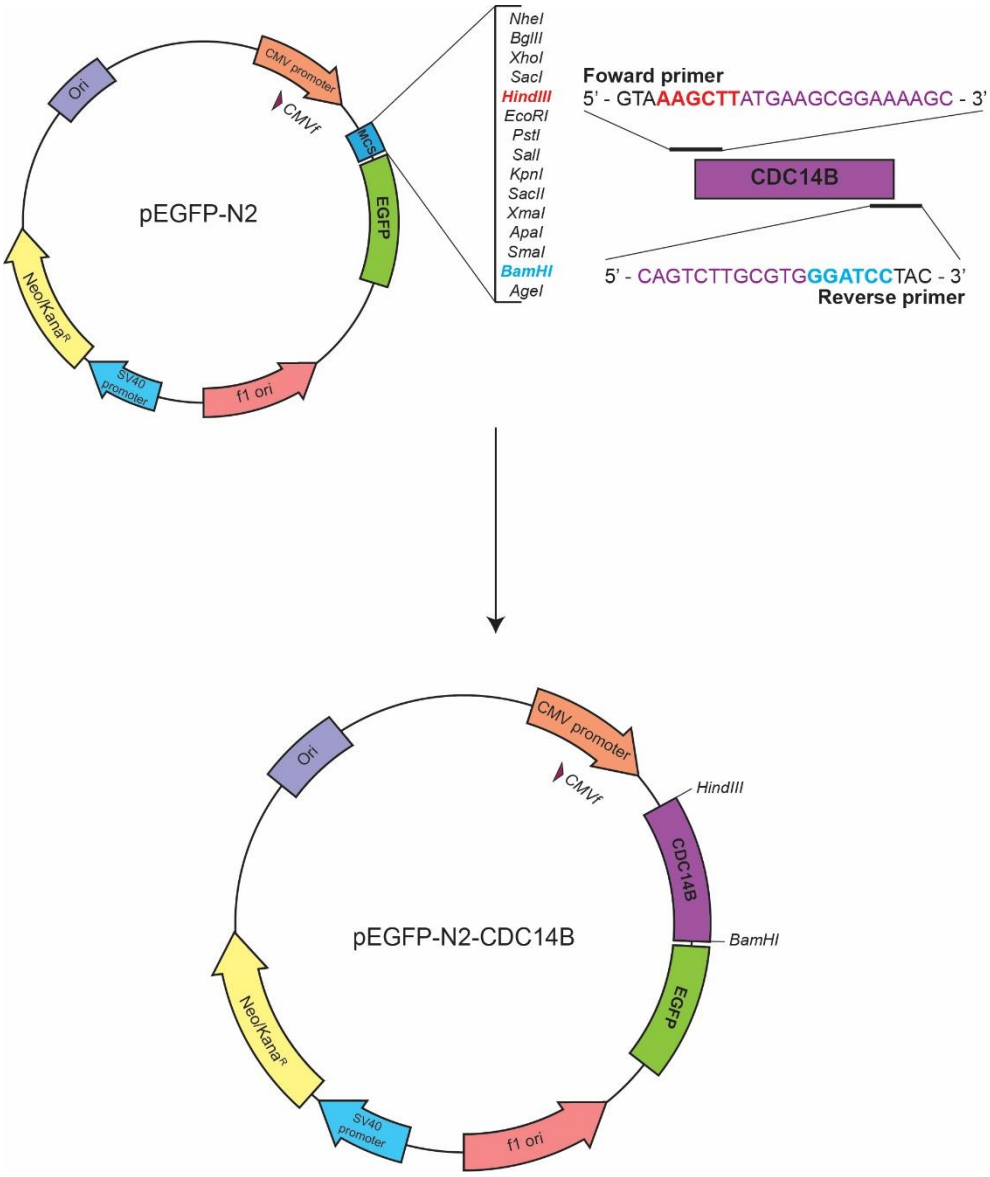

Figure 2.4 – EGFP-CDC14B cloning strategy
CDC14B constructs (wild-type and siRNA-resistant mutant) were PCR amplified to add 5' HindIII and 3' BamHI restriction digest sites. Amplified CDC14B and pEGFP-N2 plasmid were digested with HindIII and BamHI, and subsequently ligated to create GFP-tagged CDC14B expression plasmids.

CDC14B PCR products were ligated into digested GFP plasmid in a 3:1 ratio. 10 µl ligation reactions were assembled in T4 ligase buffer (Promega, Wisconsin, US) using 1 µl digested GFP plasmid, 3 µl digested CDC14B PCR product and 3 U T4 ligase (Promega). Reactions were assembled on ice and then incubated in a 37ºC water bath placed at 4 ºC overnight. Ligated plasmids were subsequently transformed into DH5α competent E. coli (Invitrogen) for amplification, and purified using alkaline lysis (described in **Sections 2.6.5.** and **2.6.6.**). Plasmid preparations with successfully ligated GFP-CDC14B were identified by restriction digest. For this, plasmids were digested using

BamHI/HindIII double digestion (as described above), and products were separated by gel electrophoresis at 130V using a 1% agarose/TAE buffer gel. Relative migration of the digested products was used to estimate size, and therefore confirm successful cloning. Ligation was further confirmed by Sanger sequencing (Source BioScience, Nottingham, UK) using a sequencing primer that anneals to the CMV promoter upstream of the GFP-CDC14B construct (pCMV forward from Source BioScience 5'-GAGCTCGTTTAGTGAACCGTC).

2.6.3. CRISPR/Cas9 gRNA design

CDC14B guide RNA (gRNA) sequences were designed using the online MIT guide design tool (http://crispr.mit.edu), which scores potential guide sequences based on the likelihood that they will generate off-target editing events (**Table 2.7**). CDC14B-specifc gRNA sequences were ordered from Sigma-Aldrich (Dorset, UK), these contained the 20 base pair CDC14B-targeting sequences with additional bases for cloning into CRISPR/Cas9 plasmids (described below).

Table 2.7 – CDC14B-targeting gRNA sequences
Sequences for CDC14B-targeting gRNAs. FWD, forward sequence; REV, reverse sequence.

gRNA	Sequence (5'-3')
Guide 2 FWD	TAAAGCTTCTACGCAGATTT
Guide 2 REV	AAATCTGCGTAGAAGCTTTA
Guide 3 FWD	TGCAGTCCATTACAATGTTA
Guide 3 REV	TAACATTGTAATGGACTGCA
Guide 4 FWD	AGACATCCTATATTCCTTTC
Guide 4 REV	GAAAGGAATATAGGATGTCT

2.6.4. CRISPR/Cas9 gRNA cloning

CDC14B-targeting guide sequences were cloned first into the PX458 plasmid (Addgene #48138) for gRNA and Cas9 expression, and later into the pU6 plasmid (Addgene #60955) for gRNA expression to be used alongside inducible Cas9 expression.

For PX458 cloning, gRNA sequences were obtained with added Bpi1 digestion site overhangs (**Figure 2.5A**). Guide RNAs were annealed in Taq polymerase buffer (Invitrogen, California, USA) by heating to 95°C for 5 minutes and then

cooling to 25°C at a rate of 5°C per minute. Annealed CDC14B gRNAs were cloned into PX458, which contains the guide RNA scaffold, Cas9 endonuclease gene, ampicillin resistance gene, and a GFP marker. For this, 100 ng PX458 was digested using 1 µl Bpi1 (Thermo Fisher Scientific, Massachusetts, USA) in fast digest buffer by incubating at 37°C for 1 hour. 1 µl annealed CDC14B gRNAs were added to the plasmid digestion along with 5 U T4 ligase (Promega, Wisconsin, US) and T4 ligase buffer. The ligation reaction was incubated at 37°C for 1 hour, after which 5 µl was transformed into competent DH5α cells (Invitrogen), and plasmid DNA was purified (described in **Sections 2.6.5.** and **2.6.6**.). DNA was Sanger sequenced (Source BioScience, Nottingham, UK) to confirm the guide sequences had been inserted correctly, using a sequencing primer that annealed upstream of the gRNA sequences (5'-GAGGGCCTATTTCCCATGATTCC).

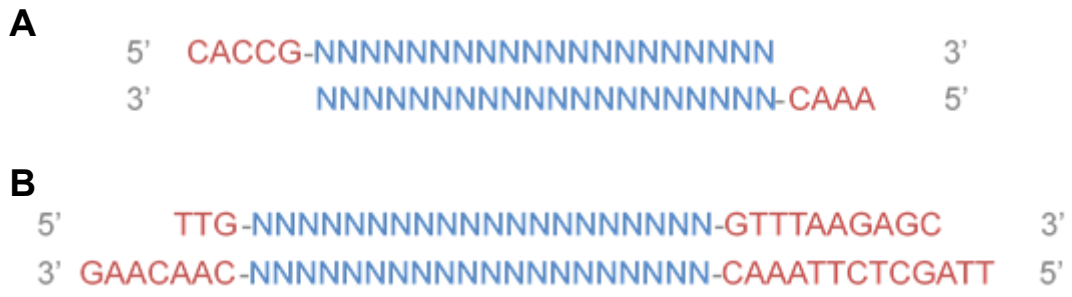

Figure 2.5 – gRNA oligos with cloning sites
Guide RNAs were obtained from Sigma-Aldrich and contained gene specific targeting regions (blue), as well as restriction digest sites (red). ***A*** *– For PX458 cloning, gRNAs with Bpi1 digestion site overhangs at either end were ordered.* ***B*** *– For pU6 cloning, gRNAs with BstXI and Blpl digestion site overhangs were ordered.*

For pU6 cloning, gRNA sequences were ordered with added BstXI and Blpl digestion site overhangs (**Figure 2.5B**). Guide RNAs were annealed in Taq polymerase buffer (Invitrogen, California, USA) by heating to 95°C for 5 minutes and then cooling to 25°C at a rate of 5°C per minute. Annealed CDC14B gRNAs were then cloned into pU6, which contains the guide RNA scaffold and a puromycin selection marker. The pU6 plasmid was digested using a 2-step method. First, 5 µg pU6 was digested with 1 µl BstXI (Thermo Fisher Scientific, Massachusetts, USA) in buffer O (Thermo Fisher Scientific) at 55ºC for 35 minutes and then 37ºC overnight. Digested pU6 was purified using the QIAquick PCR purification kit (QIAGEN, Germany). This purified product was subsequently digested with 0.5 µl Blpl (Thermo Fisher Scientific)

in Tango buffer (Thermo Fisher Scientific) at 37ºC for 2 hours, and gel purified by gel electrophoresis using the QIAquick gel extraction kit (QIAGEN, Germany). Annealed guides were ligated into the double digested pU6 vector at a ratio of 1:4 (1 µl gRNA, 4 µl pU6) using 3 U T4 ligase (Promega, Wisconsin, US) in T4 ligase buffer. Ligations were assembled on ice and incubated in a 37ºC water bath placed at 4ºC overnight. As with PX458 cloning, ligation products were transformed into DH5α cells (Invitrogen), and DNA was extracted using alkaline lysis (described in **Sections 2.6.5.** and **2.6.6.**). Sanger sequencing (Source BioScience, Nottingham, UK) was again used to confirm successful gRNA incorporation (sequencing primer 5' - GAGGGCCTATTTCCCATGATTCC).

2.6.5. Bacterial plasmid amplification

Plasmids were transformed into DH5α^{TM} competent E. coli (Invitrogen, California, USA), which was subsequently subcultured for plasmid amplification. Transformations were performed using a standard heat shock protocol. Briefly, 5 µl plasmid DNA was added to 40 µl DH5α^{TM} and incubated on ice for 30 minutes. Heat shock was then performed at 42ºC for 20 seconds, followed by a further 2 minutes on ice. E. coli was recovered in 1 ml Luria-Bertani (LB - Invitrogen) shaking at 37ºC for 1 hour, before spreading onto ampicillin or kanamycin agar plates under sterile conditions. Ampicillin (100 µg/ml final concentration) or kanamycin (50 µg/ml final concentration) was used to select for transformed E. coli, depending on the antibiotic resistance marker present in each plasmid. Agar plates were left briefly to dry at room temperature, and then incubated upside down at 37ºC for 12-16 hours. After incubation, individual colonies were picked from agar plates and subcultured in LB (+ampicillin/kanamycin). Cultures were incubated at 37ºC with vigorous shaking for 12-16 hours. MiniPrep cultures were 3 ml LB, whereas MaxiPrep cultures were 100 ml. Plasmid DNA was extracted from E. coli using alkaline lysis (described below **2.6.6.**).

2.6.6. Plasmid DNA extraction

Plasmid DNA was extracted from DH5α^{TM} cultures using QIAGEN plasmid purification kits (QIAGEN, Germany). Before extraction, cultures were centrifuged at high speed to pellet E. coli cells. QIAGEN plasmid DNA purification kits utilise a modified alkaline lysis protocol (Birnboim and Doly, 1979, Birnboim, 1983). For MiniPrep, the QIAprep spin MiniPrep kit was used according to manufacture's protocols. Briefly, bacterial cells are lysed under alkaline conditions, then neutralised and adjusted to high-salt conditions. This lysate is then applied to a silica membrane in a spin column. Plasmid DNA adsorbs to the silica membrane in high-salt buffers, and is eluted in low-salt buffers. Centrifugation steps are used to bind the lysate, wash the silica membrane to remove salts, and to elute DNA in 35 µl water. For large-scale plasmid purification, the HiSpeed plasmid maxi kit was used. Again, E.coli cells are lysed under alkaline conditions. Lysates are then bound to a QIAGEN resin under low-salt conditions. RNA, protein and low-molecular weight impurities are removed using a medium-salt wash. Plasmid DNA is then eluted in a high-salt buffer before isopropanol precipitation using the QIAprecipitator module to concentrate and desalt the DNA. Purified DNA was eluted from the QIAprecipitator modules using 1 ml TE buffer (10 mM Tris-HCL, pH 8; 1 mM EDTA).

2.6.7. T7 Endonuclease 1 (T7E1) assay

T7E1 assays were used to assess editing efficiency during CRISPR/Cas9 experiments, as described by Ran et al. (2013) (**Figure 2.6**). In the T7E1 assay, guide targeted regions of genomic DNA are amplified by high-fidelity PCR. These PCR products are denatured and reannealed, and T7E1 is then used to digest DNA duplexes with mismatches. When the digested product is separated by gel electrophoresis, multiple bands running at the correct size indicate that there were mismatches in the DNA sample, indicating gene editing.

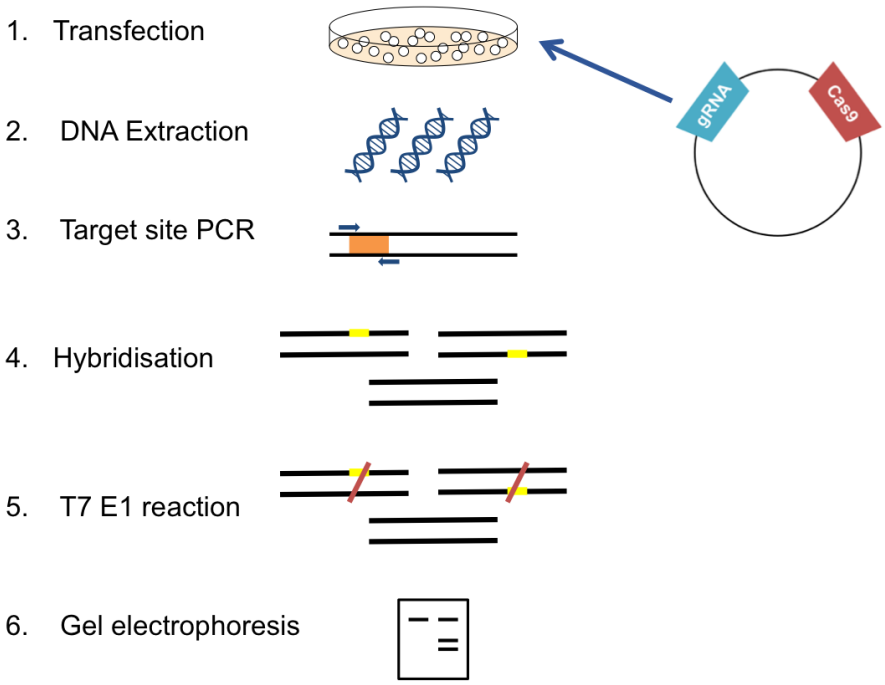

Figure 2.6 – T7 Endonuclease 1 (T7E1) assay principle
1 - Cells were transfected with CRISPR/Cas9 plasmids (PX458 or pU6). 2 – Cells were then cultured for various time periods before genomic DNA was extracted. 3 – Guide targeted DNA was amplified using high fidelity PCR. 4 – PCR products were denatured and reannealed. 5 – DNA was treated with T7E1, which cleaves at sites where the two DNA strands do not match. 6 – DNA is separated by gel electrophoresis to determine the size of resulting fragments.

In order to assess gene editing using T7E1, CRISPR/Cas9 targeted cell cultures were trypsinised and cells were pelleted at 300 xg for 5 minutes. Cell pellets were resuspended in Quick Extract (Illumina, California, USA), incubated at 65ºC for 15 minutes and then 100ºC for 2 minutes to extract genomic DNA (gDNA). PCR primers were designed to amplify *CDC14B* gene regions targeted by each of guide 2, 3 and 4 (Exons 3, 4 and 5 respectively) (**Table 2.8**). High fidelity Pfu DNA polymerase PCR reactions were performed in Pfu polymerase buffer (Promega, Wisconsin, US) using 1 µl genomic DNA, 1.24 U Pfu polymerase (Promega), primers at a final concentration of 0.4 µM, and 0.2 mM dNTPs (Promega). Thermocycling involved 40 cycles of 95ºC for 45 seconds, 55ºC for 30 seconds and 72ºC for 2 minutes with a final extension step at 72ºC for 5 minutes. PCR products were then purified using the QIAquick PCR purification kit (QIAGEN, Germany), and eluted in 35 µl EB (Elution Buffer; 10 mM Tris-Cl pH 8.5). Purified PCR products were re-hybridised in 1X NEB Buffer 2 (New England Biosciences, Massachusetts, USA), by denaturing at 95°C for 5 minutes, followed by slow cooling to allow DNA to reanneal (95°C to 25°C at a rate of 0.1°C per second). After which 1

µl T7E1 (New England Biosciences) was added and incubated at 37°C for 15 minutes to induce double stranded break formation at mismatch sites in the DNA. Digested samples were separated by gel electrophoresis at 130V on a 2% agarose gel. Gels were imaged using the Bio-Rad Molecular Imager® Gel Doc™ XR System with Image Lab™ software. Cleaved DNA of the correct size indicated successful CRISPR/Cas9 targeting.

Table 2.8 – PCR primer sequences for CDC14B guide targeted exons
PCR primer sequences to amplify CDC14B guide targeted regions for T7E1 analysis. Guide 2, 3 and 4 targeted exons 3, 4 and 5 respectively. FWD = forward sequence, REV = reverse sequence.

Target Exon	Forward (5' – 3')	Reverse (5' – 3')
Exon 3	GCAGACCAAAGAGTGCATCAA	GTCCCCCAGATCAAGCTAACA
Exon 4	CATGTGTCCATTCATGTCCCCT	CCGTGTGGTATGTAACCCATCT
Exon 5	AGGTTGCTGTGAAGAGTTGTTG	TGGTGTTATTTGCGCTCATCC

2.7. Liposomes

2.7.1. Liposome synthesis

Hydrophobic oxidovanadium liposomes (AL3) were synthesised by Ruhina Maeshima and Aris Tagalakis (Genetics and Genomic Medicine, ICH, UCL), using the thin film hydration method. AL3 was supplied in a 50:50 methanol:chloroform solution at 5 µg/ml, and stock solutions of all lipids (DOTMA, DOPC and cholesterol) were prepared at 10 mg/ml. DOTMA, DOPC (Avanti polar lipids), cholesterol (Sigma-Aldrich, Dorset, UK) and AL3 were mixed in a round-bottomed flask to a final volume of 500 µl at a molar ratio of 35 : 35 : 20 : 10 (37.5 : 37.5 : 25 for empty liposomes). A rotary evaporator (vacuum pump V-700, Rotavapor R-3 – Buchi, Switzerland) was then used at room temperature for 30 minutes to evaporate solvents leaving a thin lipid film on the bottom of the flask. Lipids were rehydrated to form liposomes by adding 1 ml nuclease free water and rotating overnight, followed by sonication for 30-40 minutes (XB3 Ultrasonic Bath).

2.7.2. Liposome dialysis

Dialysis was used to exclude any non-incorporated AL3 in solution from liposomal preparations. 500 µl of each liposome preparation was dialysed

within 48 hours of liposome synthesis using small-scale dialysis chambers (Slide-A-Lyzer™ MINI dialysis device, Thermo Fisher Scientific, Massachusetts, USA) with a molecular weight cut-off of 10 000 Da. Prior to dialysis, dialysis chambers were pre-wet with sterile water. 14 ml centrifuge tubes were then filled with 13.5 ml sterile water to be used as the dialysis buffer. Liposomal formulations were loaded into the dialysis chamber and placed into the centrifuge tubes. Tubes were placed vertically at 4ºC, shaking for 24 hours. The dialysis buffer was replaced with fresh sterile water twice during dialysis, after 4 and 18 hours.

2.7.3. Size/charge analysis

The average size and overall charge of the liposomal formulations was measured after synthesis, and again after dialysis. Size/charge analysis was performed using the Zetasizer Nano ZS system (Malvern Panalytical, UK). This machine uses dynamic light scattering to measure the average diameter of liposomes. Overall charge, or 'Zeta potential', is measured using laser Doppler velocimetry, where a voltage is applied using electrodes at either end of the cell containing the liposomal formulation and the electrophoretic mobility of liposomes is measured.

2.8. High performance liquid chromatography (HPLC)

2.8.1. cAMP HPLC

Intracellular cyclic adenosine monophosphate (cAMP) concentrations following chemical treatment were detected by reverse-phase HPLC in a novel assay developed in collaboration with Dr. Michael Orford (Stem cells and regenerative medicine, ICH, UCL). In this method, all adenine nucleotides were converted into fluorescent N^6-etheno derivatives by reacting them with chloracetaldehyde (**Figure 2.7A**). Samples were then separated by reverse-phase HPLC to allow resolution of individual adenine species, which could be detected based on fluorescence, and peak integration was used to quantify their concentrations (**Figure 2.7B**). Samples with known cAMP concentrations were used to generate a cAMP standard curve, which was then used to

determine cAMP concentration's in experimental samples (**Figure 2.7C**). This assay allows adenosine, AMP, ADP, ATP and cAMP to be detected. However, as cAMP concentrations were low compared to these other species in our samples, samples had to be run using a very sensitive scale, thus it was not possible to quantify AMP, ATP and ATP in the same run without altering the assay parameters (**Figure 2.7D**).

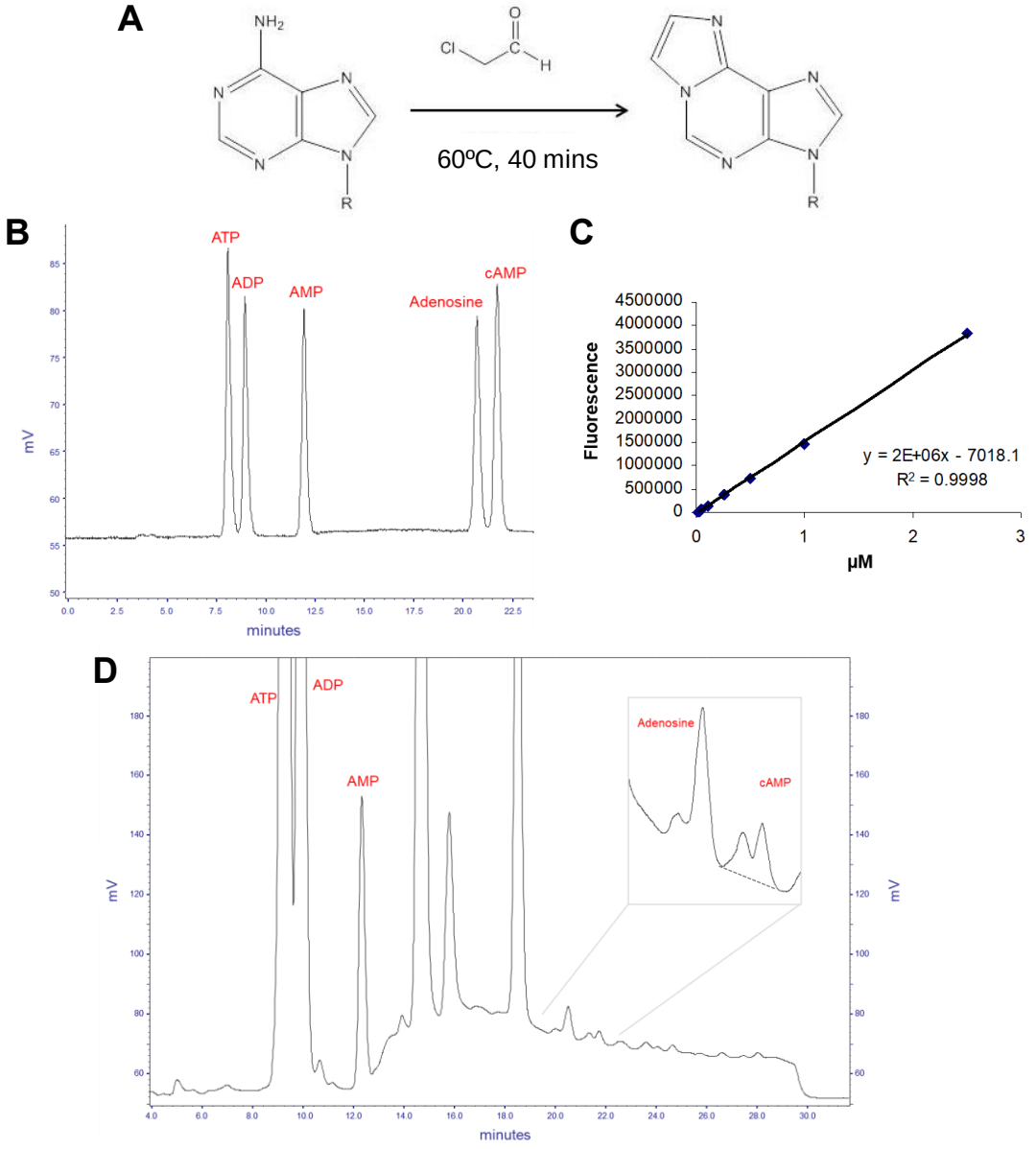

Figure 2.7 – cAMP detection by HPLC
***A** - Adenine within cAMP is reacted with chloracetaldehyde to convert it into a fluorescent N6-etheno derivative that can be detected by HPLC. **B** – Samples are separated by reverse-phase HPLC allowing individual adenine species to be detected and quantified. Plot shows HPLC using adenine standards. **C** – A cAMP standard curve was generated using known concentrations. **D** – An example of a spectra from IMR32 cells treated with 100 µM forskolin, showing that cAMP concentrations are low relative to the other adenine species. Dotted line indicates the area that was measured for cAMP quantitation.*

To prepare samples, cells were seeded into 6 well tissue culture plates, and treated with chemicals the following day. After 24 hours, cells were lysed in 300 µl ice cold 1 M perchloric acid and stored at -20ºC. A parallel set of samples were lysed for protein and assayed for protein concentration using a Bradford assay (**Sections 2.4.1.** and **2.4.2.**). Protein concentrations were used to normalise the perchloric acid samples for relative cell content. Next 160 µl 0.5 M potassium hydrogen carbonate was added to 200 µl of each cell extract, vortexed, and centrifuged at 13,000 xg for 5 minutes to remove precipitated proteins and potassium perchlorate. 100 µl clear supernatant was added to 100 µl 1 M sodium acetate, pH 4.5 and 10 µl 4 M chloracetaldehyde, and heated to 60ºC for 40 minutes. Samples were then chilled to 4ºC and 50 µl was injected into the HPLC system for adenine detection.

For reverse-phase HPLC, a JASCO Automated HPLC System was used, consisting of a column thermostat (CO-1560), sampler (AS-950), Intelligent Fluorescence Detector (FP-920), HPLC pumps (PU-1580), and degasser (DG-1580-53). A Hypersil^{TM} ODS (C18) reverse-phase HPLC column (Thermo Fisher Scientific, Massachusetts, USA – 30103-154630) was used with 3 µm particle size, 150 mm column length and 4.6 mm internal column diameter. Mobile phase A was 0.2 M potassium phosphate, pH 5.0, and mobile phase B was 0.2 M potassium phosphate, pH 5.0/ 10% acetonitrile. The HPLC was programmed with a flow rate of 0.8 ml/min and the gradient parameters shown in **Table 2.9**. Fluorescent N^6-etheno derivatives were detected by setting the fluorescence detector with the following parameters:

Excitation wavelength: 290 nm
Emission wavelength: 415 nm
Response: Standard
Gain: 100X

Table 2.9 – cAMP HPLC programme
Gradient programme for reverse-phase HPLC detection of adenine species, including cAMP. Mobile phase A, 0.2 M potassium phosphate, pH 5.0. Mobile phase B, 0.2 M potassium phosphate, pH 5.0/ 10% acetonitrile.

Time (minutes)	Mobile Phase A (%)	Mobile Phase B (%)
0	100	0
31	0	100
31.1	100	0
41	100	0

Data was collected using EZChrom Elite V 3.17 software and cAMP concentrations were quantified by determining the area under the cAMP peaks for each sample compared to the standard curve.

2.8.2. Oxidovanadium (AL3) HPLC

Reverse-phase HPLC was also used to measure the concentration of AL3 within liposomal formulations, using a novel assay set up in collaboration with Dr. Simon Eaton (Stem cells and regenerative medicine, ICH, UCL). In this assay oxidovanadium (AL3) was detected using characteristic absorbance peaks at 280 and 360 nm. A standard curve was generated using known concentrations of AL3 in ethanol, from which liposomal AL3 concentrations could be extrapolated.

To measure AL3 concentration of standards or liposomal formulations, 50 µl sample was injected into the HPLC system. A JASCO Automated HPLC System was used, consisting of a column thermostat (CO-1560), sampler (AS-950), JASCO MD-910 multiwave detector, HPLC pumps (PU-1580), and degasser (DG-1580-53). A Hypersil™ MOS-2 (C8) reverse-phase HPLC column (Thermo Fisher Scientific, Massachusetts, USA – 30305-254630) was used with 5 µm particle size, 250 mm column length and 4.6 mm internal column diameter. Mobile phase A was water and mobile phase B was 100% acetonitrile. The HPLC was programmed with a flow rate of 1.5 ml/min and the gradient parameters shown in **Table 2.10**. AL3 was detect by absorbance by programming the detector to scan between 200 and 650 nm.

Data was collected using EZChrom Elite V 3.17 software and AL3 concentrations were quantified by determining the area under the peaks for each sample compared to the standard curve. Example spectra as well as the AL3 standard curve are shown in **Figure 5.14**.

Table 2.10 – AL3 HPLC programme
Gradient programme for reverse-phase HPLC detection of oxidovanadium (AL3). Mobile phase A, water. Mobile phase B, 100% acetonitrile.

Time (minutes)	Mobile Phase A (%)	Mobile Phase B (%)
0	80	20
17	10	90
22	0	100

2.9. Statistics

Where appropriate, quantitative data were analysed using various statistical tests for significance. This included T-tests, both independent and paired, as well as analysis of variance (ANOVA). For ANOVA, post hoc testing was performed using the Dunnett test when all experimental conditions were compared to the same control, or Bonferroni when multiple comparisons were needed. Statistical tests were performed using SPSS (IBM SPSS Statistics 25) and significant changes (* $p<0.05$, ** $p<0.01$, *** $p<0.001$) are indicated throughout.

Chapter 3. Identifying pro-tumour PTPs

3.1. Introduction

As discussed previously, PTPs are an important family of signalling molecules that are under tight regulation to coordinate their roles in a vast range of cell behaviours, including differentiation, survival, proliferation, apoptosis and motility. Their role in the pathology of a number of human diseases is now being characterised, and in particular, they have been heavily implicated in cancer (Ostman et al., 2006, Motiwala and Jacob, 2006) (**Section 1.2.).** PTPs commonly act as tumour suppressors, but of particular interest to us here is that they can also be oncogenic drivers of tumourigenesis. Studying these enzymes will lead to both a better understanding of the complex mechanisms that underpin various cancers, and the identification of specific PTPs that are attractive targets for therapeutic intervention (Labbé et al., 2012, Bollu et al., 2017). Interest in therapeutically targeting PTPs was initiated by Elchebly following observations that PTP1B depletion in mice leads to increased insulin sensitivity and improved regulation of fuel metabolism (Elchebly et al., 1999). PTP1B has also been shown to have oncogenic roles in human cancers (Teng et al., 2016, Bentires-Alj and Neel, 2007). As discussed in **Chapter 1**, a range of small molecule inhibitors targeting PTP1B, as well as other oncogenic phosphatases are in development (Bollu et al., 2017).

Given the increasing description of oncogene-like roles for PTPs in various tumour types and the increased interest in the development of specific small molecule PTP inhibitors, we hypothesise that there are specific PTPs that promote growth and/or survival in neuroblastoma. As discussed in **Section 1.2.4**., a small number of PTPs have already been positively implicated in neuroblastoma, including SHP2, and to a lesser extent DUSP26 and PTPN2 (Bentires-Alj et al., 2004, Zhang et al., 2017, Shang et al., 2010, Shi et al., 2015, Young et al., 2009). Our observations that pan-inhibition of PTPs using oxidovanadium results in cytotoxicity in a panel of neuroblastoma cells further encourages this hypothesis (Clark et al., 2015). Our laboratory have begun to attempt to identify further examples of these oncogenic PTPs using RNAi. Prior to me joining the laboratory, a PTP family-wide shRNA dropout screen had been performed in two neuroblastoma cell lines, SK-N-SH and IMR32, both of

which are oxidovanadium sensitive (A. Cichon and A. Stoker, unpublished) (**Figure 3.1A**). This involved transducing cells with a pooled library of shRNA-expressing lentiviruses targeting each member of the PTP family. Viruses were prepared by Cat King (UCL Cancer Institute) using a commercial shRNAs (pGIPZ lentiviral shRNA constructs from Thermo Scientific). There were 609 shRNAs in total, with 1-13 shRNAs targeting each PTP gene. These shRNAs contained unique DNA barcodes, which facilitated their relative quantitation within total cellular genomic DNA (gDNA) after PCR and sequencing. Following transduction with the viral library, gDNA was collected after 24 hours and the relative abundance of each shRNA was thus quantified. Remaining cells were then cultured for 14 days (IMR32 cells), or for 7, 14 and 21 days (SK-N-SH cells), after which the abundance of shRNA barcodes were again quantified. ShRNAs that were less abundant in the final population of cells compared to the starting population were hypothesised to target PTPs that are critical for promoting proliferation and/or survival, as cells transduced with these shRNAs had a relative growth disadvantage. Analysis of the shRNA data generated lists of candidate oncogene-like PTP genes, which may prove to be potentially useful therapeutic targets for the treatment of neuroblastoma (**Figure 3.1B**). The IMR32 and SK-N-SH datasets were analysed by Shahzia Anjum Holtom (PURESTATS LTD) using slightly different pipelines as their growth rates and responses to pan-PTP inhibition vary. The shRNAseq R package was used for analysis of the IMR32 data, both with and without BSO (Sims et al., 2011). Note that BSO is a chemical inhibitor of glutathione synthesis that we have shown increases sensitivity to pan-PTP inhibition using oxidovanadium (Clark et al., 2015), hence it was included in this screen. In this pipeline, the log-ratios of shRNA abundance were calculated at the start of the experiment versus after 14 days of growth for each experimental replicate. The median ratio across the triplicate was then reported, using a Shapiro Wilk test to test for statistical significance, indicating depletion of specific shRNAs between time points. For SK-N-SH cells the edgeR package was used, which allows a log fold change score to be generated that reflects multiple time points, in this case 0, 7, 14 and 21 days of SK-N-SH culture after viral infection (Dai et al., 2014, Robinson et al., 2010). From analysis of both cell line data sets, PTPRN, CDC14B, ACP1 and MTMR12 were chosen for further

investigation as shRNAs targeting them either appeared in lists from both cell lines, or from IMR32 cells with and without BSO in the case of MTMR12. Note that several different shRNAs targeting ACP1, CDC14B and PTPRN were amongst the most depleted (2 out of 8, 3 out of 7, and 2 out of 6 respectively) in either or both cell lines, providing increased confidence that these were reliable candidate pro-tumour PTPs.

A

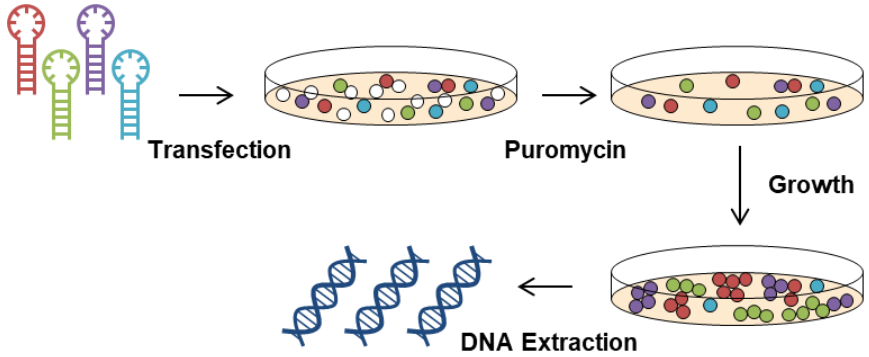

B

SK-N-SH screen

shRNA code	PTP Gene	log fold change
V3LHS_310359	***CDC14B***	-0.532
V2LHS_228508	PTEN	-0.485
V3LHS_646215	***PTPRN***	-0.480
V3LHS_369790	PTPN1	-0.472
V3LHS_406327	DUSP19	-0.465
V2LHS_242506	***ACP1***	-0.442
V3LHS_331596	MTMR6	-0.439
V2LHS_3553	DUSP8	-0.414
V3LHS_403096	DUSP2	-0.404
V2LHS_18240	DUSP8	-0.387
V3LHS_351634	PTPRE	-0.376

PTP in both cell line lists - same shRNA
PTP in both cell line lists - different shRNA
PTP in IMR32 lists +/- BSO - same shRNA
PTP in IMR32 lists +/- BSO - different shRNA

IMR32 screen

shRNA code	PTP Gene	median score
V3LHS_638599	***ACP1***	3.064
V3LHS_643062	***PTPRN***	2.466
V3LHS_325776	***MTMR12***	2.385
V3LHS_398494	PTPRT	2.384
V3LHS_639811	DUSP23	2.348
V3LHS_385799	SBF1	2.331
V2LHS_201163	DUSP6	2.149
V3LHS_375815	MTMR4	1.953
V2LHS_262421	***CDC14B***	1.883
V3LHS_378568	PTPN9	1.849
V3LHS_645217	DUSP14	1.841
V3LHS_335631	PTPN12	1.683
V2LHS_239145	PTP4A2	1.643
V3LHS_392584	PTPRF	1.589
V3LHS_321830	PTPN6	1.564
V3LHS_637582	PTPN21	1.548
V2LHS_203121	PTPN7	1.523

IMR32 + BSO screen

shRNA code	PTP Gene	median score
V3LHS_325776	***MTMR12***	3.473
V3LHS_310359	***CDC14B***	2.636
V3LHS_309710	DUSP5	2.609
V3LHS_402667	***CDC14B***	2.351
V3LHS_332279	PTPDC1	2.347
V3LHS_392583	PTPRF	2.336
V3LHS_375814	MTMR4	2.208
V3LHS_304492	MTMR7	2.028
V3LHS_637861	DUSP14	2.004

Figure 3.1 – PTP family-wide shRNA dropout screen

A *– Schematic summarising PTP family-wide shRNA dropout screen (A. Cichon and A. Stoker, unpublished). IMR32 and SK-N-SH cells were transduced with a library of viruses expressing 1 to 13 shRNAs targeting each PTP gene (609 shRNAs total). Puromycin was used to select for transduced cells. After growth periods of up to 21 days, genomic DNA was extracted and sequenced to assess relative abundance of each shRNA.* ***B*** *– Tables showing candidate tumour-promoting PTPs identified from this screen. For the SK-N-SH list, a negative log fold change indicated shRNA depletion, suggesting the corresponding PTP has a pro-tumour role. For the IMR32 lists, a positive median score indicated pro-tumour PTPs. PTPs are colour coded to indicate those which appear in multiple lists, either as the same or different shRNAs. Candidate oncogene-like PTPs that were validated in this project are shown in bold italics.*

PTPRN had been previously identified as a candidate cancer-promoting PTP in a similar phosphatase family-wide knockdown screen in HeLa cells, carried out by MacKeigan et al. (2005). Here siRNAs rather than shRNAs were used for gene knockdown, and a 96 well array format was used rather than a pooled approach followed by deconvolution as described above. PTPRN is a receptor-type PTP that is expressed in secretory granules of neuroendocrine cells. Although catalytically inactive, it is thought to play a role in insulin secretion amongst other functions (Sosa et al., 2016). PTPRN is also expressed in various tissues of the brain, and high expression has very recently been correlated with poor prognosis in glioblastoma (Shergalis et al., 2018). High *PTPRN* gene expression has also been reported in some other tumour types, including lung cancers of neuroendocrine origin (Xie et al., 1996). Furthermore, siRNA-mediated PTPRN knockdown reduced small cell lung cancer growth (Xu et al., 2016). High expression of the immature form of the closely related PTPRN2 has also been observed in various tumour types, and shRNA-mediated knockdown of proPTPRN2 led to reduced proliferation and increased apoptosis in breast cancer cell lines (Sorokin et al., 2015).

CDC14B is a DSP for which the function in mammalian cells is not well described. The yeast homolog, CDC14, is known to play a critical role in mitotic exit (Hartwell et al., 1973). The role of mammalian CDC14B, and closely related CDC14A, is not yet completely clear, but is not specifically in mitotic exit (Berdougo et al., 2008). There is growing evidence that CDC14B does play a critical role in the regulation of DNA damage repair and more generally in cell cycle regulation (Wei and Zhang, 2011). Importantly, there are now published data that support an oncogenic role for CDC14B. Chiesa et al. (2011) reported that overexpression of *CDC14B* was sufficient to drive transformation of mouse fibroblasts in culture, and tumourigenesis in mouse xenograft models. Similarly, CDC14B has been implicated in survival of laryngeal carcinoma (LC) cells (Sun et al., 2018a).

The *ACP1* gene encodes multiple isoforms of low molecular weight PTP (LMW-PTP), which have broad tissue distribution and regulate the function of several kinases (Raugei et al., 2002). ACP1 expression is upregulated in a number of cancers, including breast, colon, lung and of particular relevance

here neuroblastoma, and has been correlated with poorer outcomes (Malentacchi et al., 2005). Indeed there are a range of published data that support an oncogenic role for ACP1, however as is the case for so many signalling molecules, there are some opposing data that suggest that in specific tissue contexts and at particular stages of tumour progression, ACP1 can inhibit tumourigenesis (Alho et al., 2013, Chiarugi et al., 2004).

MTMR12 is part of the myotubularin protein family. It is catalytically inactive but acts as an adapter subunit regulating the intracellular localisation of myotubularin phosphatase (MTM1), which functions in muscle cell differentiation (Nandurkar et al., 2001, Nandurkar et al., 2003). The myotubularin protein family has been implicated in neuromuscular disease and in cancer in a very small number of cases, namely MTMR7 which has been linked to colorectal cancer (Raess et al., 2017, Weidner et al., 2016). Like PTPRN, MTMR12 was identified as a candidate oncoprotein-like PTP in the phosphatase family-wide siRNA knockdown screen performed by MacKeigan et al. (2005), however to the best of my knowledge, a role of MTMR12 in cancer has not been independently experimentally validated.

PTPRN, CDC14B, ACP1 and MTMR12 were identified as candidate neuroblastoma-promoting PTPs using our laboratory's pooled shRNA screen (described above). As is often the case with large-scale knockdown screens, the individual shRNA gene-targeting sequences had not been individually validated for on-target knockdown efficiency. Therefore some PTPs may not have been represented by the commercially-generated shRNA library, and false negatives may have been present in the final dataset. Moreover, occurrence of off-target gene knockdown events associated with the shRNAs had not been experimentally assessed, therefore false positives may also have been reported. Multiple shRNAs were used to target each PTP gene in an attempt to minimise these potential issues. Nonetheless, it is still possible that some candidate tumour-promoting PTPs are artefacts of the experimental strategy, rather than truly useful potential therapeutic targets. In the current study, I therefore aimed to further validate the role of these specific PTPs as growth and/or survival promoters in neuroblastoma.

For this loss-of-function approach, there are unfortunately very few small molecule inhibitors available that target specific PTPs (Stanford and Bottini, 2017). This is in part due to difficulties in specificity and bioavailability of molecules that bind to PTP active sites (discussed in **Section 1.2.5.**). I therefore utilised genetic technologies in order to induce loss-of-function and to validate candidate PTPs as growth and/or survival promoting proteins. This initially involved silencing the expression of each candidate PTP individually using siRNA-mediated gene knockdown. These experiments were performed in multiple neuroblastoma cell lines in order to determine whether oncoprotein-like roles could be extended to neuroblastoma more broadly, and in HEK-293T cells, in order to assess whether non-tumour cells may also rely on the expression of these enzymes. In the final experiments, CRISPR/Cas9 was employed in order to assess the effect of PTP genomic gene deletion, as opposed to transient silencing of expression using siRNA.

3.2. Results

3.2.1. Knockdown of specific PTPs reduces viability of neuroblastoma cells

Here I aimed to further validate candidate oncoprotein-like PTPs that were identified from the PTP dropout shRNA screen performed previously by our laboratory (A. Cichon and A. Stoker, unpublished). SiRNAs targeting PTPRN, CDC14B, MTMR12 and ACP1 mRNA were used to transiently knockdown gene expression. Viability assays in these transfected cells revealed whether loss of these enzymes could reduce proliferation and/or induce cell death in neuroblastoma cells. IMR32 cells were chosen for these assays because the effect of oxidovanadium (a broad-specificity PTP inhibitor) treatment in these cells is growth suppression and cytotoxicity (Clark et al., 2015), and because these cells were used in the original shRNA screen and are readily transfectable. Four, nineteen-nucleotide ON-TARGETplus siRNAs (Dharmacon, Colorado, USA) were used to target each gene. ON-TARGETplus siRNAs have chemical modifications that reduce off-target gene knockdown by blocking RNA-induced silencing (RISC) complex uptake of the

sense strand, favouring antisense strand loading, and by reducing antisense targeting of partially complimentary transcripts (Jackson et al., 2006). Just two siRNAs were used to target MTMR12, as initial knockdown efficiency testing performed by a former post doc in our group (Dr. Jessica Pickles) showed that transfection with the other two siRNAs did not substantially reduce mRNA abundance. All four siRNAs targeting PTPRN, ACP1 and CDC14B efficiently knocked down mRNA by at least 75% (**Appendix 1** – initial knockdown efficiency testing performed by Dr. Pickles).

IMR32 cells were transfected with the PTP-targeting siRNAs using RNAiMAX lipofection. After three to six days, the CCK-8 cell viability assay was used to identify any reduction in final cell density, indicating a role for the corresponding PTP in proliferation and/or cell survival (**Figure 3.2A+B**). MTMR12 was discounted as a candidate neuroblastoma-promoting PTP as transfection with neither siRNA resulted in reduced cell density compared to a non-targeting siRNA pool (SCR) **(Figure 3.2B**). In fact, one siRNA, MTMR12_12, slightly increased final cell density, although this was not statistically significant. Importantly, these studies are limited to looking for effects on final cell number, therefore any impact on other cancer phenotypes, for example motility, will not be detected. During initial experiments, including the MTMR12 data reported here (**Figure 3.2B)**, relatively high levels of siRNA was used (6 pmol per well in a 96 well plate). For PTPRN, CDC14B and ACP1 this was later reduced (3 pmol per well) to generate the data reported here (**Figure 3.2A**), which showed equivalent reductions in cell density but minimised the risk of off-target effects. For PTPRN, CDC14B and ACP1, transfection with at least one or two siRNAs resulted in a reduced final cell density. The lowest cell density values, up to 65% below the scrambled control, were observed in cells transfected with siRNAs targeting CDC14B.

CDC14B was therefore selected as the most promising candidate to pursue. I repeated the gene knockdown efficiency testing for each of the CDC14B-targeting siRNAs (**Figure 3.2C**). RNA was extracted from IMR32 cells 24 hours post transfection with the siRNAs, and qPCR using CDC14B primers was performed. According to these data, transfection with all four siRNAs reduced CDC14B expression by around 50% (Note: knockdown was less efficient in

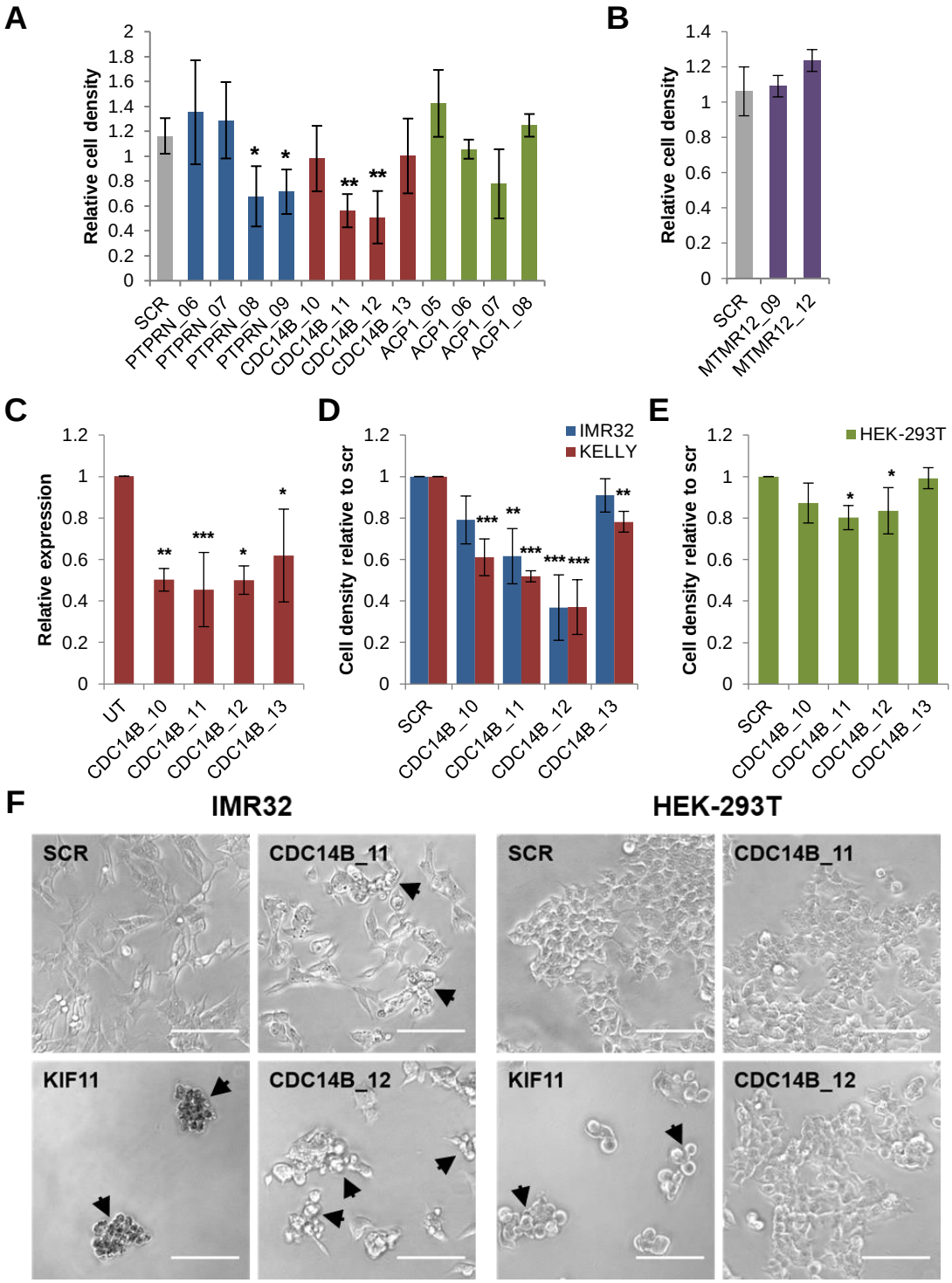

Figure 3.2 – CDC14B knockdown induced loss of cell viability in neuroblastoma cells ***A+B*** *- IMR32 cells were transfected with siRNAs targeting MTMR12, PTPRN, CDC14B and ACP1. Final cell density was quantified using CCK-8.* ***A*** *- Some siRNAs targeting PTPRN, CDC14B and ACP1 reduced final cell density compared to non-targeting control (SCR) (n=4).* ***B*** *- MTMR12 knockdown had no significant effect on cell density (n=3).* ***C*** *–CDC14B-targeting siRNA knockdown efficiency measured by qPCR in IMR32 cells (n=3).* ***D+E*** *– Final cell density measured using resazurin in cells transfected with CDC14B siRNAs.* ***D*** *- 3 out of 4 CDC14B-targeting siRNAs significantly reduced cell density in IMR32 cells, and 4 out of 4 in KELLY cells (n=3).* ***E -*** *Smaller difference in cell density were observed in HEK-293T cells (n=3).* ***F*** *– CDC14B-targeting siRNAs caused rounding up of cells indicative of cell death in IMR32 cells (black arrows), but only reduced proliferation in HEK-293T cells. Scale bar = 100 µm. All statistics – ANOVA with Dunnett post hoc, * p<0.05, ** p<0.01, *** p<0.001.*

my own experiments than in those performed by Dr. Pickles and reported in **Appendix 1**). There were substantial and replicable differences in the degree of reduction in final IMR32 cell density observed following transfection with each of the CDC14B-targeting siRNAs (**Figure 3.2A**). These differences could not completely be accounted for by differences in knockdown efficiency, although, the forth siRNA (CDC14B_13) was on average the least effective in gene silencing and had very little effect on cell viability (**Figure 3.2A+C**).

Having shown that knockdown of *CDC14B* gene expression in IMR32 cells caused reduced cell viability, these assays were extended to include other cell lines. In these experiments the concentration of siRNA used was again reduced (0.5 pmol per well in a 96 well plate), in an attempt to further minimise the risk of off-target effects. In a second neuroblastoma cell line (KELLY) a very similar pattern of final cell density was observed as with IMR32 cells, where all four siRNAs significantly reduced cell density compared to scrambled siRNA, although to differing extents (**Figure 3.2D**). In non-neuroblastoma HEK-293T cells, some significant, but much smaller changes in final cell density were detected (**Figure 3.2E**). This may indicate that CDC14B has a greater influence as a survival factor in neuroblastoma cells. Furthermore, it was observed that in IMR32 cells transfected with CDC14B-targeting siRNAs there was evidence of cytotoxicity, with cells adopting a rounder morphology, losing adhesion, and with visible dead cell debris (**Figure 3.2F-left)**. Conversely, in HEK-293T cells, there was reduced cell density at the point of assay, but the remaining cells appeared largely normal in morphology (**Figure 3.2F-right**). These data suggest that there may be a qualitative, as well as quantitative, difference in the response to CDC14B knockdown in neuroblastoma compared to non-neuroblastoma cell lines.

3.2.2. Cell viability could not be recovered using a CDC14B rescue plasmid

It is well documented that off-target gene knockdown events may occur when siRNAs are used to silence gene expression (Jackson and Linsley, 2010). We were reasonably confident that at least some of the loss of viability observed following transfection with CDC14B-targeting siRNAs was due to on-target

CDC14B gene silencing, because we had seen reduced viability with multiple siRNAs and even two distinct RNAi technologies (siRNA and the original shRNA screen). However, as there were substantial and replicable differences in cell response to each of the siRNAs targeting CDC14B in all three cell lines tested, and these could not be completely accounted for by a difference in knockdown efficiency (**Figure 3.2**), further on-target validation was required.

In an attempt to confirm that the observed cytotoxicity was largely due to CDC14B knockdown rather than an off-target effect, a CDC14B rescue plasmid was obtained (CDC14B_MUT), encoding full length isoform 2 CDC14B, but with four silent mutations in the CDC14B_12 siRNA-binding region. These mutations do not alter the amino acid sequence or gene function, but should prevent mRNA knockdown specifically by CDC14B_12 (**Figure 2.3**). Both wild-type and siRNA-resistant CDC14B overexpression plasmids were obtained from GenScript, and contain *CDC14B* genes tagged with a FLAG tag expressed under a cytomegalovirus (CMV) promotor. These plasmids were transfected into HEK-293T cells and western blotting using an anti-FLAG antibody confirmed that both constructs were expressed and produced protein of the correct size (**Figure 3.3A**). IMR32 and KELLY cells were transfected with wild-type CDC14B, and IF microscopy was performed. DAPI and anti-FLAG staining showed clear nuclear localisation of CDC14B in both IMR32 and KELLY cells, as expected (Bassermann et al., 2008, Berdougo et al., 2008, Mocciaro and Schiebel, 2010) (**Figure 3.3B**).

It was hoped that co-transfecting neuroblastoma cells with this siRNA-resistant plasmid alongside the corresponding CDC14B-targeting siRNA (CDC14B_12) would rescue cell viability, thus confirming that loss of viability is caused by knockdown of *CDC14B* gene expression. IMR32 cells were co-transfected with either wild-type or siRNA-resistant CDC14B, plus the CDC14B-targeting siRNAs. Six days after transfection, cell viability was quantified using resazurin (**Figure 3.4A**). Overexpression of either wild-type or mutant CDC14B had no effect on cell viability compared to a GFP plasmid used as a control. Transfection with the CDC14B-targeting siRNAs (CDC14B_11 and _12) reduced cell viability when coupled with overexpression of GFP or CDC14B, both wild-type and mutant. Importantly, there was no significant increase in cell

number in the rescue condition (mutant CDC14B + CDC14B_12) compared to the same siRNA co-transfected with wild-type CDC14B. Having failed to rescue cell viability in IMR32 cells, the same experiment was performed in KELLY and HEK-293T cells (**Figure 3.4B+C**). Transfection with the CDC14B-targeting siRNAs reduced cell viability in KELLY, and to a much lesser extent, HEK-293T cells as expected. However, as with IMR32 cells, cell viability could not be rescued by overexpressing siRNA-resistant mutant CDC14B.

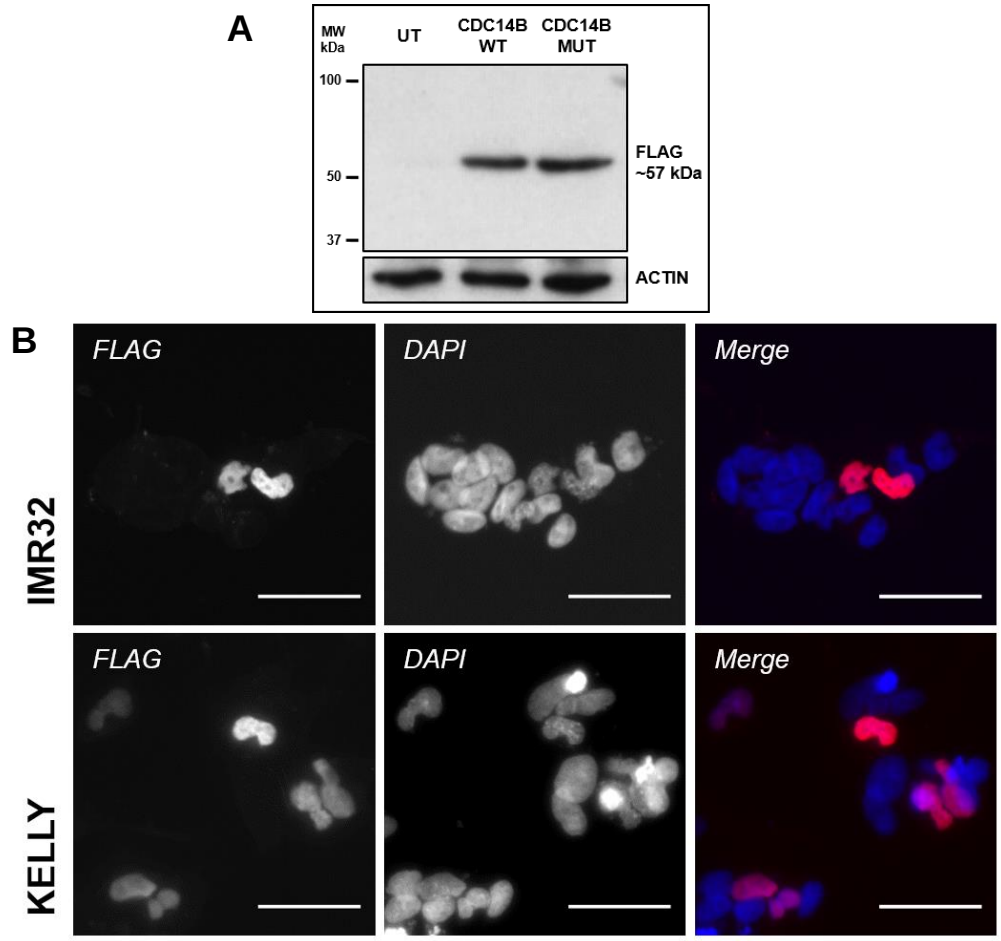

Figure 3.3 – CDC14B overexpression plasmids expressed protein of the correct size and intracellular location

***A** – Western blotting using an anti-FLAG antibody (β actin loading control) showing overexpression of FLAG-tagged wild-type (WT) and siRNA-resistant mutant (MUT) CDC14B in HEK-293T cells. **B** – IF microscopy of IMR32 (top) and KELLY (bottom) cells overexpressing FLAG-tagged wild-type CDC14B, showing nuclear localisation. Red, anti-FLAG; blue, DAPI. Scale bar = 50 µm.*

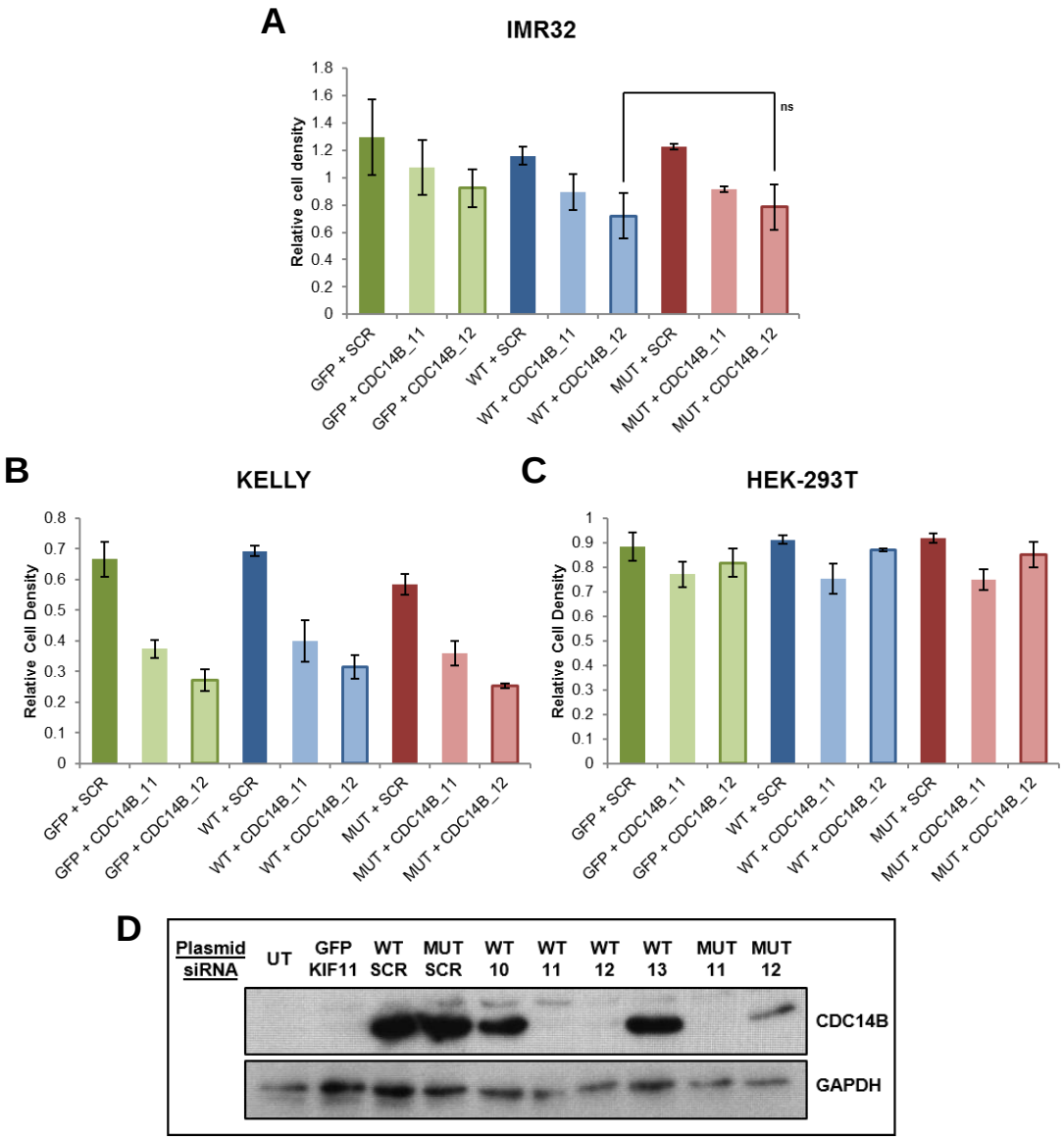

Figure 3.4 – Cell viability could not be rescued using a CDC14B rescue plasmid
A *- IMR32 cells were co-transfected with plasmid DNA (GFP, wild-type CDC14B (WT), or siRNA-resistant mutant CDC14B (MUT)) and siRNA (non-targeting scrambled (SCR), or CDC14B-targeting (11+12)). Cell density after 6 days was quantified using resazurin. Cell viability was not rescued using overexpression of mutant CDC14B. ANOVA with Bonferroni post hoc, ns=not significant (n=3).* ***B+C*** *– The same rescue experiment in KELLY cells assayed after 6 days* ***(B)****, and HEK-293T cells assayed after 4 days* ***(C)****. No rescue of cell viability observed (n=1).* ***D*** *– HEK-293T cells were co-transfected with plasmid DNA (GFP, WT CDC14B, MUT CDC14B) and siRNA (SCR, or CDC14B-targeting (10-13)). Whole cell protein lysates were analysed by western blotting using an anti-CDC14B antibody (GAPDH loading control), showing a degree of CDC14B protein rescue in the rescue condition (right hand lane).*

Western blotting for CDC14B was performed in HEK-293T cells co-transfected with plasmid CDC14B and siRNA in order to confirm that CDC14B protein was being rescued using this system (**Figure 3.4D**). CDC14B was detected in cells transfected with both wild-type and mutant constructs. Wild-type CDC14B was co-transfected with all four CDC14B-targeting siRNAs, however only CDC14B_11 and CDC14B_12 were able to prevent protein expression. This difference in apparent knockdown efficiency between siRNAs is in contrast to that which was measured by qPCR in IMR32 cells, but interestingly does somewhat correlate with their ability to cause reduction in cell viability (**Figure 3.2**). Mutant CDC14B was co-transfected with CDC14B_11 and _12. There was a low level of CDC14B protein expression in the rescue condition (final lane) suggesting that at least some protein expression can be rescued using this system. The level of CDC14B expression is still much lower here compared to the scrambled lane, even considering the slight under-loading in the final lane (evident from GAPDH loading control). This suggests that CDC14B_12 is still able to partially knockdown the siRNA-resistant CDC14B. However, expression is higher than in untreated cells, in which CDC14B was not detectable by western blotting here. This western blotting analysis confirmed that CDC14B protein expression could, to an extent, be rescued using the mutant plasmid in HEK-293T cells. However, I had difficulty showing that these plasmids were expressed at detectable levels by western blotting in the neuroblastoma cell lines. This made it difficult to ascertain whether the mutant plasmid could reliably rescue CDC14B protein expression in neuroblastoma cells, and therefore stand a chance against the siRNA at rescuing cell viability.

3.2.3. GFP-CDC14B fusions do not rescue cell viability

The difficulties in proving CDC14B overexpression in neuroblastoma cells described above led me to clone the *CDC14B* sequences into a GFP expression plasmid (**Figure 2.4**). This GFP plasmid also utilises a CMV promoter, however as other members of the laboratory and I had previously seen consistently good GFP expression in neuroblastoma cells using this plasmid, we hoped this approach would improve CDC14B expression.

Additionally, cloning the CDC14B constructs in frame to GFP meant that CDC14B proteins were now tagged with GFP, allowing detection using fluorescence microscopy, thus straightforward visualisation of the frequency of transfected cells.

CDC14B wild-type and siRNA-resistant mutant sequences were cloned in frame into the GFP expression plasmid. These were then transfected into HEK-293T, KELLY and IMR32 cells. After 24 hours, green fluorescence could be detected in all lines transfected with both plasmids (**Figure 3.5A**). Both the frequency of transfected cells, and the fluorescence intensity was highest in HEK-293T cells. Transfection and expression efficiency of both plasmids was much lower in the neuroblastoma cell lines, particularly wild-type CDC14B in IMR32 cells, however GFP could be detected in all cases. Western blotting for CDC14B was carried out using protein lysates from these transfections (**Figure 3.5B**). Unfortunately there is a background band running through the centre of the blot, however it is clear that in HEK-293T cells transfection with both the original wild-type CDC14B plasmid, and the wild-type and mutant GFP-tagged versions resulted in clearly detectable CDC14B expression. In previous experiments, I had not been able to detect CDC14B expression when neuroblastoma cells where transfected with the original CDC14B plasmids (non-GFP-tagged), however, in this experiment expression was detected in both KELLY and IMR32 cells. Furthermore, GFP-tagged CDC14B could be detected in both cell lines, although it seems that cloning them into the GFP vectors actually reduced expression rather than enhancing it.

Despite the fact that the GFP cloning did not appear to have improved CDC14B overexpression in neuroblastoma cell lines, these plasmids were used in a phenotypic rescue experiment in IMR32 cells. IMR32 cells were co-transfected with the GFP-CDC14B plasmids and the CDC14B-targeting siRNAs. After 24 hours, GFP expression was assessed using fluorescence microscopy and protein lysates were collected for western blotting to detect CDC14B expression (**Figure 3.6A+B**). The frequency of GFP positive cells was low, in particular for wild-type CDC14B. However, CDC14B-targeting siRNAs were able to reduce GFP (and therefore CDC14B) expression for the wild-type plasmid. In the case of the mutant GFP-CDC14B plasmid,

CDC14B_10 and _11 dramatically reduced GFP expression, however as predicted CDC14B_12 (the siRNA which the mutant plasmid was designed to be resistant to) did not. Less GFP knockdown was also observed in cells co-transfected with CDC14B_13, which was the siRNA that gave virtually no phenotypic response (**Figure 3.2D+E**). Western blotting for CDC14B correlated with the above analysis (**Figure 3.6B**). Briefly, overexpression using wild-type GFP-CDC14B was very weak, but was knocked down using all four siRNAs. Expression of the siRNA-resistant mutant plasmid was stronger, and could be knocked down with CDC14_10, _11 and to a lesser extent _13, but not CDC14B_12.

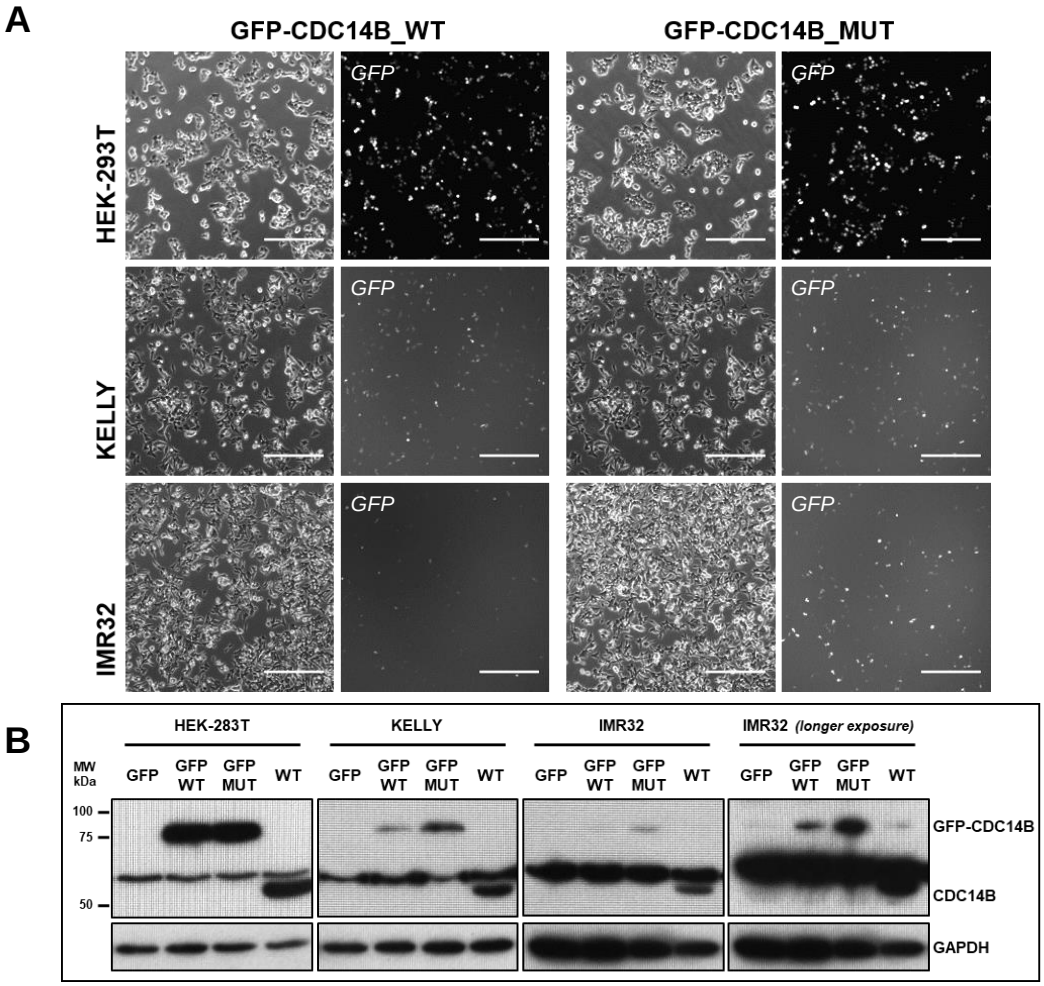

Figure 3.5 – GFP-tagged CDC14B is expressed in neuroblastoma cells
HEK-293T, KELLY and IMR32 cells were transfected GFP-tagged wild-type (WT) and siRNA-resistant mutant (MUT) CDC14B expression plasmids. ***A*** *– GFP-tagged CDC14B was detected by green fluorescence. Scale bar = 300 µm.* ***B*** *- Whole cell protein lysates were analysed by western blotting using an anti-CDC14B antibody (GAPDH loading control), showing varying levels of CDC14B expression in each cell line. Note: non-GFP-tagged wild-type CDC14B lysates were included and ran at a lower molecular weight due to absence of GFP.*

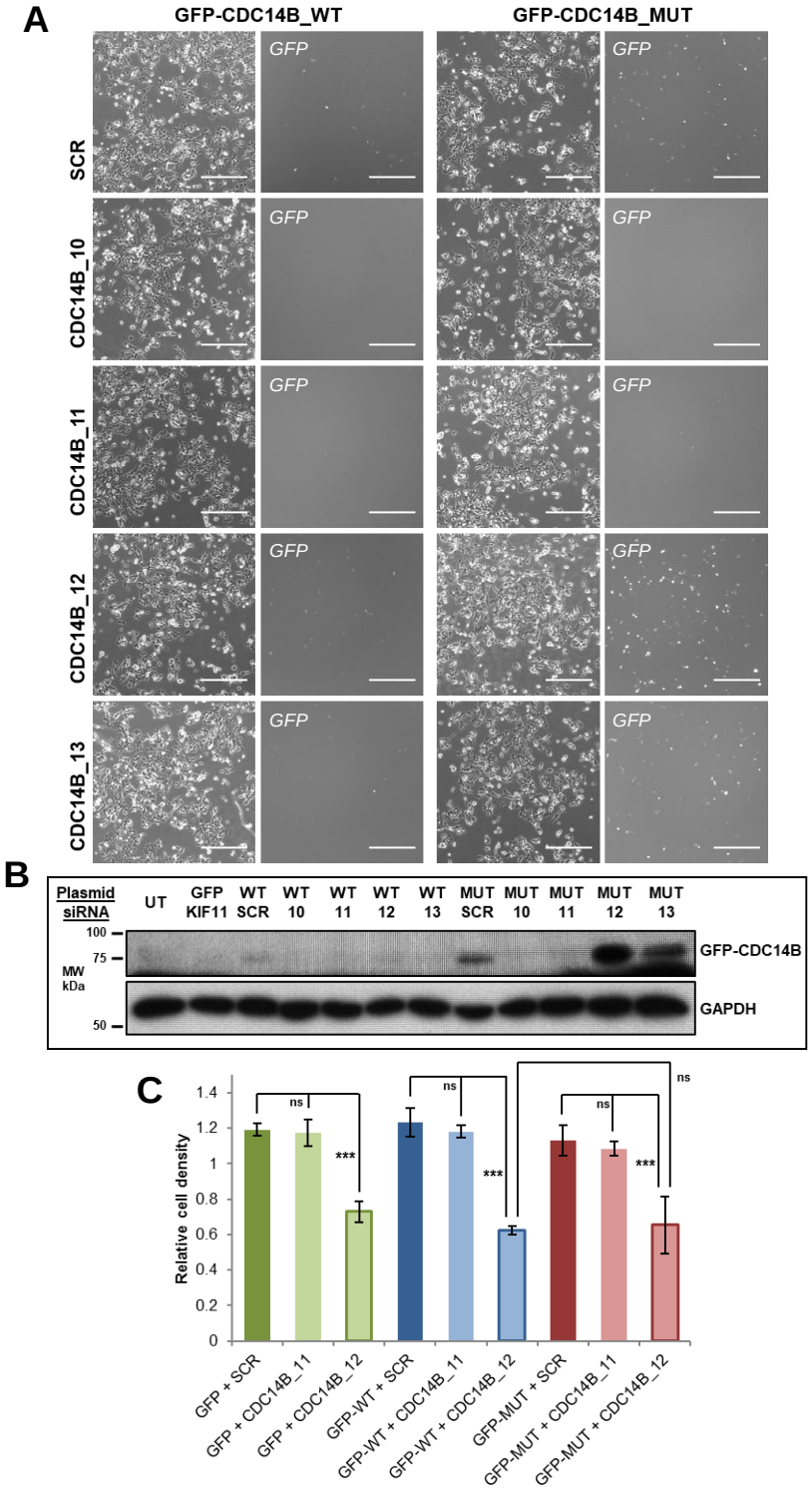

Figure 3.6 – GFP-tagged siRNA-resistant CDC14B could not rescue cell viability
IMR32 cells were transfected with GFP-tagged wild-type CDC14B (GFP-CDC14B-WT), siRNA-resistant mutant CDC14B (GFP-CDC14B-MUT) or GFP only vectors in combination with scrambled (SCR) non-targeting and CDC14B-targeting (CDC14B_10-13) siRNAs. ***A*** *– GFP fluorescence was imaged showing reduced GFP-CDC14B expression in the CDC14B siRNA knockdown conditions, but not in the rescue condition (GFP-CDC14B-MUT + CDC14B_12). Scale bar = 300 µm.* ***B*** *- Whole cell protein lysates were analysed by western blotting using an anti-CDC14B antibody (GAPDH loading control), showing CDC14B protein levels in transfected cells, including protein rescue in the GFP-CDC14B-MUT + CDC14B_12 lane.* ***C*** *– IMR32 cell viability 3 days after co-transfection assayed using resazurin, showing no rescue of cell viability. ANOVA with Bonferroni post hoc, ns=not significant, *** p<0.001 (n=3).*

These data indicated that the CDC14B rescue system can work correctly in neuroblastoma cells at the protein level. The GFP-CDC14B plasmids were used to repeat the phenotypic rescue experiment in IMR32 cells (**Figure 3.6C**). Unfortunately, as was the case for the original rescue experiments (**Figure 3.4A-C**), there was no difference in cell viability between cells transfected with CDC14B_12 alongside the wild-type compared to the siRNA-resistant mutant plasmid.

3.2.4. CRISPR/Cas9 can be used to target genomic CDC14B

The initial siRNA experiments (**Section 3.2.1.**) had shown promising data to support an oncoprotein-like role for CDC14B in neuroblastoma. Therefore, in parallel to the rescue experiments described above, gene editing was used to provide additional support for this hypothesis. CRISPR/Cas9 technology was used to knockout the *CDC14B* gene in IMR32 cells. This approach involved attempting to edit genomic *CDC14B* in neuroblastoma cells such that functional protein is not produced and therefore the gene is effectively knocked out. During CRISPR/Cas9-mediated gene editing, a bacterial endonuclease, Cas9, is introduced into cells, which creates double stranded breaks (DSBs) in DNA. Cas9 is directed to specific loci within the genome by small guide RNAs (gRNAs) that can be designed against any gene in the genome. Cells attempt to repair these DSBs via two main pathways, homology directed repair (HDR) or non-homologous end joining (NHEJ). In the absence of template DNA, as was the case for the CRISPR/Cas9 experiments described here, the NHEJ pathway is employed. This is an error-prone repair pathway, thus small insertions and deletions (indels) are introduced which in some cases cause frameshifts and premature stop codons, and therefore gene knockout (Ran et al., 2013).

CDC14B has three known isoforms in humans (**Figure 3.7A**). Isoform 2 is the longest, isoform 1 is identical except that it lacks exon 13, and isoform 3 differs only in a 5' exon. Three CDC14B-targeting guides were used in this study that target exons 2, 3 and 4, which are shared by all three isoforms. These guide targeting regions are all within the 5' core domain, upstream of the PTP catalytic motif (**Figure 3.7B**). Guides were designed using the online guide

design tool from the Zhang group at MIT (http://crispr.mit.edu), which scores potential guide sequences based on the likelihood that they will generate off-target editing events. Guide sequences that target exons towards the 5' end of the gene were favoured as frameshift in these exons will disrupt a larger proportion of the gene, minimising the chance of generating truncated, but fully or partially functional protein. Specific protospacer adjacent motif (PAM) sequences, NGG in the case of *S. pyogenes* Cas9, must occur in the target sequence immediately after the end of the gRNA sequence. This can restrict guide design, and in the case of *CDC14B* there were very few appropriate sequences that had good off-target scores and targeted at the 5' end of the gene. Nonetheless, three suitable gRNA sequences were identified (Guide 2, 3 and 4, **Table 2.7**).

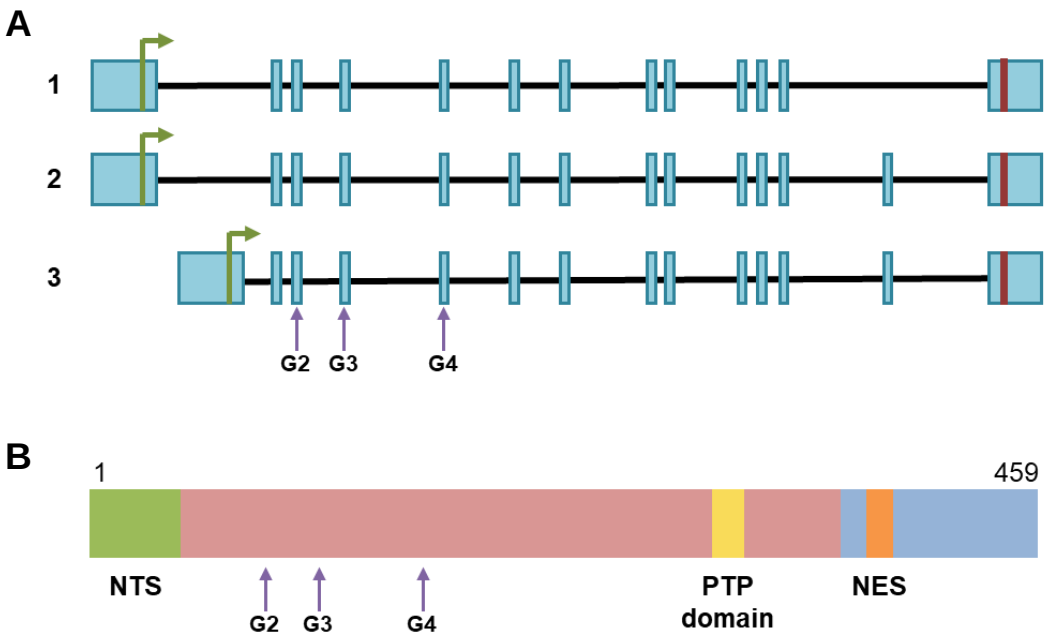

Figure 3.7 – CDC14B guide targeting
A *- Schematic showing the three human CDC14B isoforms. CDC14B-targeting guides 2, 3 and 4 (G2, G3, G4) target the 3rd, 4th and 5th exons respectively, which are common to all isoforms.* ***B*** *– CDC14B protein domain structure. Nucleolar targeting sequence (NTS), green; core domain containing guide-targeting regions, red; PTP catalytic motif, yellow; C-terminal domain, blue; nuclear export signal (NES), orange. Modified from Gray et al. (2003) and Mocciaro and Schiebel (2010).*

Initially guides 2 and 3 were cloned into the PX458 plasmid (Addgene #48138), which contains the gRNA scaffold with Bpi1 cloning sites for inserting the target specific sequences, the Cas9 gene and a GFP reporter gene. These plasmids were transfected into HEK-293T and IMR32 cells, and imaged for GFP expression after 48 hours (**Figure 3.8A**). Whilst GFP was detected in both cell

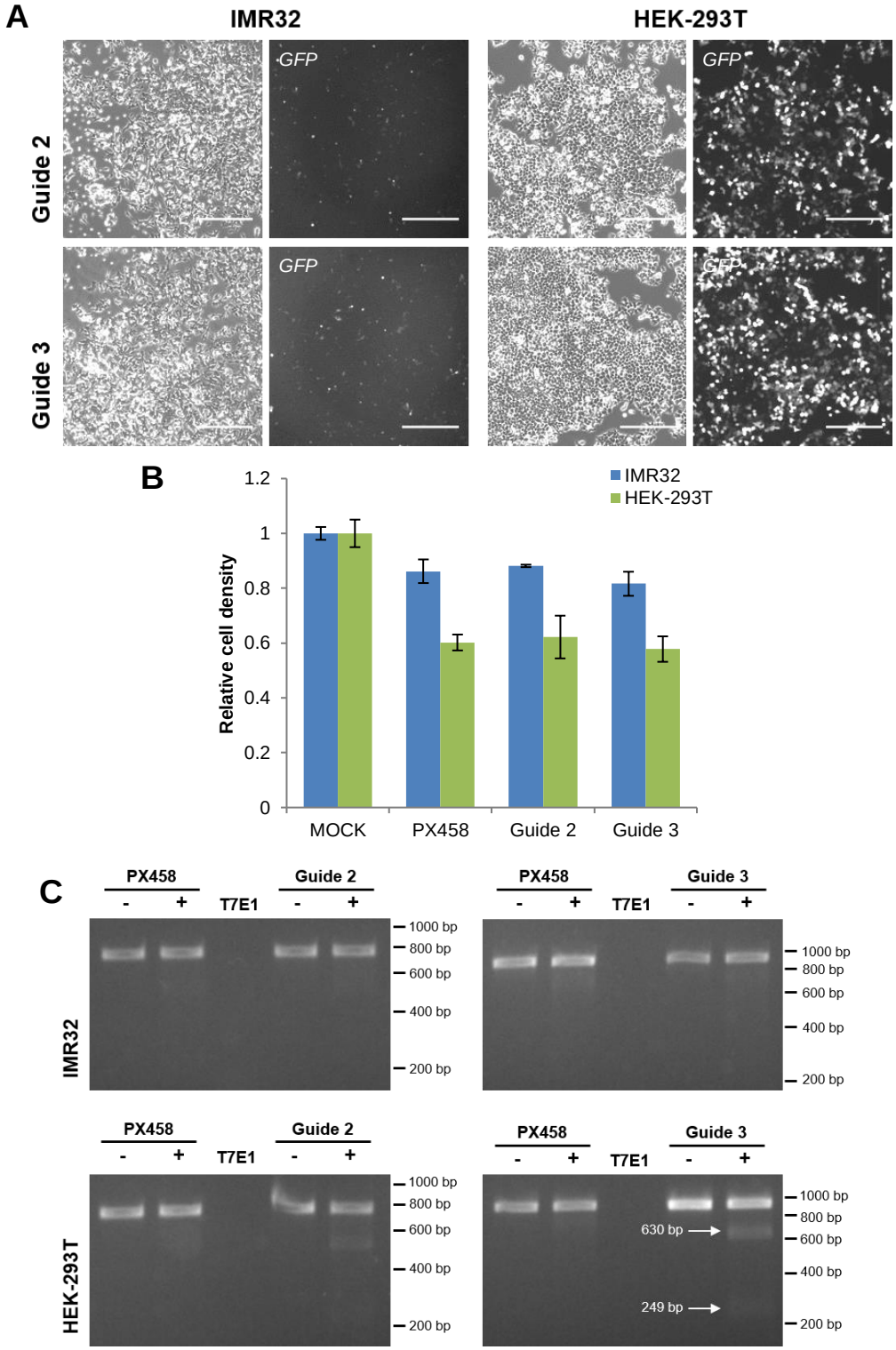

Figure 3.8 – CRISPR/Cas9 can be used to edit genomic CDC14B
IMR32 and HEK-293T cells were transfected with PX458 plasmids containing CDC14B-targeting guide 3 and 4. ***A*** *– GFP fluorescence microscopy showing that both plasmids were expressed in both cell lines, although there was much stronger expression in HEK-293T cells. Scale bar = 300 µm.* ***B*** *– Resazurin assay showed no effect on cell viability 3 days after transfection with CDC14B-targeting plasmids compared to the PX458 plasmid with no gRNA targeting sequence (n=1).* ***C*** *– T7E1 assay showed gene editing in HEK-293T cells (bottom), but not IMR32 cells (top), transfected with CDC14B-targeting plasmids. The digested bands are of the predicted size for guide 3 but not for guide 2 (predicted digested lengths in bp indicated)*

lines, confirming CRISPR/Cas9 machinery expression, the signal was much higher in HEK-293T cells. If CDC14B is required for cell survival, cells in which CDC14B is knocked out by CRISPR/Cas9 should have reduced viability and/or growth rate. IMR32 and HEK-293T cells were assayed for cell viability using resazurin three days after transfection with the guide 2 and 3 plasmids, as well as empty PX458 with no guide targeting sequence (**Figure 3.8B**). There was a reduction in final cell number in both cell lines transfected with the CRISPR/Cas9 plasmids. However, there were no significant changes in cell viability in either cell line when CDC14B-targeting plasmids were compared to empty PX458 using these pooled cultures.

In order to confirm that these plasmids were inducing gene editing, genomic DNA was extracted from IMR32 and HEK-293T cells 48 hours after transfection with PX458 plasmids. Guide targeted regions were amplified by PCR and a T7E1 assay was used to assess editing efficiency (**Figure 3.8C**). Faint digested bands of the predicted size can be seen in HEK-293T cells transfected with guide 3 plasmids (predicted digested fragments were 630 and 249 base pairs long), suggesting that this guide sequence is capable of inducing gene editing. A faint band below that of the undigested PCR product can also be seen in HEK-293T cells transfected with the guide 2 plasmid; however, this does not correlate with the predicted band sizes (616 and 118 base pairs). Convincing gene editing was not detected in IMR32 cells, perhaps not surprising given the comparatively low GFP signal.

The data shown so far indicate that guide 3 is able to induce *CDC14B* gene editing in HEK-293T cells, however plasmid expression is perhaps too low to detect editing in IMR32 cells. The GFP reporter in the PX458 plasmid can be used to select for successfully transfected cells, therefore enriching the population for cells that are expressing the CRISPR machinery. IMR32 cells were transfected with the guide 3 plasmid, or with empty PX458, and GFP expression was confirmed after 48 hours using fluorescence microscopy (**Figure 3.9A**). After which cells were sorted for GFP expression using FACS. GFP-positive cells were sorted both into a group population and into single cell cultures in 96 well plates, which were propagated into clonal cultures. Both the

group and clonal cultures could then be used to assess editing efficiency, and for growth assays (**Figure 3.10**).

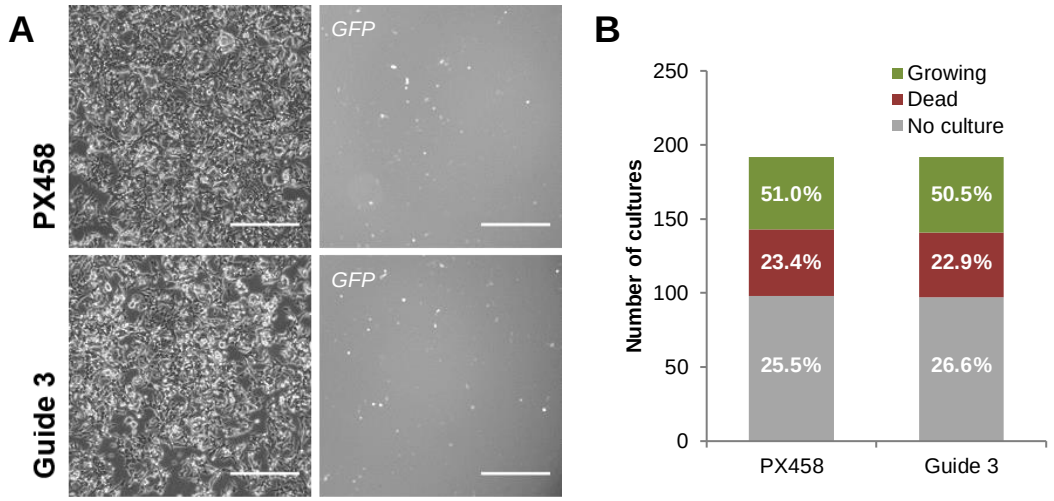

Figure 3.9 – CDC14B CRISPR/Cas9 targeting did not effect single cell recovery
IMR32 cells were transfected with empty PX458 and PX458 containing CDC14B-targeting guide 3. ***A*** *– GFP fluorescence confirming plasmid expression 48 hours post transfection.* ***B*** *– GFP-positive cells were single cell sorted into 96 well plates. After 12 days, clonal cultures were assessed for viability and scored as growing, dead, or no culture, where no cells could be seen. The number of cultures in each state was virtually identical between PX458 and guide 3 cultures (n=1).*

If CDC14B does promote growth and survival in neuroblastoma cells, including the IMR32 cells used in these experiments, it is possible that knockout was lethal to cells and therefore many of the edited cells did not survive. The number of clonal cultures that were successfully recovered from single cell sorting, and that were still growing 12 days after the sort, for both targeted and non-targeted cells were counted (**Figure 3.9B**). There was virtually no difference in the number of growing cultures, with 49 and 51 out of 192 cultures surviving in PX458 and guide 3-transfected cells respectively. The guide 3-targeted clonal cultures were expanded over a period of around 6 weeks, at which point gDNA was extracted and used in T7E1 assays to assess gene editing. Initially gDNA was pooled into groups of four to allow screening for edited cells. Four out of five of these groups displayed gene editing and were subsequently de-convoluted to allow individual cultures with successful gene editing to be identified (**Figure 3.11A**). Group cultures for both empty PX458 and guide 3 were also included in this T7E1 analysis. Six, CDC14B-targeted clonal cultures showed gene editing in this assay at a range of efficiencies, these are referred to as 4D10, 4F10, 4D11, 4F7, 3F10 and 3G9.

Morphologically these cultures appear very similar to wild-type IMR32 cells and to IMR32 cells transfected with empty PX458 (**Figure 3.11B**). Growth assays were performed using these cultures to assess whether gene editing had any effect on the rate of proliferation (**Figure 3.11C+D**). These data show that there were no significant differences between the rates of proliferation in the CDC14B-edited cells compared to wild-type IMR32 cells.

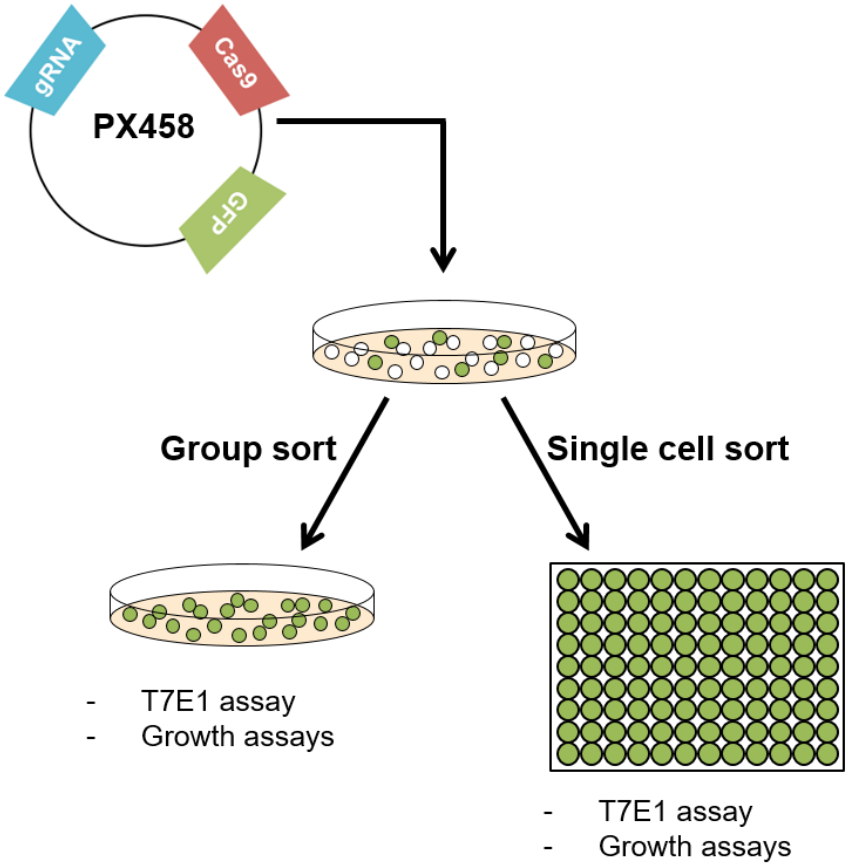

Figure 3.10 – GFP sorting can be used to select PX458 transfected cells
IMR32 cells were transfected with PX458 plasmids with and without CDC14B-targeting guide 3. After 48 hours, cells were GFP-sorted by FACS. GFP-positive cells were sorted into a mixed population and single cells. Both mixed population and single cell cultures were expanded and used for growth assays and T7E1 assays to estimate editing efficiency.

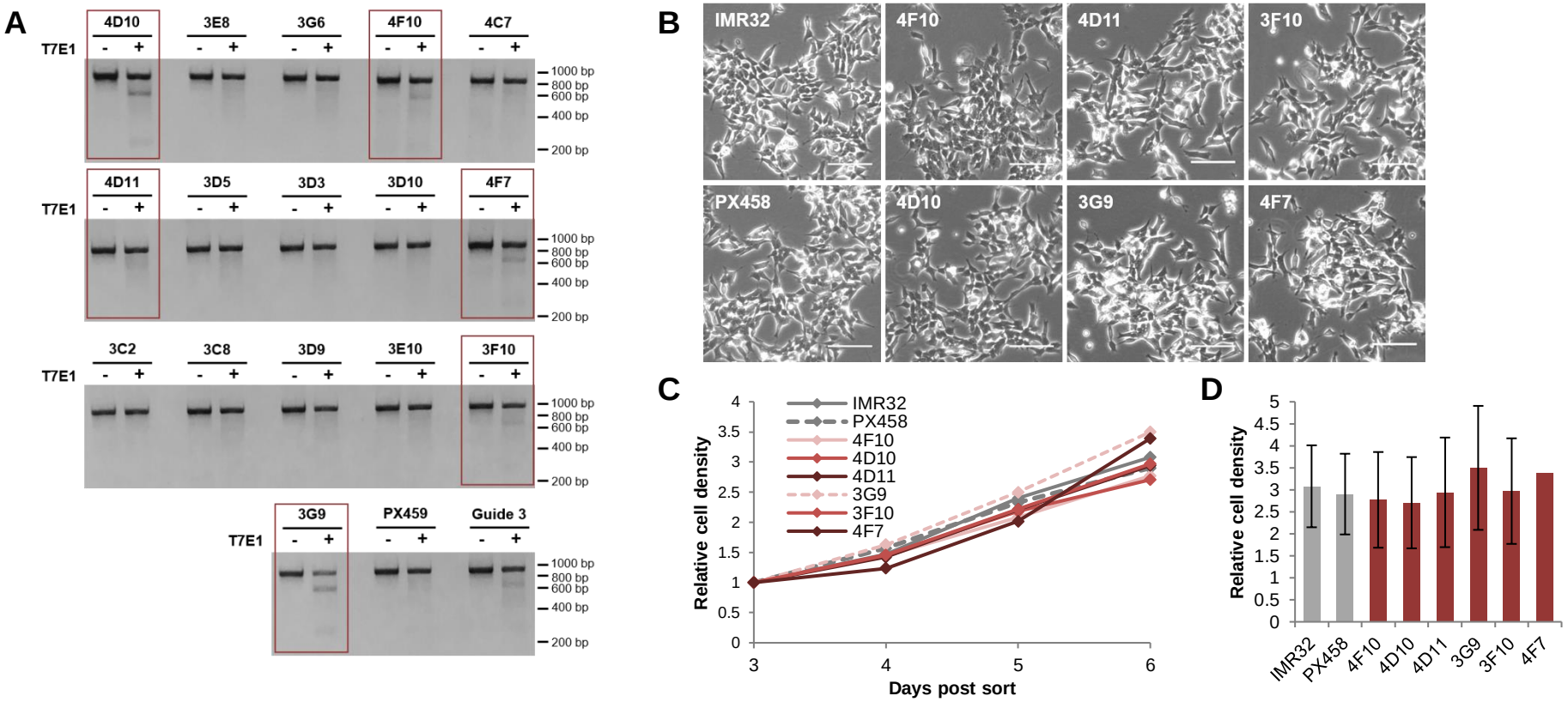

Figure 3.11 – CDC14B editing did not correlate with reduced proliferation in single cell cultures

IMR32 cells transfected with guide 3 PX458 plasmid where sorted for GFP 48 hours post transfection. GFP-positive cells were seeded as single cell cultures, and expanded. ***A*** *– T7E1 assay to assess the degree of CDC14B-editing in clonal cultures. Group empty PX458 and guide 3-targeted cultures were also included. 6 out of 16 single cell cultures had detectable on-target editing (red boxes).* ***B*** *– Phase-contrast microscopy of CDC14B-edited clonal cultures. No observable differences in morphology compared to parental, wild-type IMR32 cells and empty PX458 transfected cells.* ***C+D*** *– Resazurin growth assays showed no differences in growth between the CDC14B-edited single cell cultures and parental IMR32 cells (n=3, n=1 for 4F7).* ***C*** *– Resazurin assays from day 3 to 6.* ***D*** *- Difference in cell density between 3 and 6 days after seeding.*

3.2.5. Inducible Cas9 expression can be used to target the CDC14B gene

The initial CRISPR/Cas9 experiments performed using guides targeting *CDC14B* did not provide any data to suggest that gene editing reduced cell viability, however there had been problems expressing the CRISPR machinery at a high level in neuroblastoma cells. A post doc in the group, Dr. Vruti Patel, had also recently developed an inducible CRISPR/Cas9 system whereby Cas9 expression is under the control of a tetracycline-on (TET-On) system. The advantage of this system is that an IMR32-derived cell line was created with inducible Cas9 expression, into which a plasmid containing the gRNA with a selectable puromycin marker is transfected. Therefore, following puromycin selection, all cells in the population should express both Cas9 and gRNA.

The edit-R inducible lentiviral Cas9 expression vector from Dharmacon was used to create the Cas9 inducible IMR32 cell line. In this vector, the Cas9 gene is downstream of a tetracycline response element (TRE). A reverse tetracycline-controlled transactivator (rtTA) is constitutively expressed from the same plasmid and binds to the TRE, suppressing Cas9 expression. When a tetracycline antibiotic, in this case doxycycline, is applied, rtTA dissociates from the TRE, thereby allowing Cas9 gene expression (**Figure 3.12A**). It is important that the regulation of Cas9 expression is very tight so that gene editing does not occur prior to induction. Historically TET-On systems have been reported to be leaky, however this vector uses the Tet-ON 3G® system, which has optimised spacer sequences within the TRE resulting in reduced background expression and therefore very tight regulation of gene expression (Loew et al., 2010).

Dr. Patel created an IMR32-derived, Cas9-inducible cell line named 2E11 (**Figure 3.12B**). Briefly, IMR32 cells were transduced with the Edit-R inducible lentiviral Cas9 expression vector and selected using blasticidin. These cells were seeded as single cells and clonally expanded. Resulting clonal cell lines were tested for Cas9 inducibility and transfection efficiency, and 2E11 was selected as the most useful cell line to take forward. For gene editing, a second expression vector (pU6-sgRNA EF1Alpha-puro-T2A-BFP, Addgene #60955,

referred to as pU6 from this point on) was used to express gRNAs (Gilbert et al., 2014). Gene specific gRNAs can be cloned into this vector, but the original plasmid contained GFP-targeting gRNA, which was used to test the inducible Cas9 system. Dr. Patel transfected 2E11 cells with GFP or GFP and the pU6 plasmid, and then induced Cas9 expression with doxycycline (**Figure 3.13A,** figure and data kindly provided by Dr. Patel). 24 hours after induction, a visible reduction in GFP expression could be seen using fluorescence microscopy, confirmed by western blotting for Cas9 and GFP (**Figure 3.13B+C**).

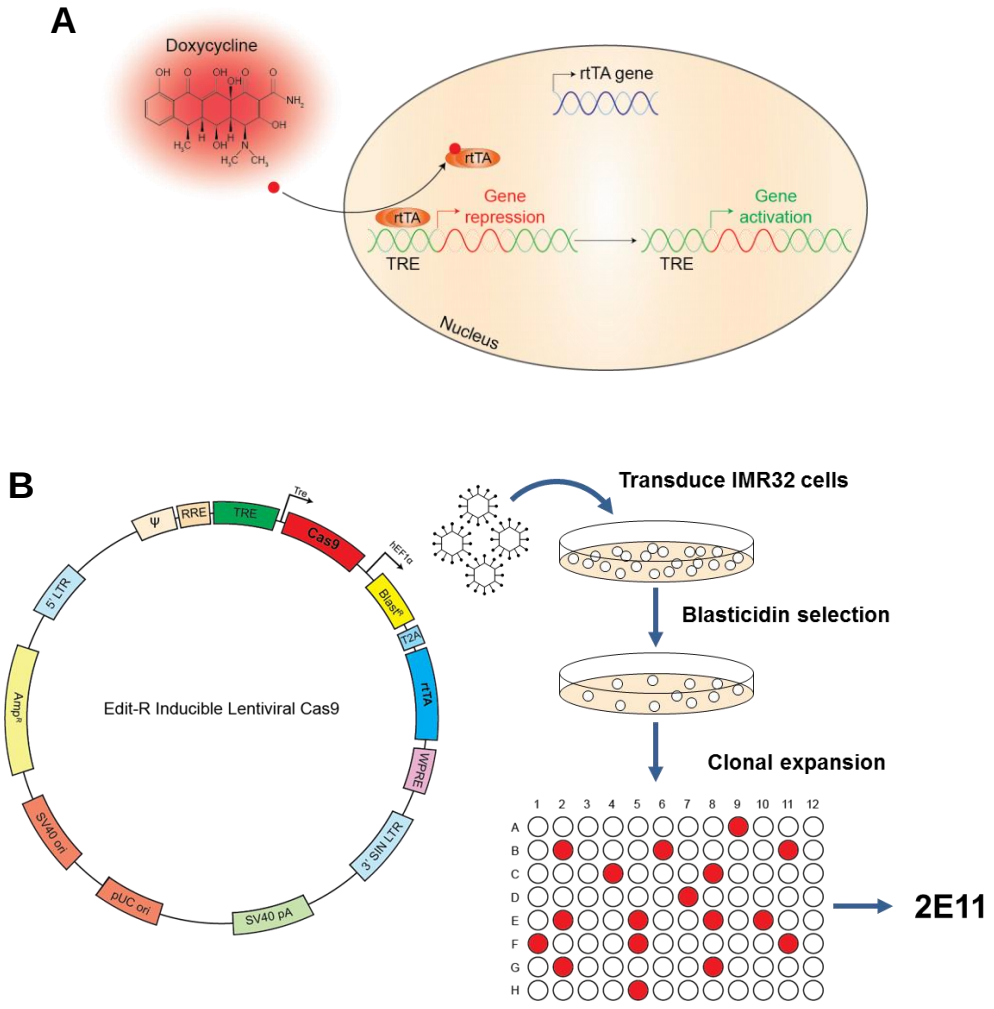

Figure 3.12 – 2E11 was derived from IMR32 cells and has inducible Cas9 expression (Dr. Vruti Patel)
Schematic describing the derivation of a Cas9-inducible IMR32 cell line. ***A*** *– Cas9 expression is under the control of a Tet-ON 3G© system, where reverse tetracycline-controlled transactivator (rtTA) is constitutively expressed and inhibits Cas9 expression. The addition of doxycycline dissociates rtTA from the tetracycline response element (TRE) activating Cas9 gene expression.* ***B*** *– To create the inducible Cas9 cell line, IMR32 cells were transduced with this Edit-R inducible lentiviral Cas9 vector (Dharmacon). Following blasticidin selection, cells were seeded at 1 cell per well into 96 well plates and those that were viable (red) were expanded. 2E11 was the clonal culture chosen to take forward to further experiments.*

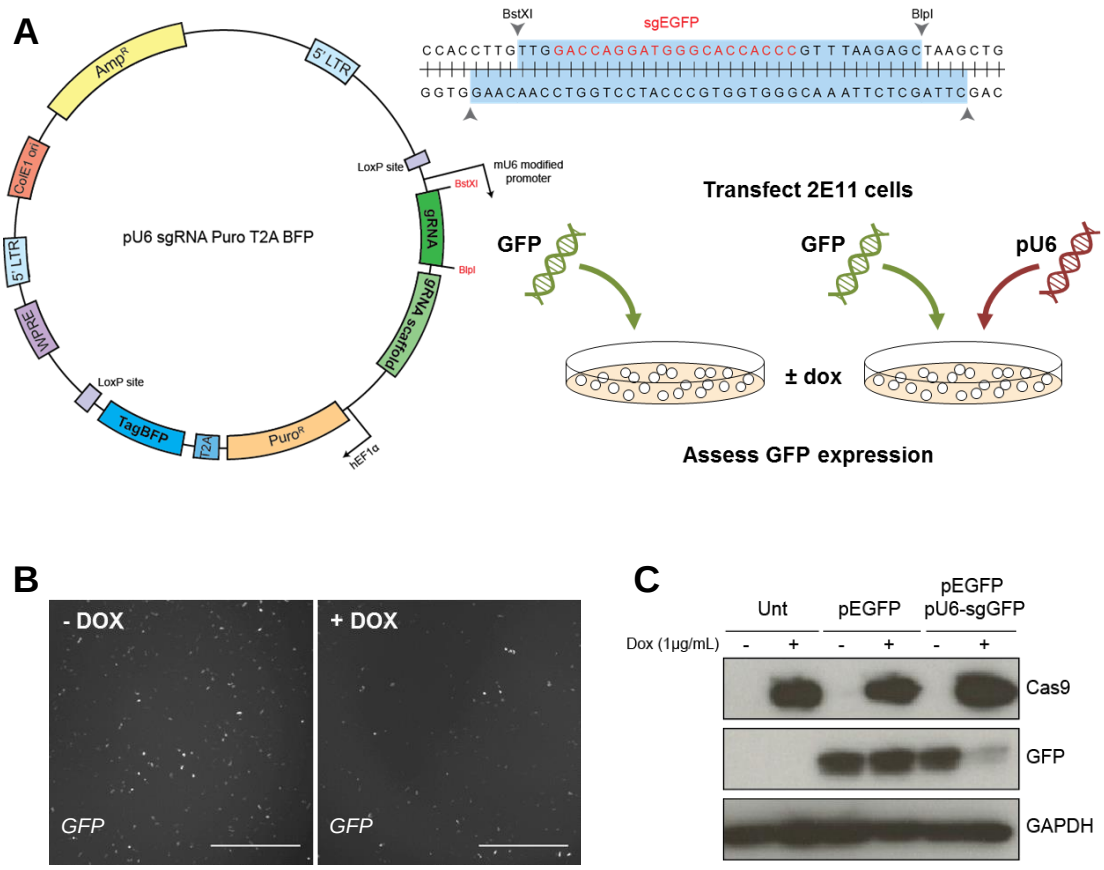

Figure 3.13 – GFP-targeting using the inducible CRISPR/Cas9 system reduced GFP expression (Dr. Vruti Patel)

The pU6 sgRNA Puro T2A BFP plasmid (Addgene #60955) originally contained a GFP-targeting gRNA, which was used to test the CRISPR/Cas9 system in the 2E11 clone. ***A*** *– 2E11 cells were transfected with a GFP expression plasmid +/- pU6 vector (containing GFP-targeting gRNA) +/- doxycycline (DOX).* ***B*** *– GFP expression was reduced in guide-transfected cells treated with doxycycline, assessed by fluorescence microscopy 24 hours post transfection. Scale bar = 300 µm.* ***C*** *– Western blotting using an anti-Cas9 antibody confirmed inducible Cas9 expression, and using an anti-GFP antibody confirmed reduced GFP expression (GAPDH loading control).*

CDC14B-targeting guides 3 and 4 were cloned into the pU6 plasmid utilising the BstX1 and Blpl cloning sites. These plasmids were transfected into 2E11 cells, and puromycin was used to select for transfected cells. 11 days after selection, Cas9 expression was induced for 24, 48 and 72 hours and gDNA was collected. A T7E1 assay was performed to assess gene editing (**Figure 3.14A**). Cleaved bands of the predicted sizes were detected after 48 and 72 hours induction for guide 4 and 3 respectively, indicating that Cas9 expression had been induced and gene editing had occurred. These cells were cultured in puromycin for six weeks in order to create a population with stable gRNA expression. At this stage, another T7E1 assay was performed using cultures where Cas9 expression had been induced for 7 days (**Figure 3.14B**). Very

clear on-target editing could be seen for guide 3 but not guide 4. Growth assays were also carried out using 2E11 cells stably expressing each guide with Cas9 induction for 7 days (**Figure 3.14C**). There was no statistically significant difference in final cell density comparing guide 3- and 4-expressing cells with and without doxycycline (ANOVA with Bonferroni post hoc).

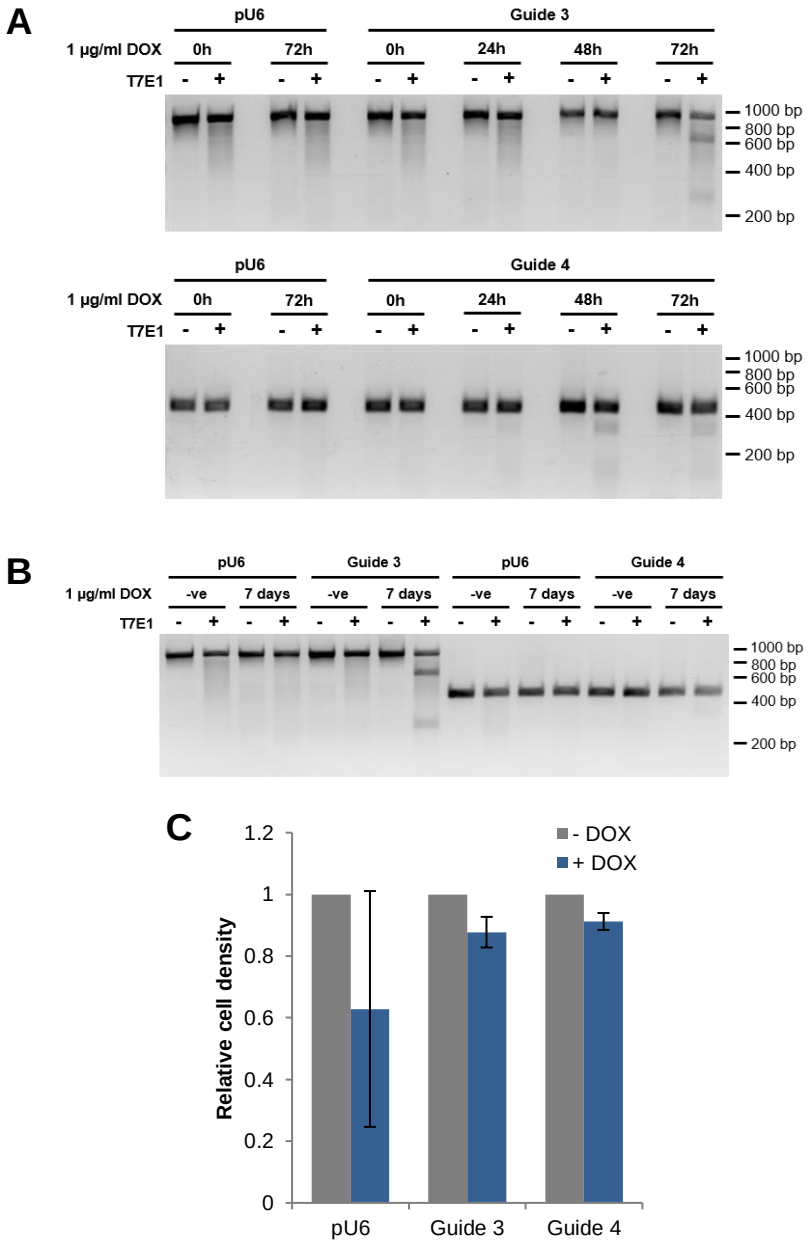

Figure 3.14 – CDC14B gene editing using inducible CRISPR/Cas9 did not reduce cell viability

2E11 cells were transfected with the original pU6 vector, or pU6 with CDC14B-targeting guides 3 and 4. ***A*** *– T7E1 assay to assess editing efficiency 24, 48 and 72 hours after Cas9 induction, confirming on-target editing using guides 3 and 4 (bands at 249 and 630 base pairs for guide 3, and 309 and 129 base pairs for guide 4).* ***B*** *– T7E1 assay after 7 days Cas9 induction in 2E11 cells with stable guide 3 and 4 expression, showing editing with guide 3 but not guide 4.* ***C*** *– Resazurin cell viability assay after 7 days Cas9 induction showing no significant changes in final cell density in pU6, guide 3 and guide 4 cultures with and without doxycycline-mediated Cas9 expression. ANOVA with Bonferroni post hoc, no significant differences (n=3).*

A long-term Cas9 induction experiment was performed where 2E11 cells stably expressing CDC14B-targeting guide 3 or guide 4 were cultured in doxycycline for up to 53 days. Halfway through the experiment, doxycycline was removed from one set of cultures to see if the cells would recover from gene editing. It was hypothesised that if CDC14B knockout is detrimental to cell viability, then when doxycycline is removed and therefore gene editing stops, any wild-type cells in the population will have a growth advantage over edited cells. At multiple time points throughout the experiment cells were fixed and stained with crystal violet (**Figure 3.15A**). As had been observed in the shorter time point experiments previously, there was no effect on cell number in guide 3 and guide 4 cultures when Cas9 expression was induced up to 25 days. From 38 days there were fewer cells in the doxycycline-treated cultures, however the negative controls (parental 2E11 cells, and 2E11 expressing the original pU6 plasmid with GFP-targeting guide) also had a large drop off in cell number. Even 28 days after doxycycline had been removed, no recovery in cell number was observed in any of the cultures. T7E1 analysis was also performed at each time point (**Figure 3.15B**). On-target gene editing was observed in both CDC14B-targeting guide cultures after 10 and 25 days of Cas9 induction. There was no effect on the proportion of CDC14B-edited cells when doxycycline was removed for up to 28 days, suggesting that the wild-type cells had no growth advantage. Interestingly, the proportion of edited cells in the guide 3 cultures did not increase between 10 days all the way to 53 days Cas9 induction. There appears to be a decrease in edited cells across these time points for guide 4 cells, although this is likely to be an artefact of gel loading and imaging.

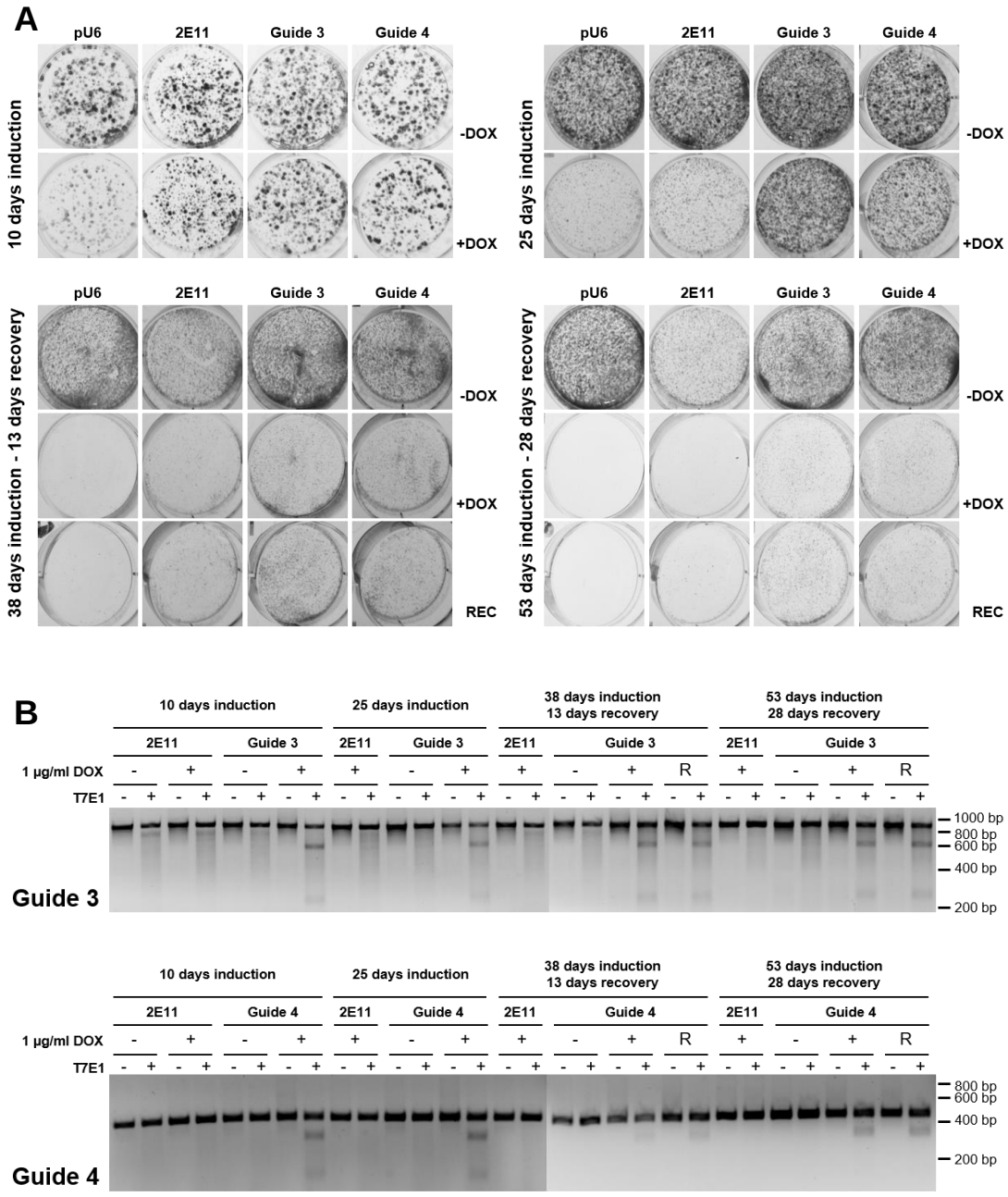

Figure 3.15 – Long-term Cas9 expression did not lead to further CDC14B editing
2E11 cells were transfected with the pU6 vector, or pU6 with CDC14B-targeting guides 3 and 4, and cultured in doxycycline (inducing Cas9 expression) for up to 53 days. After 25 days one set of cultures were left to recover (REC) by removing doxycycline. ***A*** *– Crystal violet staining showed that there was no loss of cell number induced by doxycycline in the CDC14B-targeted cultures greater than that observed in the pU6 and 2E11 negative control cultures. Removing doxycycline (recovery condition) had no effect in any of the cultures.* ***B*** *– T7E1 analysis showed that whilst both guide 3 and guide 4 induced on-target CDC14B gene editing, the degree of edited cells did not increase with time, and there was no difference in proportion of edited DNA in the recovery cultures (R).*

3.3. Discussion

Here I have presented some evidence that silencing specific PTP genes in neuroblastoma cell lines reduces cell viability, suggesting that there are indeed specific PTPs that are critical for neuroblastoma cell survival and proliferation. The shRNA screen performed before I joined the laboratory (A. Cichon and A. Stoker, unpublished) indicated that PTPRN, CDC14B, ACP1 and MTMR12 might have oncogene-like roles in neuroblastoma. Support for an pro-tumour role of PTPRN, CDC14B, ACP1, and to a lesser extent MTMR12 can be found in the literature (MacKeigan et al., 2005, Shergalis et al., 2018, Xu et al., 2016, Chiesa et al., 2011, Sun et al., 2018a, Malentacchi et al., 2005, Alho et al., 2013, Hnia et al., 2012). In my initial siRNA experiments using IMR32 cells, a degree of loss of cell viability or reduced proliferation was observed following PTPRN, CDC14B and ACP1 siRNA targeting (**Figure 3.2A**). CDC14B was selected as the candidate to take forward, as its knockdown provided the most promising data, with at least three out of the four siRNAs causing cytotoxicity in neuroblastoma cells (**Figure 3.2D**). The degree of mRNA knockdown did not fully correlate with the extent of cytotoxicity observed following transfection with the four CDC14B-targeting siRNAs (**Figure 3.2C**), leading to concerns that the loss of neuroblastoma cell viability may have been partially due to off-target events. Western blotting, as well as fluorescence microscopy, revealed that siRNA knockdown efficiency at the protein level did somewhat agree with the observed differences in cell viability (**Figure 3.4D** and **3.6A+B**). However, these data were variable and should be repeated several times further to determine relative protein knockdown for each siRNA with confidence. Importantly, we are now aware that according to cBioportal, *CDC14B* is homozygously deleted in KELLY cells, based on data from the Cancer Cell Line encyclopaedia (Cerami et al., 2012, Gao et al., 2013, Barretina et al., 2012). This somewhat brings into question the loss of viability observed following siRNA-mediated CDC14B knockdown in KELLY cells specifically (**Figure 3.2D**), in particular as we have been unable to detect endogenous protein expression in these cells by western blotting. A siRNA rescue experiment and *CDC14B* gene deletion using CRISPR/Cas9 were performed with the aim of demonstrating that the observed cytotoxicity was indeed an on-

target effect, and that CDC14B has pro-tumour activity in neuroblastoma cells that could be targeted therapeutically. Unfortunately, I was unable to rescue cells from the cytotoxicity observed following siRNA-mediated CDC14B knockdown by overexpression of siRNA-resistant CDC14B. Neither have I been able to report any evidence that *CDC14B* gene loss-of-function using CRISPR/Cas9 leads to reduced proliferation or cell survival in neuroblastoma cells. Although there are some caveats to the approaches used here, which will be discussed below, much more validation would be required to label CDC14B as having oncogene-like properties in neuroblastoma tumour cells.

It was disappointing that neuroblastoma cell viability could not be rescued by co-transfection with the siRNA-resistant CDC14B overexpression plasmid, despite some evidence of protein rescue (**Figure 3.4** and **3.6**). However, the rescue experiment was not without its flaws. Western blotting confirmed that transfection with the CDC14B overexpression vectors resulted in increased protein expression compared to control, untransfected cells (where expression was too low to be detected with the antibody used here). However, the use of GFP-CDC14B fusion constructs revealed that the frequency of transfected cells within the population was low (**Figure 3.5A** and **3.6A**). Therefore, the proportion of cells that are overexpressing CDC14B within the population may not be high enough for rescue effects to be detected in the pooled cell viability assays. A good approach to use in the future would be to create stable CDC14B wild-type and mutant overexpression cell lines and use these to attempt the phenotypic rescue. In this case, all cells should be overexpressing CDC14B. It is also possible that overexpression of CDC14B, above physiological expression levels, had been toxic to neuroblastoma cells. This 'Goldilocks effect' has been reported for other signalling molecules and pathways, where both too much or too little can be detrimental to cells (Wang et al., 2014, Braune and Lendahl, 2016). However, cytotoxicity above normal lipofectamine toxicity was not observed in cells transfected with CDC14B overexpression plasmids, and quantitation of cell viability in the rescue experiments did not generally show reduced viability associated with the overexpression plasmids alone (**Figure 3.4A-C** and **3.6C**). Furthermore, IF microscopy showed that IMR32 and KELLY cells overexpressing wild-type

CDC14B were viable and had apparently healthy nuclei according to DAPI staining (**Figure 3.3B**).

Although phenotypic rescue has been described as the gold standard for on-target validation in RNAi experiments, and in theory it is straightforward, numerous complications could lead to failure. Achieving co-expression of both the overexpression and RNAi constructs can be very challenging. Additionally, protein tags (e.g. the FLAG and GFP tags in the CDC14B vectors) can interfere with protein localisation and function, and unreported alternative gene products that are silenced by RNAi but not accounted for by rescue expression may occur (Ma et al., 2007). Furthermore, the silent mutations used to confer RNAi resistance in rescue vectors do not affect amino acid sequence, but may affect mRNA dynamics (Plotkin and Kudla, 2011). In a study by Datler and Grimm (2013), 19 distinct RNAi constructs were used to silence mitochondrial creatine kinase-1 (CKMT1) expression. In all cases the degree of knockdown correlated with the observed effect of mitochondrial depolarisation, however despite very thorough troubleshooting that addressed all of the complications described above, phenotypic rescue could not be achieved. They concluded that it is unlikely that the observed phenotype is due to off-target effects considering the large number of distinct RNAi constructs used in the study. Instead, they suggest that the failed rescue may be due to a 'Goldilocks effect' as described above. Achieving expression of an RNAi-resistant protein that is equivalent to physiological levels is very challenging. A potential, alternative approach may be to use rapidly advancing base editing technologies to introduce the RNAi resistance mutations into the endogenous gene itself.

CRISPR/Cas9 is an extremely powerful technique that is revolutionising the ways in which gene function can be investigated. In this study, indel disruption using CRISPR/Cas9 was used in an attempt to knockout genomic CDC14B in neuroblastoma cells. Initial experiments used transfection with single plasmids containing genes for *S. pyogenes* Cas9 and CDC14B-targeting gRNAs. Later experiments involved transfecting a Cas9 inducible cell line (developed by Dr. Vruti Patel) with plasmids containing the gRNA sequences. Both systems were successful in editing the *CDC14B* gene (**Figure 3.11A** and **3.14A+B**); however, no difference in cell viability or the rate of proliferation was observed

(**Figure 3.11C+D** and **Figure 3.14C**). Even when Cas9 expression was induced for up to 53 days, no changes in cell viability above those observed for the control cultures were detected (**Figure 3.15A**). Furthermore, when doxycycline was removed, attenuating Cas9 expression and gene editing, there was no recovery of wild-type CDC14B, suggesting there was no survival advantage associated with CDC14B expression (**Figure 3.15B**). These data certainly do not support an oncogenic role of CDC14B in neuroblastoma. However, as for the siRNA rescue experiment, there are a number of experimental challenges to consider.

The targeting strategy used here was to induce frame shift mutations at the 5' end of the *CDC14B* gene that would effectively knockout protein expression (**Figure 3.7**). A significant proportion of cells however are likely to have small in-frame CDC14B indels. These may produce at least partially functional protein, given that indels would be upstream of the catalytic domain, and within linker regions of the protein (**Figure 3.16A**). The online tool SNAP^2 (from the Rost group, Munich, Germany) can be used to predict the likelihood that amino acid substitutions at specific sites will impact on protein function (Hecht et al., 2015). Based on these predictions, it is unlikely that small in frame indels at the guide 3 targeting site will impact on CDC14B activity, however changes at the guide 4 target site may have functional consequences (**Figure 3.16B**). However, importantly, this software was designed to predict the effect of substitutions rather than insertions and deletions. It is also possible that some cells expressed truncated CDC14B due to premature stop codons, although these are unlikely to be functional as CDC14B catalytic activity is mostly encoded by exons 8 and 9 towards the 3' end of the gene (Guillamot et al., 2011). An important limitation of these experiments is that I have not been able to show that homozygous knockout cells, with no functional CDC14B protein, were generated with high efficiency. It is possible that heterozygous knockout cells have no growth disadvantage compared to wild-type cells, therefore if homozygous knockouts are not generated with reasonably high efficiency, overall growth defects will not be detected. If indeed the rate of homozygous knockout generation was low, it is possible that the CRISPR/Cas9 targeted cultures contained largely wild-type and heterozygous knockout cells, with any

low abundance homozygous knockouts quickly dropping out of the population. Similarly, frameshift knockouts may have had the same fate, with only cells with small in-frame indels that do not affect protein function surviving. It was hoped that DNA sequencing of clonal CRISPR/Cas9 cultures (**Figure 3.9** and **3.11**) could address this issue, as if only wild-type and heterozygous clones were recovered then we could perhaps infer that homozygous knockouts were non-viable. However, T7E1 analysis of these cultures revealed a wide range of editing efficiencies. This suggested that the cultures were not clonal and that editing had continued to occur following the single cell sorting, therefore homozygosity could not be determined (**Figure 3.11A**).

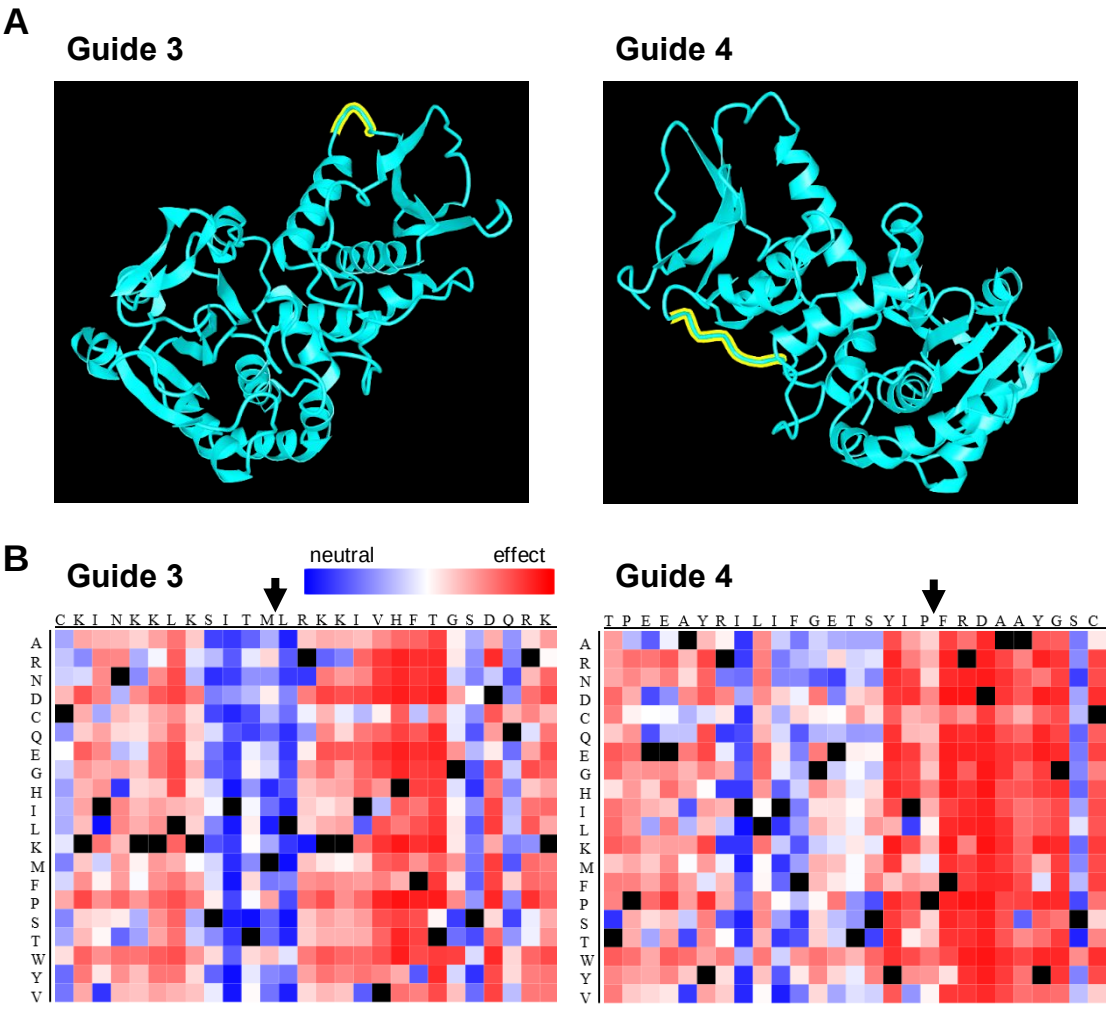

Figure 3.16 – Structural impact of CDC14B-targeting
***A** – Human CDC14B isoform 2 crystal structure from Gray et al. (2003) (PDB ID: 1OHE) visualised using the NCBI web-based 3D structure viewer (iCn3D). Guide 3- (left) and guide 4- (right) targeted regions are highlighted in yellow and are within linker structures. **B** – Functional predictions for amino acid substitutions at guide-targeted regions. Substitutions predicted to have functional consequences are show in red, and neutral changes in blue. Generated using SNAP[2] from the Rost laboratory (Munich, Germany). Predicted CRISPR/Cas9 double stranded break sites marked with arrows.*

Some indirect evidence to support the hypothesis that heterozygous, but not homozygous, CDC14B knockout cells were viable came from the T7E1 analysis of long-term CRISPR/Cas9 induction experiments, where the proportion of edited cells did not increase over the course of the experiment (**Figure 3.15B**). One explanation for this could be that once all cells became heterozygous, or homozygous but with fully or partially functional protein, no further editing could be detected, as cells that acquired additional editing leading to complete CDC14B functional knockout were non-viable. This may also explain the lack of wild-type CDC14B rescue that was observed during the recovery phase of this experiment, because if cells with heterozygous CDC14B deletion do not have a growth disadvantage compared to wild-type cells, there would be no driving force for rescue of wild-type cells. To address these issues, future experiments should involve expanding clonal cultures from targeted populations, sequencing them to identify heterozygous knockouts and retargeting these cells with the same CDC14B gRNAs. In this scenario, a larger proportion of homozygous knockouts should be generated, allowing detection of a drop off in cell number if CDC14B really does have a role in neuroblastoma cell survival. This would also allow sequencing of clonal edited populations, which would allow me to determine whether small in frame indels that likely don't impact on CDC14B functions are occurring, and perhaps being selected for. Due to time limitations and the lack of a clear phenotype with the current CRISPR/Cas9 approaches, I did not prioritise this further.

In this chapter, I have initially presented some data that may point to an oncogene-like role for CDC14B in neuroblastoma, however the validation data do not all currently support this hypothesis and clearly much more validation is required. The lack of agreement between the RNAi and CRISPR/Cas9 data described here could represent a genuine difference in the response of neuroblastoma cells to short-sharp gene knockdown using siRNAs, as opposed to the slower changes brought about using CRISP/Cas9. Several instances where there is a difference in cellular response to gene knockdown verse knockout have been described in various systems (El-Brolosy and Stainier, 2017, Karakas et al., 2007, Morgens et al., 2016). Indeed, a difference in cellular response to RNAi versus germline CDC14B knockout was proposed

by Mocciaro and Schiebel (2010) in a review of functional data relating to mammalian CDC14 proteins. The slower dynamics of the CRISPR/Cas9 approach may allow cells sufficient time to adapt to loss of CDC14B, for example by upregulating other phosphatases including CDC14A, which may have some functional redundancy with CDC14B (Mocciaro and Schiebel, 2010, Mocciaro et al., 2010, Lin et al., 2015). Rossi et al. (2015) reported that knockdown of an extracellular matrix (ECM) gene in zebrafish led to vascular defects, but no phenotype was observed following deleterious mutations in the same gene, due to upregulation of other compensatory ECM genes. They used rescue experiments to confirm that the knockdown effect was not due to off-target effects of RNAi (Rossi et al., 2015). El-Brolosy and Stainier (2017) also suggest that epigenetic changes that occur following DNA damage, including DSBs during CRISPR/Cas9 gene editing, may confer a compensatory response following gene knockout but not knockdown. Alternatively, this apparent difference in cellular response to siRNA-mediated gene knockdown versus CRISPR/Cas9-mediated knockout may be due to an experimental problem with either approach. The most obvious explanation is perhaps that the loss of cell viability observed following siRNA knockdown was due to an off-target effect, in particular because cell viability could not be rescued using overexpression of siRNA-resistant mutated CDC14B. However, importantly we have also shown a growth disadvantage in neuroblastoma cells with shRNA-mediated CDC14B knockdown, with significant depletion of three distinct CDC14B-targeting shRNAs in our pooled dropout screen (A. Cichon and A. Stoker, unpublished, **Figure 3.1B**). Thus two RNAi technologies that utilise distinct biochemistry as well as different CDC14B-targeting sequences, both support a pro-growth or –survival role for CDC14B in neuroblastoma cells. Furthermore, using an online gene expression database (R2: Genomics Analysis and Visualization Platform (http://r2.amc.nl)), high CDC14B expression is correlated with poor prognosis in neuroblastoma patient cohorts, independently of the most common poor prognosis indicator, MYCN status (**Figure 3.17**). Importantly, this correlation does not necessarily confirm CDC14B as an oncogenic, and may alternatively point to a role in drug resistance for example. Based on the data presented here, it is not possible to conclude whether CDC14B really does have pro-tumour activity in

neuroblastoma cells, and if it does, the mechanisms driving this activity remain unclear.

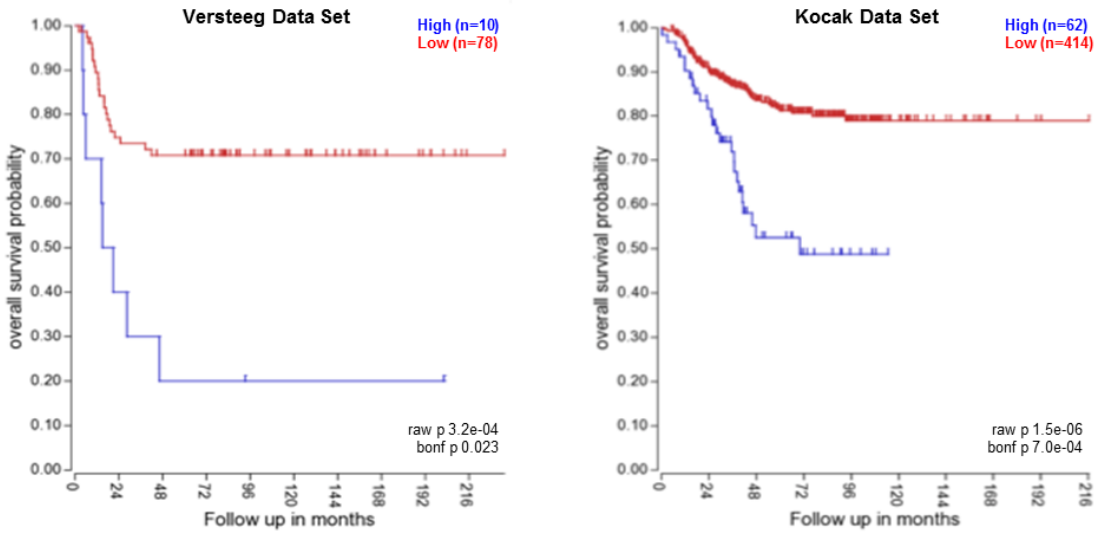

Figure 3.17 – High CDC14B expression correlates with poorer prognosis in neuroblastoma
Kaplan-Meier plots generated using an online genomic analysis platform developed at the Academic Medical Centre, Amsterdam (R2: Genomics Analysis and Visualization Platform (http://r2.amc.nl) with two neuroblastoma patient data sets (Versteeg, left; Kocak, right). High CDC14B expression is show in blue, and low in red.

The precise functions of CDC14B in normal cells, and in particular in cancer, are not entirely clear, however mammalian CDC14B has been implicated in regulating progression through the cell cycle and in DNA damage repair (DDR) (Tumurbaatar et al., 2011, Bassermann et al., 2008, Mocciaro et al., 2010). Bassermann et al. (2008) proposed that CDC14B is involved in activation of the G2 DNA damage checkpoint, whereas Mocciaro et al. (2010) reported that this checkpoint was intact in when CDC14B was knocked out, although the knockout cells did acquire spontaneous DNA damage more frequently and were slower to repair it. The discrepancy between the findings of these studies may be due to the use of siRNA-mediated *CDC14B* gene silencing in the former versus gene knockout in the latter (Mocciaro and Schiebel, 2010). Nevertheless, further support for a role of CDC14B in DDR, if not the G2 checkpoint specifically, comes from Peddibhotla et al. (2011), who showed that CDC14B translocates from the nucleolus from the nucleoplasm following ionising radiation (IR)-induced DNA damage, and Wei et al. (2011) who reported early onset aging and DDR defects in CDC14B knockout mice.

A role in the coordination of DDR during the mammalian cell cycle perhaps logically points to a tumour suppressive, rather than oncogenic, role for CDC14B. Indeed, low CDC14B expression has been reported in breast, prostate, ovary, liver, brain and kidney tumours (Bassermann et al., 2008, Kim et al., 2014). However, there are also data that suggest an oncogenic role for CDC14B. CDC14B overexpression was sufficient to drive transformation of normal murine fibroblasts, with cells displaying disruption of the F-actin cytoskeleton and loss of contact inhibition leading to fibroblasts forming colonies in soft agar. These cells went on to develop tumours when injected into SKID mice or chick embryos (Chiesa et al., 2011). CDC14B overexpression has also been reported in laryngeal carcinoma (LC), where reduced CDC14B expression was coupled to G1/S cell cycle arrest, reduced proliferation and increased apoptosis (Sun et al., 2018a).

Although much of the literature surrounding CDC14B thus far focusses on its possible role in cell cycle regulation and in particular DDR, leading to its tentative labelling as a tumour suppressor, it may have distinct roles during tumour progression. Virtually all cancer cells have mutations that compromise DDR machinery leading to genomic instability, one of the hallmarks of cancer (Knijnenburg et al., 2018, Hanahan and Weinberg, 2011). This leaves tumour cells extremely reliant on other DDR pathways, and targeting these dependencies is being successfully investigated for cancer therapy (O'Connor, 2015). Perhaps neuroblastoma cells are sensitive to CDC14B knockdown due to distinct DDR defects, thus when CDC14B is lost, cells have insufficient repair pathways to prevent mitotic catastrophe and ultimately cell death. In order to have any confidence in this hypothesis and to consider CDC14B as a therapeutic target, substantial further validation of both the oncogenic role of CDC14B in neuroblastoma, and its role in DDR will be required.

Chapter 4. Characterisation of the mechanisms underlying oxidovanadium-induced inhibition of cancer cell phenotypes

4.1. Introduction

The use of vanadium-derived compounds in cancer has been well described, and the anti-cancer effects of these compounds have been reported in numerous preclinical studies using cell-based and animal models of cancer (Evangelou, 2002, Irving and Stoker, 2017) (**Tables 1.3** and **1.4**). As described previously, the vanadate form of the vanadium ion inhibits PTPs; therefore, PTP inhibition is likely to contribute to the anti-cancer efficacy of vanadium-derived compounds (Peters et al., 2003, Crans et al., 2004). Our group have previously reported that global inhibition of PTPs, using the oxidovanadium derivative BMOV, induces cytotoxicity or differentiation in a range of neuroblastoma cell lines (Clark et al., 2013, Clark et al., 2015). BMOV-induced cytotoxicity was at least partially driven by apoptosis, and was enhanced by BSO-mediated glutathione blockade (Clark et al., 2015). These findings provide some support for the hypothesis that there are specific PTPs that are required for cell survival in neuroblastoma. However, as outlined in **Chapter 1**, there are alternative possible mechanisms, other than PTP inhibition, that may be driving oxidovanadium-induced cytotoxicity. Some of these have been addressed previously by our group and are described below (Clark et al., 2015).

As well as PTPs, oxidovanadium compounds can inhibit ion channel ATPases (Nechay, 1984). Clark et al. (2015) reported that ion channel blockage is toxic to neuroblastoma cells. Specifically, both BMOV-sensitive and resistant neuroblastoma cell lines were treated with ouabain and thapsigargin to block Na^+/K^+ and Ca^{++} channels respectively. Cell death was observed in all cell lines, and importantly, the levels of cytotoxicity did not correlate with BMOV sensitivity, suggesting that ion channel inhibition is not the mechanism driving BMOV-induced cytotoxicity. Activation of p53 signalling triggers the expression of a plethora of genes involved in DNA damage and cell cycle regulation, and is considered a hallmark of genotoxicity (Reinhardt and Schumacher, 2012, Zerdoumi et al., 2015). Induction of the p53 response can therefore be used as a marker of genotoxicity in cells following chemical treatment. It is clear from the literature that at high concentrations some specific vanadium compounds

can induce genotoxicity, which may be responsible for their observed cytotoxicity (Huang et al., 2000a, Harding and Mokdsi, 2000, Köpf-Maier et al., 1983). However, p53-mutant KELLY cells are sensitive to BMOV, therefore BMOV sensitivity in neuroblastoma cell lines does not correlate with p53 status. Additionally, there was no induction of p53 protein expression when neuroblastoma cells were treated with BMOV (Clark et al., 2015). This suggests that genotoxicity is not a factor contributing to BMOV-induced cytotoxicity in neuroblastoma cells. Mutations in p53 and related pathways are common in relapsed neuroblastoma (Carr-Wilkinson et al., 2010, Tweddle et al., 2001). Thus, the fact that oxidovanadium-induced cytotoxicity appears to be independent of p53 may prove to be an advantage, as both relapsed and primary neuroblastoma may respond to oxidovanadium-based therapy.

As has been previously mentioned, cycling between vanadyl and vanadate can produce ROS within the cell (Nechay, 1984, Sakurai et al., 1980). This increase in ROS may lead to oxidative stress and ultimately cell death, and is therefore a candidate mechanism for BMOV-induced cytotoxicity. However, again this also does not appear to account for BMOV-induced cytotoxicity in neuroblastoma cells. Although there was a modest increase in ROS following BMOV treatment in KELLY cells, a similar increase was detected in SK-N-AS cells, which are resistant to BMOV. Furthermore, there was no significant further increase in ROS in either cell lines when BSO was added alongside BMOV, which phenotypically enhanced BMOV cytotoxicity (Clark et al., 2015). The studies described above, which had been carried out prior to me joining the laboratory (Clark et al., 2015), go some way to rule out ion channel blockage, genotoxicity, and oxidative stress as mechanisms driving BMOV-induced cytotoxicity in neuroblastoma cells. This leaves PTP inhibition, leading to altered signal transduction within networks that effect proliferation and cell survival, as the most likely mechanism.

Nevertheless, progression of oxidovanadium compounds including BMOV into clinical trials for cancer therapy has been hindered in part by concerns regarding off-target toxicity. These compounds clearly have very broad activity in inhibiting all PTPs as well as other phosphate binding enzymes, and potentially inducing oxidative stress (Nechay, 1984). Accumulation of

vanadium species in high phosphate tissues such as bone has also been reported (Parker et al., 1980, Setyawati et al., 1998). The identification of specific, critical BMOV effectors that drive oxidovanadium activity and that could themselves be therapeutically targeted, may allow the use of vanadium itself to be avoided. This, along with a better understanding of how BSO is able to enhance BMOV-induced activity in neuroblastoma cells, may prove to be crucial in maximally harnessing BMOV-induced cytotoxicity and differentiation for improved therapeutic interventions in this and perhaps other cancers. Therefore in this chapter my focus was to examine the possible molecular mechanisms by which vanadium induces neuroblastoma cell cytotoxicity or differentiation. To do this, I have examined the role of AKT and ERK pathways in vanadium activity, and also performed an RNAseq experiment to characterise the global transcriptional response to oxidovanadium and BSO.

Clark et al. (2013 and 2015) showed increased phosphorylation of AKT and ERK in neuroblastoma cells treated with oxidovanadium. This may be due to inactivation of PTPs that negatively regulate these signalling pathways, for example DUSP6, which dephosphorylates phosphorylated ERK (Law et al, 2017). The data in these papers indicate that these pathways are unlikely to be drivers of BMOV-induced cytotoxicity, even though their activation did somewhat correlate with BMOV sensitivity. In this chapter I first aimed to investigate further any requirement for activation of AKT and ERK in BMOV activity, and in particular to ask whether these pathways may act redundantly to regulate cell survival.

In a second approach to characterise the pathways that drive BMOV-induced activity in neuroblastoma cells, I utilised unbiased, genome-wide transcriptomics in IMR32 and KELLY cells treated with BMOV. This transcriptomic analysis builds upon a previous study carried out in the laboratory, exploring the mechanisms driving BMOV-induced differentiation, and in particular BMOV-enhanced retinoic acid-induced differentiation. This previous RNAseq experiment revealed a significant transcriptional response to BMOV in two neuroblastoma cell lines that differentiate in response to BMOV treatment, SK-N-SH and LAN5, perhaps not surprisingly given that BMOV increases phosphorylation and activation of ERK (A. Di Florio and A.

Stoker, unpublished). I used these data along with new RNAseq data that I derived in KELLY and IMR32 cells, to specifically define the common transcriptional changes that occur following BMOV treatment in multiple neuroblastoma cell lines. It is these common gene expression changes that are most likely to be involved in critical signalling networks that are required for BMOV-driven cytotoxicity and differentiation in neuroblastoma cells.

The transcriptomics approach was also employed to address the additional question of how BSO enhances BMOV-induced cytotoxicity (Clark et al., 2015). The study published by our group prior to my project showed that BMOV-induced cell death is dependent on an oxidising cellular environment, as treatment with the ROS scavenger N-acetyl L-cysteine (NAC) reduced BMOV sensitivity (Clark et al., 2015). This may be because an oxidising environment likely favours the PTP-inhibiting vanadate (+5) state of the vanadium ion (Swarup et al., 1982), whereas NAC will encourage a reducing environment that favours the non-PTP-inhibiting vanadyl (+4) ion. In the same study, the addition of BSO in combination with BMOV greatly enhanced cytotoxicity in BMOV-sensitive cell lines, and induced some cell death in BMOV-resistant lines (Clark et al., 2015). BSO is a chemical inhibitor of the rate-limiting enzyme in glutathione synthesis, compromising glutathione as a major antioxidant defence (Griffith and Meister, 1979). Treatment with BSO may therefore act in the opposite way to NAC, increasing BMOV-induced cytotoxicity by promoting the active vanadate form of the vanadium ion. This forms the hypothesis for the final objective of this chapter, to understand at a transcriptional level whether BSO simply enhances BMOV-induced gene expression changes, or induces a unique transcriptional response.

4.2. Results

4.2.1. BMOV induces cytotoxicity that can be enhanced by BSO

I began by replicating previous findings from our group showing that BMOV induces cytotoxicity in neuroblastoma cell lines in 2D culture (Clark et al., 2015). In IMR32 and KELLY cells, three days of treatment with 10 µM BMOV was sufficient to cause rounding up of cells and loss of adhesion, indicative of

cytotoxicity that will lead to cell death (**Figure 4.1A**). 10 µM BSO alone resulted in no visible changes to cell morphology. However, when BMOV and BSO were combined, increased cytotoxicity, above that which was seen with BMOV alone, was observed in both cell lines. This microscopy clearly shows loss of adhesion in treated cells, but does not definitively confirm cell death. However, previous experiments performed by our group have shown that BMOV and BSO-treated cells undergo apoptosis (Clark et al., 2015). Crystal violet staining was used to quantify these observations in IMR32 cells, showing that there was a statistically significant reduction in cell density following BMOV treatment (**Figure 4.1B**). There was also a significant reduction in cell density following BMOV/BSO combination treatment compared to BMOV alone. An MCB assay (**Section 2.2.4.**) was used to confirm BSO activity in depleting intracellular glutathione (**Figure 4.1C**). IMR32 and KELLY cells were treated with increasing concentrations of BSO (0 – 400 µM) for 6, 24 and 48 hours, after which reduced glutathione levels were assessed using MCB fluorescence. With 24 hour treatment, 10 µM BSO was sufficient to deplete glutathione levels in IMR32 and KELLY cells by around 40% and 70% respectively. Higher concentrations of BSO had a modestly larger effect in IMR32, but not KELLY cells. After 48 hours there were no significant additional changes in KELLY cells compared to 24 hours, but IMR32 cell glutathione levels were reduced further, almost reaching zero when BSO was administered at 50 µM.

Having confirmed that BMOV, in particular with the addition of BSO, induces morphological changes indicative of loss of cell viability in these two neuroblastoma cell lines, I subsequently extended these qualitative observations to include a wider panel of neuroblastoma and non-neuroblastoma cell lines (Summary table in **Figure 4.2A,** microscopy **Appendix 2**). Cells were treated with 10 µM BMOV and BSO for 3 days, after which morphology was assessed looking for characteristic changes associated with cytotoxicity such as reduced final cell number, rounding up of cell bodies and loss of adhesion. As already discussed, IMR32 and KELLY cells were sensitive to BMOV alone, resistant to BSO alone, and highly sensitive to the

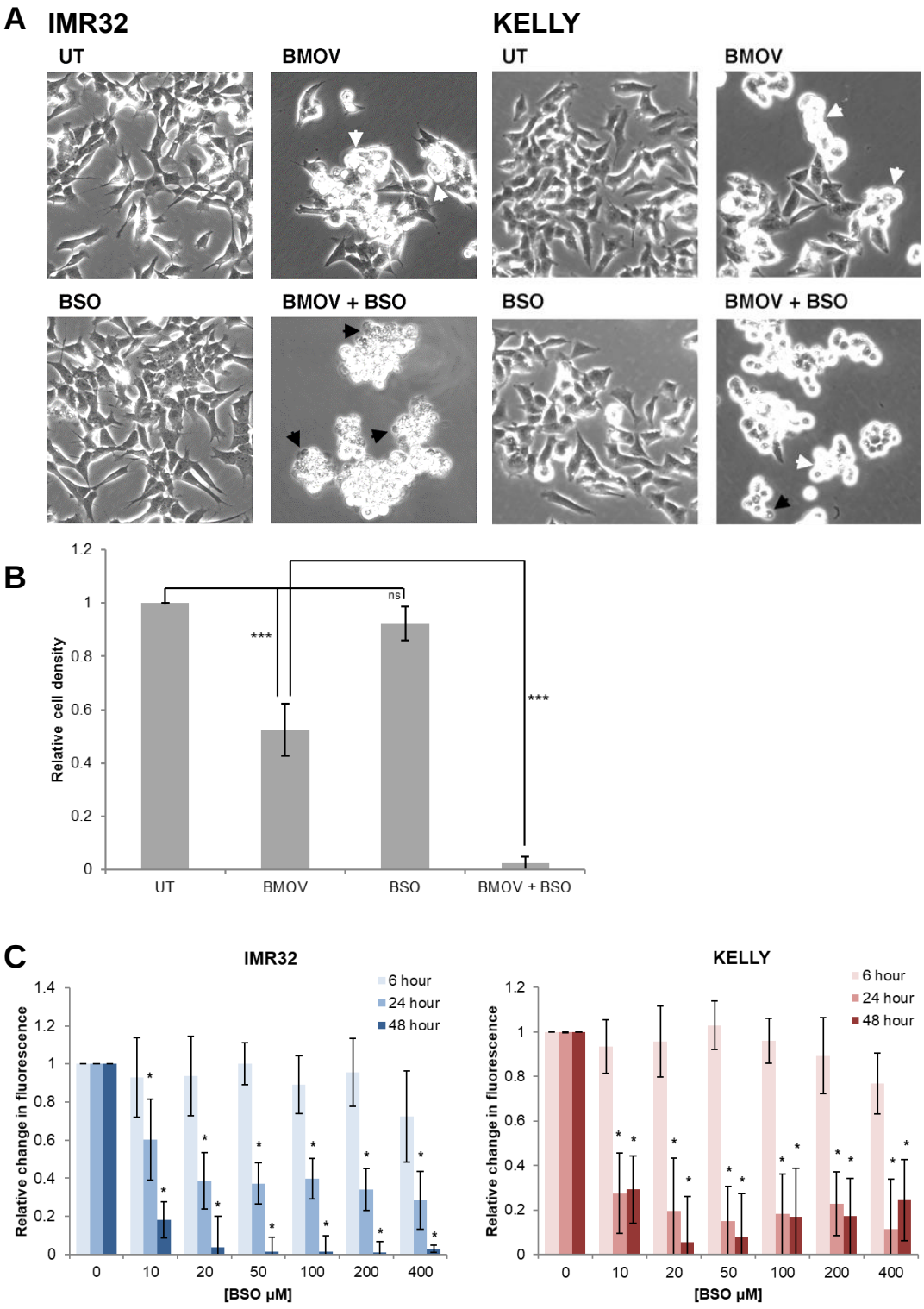

Figure 4.1 –BSO-mediated glutathione depletion enhanced BMOV-induced cytotoxicity in neuroblastoma cells

A *– IMR32 (left) and KELLY (right) cells treated with 10 µM BMOV and BSO for 3 days. White and black arrows indicating dying and dead cells respectively.* ***B*** *– IMR32 cells treated with 10 µM BMOV and BSO for 3 days, and quantitatively assessed for relative cell density using crystal violet staining and solubilisation. ANOVA with Bonferroni post hoc, ns = not significant *** p<0.001 (n=3).* ***C*** *- IMR32 (left) and KELLY (right) cells treated with increasing concentrations of BSO up to 400 µM for 6, 24 and 48 hours. Relative levels of reduced glutathione detected using MCB fluorescence. ANOVA with Dunnett post hoc, * p<0.05 (n=3).*

combination. The neuroblastoma cell lines SK-N-AS, SK-N-DZ and SK-N-BE(2) had either low or no sensitivity to BMOV alone, but were more sensitive to the BMOV/BSO combination. Unlike the cell lines previously discussed, SK-N-DZ and SK-N-BE(2) were highly sensitive to BSO in monotherapy. There are published data showing that glutathione depletion using BSO is cytotoxic in some neuroblastoma cell lines, and may be a useful therapeutic in its own right or in combination with other cytotoxic agents (Dukhande et al., 2013, Anderson et al., 2001). Specifically, it has been reported that BSO induces cell death in SK-N-BE(2) cells with an IC_{90} of 4.6 µM, in agreement with my data (Anderson et al., 1997). In general however, my data show resistance to BSO in most neuroblastoma cell lines.

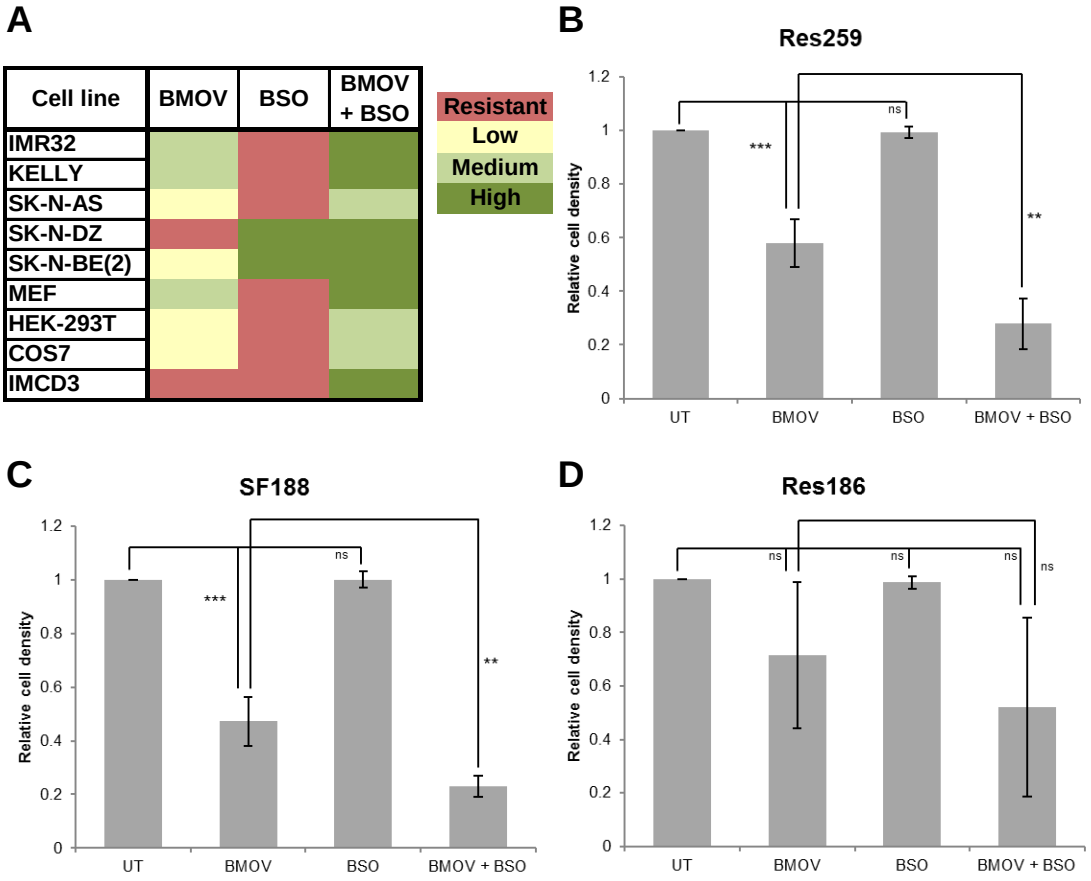

Figure 4.2 – BMOV/BSO sensitivity varied across different cell types
A *– Cytotoxicity was qualitatively assessed as high, medium, low, or resistant in a panel of cell lines following 3 days treatment with 10 µM BMOV and BSO. Reduced cell number, rounding up of cell bodies and loss of adhesion were used as observable indications of loss of cell viability. Microscopy shown in* ***Appendix 2****.* ***B-D*** *– Three paediatric brain tumour cell lines were treated with 10 µM BMOV and BSO for 3 days, after which final cell density was quantitatively assessed using resazurin. ANOVA with Bonferroni post hoc, ns = not significant ** p<0.01 *** p<0.001 (n=3).*

The non-neuroblastoma cell lines HEK-293T, COS7, IMCD3 and MEF had varying degrees of sensitivity to BMOV, but all were more sensitive to the combination with BSO. There was not a strikingly clear definition between the neuroblastoma cell lines versus the control cell lines, where the tumour lines were more sensitive to oxidovanadium treatment. However, importantly, there were some cell lines that displayed resistance (namely SK-N-DZ and IMCD3), indicating that BMOV is not generally cytotoxic to all cells. I also treated a small panel of paediatric brain tumour lines with BMOV and BSO (**Figure 4.2B-D**). Two of these cell lines, Res259 and SF188, were highly sensitive to BMOV and even more so to the BMOV/BSO combination. Res186 cells showed a much more varied response across the repeated experiments, although they are likely to be partially sensitive to BMOV and BMOV/BSO. This variation may have been due to a density dependency, where small variations in cell density between the replicates had large effects on BMOV sensitivity. This would be an important point to consider if these compounds were to be used *in vivo* where the density of cells cannot be controlled.

4.2.2. BMOV induces differentiation

As discussed previously, our group and others have previously shown that vanadium-derived compounds, including BMOV, can also drive differentiation in neuroblastoma cell lines (Clark et al., 2013, Rogers et al., 1994). I have replicated these findings in SK-N-SH cells. 5 days treatment with 10 µM BMOV was sufficient to induce significant neurite outgrowth, characteristic of differentiated cells (**Figure 4.3A+B**). There were no observed morphological signs of toxicity in these cells at 10 µM BMOV, and when cell viability was measured by nuclei counting in cells treated with increasing concentrations of BMOV, significant cytotoxicity was only detected from 20 µM (**Figure 4.3C**). In fact at lower concentrations between 1.25 and 5 µM, increased cell numbers were observed, although these were not statistically significant compared to untreated cell numbers according to ANOVA testing for significance (Dunnett post hoc). It is worth noting that when SK-N-SH cells are treated with oxidovanadium-derived compounds, they scatter rather than remain as 3D clusters as untreated cultures often do (**Figure 4.3A**). This may allow cells to divide more rapidly, accounting for the apparent increase in cell number at low

BMOV concentrations. Alternatively, this scattering of cells may simply allow nuclei counting with higher accuracy.

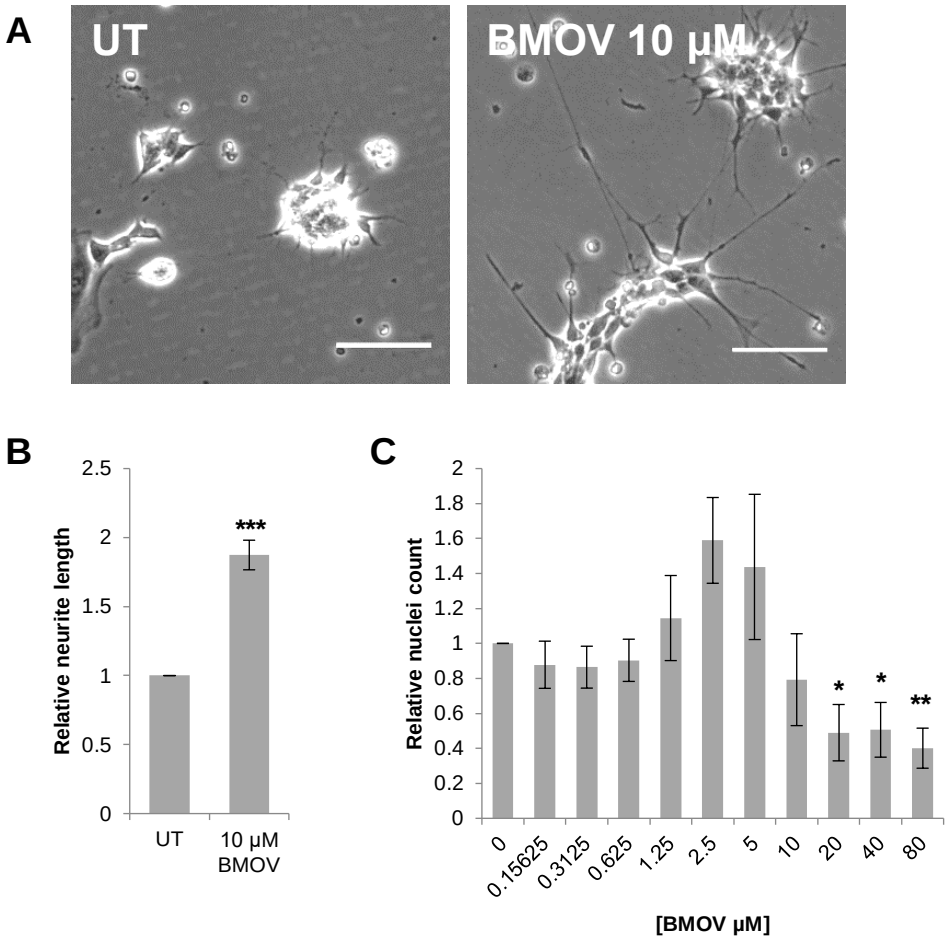

Figure 4.3 – BMOV treatment induced differentiation in SK-N-SH cells
A *– SK-N-SH cells treated with 10 µM BMOV for 5 days. Scale bar = 100 µm.* ***B*** *– Neurite length was measured in SK-N-SH cells treated with 10 µM BMOV for 5 days. Independent T-test, *** p<0.001 (n=3).* ***C*** *– Nuclei counting following 5 days treatment with increasing concentrations of BMOV up to 80 µM. ANOVA with Dunnett post hoc, * p<0.05, ** p<0.01 (n=3).*

4.2.3. AKT and ERK activation are not required for BMOV-induced cytotoxicity

Our group has previously shown increased phosphorylation of AKT and ERK in neuroblastoma cells following treatment with BMOV (Clark et al., 2013, Clark et al., 2015). This may be due to inhibition of PTPs that ordinarily damped down signalling via these kinase cascades. For example, knockdown of PTPN2, PTPRJ and PTEN has been shown to enhance AKT activation (Omerovic et al., 2010). In order to assess whether activation of these pathways is required for BMOV-induced cytotoxicity, I obtained chemical

inhibitors of the AKT and ERK pathways (**Figure 4.4A**). In order to be consistent with our laboratory's previously published work, MK-2206 and U0126 were chosen to inhibit AKT and MEK respectively (Clark et al., 2013, Clark et al., 2015). Given that both pathways are involved in growth and survival, it was first necessary to determine whether their inhibition would be tolerated in neuroblastoma cell lines.

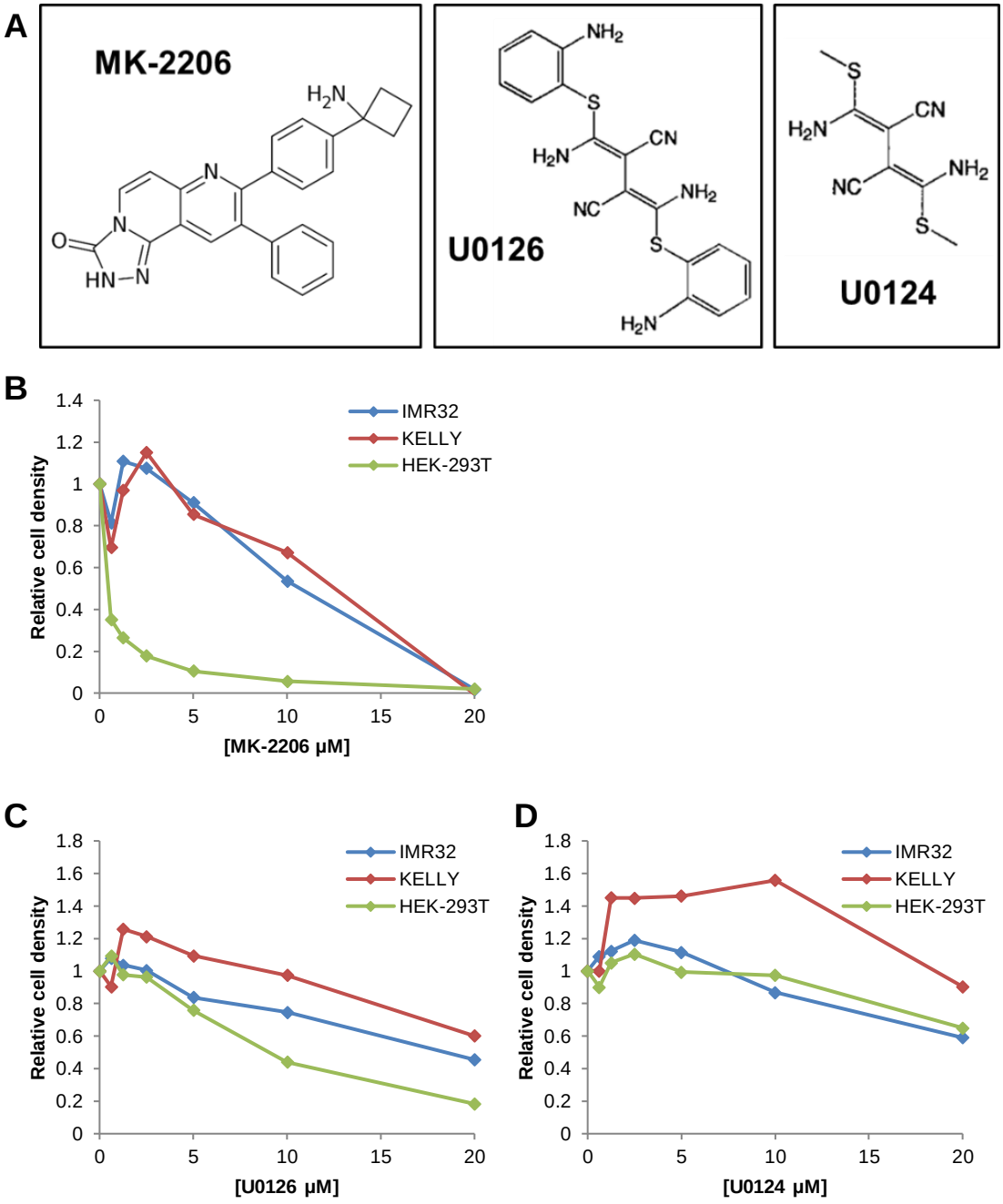

Figure 4.4 – Neuroblastoma cells were partially sensitive to AKT and MEK inhibition
A *– Chemical structures of the AKT inhibitor MK-2206 (left), MEK inhibitor U0126 (middle) and its inactive structural analogue U0124 (right).* ***B-D*** *– Cell viability assessed using a resazurin assay following 3 days treatment with increasing concentrations up to 20 µM of MK-2206 (**B**), U0126 (**C**) and U0124 (**D**) in IMR32, KELLY and HEK-293T cells (n=1).*

MK-2206 is an allosteric pan-AKT inhibitor that is being investigated as a combination partner to increase the cytotoxicity of a range of anti-cancer agents. It has produced promising data both in preclinical studies and in patients for the treatment of a wide range of tumour types, e.g. colorectal, breast and lung (Hirai et al., 2010, Narayan et al., 2017). In this case, I hypothesised that combining BMOV with MK-2206 may have the reverse effect, i.e. that it may protect neuroblastoma cells from BMOV-induced cytotoxicity, since high levels of phosphorylated AKT and cytotoxicity are generated by BMOV treatment (Clark et al., 2015). Initial dose response cell viability data showed that MK-2206 was tolerated in IMR32 and KELLY cells up to around 5 µM (**Figure 4.4B**). It has been previously reported that MK-2206 can completely inhibit phosphorylation of AKT at 1 µM in a range of cell types (Hirai et al., 2010, Sefton et al., 2013, Narayan et al., 2017), therefore it was deemed that it would be possible to inhibit AKT without effecting IMR32 and KELLY cell viability.

U0126 is a non-competitive inhibitor of both MEK1 and MEK2 that prevents phosphorylation of ERK, and may be of use in the treatment of some cancers, specifically those driven by oncogenic RAS (Favata et al., 1998). IMR32, KELLY and HEK-293T cells were treated with increasing concentrations of U0126 and the structurally similar but inactive analogue U0124 (Favata et al., 1998) (**Figure 4.4C+D**). U0126 was tolerated in KELLY cells up to 10 µM, and only modestly effected the final cell density in IMR32 cells, whereas HEK-293T cells were more sensitive. As expected, all lines were less sensitive to the inactive analogue U0124. Several studies using a range a cell lines have reported that 10 µM U0126 is sufficient to inhibit phosphorylation of ERK (Favata et al., 1998, Marampon et al., 2009, Lim et al., 2013, Ramos-Nino et al., 2002). Therefore, as with MK-2206 it was deemed that it should be possible to inhibit pathway activation without causing extreme levels of toxicity using this compound in IMR32 and KELLY cells.

In order to determine whether increased phosphorylation of AKT and/or ERK was required for BMOV-induced cytotoxicity, IMR32 and KELLY cells were treated with 10 µM BMOV alone and in combination with 1 µM MK-2206 or 10 µM U0126/U0124. Western blotting for phosphorylated and total AKT and ERK

was performed using protein lysates extracted after 24 hours chemical treatment, in order to confirm that the inhibitors were acting as expected (**Figure 4.5A**). 1 µM MK-2206 was sufficient to completely inhibit phosphorylation of AKT with and without BMOV treatment in both IMR32 and KELLY cells. 10 µM U0126 completely inhibited phosphorylation of ERK in IMR32 cells with and without BMOV and KELLY cells without BMOV. Phosphorylation of ERK was reduced but not completely inhibited in KELLY cells treated with BMOV. As expected, U0124 had no effect on ERK phosphorylation. The effect of these chemical combinations on cell viability was assessed using nuclei counting assays following 3 days of treatment (**Figure 4.5B**). In IMR32 cells, as expected there was a significant reduction in final cell nuclei counts in cells treated with BMOV. The addition of MK-2206 or U0126 had no effect on BMOV sensitivity, indicating that activation of neither AKT nor ERK is required for the observed cytotoxicity. In these experiments, the effect of single treatment with the MEK and AKT inhibitors on KELLY cells was larger than that of BMOV. Therefore, it was not possible to quantify the effect of these inhibitors on BMOV sensitivity in KELLY cells with this assay. Importantly, KELLY cells did appear very unhealthy following BMOV treatment with cell bodies rounding up considerably. However, as they do not lose adhesion as readily as IMR32 cells, this cytotoxicity is under-represented by the nuclei counting assay. Assaying cell viability with commonly used metabolic activity-based assays is challenging when using oxidovanadium compounds, due to an apparent effect of vanadium on levels of cellular dehydrogenases. After testing several cell viability assays, nuclei counting was deemed to be the most accurate when using oxidovanadium compounds, these experiments and justifications are described in (**Appendix 3**).

These data indicate that increased phosphorylation of AKT or ERK are not required for BMOV-induced cytotoxicity and are therefore not part of the cellular mechanisms driving this cell death, at least in IMR32. It is possible that there is some redundancy between these two signalling pathways, whereby either one, but not both, are required for BMOV-induced cytotoxicity. In order to test this hypothesis, IMR32 cells were treated with BMOV with and without MK-2206, U0126, or both together (**Figure 4.5C**). No protection from

cytotoxicity was observed even when both pathway inhibitors were administered alongside BMOV, suggesting that activation of neither pathway is required for cytotoxicity.

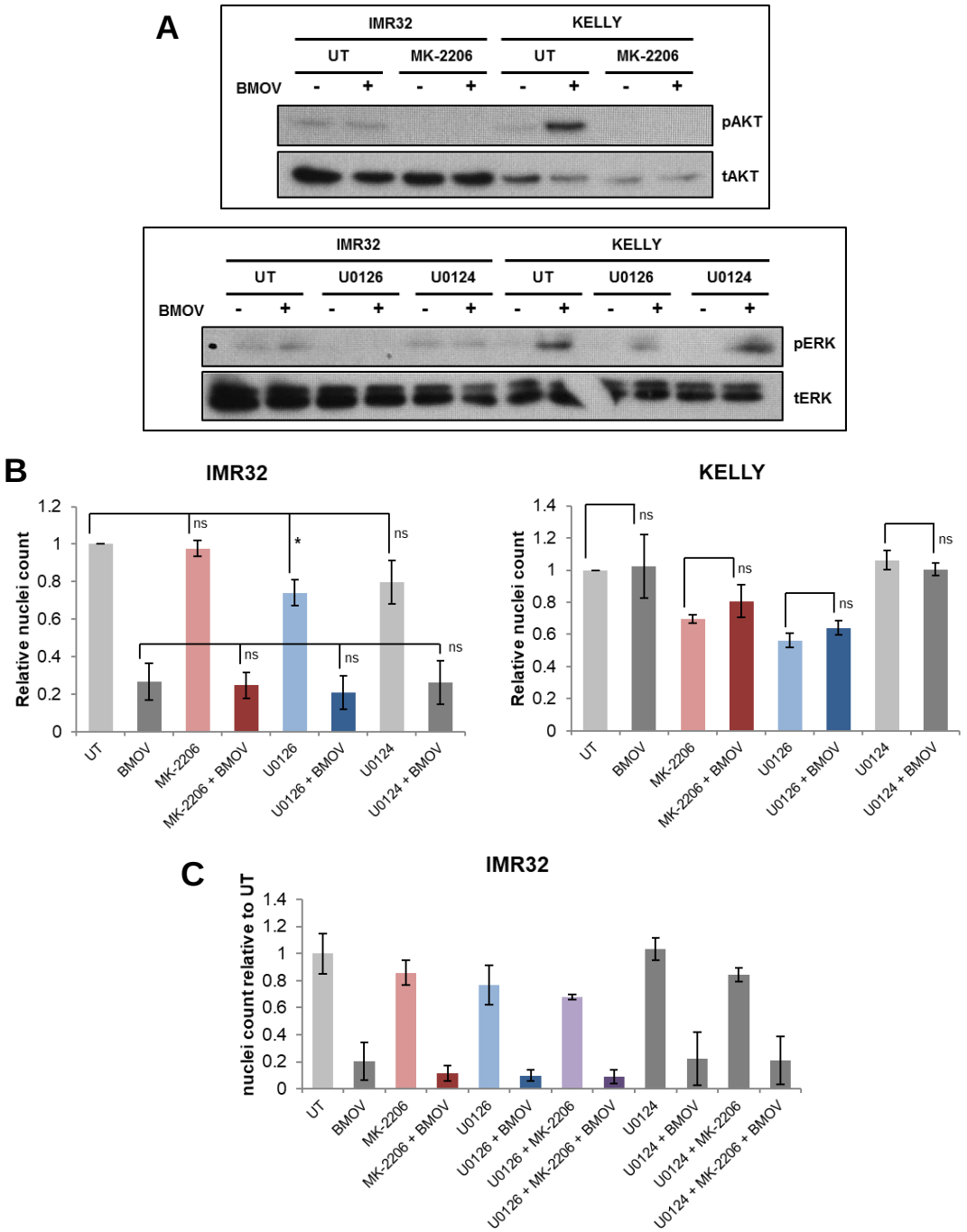

Figure 4.5 – AKT or MEK inhibition did not rescue neuroblastoma cells from BMOV-induced cytotoxicity

A *– Western blotting for phosphorylated and total AKT (top) and ERK (bottom) in IMR32 and KELLY cells treated with 1 μM MK-2206 or 10 μM U0126/U0124 with and without 10 μM BMOV for 24 hours.* ***B*** *– Nuclei counting in IMR32 (left) and KELLY (right) cells treated with 1 μM MK-2206 or 10 μM U0126/U0124 with and without 10 μM BMOV for 3 days. ANOVA with Bonferroni post hoc, ns = not significant * p<0.05 (n=3).* ***C*** *– Nuclei counting in IMR32 cells treated with 1 μM MK-2206 and 10 μM U0126/U0124 with and without 10 μM BMOV for 3 days (n=1).*

4.2.4. Transcriptomic analysis of BMOV/BSO-treated neuroblastoma cells

In a further approach to unpick the pathways that drive oxidovanadium and BSO-induced cytotoxicity, a transcriptomic were employed. For this study, RNAseq analysis was performed in IMR32 and KELLY cells, two neuroblastoma cell lines that die in response to BMOV and that are particularly sensitive to the BMOV/BSO combination. Cells were treated with 10 μM BMOV or BSO, or both in combination for 24 hours, after which RNA was extracted and cDNA libraries were synthesised. After next generation sequencing, sequence alignment, and normalisation, the DESeq2 algorithm was used to calculate differential expression between the chemical treatments for every known gene (performed by Tony Brooks, UCL Genomics). Principle component analysis (PCA) confirmed that the three replicates for each condition clustered tightly (**Figure 4.6A**). This plot also suggests that there is surprisingly little transcriptional response to BSO in either cell line, since the BSO-treated samples cluster closely with the untreated samples. In KELLY cells both the BMOV and BMOV/BSO samples cluster distinctly, suggesting that there are gene expression changes induced by BMOV and additional changes in the combination. In contrast, in IMR32 cells the BMOV and BMOV/BSO samples cluster tightly together, suggesting that there is a transcriptional response to BMOV, but very few additional changes when BSO is co-administered. This indicates already that the two cell lines may be distinct in their response to co-treatment with BSO. A parallel set of 48-hour chemical treatments were carried out in the same cells to allow morphological signs of cell death to appear, these are not visible after 24 hours. This confirmed that the chemicals had been active in inducing cytotoxicity in these experiments (**Figure 4.6B**). These morphological changes included rounding up of cell bodies and loss of adhesion, mirroring those that had been seen previously (**Figure 4.1A** and Clark et al., 2015). Gene lists were generated, comparing gene expression in each chemical treatment within each cell line. These lists were filtered for significance (adjusted p value < 0.05) and a fold change cut-off (log2 fold change >0.3 or <-0.3) to generate lists of genes that were considered to be differentially expressed between each condition. The number

of genes that were differentially expressed in each comparison are shown in **Table 4.1**. These values corroborate the conclusions drawn from the principle component analysis above.

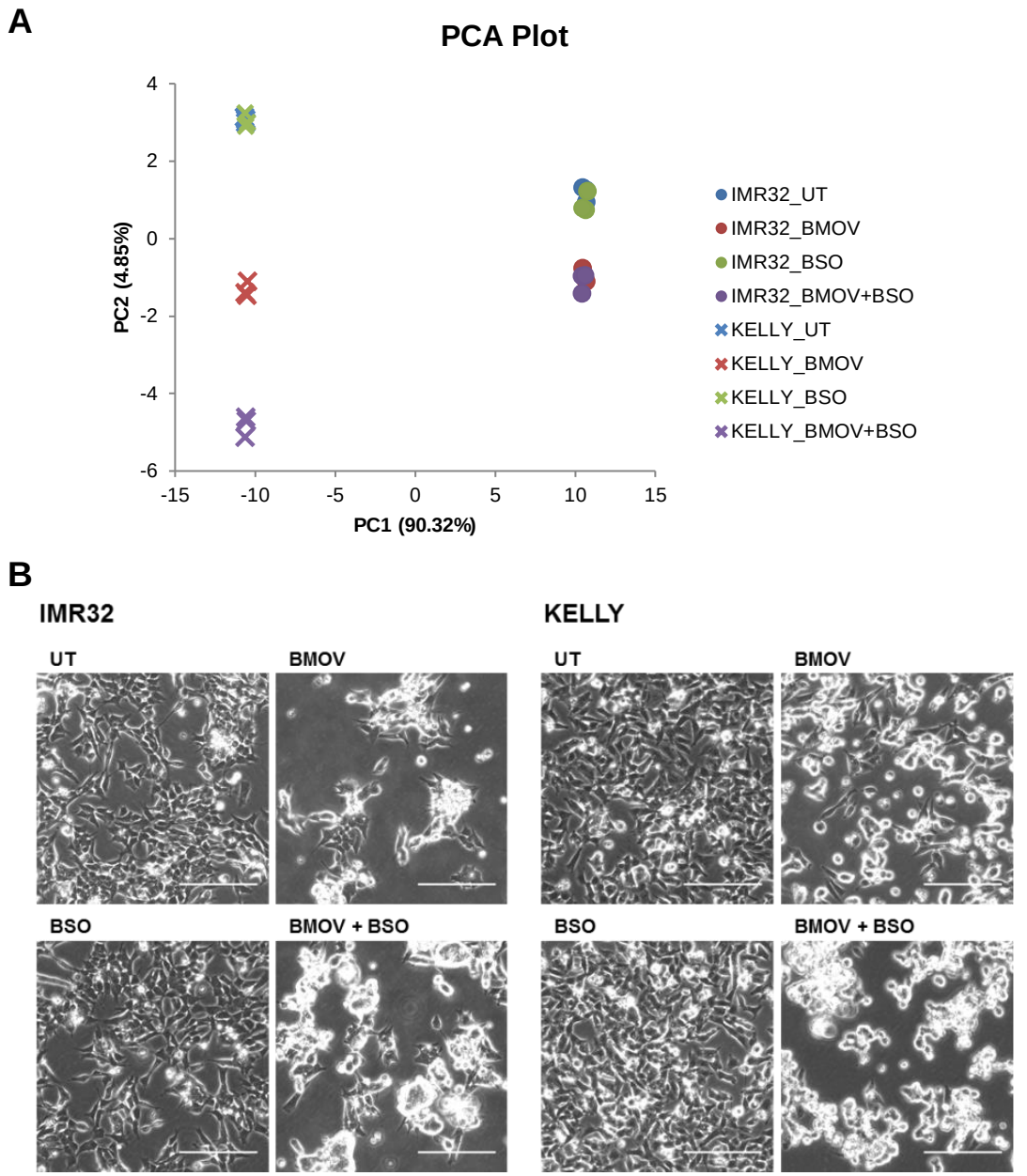

Figure 4.6 – BMOV/BSO induced transcriptional changes in neuroblastoma cells
A *– Principle component analysis (PCA) of the IMR32 and KELLY RNAseq datasets showing clear clustering of the triplicates within each sample.* ***B*** *- Parallel set of chemical treatments (10 µM BMOV/BSO, 48 hours) carried out alongside those used for RNAseq, confirming that the chemicals were active in inducing rounding up of cell bodies and loss of adhesion indicative of cytotoxicity. Scale bar = 150 µm.*

Table 4.1 – Significantly differentially expressed genes in neuroblastoma cells treated with BMOV/BSO

Numbers of genes that were differentially expressed in IMR32 and KELLY cells for each chemical comparison generated using the DESeq2 algorithm. Gene lists were filtered using an adjusted p value cut off of <0.05 and a log2 fold change cut off of >0.3 or <-0.3.

	IMR32	KELLY
UT vs BMOV	507	1879
UT vs BSO	0	0
UT vs BMOV+BSO	547	4763
BSO vs BMOV+BSO	440	4795
BMOV vs BMOV+BSO	1	1835

4.2.5. BSO enhances BMOV-induced transcriptional changes

The RNAseq data presented here reveal that there is a significant and widespread transcriptional response to oxidovanadium treatment in both IMR32 and KELLY cells (**Table 4.1**), as was the case for the two cell lines that had been previously analysed by our group, SK-N-SH and LAN5 (A. Di Florio and A. Stoker, unpublished). Perhaps surprisingly, there were no significant changes in gene expression in the BSO treatment in either cell line, confirmed by tight grouping of BSO-treated cells with untreated cells in the PCA plot (**Figure 4.6A**). This striking result suggests that these specific neuroblastoma cells are able to tolerate glutathione depletion when no additional stress is applied, in agreement with the lack of any morphological change when cells are treated with BSO alone (**Figure 4.6B,** and Clark et al., 2015).

A key aim of this transcriptomic experiment was to ask how BSO enhances BMOV-induced cytotoxicity. Specifically, whether BSO chemically enhances BMOV activity and therefore BMOV-induced gene expression changes, rather than inducing its own unique changes. When BMOV and BSO were co-dosed in KELLY cells, 1835 genes were differentially expressed compared to BMOV alone. Of these 1835 genes, 656 also appeared in the filtered list of genes that were differentially expressed in BMOV-treated compared to untreated cells. The other 1179 genes were only significantly differentially expressed after combination treatment (**Figure 4.7A**). The top 100 genes from the 1835 genes that were differentially expressed in combination-treated cells compared to BMOV-treated cells (BMOV vs [BMOV+BSO]) were assessed in more detail. Of these 100 genes, 70 also appeared in the filtered list of genes for untreated

compared to BMOV-treated cells (i.e. they had a fold change greater than 0.3 or less than -0.3, and an adjusted p value less than 0.05 in untreated compare to BMOV-treated cells), and importantly, expression was altered in the same direction in both conditions. Of the remaining 30 genes, expression of 26 did change in the same direction in both untreated compared to BMOV and BMOV compared to combination-treated cells; however, in the case of untreated compared to BMOV the log2 fold change was below the cut off (1 gene), the adjusted p value was greater than 0.05 (8 genes), or both (17 genes). Just 4 genes had an expression change in the opposite direction, and none of these had significant p values ($p<0.05$) or log2 fold changes greater than 0.3 (**Figure 4.7A**). To demonstrate this point, the normalised counts for genes in untreated KELLY cells, BMOV-treated cells and doubled-treated cells were plotted for the top 50 of these 100 'BMOV vs [BMOV+BSO]' genes (**Figure 4.7B**). This plot shows that in the vast majority of cases (49 out of 50 genes), the addition of BSO increased the change in gene expression, rather than changing the direction. That is, genes for which expression is increased by BMOV, are further increased in the combination treatment such that they may become significant according to my parameters (log2 fold change > 0.3 or < -0.3 and adjusted p value < 0.05). In fact when I looked at the whole list of 1179 genes that were only significantly differentially expressed in combination-treated compared to BMOV-treated cells 'BMOV vs [BMOV+BSO]', 897 genes (76%) changed in the same direction in untreated compared to BMOV-treated cells (**Figure 4.7A**). Of those that changed in the opposite direction, only 9 had an adjusted p value less than 0.05, and less than half had a log2FC greater than 0.1 or less than -0.1. Therefore these genes actually had extremely low changes in gene expression that were mostly not significant and can therefore likely be eliminated as experimental noise. These findings suggest that the addition of BSO alongside BMOV largely enhances BMOV-driven gene expression changes in KELLY cells, rather than generating a unique, combination specific transcriptional response.

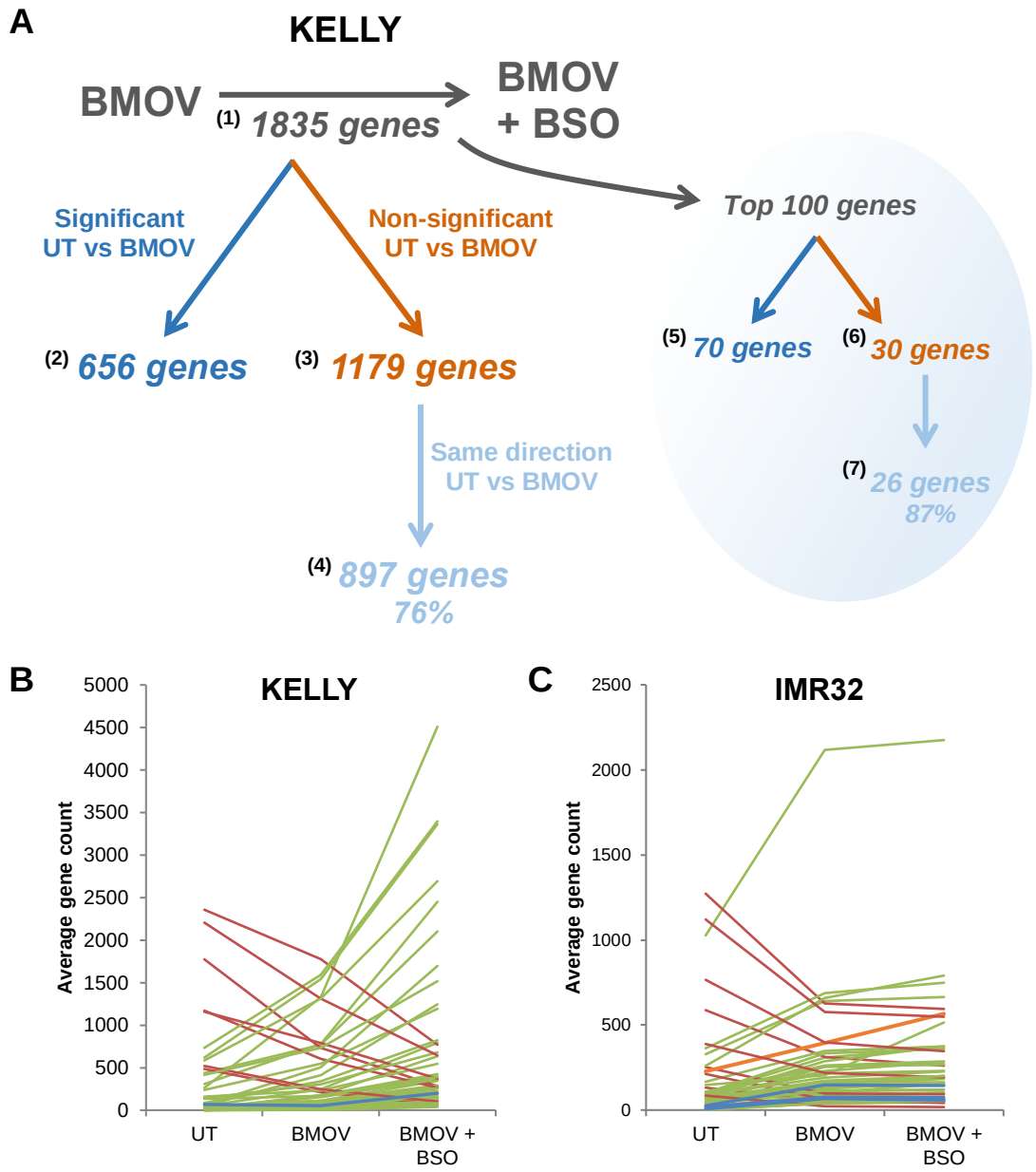

Figure 4.7 – BSO enhances BMOV-driven gene expression changes
A *- Using an adjusted p value cut off of p<0.05 and a log2 fold change cut off of >0.3 or <-0.3, 1835 (1) genes were differentially expressed between BMOV-treated and BMOV/BSO-treated KELLY cells. 656 (2) of these were common to the untreated (UT) versus BMOV list using the same cut offs, whereas 1179 (3) were not. Of these 1179 genes, expression of 76% (897 genes) (4) were altered in the same direction in UT versus BMOV compared to BMOV versus BMOV/BSO, although not meeting the filtering cut offs. Of the top 100 differentially expressed genes in BMOV compared to double-treated cells, 70 (5) were significantly differentially expressed in the same direction in UT versus BMOV-treated cells. Of the remaining 30 genes (6), expression of 26% (7) were altered in the same direction in UT versus BMOV-treated cells, although not significantly.* ***B+C*** *- Normalised gene counts for the top 50 differentially expressed genes in BMOV versus combination-treated KELLY cells (**B**), and in UT versus combination-treated IMR32 cells (**C**). Genes that are up-regulated in BMOV-treated cells, and further up-regulated in BMOV/BSO are in green. Red lines represent genes that are down-regulated by BMOV and further down-regulated in the combination. Blue lines represent genes where the direction of regulation is different in the combination compared to BMOV alone. The orange line in **C** represents the one gene, NQO1, which is significantly differentially expressed in combination-treated IMR32 cells compared to BMOV alone.*

Surprisingly, in IMR32 cells there was just one additional gene expression change in the BMOV+BSO double treatment compared to BMOV alone, despite the very clear increase in cytotoxicity (**Figure 4.6B**). This gene was *NQO1* (**Figure 4.7C** orange line), and the log2 fold change increase in expression between BMOV-treated and combination-treated cells was only 0.37. When the normalised gene counts for the top 50 differentially expressed genes in untreated compared to BMOV+BSO-treated IMR32 cells were plotted, it became clear that in most cases gene expression changes induced by BMOV were modestly enhanced by the addition of BSO, although in all but one case not to a level that crossed the original gene filtering for significance and fold change (**Figure 4.7C**). Only 4 of these top 50 genes (blue lines in **Figure 4.7C**) had a change of expression in the opposite direction in combination-treated cells compared to BMOV alone, and none of these had a significant adjusted p value or a log2 fold change greater than 0.3. Furthermore, when expression of all 507 genes that were significantly differentially expressed in BMOV compared to untreated cells were assessed in combination-treated cells, 213 had gene expression changes in the opposite direction, however none of these were significant, and only 14 had a log2 fold changer greater than the lower cut off of 0.1 (or less than -0.1). It can therefore be concluded that the addition of BSO also does not induce a unique transcriptional response in IMR32 cells. In fact these data indicate that BSO does not induce a significant transcriptional response in IMR32 cells at all, neither as a monotherapy nor in combination with BMOV.

4.2.6. Candidate BMOV effectors

The other key aim of the RNAseq experiment was to more broadly understand the mechanisms that drive oxidovanadium activity in neuroblastoma cell lines, including both cytotoxicity and differentiation. Genome-wide transcriptomics using oxidovanadium, to our knowledge, has not been previously reported and we predicted that it would provide novel insight into vanadium action. Lists of genes that are differentially expressed in BMOV-treated compared to untreated cells were generated for the four cell lines for which I now had RNAseq data: IMR32, KELLY, LAN5 and SK-N-SH. The IMR32 and KELLY data was obtained in this project, whilst the LAN5 and SK-N-SH data came

from a previous project in our laboratory (A. Di Florio and A. Stoker, unpublished). These gene lists were compared in order to identify genes that are altered by BMOV treatment in multiple cell lines, and are therefore more likely to be critical for BMOV-induced cytotoxicity and/or differentiation (**Figure 4.8**). The morphological response of these four cell lines to oxidovanadium does differ. IMR32 and KELLY cells display a cytotoxic response, whereas SK-N-SH cells undergo neurite extension indicative of differentiation. LAN5 cells display a mixed cytotoxic/differentiation response (Clark et al., 2013, Clark et al., 2015). It is therefore unsurprising that the transcriptional responses to BMOV treatment in these cell lines also differed substantially. Nonetheless, there are 33 genes that are differentially expressed in all four cell lines, and a further 150 genes that are differentially expressed in the three cell lines in which oxidovanadium is cytotoxic (LAN5, IMR32 and KELLY) (gene lists shown in **Appendix 4**). These common genes are of greatest interest in increasing understanding of the mechanisms that drive oxidovanadium activity in neuroblastoma cells.

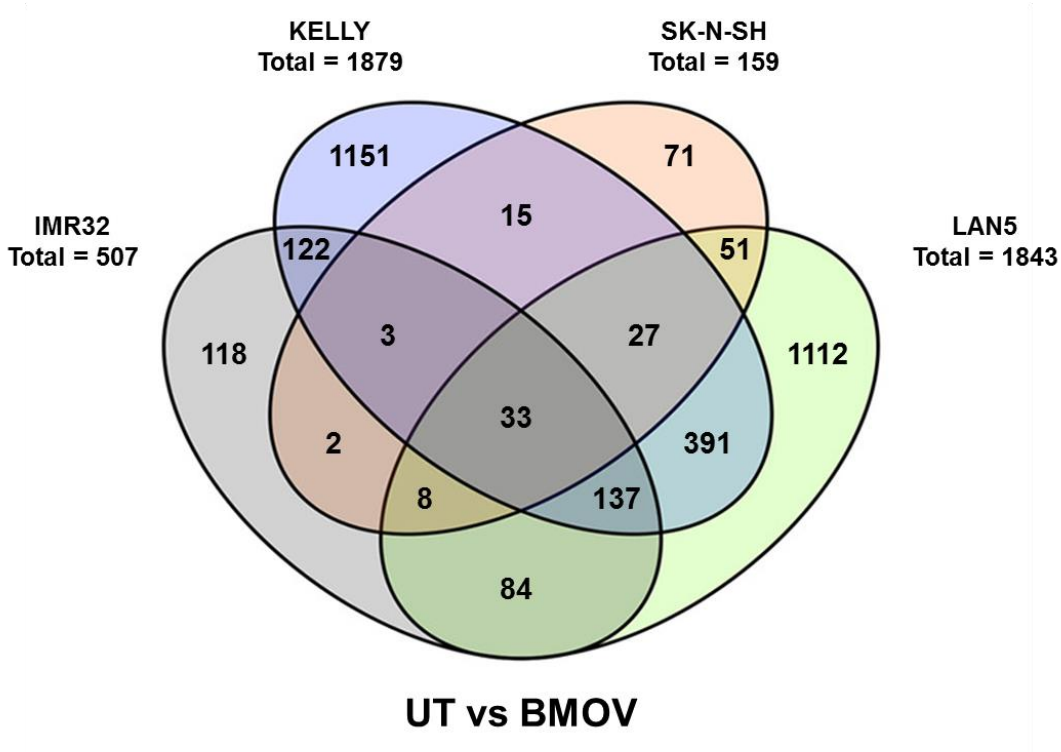

Figure 4.8 – Many common and unique BMOV-induced transcriptional changes exist between neuroblastoma cell lines
Venn diagram showing the numbers of differentially expressed genes that are common and unique to each of four neuroblastoma cell lines. For IMR32, KELLY and LAN5 cells, genes with p<0.05 and log2 fold change >0.3 or <-0.3 were considered to be differentially expressed. For SK-N-SH cells, the significance cut off was p<0.1.

Clearly a large number of genes were differentially expressed in response to BMOV in neuroblastoma cells, thus selecting targets for further analysis was challenging. A siRNA gene knockdown approach was going to be used to validate potential targets; I therefore focussed on genes that were down regulated in response to BMOV. In practical terms, these proteins may also be more amenable for therapeutic targeting in the future, by using small molecule inhibitors for example. A panel of 24 significantly down-regulated genes was selected based on various criteria (**Table 4.2**). Genes that had altered expression in IMR32, KELLY and LAN5 were prioritised, as a cell viability read out was going to be used to assess the effect of gene knockdown and BMOV is not highly cytotoxic to SK-N-SH cells. Genes with a significant log2 fold change less than -0.5 in all four cells lines or in some cases in at least three out of four cell lines were included. Genes with a significant fold change less than -1 in at least two of KELLY, IMR32 and LAN5, or those in the top 30% most altered genes in all three of these lines were also included.

It was hypothesised that some of these 24 target genes identified may be important in the mechanisms driving BMOV-induced cytotoxicity. Thus, they may be critical for the growth and survival of neuroblastoma cells, making them potentially useful therapeutic targets. Expression of these genes was knocked down in IMR32 and KELLY cells using siRNA pools targeting each gene (ON-TARGETplus siRNAs, Dharmacon) (**Figure 4.9A+B**). A scrambled, non-targeting siRNA pool was used as a negative control, and KIF11 and CDC14B-targeting siRNAs were used as positive controls. The experimental error across the replicates for these experiments was high due to lipofectamine toxicity that is extremely dependent on incubation times of transfection mixtures. Nonetheless, it was clear from these data that knocking down some of these genes had a significant, negative impact on cell viability. *DCTN1*, *PDE2A*, *TUBGCP6* and *GLMP* were chosen for further analysis, as knockdown of these genes was associated with a large, and in most cases statistically significant, loss of viability in both neuroblastoma cell lines. The resazurin assay used here to assess cell viability following gene knockdown provides a measure of the relative quantity of metabolically active cells, therefore both cytotoxicity and changes in the rate of proliferation will be

Table 4.2 – Candidate BMOV effector genes

24 genes that encode candidate BMOV effectors identified from RNAseq analysis. Log2 fold changes (Log2FC) and associated adjusted p (AdjP) values taken from DESeq2 analysis of RNAseq data from the current study (IMR32 and KELLY), and a previous data set from the laboratory (SK-N-SH and LAN5) (A. Di Florio and A. Stoker, unpublished). NA = not assessed, as gene counts were very low or zero.

Gene	Description	IMR32		KELLY		SK-N-SH		LAN5	
		Log2FC	Adj P	Log2FC	Adj P	Log2FC	Adj P	Log2FC	Adj P
ANKRD39	Ankyrin Repeat Domain 39.	-0.6035	3.01E-05	-0.8237	1.15E-05	-0.7148	0.2775	-0.9178	0.00453
CALHM2	Calcium homeostasis modulator family member 2, implicated in ALZ and CJD (Calero et al., 2012, Shibata et al., 2010).	-0.5918	7.31E-05	-1.3159	2.49E-14	0.3384	0.9537	-0.3400	0.2636
CCDC61	Coiled-coil domain containing 61.	-0.5998	5.10E-05	-0.9895	2.75E-10	NA	NA	NA	NA
COX20	Cytochrome C Oxidase Assembly Factor, mutations associated with ataxia and muscle hypotonia (Szklarczyk et al., 2013).	-0.7825	2.99E-13	-0.8680	1.12E-22	-0.3886	0.5883	-0.8073	4.46E-13
DCTN1	Encodes the largest subunit of dynactin, mutations can cause neurodegenerative disease (Hwang et al., 2016), and DCTN1-ALK fusions have been reported in tumour cells (Cohen et al., 2018).	-0.6293	4.36E-22	-0.9483	2.06E-49	-0.6864	0.05038	-0.7438	0
EMG1	Encodes an 18S ribosome assembly protein, mutation associated with Bowen–Conradi syndrome, other proteins within complex (responsible for 18S maturation) implicated in ovarian cancer (Sondalle and Baserga, 2014).	-0.9591	5.32E-31	-0.9351	1.59E-19	NA	NA	NA	NA
FAXDC2	A member of the fatty acid hydroxylase superfamily with a role in megakaryocytes. Deregulation associated with increased ERK signalling and leukaemia (Jin et al., 2016).	-0.1247	NA	-2.1557	8.15E-31	-1.2426	0.08795	-0.6139	0.6578
G6PC3	Glucose-6-Phosphatase Catalytic Subunit 3, deficiency associated with congenital neutropenia (Notarangelo et al., 2014).	-0.5485	7.98E-13	-0.6146	2.41E-13	-0.4474	0.1415	-0.7801	3.25E-09
GLMP	Glycosylated Lysosomal Membrane Protein, knockout leads to liver fibrosis in mice (Nesset et al., 2016).	-1.1477	1.09E-19	-1.0035	2.66E-19	NA	NA	NA	NA
IL17RC	Interleukin-17 receptor C, overexpressed in prostate tumours (You et al., 2007).	-0.5632	3.01E-05	-0.5111	0.00362	-0.0932	0.9999	-0.6284	0.01874
ITFG2	Integrin Alpha FG-GAP Repeat Containing 2, part of the KICSTOR complex that negatively regulates mTORC1 signalling, which is involved in neurological disease and cancer (Wolfson et al., 2017).	-0.4905	1.65E-05	-1.1087	2.82E-17	-1.0757	0.09261	-1.1827	0
LPCAT3	Involved in phospholipid remodelling, Lpcat3 deficiency increases cholesterol synthesis and promotes stem cell proliferation encouraging tumourigenesis (Wang et al., 2018).	-0.9627	1.28E-14	-1.6155	1.48E-36	-0.8385	0.0345	-1.4504	0
LRRC75B	Leucine rich repeat containing 75B negatively regulates of myogenic differentiation by modulating ERK signalling (Zhong et al., 2016).	-0.5807	0.00011	-1.0063	3.87E-07	NA	NA	NA	NA
LYSMD1	LysM domain containing 1.	-0.5997	9.54E-06	-0.7759	1.40E-07	-0.4988	0.4023	-0.8725	8.00E-07
MRPL30	A mitochondrial ribosomal protein, possibly involved in type 2 diabetes (Chen et al., 2013).	-0.6388	1.07E-12	-0.8620	7.40E-24	-0.6781	0.1099	-0.7535	1.07E-12
PDE2A	cGMP-dependent 3',5'-cyclic phosphodiesterase involved in regulating cAMP signalling, implicated in various human diseases including cancer (Hiramoto et al., 2014).	-0.2342	0.03649	-0.6681	8.87E-14	-0.9171	0.00085	-0.5082	0.00191
PTGES2	Synthesises prostaglandin E2, implicated in cancer, specifically high expression promotes proliferation and invasion in endometrial tumour cells (Ke et al., 2016).	-0.8946	3.64E-25	-0.8036	1.80E-21	-0.8784	2.48E-05	-0.7763	0.00025

Table 4.2 continued

SARS2	Mitochondrial seryl-tRNA synthetase, mutations can cause the rare mitochondrial disease HUPRA syndrome (Rivera et al., 2013).	-0.7045	4.68E-10	-0.5007	9.29E-06	-0.7628	0.4747	-1.5087	0
SEPW1	Encodes selenoprotein W, implicated in cancer as depletion causes a delay in cell cycle progression at the G1/S transition by regulating p53 and p21 (Hawkes and Alkan, 2011).	-0.8611	5.23E-21	-1.1029	2.91E-41	-0.5142	0.2226	-0.8930	0
SGSH	Encodes sulfamidase, mutations can cause lysosomal storage disease (Lau et al., 2017).	-0.5255	0.00053	-0.6391	5.82E-05	-0.8265	0.00245	-0.5566	0.00021
SHPK	Sedoheptulokinase, mutations possibly related to the lysosomal storage disorder cystinosis (Phornphutkul et al., 2001).	-0.7867	6.25E-12	-0.8578	7.42E-11	NA	NA	NA	NA
TLCD1	TLC Domain Containing 1.	-0.8646	1.84E-10	-0.7909	0.00015	-0.4849	0.9537	-1.8330	0.00159
TMEM240	Transmembrane Protein 240, mutations result in spinocerebellar ataxia 21 (Delplanque et al., 2014).	-0.1731	0.33950	-1.0221	3.71E-07	-1.2158	0.04449	-2.0871	9.20E-08
TUBGCP6	Gamma-tubulin complex component 6, required for centriole biogenesis, mutations related to various congenital anomalies (Martin et al., 2014).	-0.5343	3.40E-07	-0.6316	5.14E-10	-0.4985	0.5847	-0.6866	1.60E-07

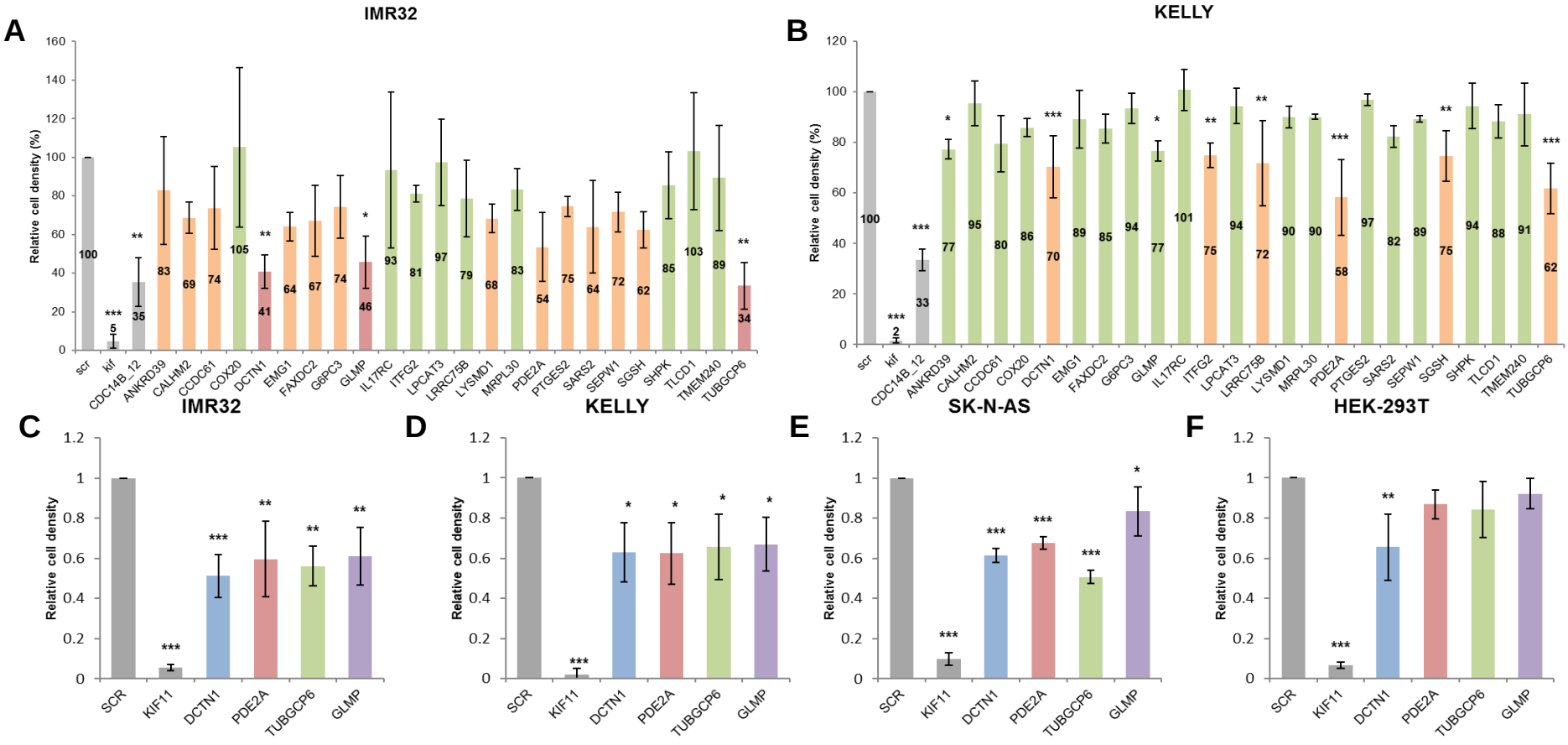

Figure 4.9 – Knockdown of some candidate BMOV effectors led to reduced neuroblastoma cell numbers

A-B *– Resazurin cell viability assays in IMR32 (**A**) and KELLY (**B**) cells 6 days following siRNA transfection. Results are colour coded based on percentage cell density compared to cells transfected with a scrambled (SCR) non-targeting control siRNA. Red <50% cells compared to scrambled, orange <75%, green >75%, grey - control conditions. ANOVA with Dunnett post hoc, * p<0.05 ** p<0.01 *** p<0.001 (n=3).* ***C-F*** *- Resazurin cell viability assay in IMR32 (**C**), KELLY (**D**), SK-N-AS (**E**) and HEK-293T (**F**) cells 6 days following siRNA transfection. ANOVA with Dunnett post hoc, * p<0.05 ** p<0.01 *** p<0.001 (n=3).*

reflected in these values. Microscopy was taken of IMR32 cells transfected with each of the siRNAs (**Figure 4.10A**). There is clear rounding of cells, characteristic of cell death in DCTN1, PDE2A and to an extent TUBGCP6 knockdown cells, whereas there appear to just be fewer GLMP knockdown cells with no clear morphological effects. These differences may reflect distinct roles of these proteins in survival and proliferation.

Having selected four targets and shown promising data in IMR32, the knockdown experiments were extended to include SK-N-AS cells and HEK-293T cells (**Figure 4.9C-F**). It was reassuring that knockdown of these genes in HEK-293T cells had no significant effect on final cell density, except a modest reduction for DCTN1, indicating some specificity of the potential role of these proteins in tumour cell growth and survival. SK-N-AS cells are more resistant to a range of chemicals, including oxidovanadium than IMR32 or KELLY (**Figure 4.2A** and Clark et al., 2015). Therefore, it was interesting that knockdown of these genes still resulted in reduced cell numbers. It is worth noting that in contrast to the morphological effects in IMR32 cells, none of the knockdown SK-N-AS cells display morphology indicative of cell death. Rather there seem to be simply fewer cells, perhaps due to reduced proliferation (**Figure 4.10B**). Furthermore, SK-N-AS cells are more resistant to BMOV, but are partially sensitive to the BMOV/BSO combination (**Figure 4.2A** and Clark et al., 2015). Therefore, it is likely that they have a high threshold for BMOV sensitivity, and perhaps knockdown of these genes using siRNAs was sufficient to cross that threshold.

Quantitative PCR primers were designed for DCTN1, PDE2A, TUBGCP6 and GLMP, and used to confirm siRNA knockdown efficiency in IMR32 cells (**Figure 4.10C**). Good knockdown was achieved for PDE2A and DCTN1, around 50% and 60% respectively. The siRNAs targeting TUBGCP6 and GLMP were much less efficient, only knocking down 15% and 30% in this single experiment. However, the fold changes in gene expression observed in the RNAseq experiment were small, therefore very strong gene knockdown should not be required to mimic these changes. The qPCR primers were next used to assess expression of the 4 target genes in a panel of 8 neuroblastoma cell lines following BMOV treatment (**Figure 4.11**). This experiment served two

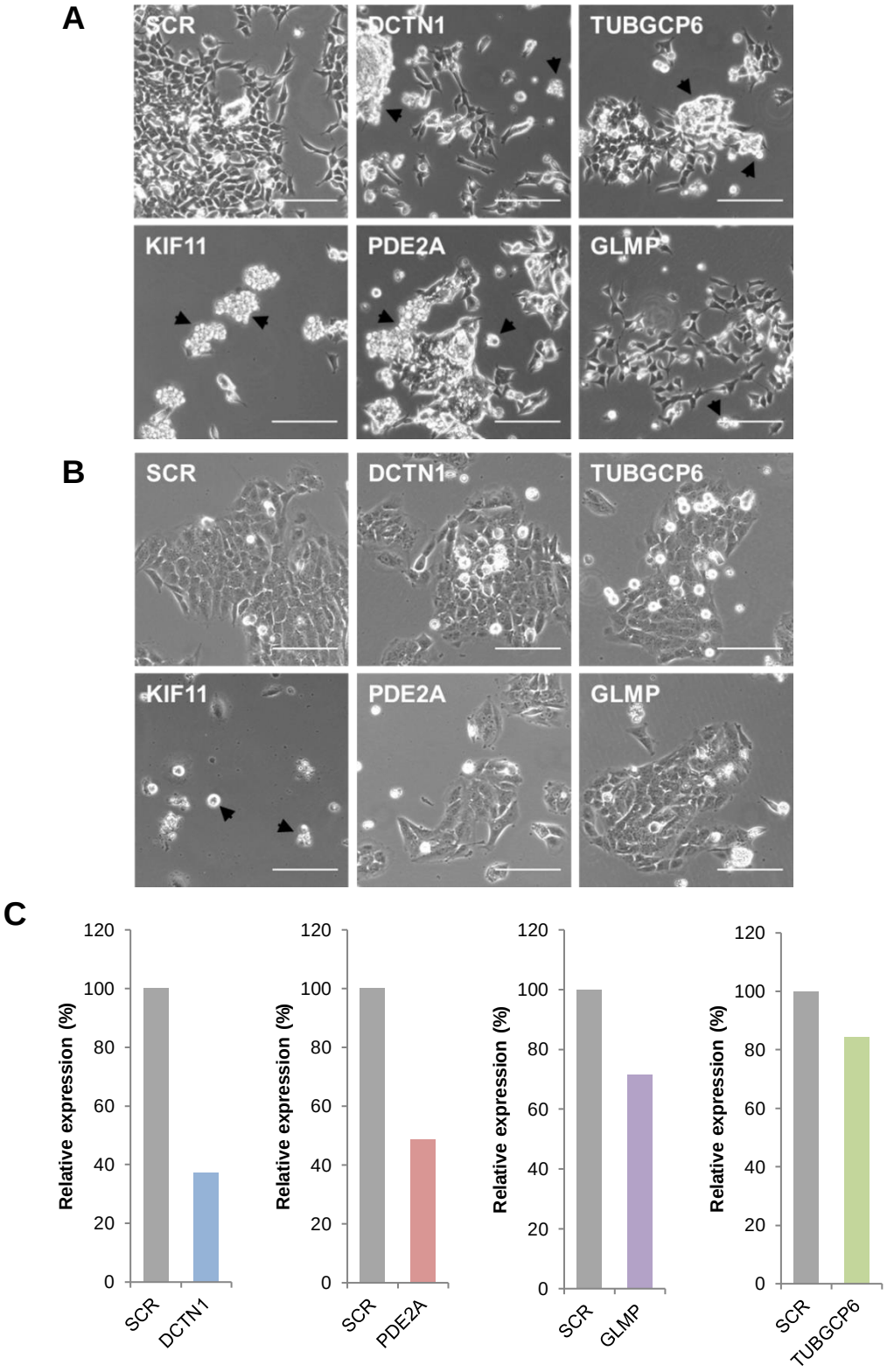

Figure 4.10 – Knockdown of candidate BMOV effectors caused cytotoxicity or reduced proliferation in distinct neuroblastoma cell lines

A+B *– IMR32 (**A**) and SK-N-AS (**B**) cells 6 days following siRNA transfection. Black arrows indicating dead or dying cells. Scale bar = 150 µm.* ***C*** *– SiRNA knockdown efficiency in IMR32 cells 24 hours post transfection, assayed by qPCR (n=1).*

purposes, first to validate the changes in gene expression observed in the RNAseq experiment, and second to determine whether these findings can be extended to other neuroblastoma cell lines. Cell lines with varying sensitivity to BMOV were chosen to assess any correlation between sensitivity and the degree of knockdown for these 4 genes (**Figure 4.11A**). All 8 cell lines were treated with 10 µM BMOV for 24 hours, before RNA extraction, cDNA synthesis, and qPCR using primers against the 4 target genes (**Figure 4.11B+C**). In general, the target genes were knocked down to a greater extent in cell lines that were more sensitive to BMOV, either in terms of cytotoxicity or differentiation. IMR32, KELLY, LAN5 and SK-N-SH are all sensitive to BMOV and in most cases, as expected based on RNAseq analysis, all 4 genes were down regulated in response to BMOV treatment. SK-N-BE(2) are partially BMOV-sensitive, displaying some rounding of cell bodies indicative of cytotoxicity, and expression of all four genes was reduced, although this was only statistically significant for DCTN1 and GLMP. SK-N-AS are only very slightly sensitive to BMOV, and had a small but insignificant reduction in PDE2A, DCTN1 and GLMP expression. LAN1 and SK-N-DZ are resistant to BMOV in terms of both cytotoxicity and differentiation, and none of the genes were significantly down regulated following BMOV treatment. Although purely correlative at this stage, these data suggest knockdown of these 4 target genes may play a causal role in BMOV-induced cytotoxicity and/or differentiation, and that they may act to promote survival in neuroblastoma cells.

If these genes are indeed drivers of BMOV-induced cytotoxicity, we would expect that their expression would be further down-regulated in BMOV/BSO-treated cells, given that we have concluded that BSO enhances BMOV-driven transcriptional changes, in KELLY cells at least. Indeed, gene expression for *PDE2A*, *DCTN1*, *GLMP* and *TUBGCP6* mirrors the trends shown in **Figure 4.7B+C** (**Figure 4.12A**). In KELLY cells, all four genes were further significantly down-regulated in BMOV/BSO-treated cells compared to BMOV alone (BMOV vs [BMOV +BSO]), whereas in IMR32 cells there is no further significant change in expression (**Figure 4.12B**).

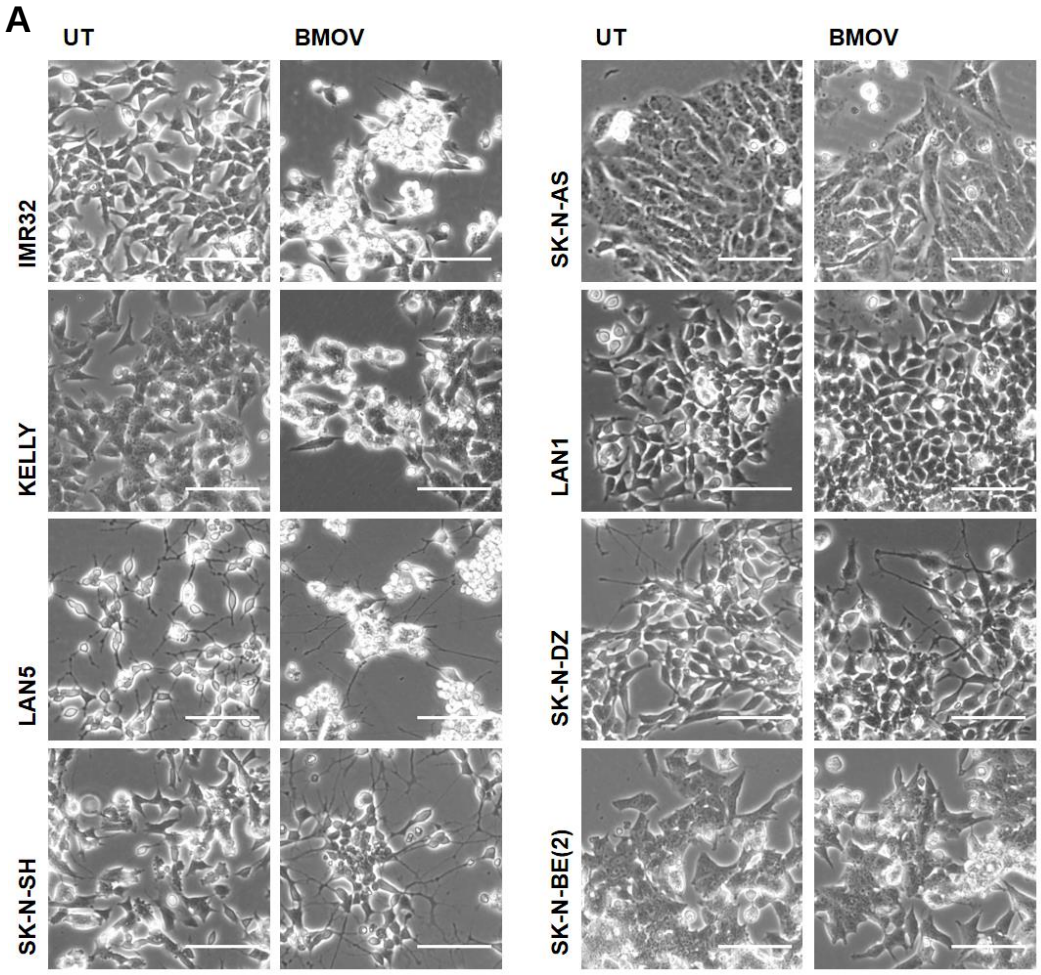

Figure 4.11 – Reduced expression of effector genes following BMOV treatment correlated with BMOV sensitivity

A *– Neuroblastoma cell lines treated with 10 µM BMOV for 5 days. Scale bar = 100 µm.* ***B*** *(next page) – qPCR showing DCTN1, PDE2A, GLMP and TUBGCP6 gene expression in neuroblastoma cell lines treated with 10 µM BMOV for 24 hours. ANOVA with Bonferroni post hoc, ns = not significant * p<0.05 ** p<0.01 *** p<0.001 (n=3).* ***C*** *(next page) – Table qualitatively summarising morphological BMOV sensitivity and BMOV-induced gene expression changes in neuroblastoma cell lines. Morphological BMOV sensitivity (second column) was scored based on qualitative observations, including cell density, rounding up of cell bodies and loss of adhesion, all indicative of cytotoxicity, as well as neurite extension, which is observed in SK-N-SH cells following BMOV treatment and is indicative of differentiation. Gene expression changes were summarised from the qPCR analysis presented in* ***B****.*

Figure 4.11 continued

B

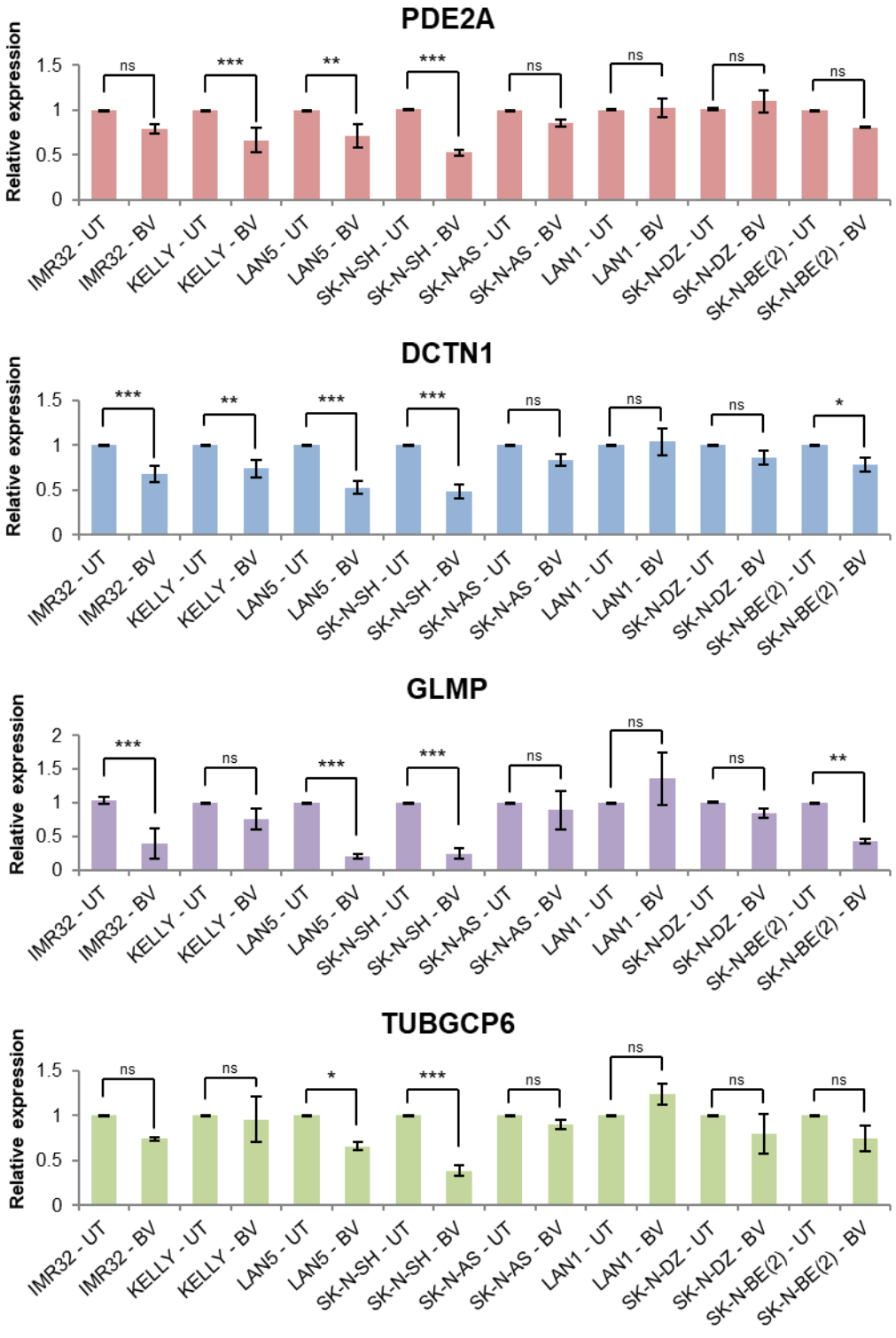

C

	BMOV sensitive	Gene knock-down			
		PDE2A	DCTN1	TUBGCP6	GLMP
IMR32	S	(Y)	Y	(Y)	Y
KELLY	S	Y	Y	N	(Y)
LAN5	S	Y	Y	Y	Y
SK-N-SH	S	Y	Y	Y	Y
SK-N-AS	(S)	(Y)	(Y)	N	(Y)
LAN1	R	N	N	N	N
SK-N-DZ	R	N	(Y)	(Y)	(Y)
SK-N-BE(2)	(S)	(Y)	Y	(Y)	Y

S = Sensitive
(S) = Slightly sensitive
R = Resistant
Y = knock-down
(Y) = non-significant knock-down
N = no knock-down

A

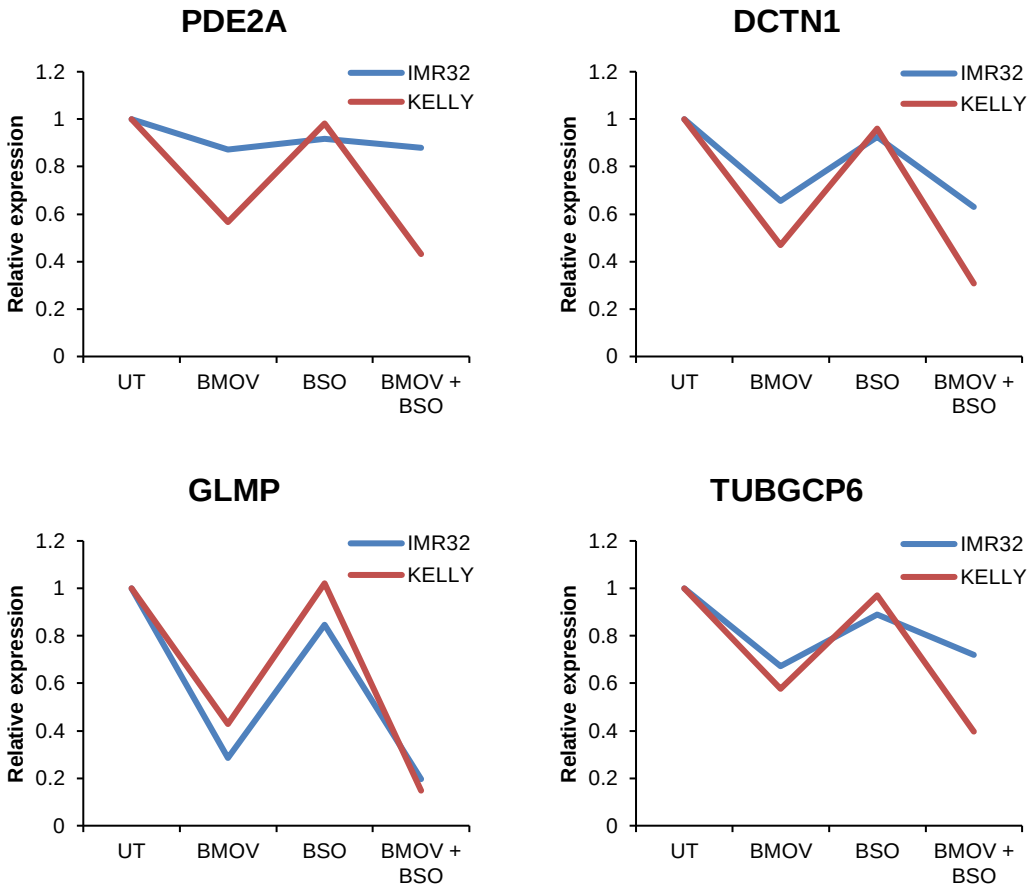

B

IMR32	PDE2A		DCTN1		GLMP		TUBGCP6	
	Log2FC	Adj P	Log2FC	Adj P	Log2FC	Adj P	Log2FC	Adj P
UT vs BMOV	-0.234	0.036	-0.629	4.36E-22	-1.148	1.09E-19	-0.534	3.40E-07
UT vs BSO	-0.050	1.000	-0.045	1.000	-0.107	1.000	-0.078	1.000
UT vs BMOV+BSO	-0.173	0.570	-0.623	2.94E-12	-1.443	6.05E-24	-0.407	0.005
BMOV vs BMOV+BSO	0.035	1.000	-0.016	1.000	-0.137	1.000	0.084	1.000

KELLY	PDE2A		DCTN1		GLMP		TUBGCP6	
	Log2FC	Adj P	Log2FC	Adj P	Log2FC	Adj P	Log2FC	Adj P
UT vs BMOV	-0.668	8.87E-14	-0.948	2.06E-49	-1.004	2.66E-19	-0.632	5.14E-10
UT vs BSO	0.016	1.000	-0.001	1.000	0.037	1.000	0.004	1.000
UT vs BMOV+BSO	-1.093	7.82E-33	-1.587	6.15E-126	-2.501	1.45E-61	-1.208	7.10E-30
BMOV vs BMOV+BSO	-0.378	1.91E-04	-0.605	4.11E-21	-1.182	9.68E-15	-0.508	5.65E-06

Figure 4.12 – BMOV effector gene expression in BMOV, BSO and combination-treated cells

A *- Relative expression of PDE2A, DCTN1, GLMP and TUBGCP6 in BMOV, BSO and combination-treated IMR32 (blue) and KELLY (red) cells, extracted from RNAseq data. Mean normalised gene counts for each condition were calculated and normalised to untreated cells.*
B *- Log2 fold changes (Log2FC) and associated adjusted p values (AdjP) from DESeq2 analysis of comparative PDE2A, DCTN1, GLMP and TUBGCP6 gene expression between various chemical treatments. Colour coded to show whether genes met the original criteria to be considered significantly differentially expressed, and therefore appeared in filtered gene lists (log2 FC >0.3 or <-0.3, AdjP<0.05). Green = significant, orange = non-significant.*

4.2.7. IPA analysis of BMOV-treated cells

Another approach to utilise these RNAseq data for understanding BMOV cytotoxicity mechanisms is to use pathway analysis. IPA is a network analysis tool produced and maintained by QIAGEN, which correlates expression data with known signalling networks and upstream molecules. Any list of genes, along with corresponding relative expression values, can be imported, and the analysis generates a list of known networks associated with similar gene expression changes. Similarly, the software generates a list of upstream regulators, including chemicals, transcription factors etc., that cause similar gene expression changes to those within the imported list. Using this analysis, I hoped to gain insight into the cellular networks that may be involved in the mechanism by which BMOV induces cytotoxicity and differentiation in neuroblastoma cells.

IPA analysis was performed using gene lists that were significantly up or down regulated in response to BMOV from both the current RNAseq experiment using IMR32 and KELLY cells, and the previous experiment using SK-N-SH and LAN5 cells (A. Di Florio and A. Stoker, unpublished). The findings from this analysis were, however, very difficult to interpret. Many networks and upstream regulators were identified, but in the vast majority of cases, the overlap with the experimental data sets was insignificant and based on gene associations with limited functional data. Furthermore, there were very few examples of networks that were detected in gene lists from multiple cell lines, making it difficult to identify pathways that are likely to be relevant in BMOV-induced cytotoxicity and differentiation. For example, the top four pathways that correlated to the experimental data for BMOV-treated IMR32 cells all related to cholesterol biosynthesis. When these networks were investigated, correlations were based on very small numbers of genes, even fewer of which actually correlated with the experimental data (5 out of 28 genes for the first pathway and 3 out of 13 for the other 3). *LPCAT3* was one of these genes, and was significantly down regulated in response to BMOV in all four cell lines (**Table 4.2**). However, siRNA-mediated knockdown of LPCAT3 did not induce loss of cell viability in IMR32 or KELLY cells (**Figure 4.9A+B**). Reduced expression of LPCAT3 has been linked to increased cholesterol synthesis,

which can led to enhanced proliferative signalling that may promote tumourigenesis (Wang et al., 2018). Increased levels of cholesterol have been previously reported in cancer, in particular in breast cancer where high plasma cholesterol is reported to enhance tumour aggressiveness (Aylon and Oren, 2016, Llaverias et al., 2011). It is therefore unlikely that cholesterol biosynthesis plays a causal role in BMOV-induced cytotoxicity, given that LPCAT3 expression is reduced, rather than enhanced by BMOV treatment. Activation of the non-canonical Wnt-calcium signalling pathway was correlated with the BMOV-treated KELLY cell RNAseq data. Wnt signalling and in particular the Wnt-calcium pathway has been heavily implicated in various cancers including neuroblastoma (De, 2011, Blanc et al., 2005), however activation of Wnt signalling was not correlated with the data from the other three cell lines.

4.2.8. BMOV induces activation of cAMP signalling

Although it was difficult to discern patterns in the IPA analysis, I did identify one potential pathway that showed more promise as a BMOV effector. IPA analysis using both the current KELLY RNAseq data, and the previous SK-N-SH and LAN5 data, identified significant overlap between the forskolin activation network and my experimental data (**Figure 4.13A+B).** Forskolin is a naturally occurring diterpene found in the roots of the *Coleus forskohlii* plant, which has been used in traditional medicine for many centuries (Kanne et al., 2015). It directly activates adenylyl cyclase (AC) and therefore elevates intracellular cAMP levels, resulting in increased cAMP-mediated signalling events (Seamon et al., 1981) (**Figure 4.13C**). One of the major implications of elevated cAMP is increased protein kinase A (PKA) signalling, which is involved in many cell behaviours including proliferation, apoptosis and differentiation, and is therefore highly relevant to cancer biology (Sapio et al., 2017). Several published studies have demonstrated anti-cancer properties of forskolin and other agents that increase cAMP signalling in range of tumour types. These properties include reduced proliferation, reduced migration, and increased epithelial morphology (Pattabiraman et al., 2016, Chen et al., 1998). Of particular interest, forskolin is able to induce differentiation in neuroblastoma cell lines (Radha et al., 2008). Interestingly, *PDE2A*, one of the

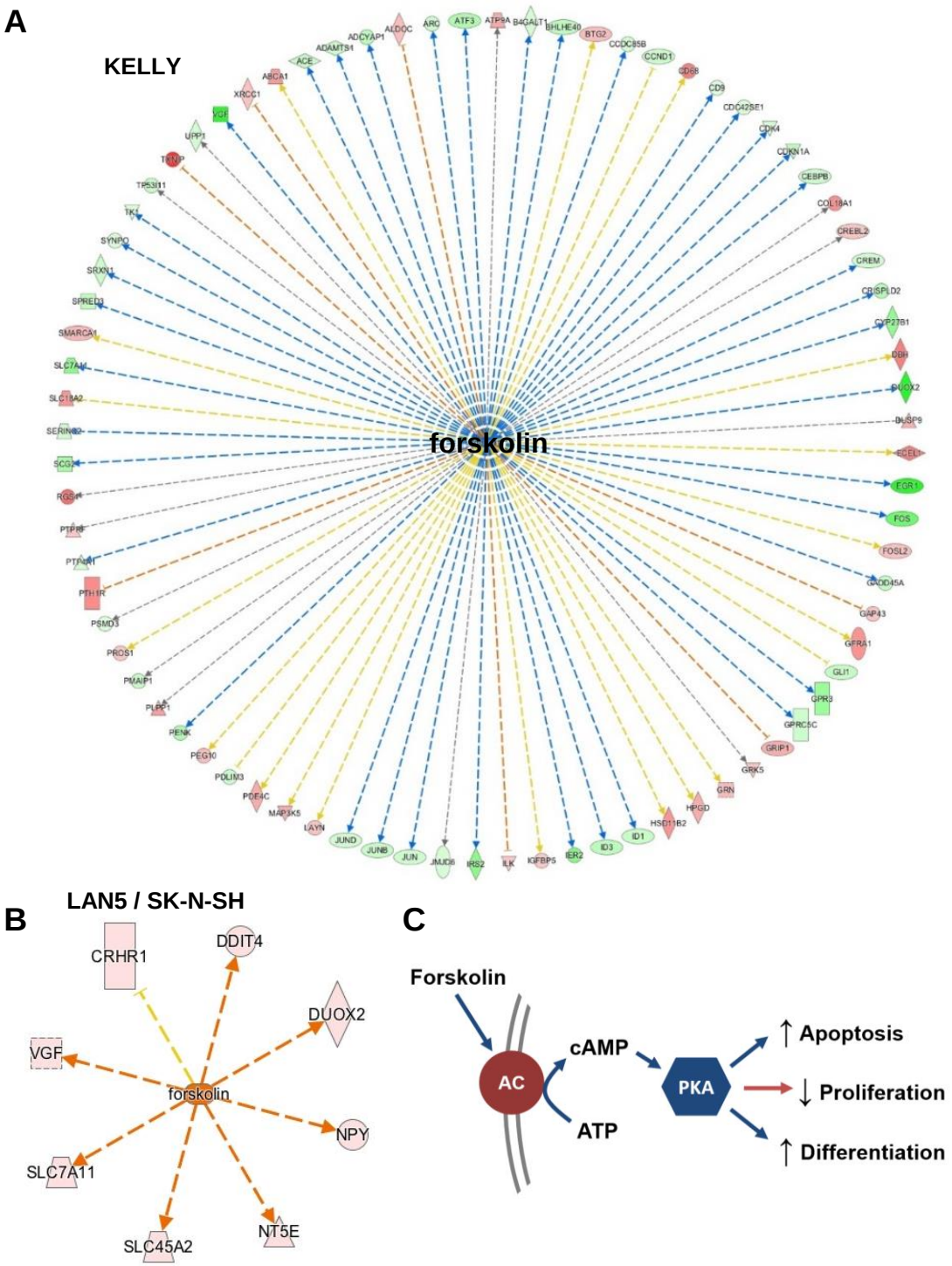

Figure 4.13 – BMOV-induced transcriptional changes were consistent with activation of the forskolin/cAMP signalling network

A+B *– IPA network analysis showed correlation between forskolin associated genes and transcriptional changes from BMOV-treated KELLY (**A**) and LAN5/SK-N-SH (**B**) RNAseq data sets. Genes in red symbols had increased expression in BMOV-treated cells and genes in green had decreased expression. Orange and blue lines indicate agreement between the predicted and observed transcriptional changes, yellow lines indicate disagreement. In all cell lines the observed gene expression changes broadly correlate with the predicted forskolin activation network. © 2000-2017 QIAGEN.* ***C*** *– Simplified forskolin/cAMP signaling pathway. AC = adenylyl cyclase, PKA = protein kinase A. Forskolin activates AC, which in turn activates PKA-mediated signaling pathways via increased cAMP, leading to increased apoptosis and differentiation and reduced proliferation (Chen et al., 1998).*

genes that is down-regulated following BMOV treatment (**Table 4.2** and **Figure 4.11B**), and for which knockdown caused a loss of cell viability in neuroblastoma cells (**Figure 4.9 + 4.10**), is involved in cAMP signalling. PDE2A is a dual substrate cyclic nucleotide phosphodiesterase (PDE), which hydrolyses both cAMP and cGMP (Martins et al., 1982). Hydrolysis and degradation of these second messengers is critical for the proper regulation of their activity and the pathways that they regulate. PDE2A is unique in that its cAMP hydrolysis activity is enhanced by cGMP binding, allowing crosstalk between these pathways (Beavo et al., 1971, Martinez et al., 2002, Russwurm et al., 2009).

As BMOV appeared to enhance signalling along the forskolin network according to IPA and the transcriptomic data, I hypothesised that activation of this network may induce some BMOV-like morphological changes. Neuroblastoma cells were treated with forskolin to activate signalling, and cell viability and differentiation was assessed (**Figure 4.14A+B**). IMR32 cells treated with 100 µM forskolin for 6 days began to round up and lose adhesion typical of cytotoxicity. IMR32 as well as KELLY, LAN5, SK-N-SH and HEK-293T cell viability following 3 days treatment with 100 µM forskolin was then assayed using resazurin (**Figure 4.14B**). IMR32, LAN5 and HEK-293T cells were sensitive to forskolin under these conditions. SK-N-SH cells did not display a loss of cell viability. However, there were subtle signs of differentiation after 6 days forskolin treatment, namely increased neurite length and rounding and elongation of cell bodies, and cells appeared to have scattered rather than growing in clusters (**Figure 4.14A**). This partially mimics the phenotype observed following BMOV treatment at least qualitatively (**Figure 4.3**). KELLY cells were not sensitive to forskolin treatment.

With help from Dr. Michael Orford (Stem cells and regenerative medicine, ICH, UCL), we were able to measure cAMP concentrations using HPLC in cells treated with BMOV or forskolin for 24 hours (**Figure 4.14C**). In SK-N-SH cells, intracellular cAMP concentration was increased following treatment with both forskolin and BMOV, although this did not reach statistical significance using ANOVA with Dunnett post hoc testing. Forskolin modestly increased cAMP concentration in BMOV-resistant SK-N-AS cells, however BMOV had no

effect. Interestingly there were no changes in cAMP concentration following treatment with BMOV or forskolin in KELLY cells, despite activation of the forskolin gene expression network being highlighted in BMOV-treated KELLY cells in the IPA analysis. Nonetheless, taken together these data indicate that increased cAMP, perhaps due to reduced PDE2A expression, may form part of the mechanisms that drive cytotoxicity and differentiation following BMOV treatment in some neuroblastoma cell lines (**Figure 4.15**).

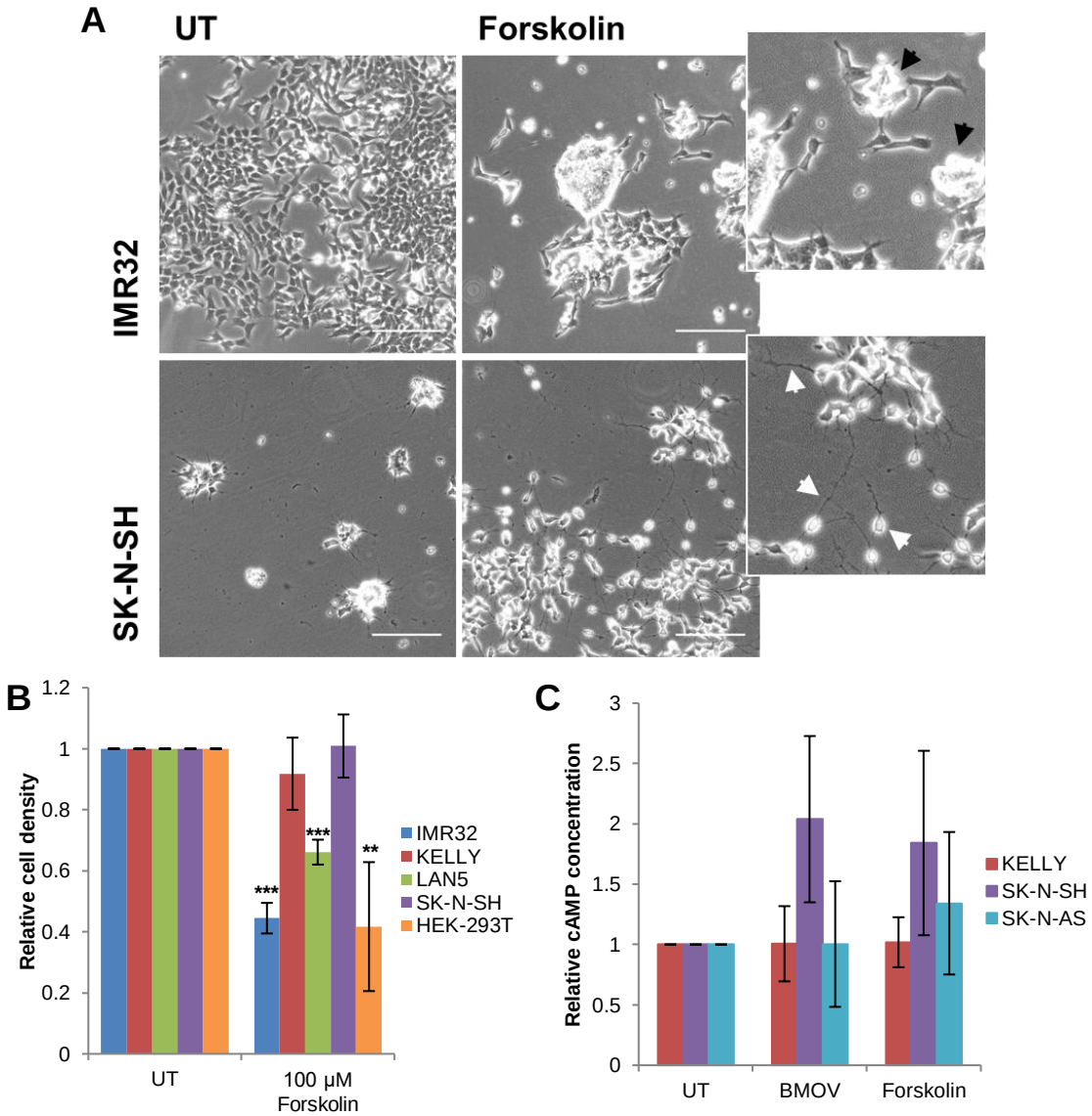

Figure 4.14 – cAMP signalling may contribute to BMOV-induced cytotoxicity
***A** – IMR32 and SK-N-SH cells treated with 100 µM forskolin for 6 days showing BMOV-like morphological changes. Black arrows indicate loss of adhesion indicative of non-viable cells. White arrows indicate neurite extension and rounded elongated cell bodies, indicative of differentiation. Scale bar = 150 µm. Images on the right are zoomed in fields of view for forskolin-treated cells. **B** – Resazurin cell viability assay in IMR32, KELLY, LAN5, SK-N-SH and HEK-293T cells treated with 100 µM forskolin for 3 days. Independent T-tests comparing forskolin-treated to untreated (UT) cells for each cell line, ** p<0.01 *** p<0.001 (n=3). **C** – cAMP concentration measured by HPLC in KELLY, SK-N-SH and SK-N-AS cells treated with 10 µM BMOV or 100 µM forskolin for 24 hours (n=3). No statistical significance using ANOVA with Dunnett post hoc.*

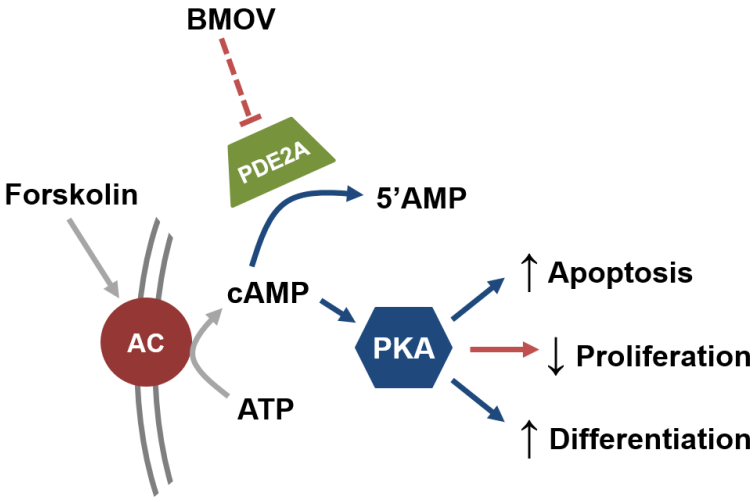

Figure 4.15 – Proposed BMOV mechanism of action
AC = adenylyl cyclase, PKA = protein kinase A. PDE2A was downregulated following BMOV treatment in the RNAseq experiment. Reduced PDE2A expression inhibits cAMP degradation, resulting in enhanced cAMP-mediated signalling, including the PKA pathway, leading to increased apoptosis and differentiation and reduced proliferation (Chen et al., 1998).

4.3. Discussion

Here I have confirmed that the oxidovanadium derivative BMOV is able to drive cytotoxicity and/or differentiation in a subset of neuroblastoma cell lines (**Figures 4.1-3**). This has been previously published by our group (Clark et al., 2013, Clark et al., 2015), and the anti-cancer effects of BMOV and other oxidovanadium compounds have been widely described in other tumour types (Dąbroś et al., 2011, Sálice et al., 1999, Evangelou, 2002). The mechanisms that drive these BMOV-induced morphological changes in neuroblastoma cell lines, and more broadly the anti-cancer effects of oxidovanadium compounds in various cancer models had, however, remained somewhat unclear. Here, I have presented data indicating that oxidovanadium can generate a broad and complex transcriptional response in these tumour cells. The data point to a role of the cAMP signalling network, perhaps including PDE2A, as a novel mechanism underlying some of the observed oxidovanadium effects.

When considering chemicals for therapeutic use it is important to consider their effects on off-target tissues. In this study, I treated a range of neuroblastoma and non-neuroblastoma cell lines with BMOV and BSO (**Figure 4.2A** and **Appendix 2**). Although there was a range of sensitivities to BMOV, these did not group into sensitive tumour and resistant non-tumour cell lines. Nonetheless, the fact that oxidovanadium was not generally toxic to all cell

lines was reassuring. SK-N-SH cells show morphological changes indicative of differentiation following oxidovanadium treatment (**Figure 4.3**). However, it is possible that this may be associated with a generalised stress response. Furthermore, human phase I and phase IIa clinical trials using BEOV, an ethyl analogue of BMOV, in the diabetes field have been performed, reporting no major adverse effects (Thompson et al., 2009). It should however be noted that the maximum plasma concentration of BEOV in these clinical trials was 170 ng/ml, which is equivalent to 493 nM and is thus much lower than the 10 μM used in most of the *in vitro* assays reported here (Thompson and Orvig, 2006). BSO was generally tolerated by most neuroblastoma and non-neuroblastoma cell lines tested here, although this somewhat contradicts previously published data (Anderson et al., 1997, Dukhande et al., 2013). BSO has also been used and tolerated in human clinical trials to enhance the anti-cancer action of other therapeutic agents at concentrations that exceed those used in this project (Bailey et al., 1994, Anderson et al., 2001). The combination of BMOV with BSO induced some level of cytotoxicity in all cell lines treated in this study. Therefore, while clear that BSO enhances oxidovanadium action, biochemically, transcriptionally and cytotoxically, it remains to be seen whether such a combination would remain tolerated in *in vivo* tumour models and therefore be useful ultimately in humans. Nonetheless, advances in delivery methods such as targeted nanoparticles may allow a combination of oxidovanadium with glutathione blockage to be safely delivered to tumour cells (addressed in part in **Chapter 5**). Alternatively, a better understanding of the mechanisms that drive BMOV activity in neuroblastoma cells, as I aimed to achieve here, may itself lead to the identification of novel druggable therapeutic targets that will not require use of oxidovanadium itself.

Work previously published by our group and described in **Section 4.1.** indicated that BMOV-induced cytotoxicity was unlikely to be driven by ion channel blockage, genotoxicity, or ROS production (Clark et al., 2015). In the same paper it was reported that phosphorylation of AKT and ERK are increased after treatment with BMOV, and that these increases in phosphorylation somewhat correlate with BMOV sensitivity. This is perhaps

surprising given that both Ras-MAPK and PI3K/AKT pathways are for the most part considered positive regulators of cell proliferation and survival, and activating mutations in both pathways are very common in virtually all cancers (McCubrey et al., 2007, Hennessy et al., 2005). However, it is rarely the case that signalling molecules and pathways are purely cancer promoting or inhibiting, most can have opposing roles in specific contexts (Sever and Brugge, 2015). This is true for both AKT and ERK pathways. For example, whilst AKT is often pro-survival, activation of AKT can also sensitise tumour cells to ROS-mediated apoptosis (Los et al., 2009, Nogueira et al., 2008). Similarly, sustained activation of ERK can promote apoptosis, autophagy and senescence (Cagnol and Chambard, 2010). Moreover in neuroblastoma specifically, where retinoic acid is used therapeutically, activation of both AKT and ERK is observed during retinoic acid-induced differentiation in SH-SY5Y cells (Singh et al., 2003, López-Carballo et al., 2002). In the current study, I have shown that increased phosphorylation of AKT and ERK is unlikely to be a driver of BMOV-induced cytotoxicity in neuroblastoma cells. These signalling events are certainly not required for loss of viability to occur, as inhibition of MEK and AKT did not reduce sensitivity to BMOV (**Figure 4.5**). In particular, I wanted to ask whether these pathways act redundantly, such that inhibition of either MEK or AKT would not affect BMOV-induced cytotoxicity. However even when both inhibitors were administered together, IMR32 cells were not protected from cytotoxicity induced by BMOV (**Figure 4.5C**). I was able to confirm that these MEK and AKT inhibitors were active in reducing phosphorylation of ERK and AKT (Figure 4.5A). However, as basal levels of phospho-EKR and AKT were fairly low in IMR32 and KELLY cells, acute pathway activation followed by inhibitor treatment, may have produced more convincing data. Nevertheless, these findings build on the laboratory's previous report that increased phosphorylation of AKT and ERK is also not required for BMOV-induced differentiation in SK-N-SH and LAN5 cells (Clark et al., 2013). Phosphorylation of AKT and ERK was assessed following relatively long time points of BMOV treatment, 48 or 72 hours in this study and 24 hours in previous publications from the lab (Clark et al., 2012, Clark et al., 2015). Therefore, these signalling changes are likely to be indirect effects. It is possible that increased signalling down these pathways is a survival feedback

mechanism, which occurs in these cells to counteract the growth inhibitor and cytotoxic effect of BMOV. Regardless, increased phosphorylation of AKT and ERK can nonetheless be used as a marker of oxidovanadium activity, as these events seem to occur whenever BMOV is active, regardless of whether the cellular response is cytotoxicity or differentiation.

Having eliminated activation of AKT and/or ERK as the key mechanisms driving BMOV-induced toxicity, genome-wide transcriptomics was then used in attempt to identify alternative pathways. The unbiased RNAseq analysis presented here clearly demonstrates that there is a complex transcriptional response to BMOV, and the BMOV+BSO combination, in neuroblastoma cells. The decision to use a transcriptomic approach was not necessarily an obvious one. As discussed previously, oxidovanadium, specifically the vanadate ion, is a broad-specificity inhibitor of PTPs (Swarup et al., 1982). If PTP inhibition is the primary mechanism of action of BMOV, then phospho-mass spectrometry looking for differences in the phospho status of all proteins that are phosphorylated on tyrosine residues may be a good, although still complex, approach to look for mechanistic insight. This is certainly true; however, the laboratory had previously established that there is a transcriptional response to BMOV in SK-N-SH and LAN5 cells (A. Di Florio and A. Stoker, unpublished); therefore, it was reasonable to expand on this approach to look for mechanisms of BMOV-induced cytotoxicity in IMR32 and KELLY cells. Furthermore, this would allow four data sets from four distinct neuroblastoma cell lines to be directly compared, hopefully leading to the identification of transcriptional changes that are relevant for BMOV activity across a range of neuroblastoma cell lines.

One key question that I wanted to answer using the RNAseq data was how BSO enhances BMOV-induced cytotoxicity in neuroblastoma cell lines. RNAseq was performed in IMR32 and KELLY cells treated with BMOV with and without BSO. In KELLY cells there were 1835 significant gene expression changes in BMOV+BSO-treated cells compared to BMOV alone (BMOV vs [BMOV + BSO]) (**Figure 4.7A**). Of these 1835 genes, expression of over 80% were also altered in the same direction by BMOV alone, although not always significantly (**Figure 4.7A+B**). This strongly suggests that BSO chemically

enhances BMOV activity, therefore enhancing BMOV-induced transcriptional changes, rather than generating a unique, combination-specific response. Although a small proportion of genes (17%) were seemingly uniquely differentially expressed in the opposite direction in combination-treated cells compared to BMOV-treated cells, these were mostly associated with extremely low and non-significant fold changes and are therefore unlikely to be relevant. Further support for the conclusion that BSO does not induce a unique combination-specific response comes from the IMR32 data. In contrast to in KELLY cells, there was surprisingly only one significant gene expression change in BMOV+BSO-treated IMR32 cells compared to BMOV alone (BMOV vs [BMOV + BSO]), despite clear increased cytotoxicity (**Figure 4.1A, 4.6B** and Clark et al., 2015). The genes with the highest fold changes in untreated compared to combination-treated IMR32 cells were modestly up- or down-regulated in the same direction in the combination treatment compared to BMOV alone, although these additional changes were mostly not significant (**Figure 4.7C**). This difference between IMR32 and KELLY cell response to the BMOV+BSO combination was very unexpected, and suggests that perhaps in IMR32 cells BMOV alone is sufficient to drive the gene expression changes required for BMOV-induced cytotoxicity. Phenotypically IMR32 cells are more sensitive to BMOV in monotherapy than KELLY cells; therefore, it is plausible that more of the genes responsible for BMOV-induced cell death are already altered maximally following BMOV treatment alone in IMR32 cells compared to KELLY cells. However, importantly, there is still an additional cytotoxic effect of BMOV+BSO co-treatment compared to BMOV alone in IMR32 cells (**Figure 4.1A**), that may therefore be driven by biochemical rather than transcriptional changes. In order to assess whether the biochemical response to BMOV is enhanced by BSO in IMR32 as well as KELLY cells, phosphoproteomics could be employed. Nonetheless, these data suggest that in KELLY cells at least, BSO enhances BMOV-driven transcriptional changes, and this may explain in part the increased cytotoxicity observed in combination-treated cells.

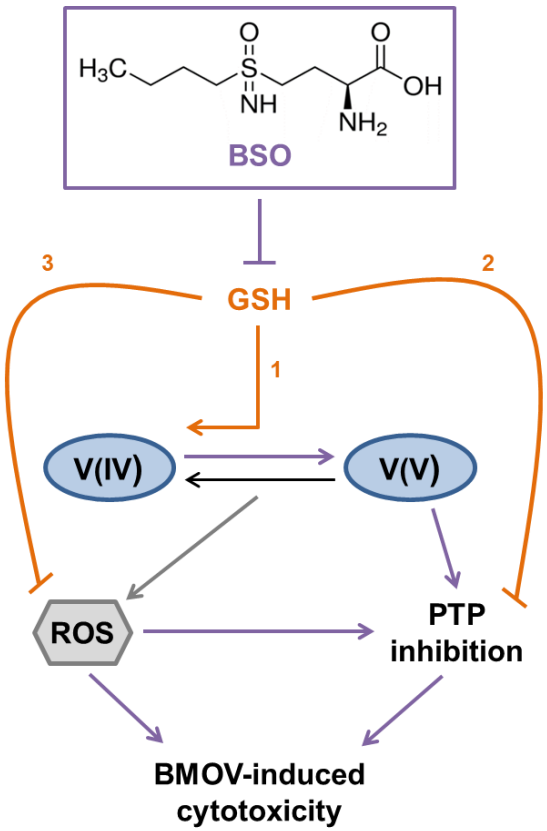

Figure 4.16 – BSO chemically enhances BMOV activity
*Proposed mechanisms by which BSO enhances BMOV-induced cytotoxicity in neuroblastoma cells. BSO-induced depletion of glutathione (GSH) likely encourages the cytoplasmic equilibrium of vanadyl (V(IV)) to vanadate (V(V)) to shift to favour PTP-inhibiting vanadate, contributing to BMOV-induced cytotoxicity (**1**). Vanadyl-to-vanadate cycling produces reactive oxygen species (ROS), which may contribute directly to BMOV-induced cytotoxicity via non-PTP related mechanisms, or indirectly via PTP inhibition by active site cysteine oxidation. BSO may further enhance BMOV-induced cytotoxicity both by preventing GSH-mediated PTP active site reactivation (**2**), and by preventing GSH-mediated ROS clearance (**3**).*

The hypothesis that BSO enhances BMOV cytotoxicity by chemically enhancing its activity is logical based on glutathione activity (**Figure 4.16**). As stated previously, BSO is a chemical inhibitor of the rate-limiting enzyme in glutathione synthesis, and therefore depletes intracellular glutathione (**Figure 4.1C**). Macara et al. (1980) reported that reduction of vanadate to vanadyl, was dependent on intracellular glutathione. Therefore BSO-mediated glutathione depletion likely promotes the PTP-inhibiting vanadate form of the vanadium ion. Furthermore, PTPs can be inhibited by oxidation of their active site cysteine, either by vanadium compounds directly, or by ROS produced during vanadyl-to-vanadate cycling (Peters et al., 2003, Barford, 2004, Ostman et al., 2011). This inhibition is reversible as cysteine residues can be reduced,

coupled to glutathione oxidation (den Hertog et al., 2005). Therefore, depletion of glutathione may also directly induce sustained PTP inhibition.

BSO may also increase BMOV-induced cytotoxicity by sensitising cells to oxidative stress (**Figure 4.16**). Glutathione is one of the cell's major antioxidant defences as it sequesters ROS. Therefore, depletion of glutathione may leave neuroblastoma cells more susceptible to oxidative damage. Cancer cells notoriously have higher basal levels of oxidative stress, a feature that has been exploited therapeutically over many decades (Fang et al., 2007). BSO has been reported to enhance cytotoxicity of other chemotherapeutic drugs in neuroblastoma, perhaps by sensitising cells to oxidative damage (Anderson and Reynolds, 2002), and has even been found to induce cytotoxicity as a monotherapy in some neuroblastoma cell lines (Dukhande et al., 2013, Anderson et al., 1997, Anderson et al., 2001). Although IMR32 and KELLY cells were not sensitive to BSO in monotherapy in our hands, we did see high levels of toxicity in SK-N-DZ and SK-N-BE(2) cells in agreement with data reported by Anderson et al. (1997) (**Figure 4.2A**). It has been suggested that BSO sensitivity across different neuroblastoma cell lines is dependent on the overall redox status of the cell (Marengo et al., 2008). Therefore, it is possible that IMR32 and KELLY cells are resistant to BSO alone, due to high levels of redox tolerance, but glutathione depletions renders them extremely sensitive to even the fairly low increases in ROS associated with BMOV treatment (Clark et al., 2015). In this model, even if oxidative stress is not the primary mechanism driving BMOV-induced cytotoxicity, it may come into play when glutathione is depleted. This may explain why cell lines that are resistant to BMOV alone were sensitive to the combination (**Figure 4.2A**). If this were to be true, we would expect unique transcriptional changes associated with oxidative stress to occur in BMOV/BSO-treated cells, qualitatively different from those observed in cells treated with BMOV alone. Although importantly, increased ROS produced as a result of vanadyl-to-vanadate cycling, and sustained due to BSO-induced glutathione depletion, may contribute directly to PTP inhibition via cysteine oxidation, and this may also contribute to increased cytotoxicity (Barford, 2004) (**Figure 4.16**).

In general, analysis of the RNAseq data did not support non-specific oxidative damage as the mechanism for BMOV/BSO driven cytotoxicity. IPA analysis did provide weak a correlation between activation of the NRF2-mediated oxidative stress pathway and the experimental expression data from KELLY cells treated with BMOV+BSO compared to BMOV alone. NRF2 is a transcription factor that translocates to the nucleus following increased ROS, where it regulates the expression of genes involved in antioxidant and anti-inflammatory defences (Kumari et al., 2018). Activation of this pathway would indicate that KELLY cells treated with BMOV in combination with BSO are subjected to oxidative stress. However, we deemed this correlation to be insignificant as the overlap between the expected gene expression changes when the NRF2-mediated oxidative stress response pathway is active and the observed experimental changes was only 5.7%, with expression of just 11 out of 193 associated genes changing in the correct direction. Furthermore, this correlation, and others, may occur purely as a consequence of apoptosis rather than a cause, i.e. these genes may be up or down regulated due to apoptosis, and are not themselves initiating apoptosis. Further analysis using RNA extracted from cells treated with BMOV over a range of time points would be required to separate gene expression changes that likely occur as a consequence of the initiation of cell death. Importantly, previous published work by our group reported that whilst ROS are modestly increased by BMOV, this occurs in both BMOV-sensitive and resistant neuroblastoma cell lines, and there is no further increase when cells are treated with BMOV and BSO in combination (Clark et al., 2015). Thus to date we feel the most likely explanation for BSO enhancing BMOV-induced cytotoxicity is that depletion of glutathione encourages the cytoplasmic equilibrium of oxidovanadium to shift to the PTP-inhibiting vanadate form of the vanadium ion, therefore chemically enhancing BMOV activity. Nonetheless, a role for ROS production in the observed cell death cannot be entirely ruled out given the apparent complexity of BMOV's actions. In either case, it is clear that combining BMOV with BSO-mediated glutathione suppression enhances the therapeutic potential of this oxidovanadium compound.

The other main aim of the RNAseq data analysis was to identify specific BMOV effector pathways and molecules that drive BMOV-induced cytotoxicity and differentiation in neuroblastoma cells. For this I used BMOV-treated IMR32 and KELLY cells from my data set, as well as SK-N-SH and LAN5 from a previous data set obtained by the team (A. Di Florio and A. Stoker, unpublished). Comparison of lists of genes that are differentially expressed following BMOV treatment in each of the cell lines revealed many similar and unique gene expression changes (**Figure 4.8**). Genes that were differentially expressed in multiple cell lines were assumed to be most critical for BMOV activity. Two approaches were then taken in identifying mechanisms that might be important for BMOV-induced cytotoxicity. First, careful filtering of gene lists led to the selection of 24 candidate BMOV effector genes that were down-regulated in response to BMOV in multiple cell lines (**Table 4.2**). The majority of these genes had not been previously convincingly implicated in cancer, but as I was attempting to identify novel targets using hypothesis-free analysis, they were all taken forward for further validation. Initial siRNA-mediated knockdown experiments were performed revealing a wide range of final cell densities following transfection with each siRNA pool (**Figure 4.9A+B**). The majority of the siRNAs reduced cell viability or proliferation fairly modestly. This is perhaps not surprising given that the gene expression changes observed in the RNAseq experiment had fairly low fold changes. Furthermore, the degree of cell death observed following BMOV treatment is almost certainly driven by the combined effect of several transcriptional and post-translational changes. It is therefore unlikely that a similar level of cytotoxicity could be achieved by silencing one candidate BMOV effector in isolation. Nonetheless, significant differences in cell viability following knockdown of the 24 genes were indeed observed in IMR32, KELLY and SK-N-AS cells for four genes in particular, *DCTN1*, *PDE2A*, *TUBGCP* and *GLMP* (**Figure 4.9C-F**). When gene expression following BMOV treatment was assessed in a wider panel of neuroblastoma cell lines, reduced expression of these genes broadly correlated with BMOV sensitivity (**Figure 4.11**). These genes and their encoded proteins may therefore play a critical role in BMOV-induced cytotoxicity, and by extrapolation in normally sustaining neuroblastoma cell proliferation or survival. They could therefore form the initial basis for future

research into novel targeted therapies. Importantly, due to time limitations, genes that were upregulated have not yet been analysed in detail, and may well provide further insights into the mechanisms driving BMOV activity in neuroblastoma cell. I chose to prioritise down regulated genes as this may be more easily targeted using small molecules for example.

The second approach that I took in identifying signalling pathways that drive BMOV activity was network analysis using IPA (QIAGEN). For this, lists of genes that were significantly up or down regulated following BMOV treatment were analysed. As with the gene list filtering, I intended to use this analysis in an unbiased and hypothesis-free manner. However, due to the complexity of the output of network analysis described previously, it was very difficult to identify meaningful candidate pathways that may play a role in BMOV activity. Network analysis using large datasets such as these is notoriously complicated, in particular when using chemicals with broad activity like BMOV. We therefore decided to focus on a network identified using the IPA analysis for which there was a good basis for a role in cancer based on the literature. Gene expression changes associated with forskolin correlated with our experimental datasets for KELLY, LAN5 and SK-N-SH based on IPA analysis. Forskolin activates cAMP signalling, which has been previously implicated in cell survival, proliferation and differentiation (Chen et al., 1998, Sapio et al., 2017). Furthermore, *PDE2A*, one of the genes identified as a candidate BMOV effector, is implicated in cAMP signalling. This gave us some confidence in pursuing cAMP signalling as a potential BMOV effector pathway. Alternative pathway analysis tools such as Gene Set Enrichment Analysis and WebGesalt are available, and these could be used to reanalyse the RNAseq data. This may both identify alternative interesting potential BMOV effector pathways, and validate the forskolin network correlation that was identified using IPA.

I have presented some initial data that provide some support for a role of cAMP signalling in BMOV-induced cytotoxicity and differentiation in neuroblastoma cell lines. Neuroblastoma cells treated with forskolin for the most part mirrored the morphological changes observed following BMOV treatment (**Figure 4.14A+B**). Given the role of forskolin in activating cAMP-mediated signalling (Seamon et al., 1981), I measured cAMP concentrations in cells treated with

BMOV and forskolin to see if BMOV really did activate this pathway (**Figure 4.14C**). HPLC was used to measure cAMP concentrations. This was a new and challenging assay developed in collaboration with Dr. Michael Orford (Stem cells and regenerative medicine, ICH, UCL) and probably requires further validation since cAMP concentrations were very close to the lower detection limit. Nonetheless, initial data suggest that in SK-N-SH cells at least, BMOV increases cAMP to a similar level compared to forskolin, although these data are not yet significant. This supports a role of cAMP signalling in BMOV activity. It is interesting that KELLY cells were resistant to forskolin in terms of both cytotoxicity and increased cAMP concentration (**Figure 4.14B+C**). BMOV also did not increase cAMP concentrations in these cells, despite the forskolin network being identified by IPA using the KELLY data set. It seems therefore that KELLY cells do not require increased cAMP itself in order to be killed by BMOV, however this cytotoxicity may still be dependent on changes to signalling further down the cAMP network.

First described in the 1950s, cAMP is an important second messenger that leads to activation of PKA (Rall and Sutherland, 1958, Walsh et al., 1968, Caretta and Mucignat-Caretta, 2011). PKA is activated via cAMP binding to regulatory subunits, allowing activation of the catalytic subunits (Caretta and Mucignat-Caretta, 2011). Active PKA is then able to phosphorylate a number of targets, contributing to the role of cAMP/PKA signalling in numerous cell behaviours including cell survival, proliferation and differentiation (**Figure 4.13C**) (Chen et al., 1998, Sapio et al., 2017). Given this role in the regulation of cell viability and differentiation, it is unsurprising that this pathway is heavily implicated in cancer. Although activation of PKA is the most well described effect of increased cAMP, it can also act directly on other signalling molecules, for example, ion channels and guanine nucleotide exchange factors and these effects may also be relevant to cancer (Biel, 2009, de Rooij et al., 1998).

Intracellular levels of cAMP are controlled by the opposing action of AC and PDEs, which catalyse the formation of cAMP from ATP and the hydrolysis of cAMP to 5'AMP respectively (Fertig and Baillie, 2018). Although enhanced signalling down the cAMP/PKA pathway has been positively implicated in tumour initiation and development, and therapeutic inhibition of this network

has been described, there are also studies showing that elevating cAMP can have beneficial outcomes in cancer cells (Insel et al., 2012). These outcomes include induction of mesenchymal-to-epithelial transition, reduced proliferation, apoptosis, differentiation, and reduced motility (Sapio et al., 2017, Naviglio et al., 2010, Burdyga et al., 2013, Dong et al., 2015, Follin-Arbelet et al., 2015, Pattabiraman et al., 2016, Perez et al., 2016). Lower risk of colorectal cancer has been reported in patients taking long-term antidepressants that enhance cAMP signalling (Chubak et al., 2011). Murata et al. (2000) showed that inhibition of PDE4 using rolipram elevated cAMP levels in colon cancer cells, leading to suppression of the invasive properties of these cells. Anti-cancer effects of the PDE4-specific inhibitor rolipram have also been shown in chronic lymphocytic leukaemia (CLL) and glioma (Kim and Lerner, 1998, Chen et al., 2002). Daniel et al. (2016) used data sets from The Cancer Genome Atlas (TCGA) to show that suppression of the cAMP signalling pathway is common in many cancer types, including glioblastoma, lung adenocarcinoma, bladder urothelial carcinoma and uterine endometrial carcinoma. Using the human protein atlas, they also showed that PRKACA (a catalytic subunit of PKA) was downregulated in a number of cancers. Finally, they report that activation of cAMP signalling using forskolin and a PDE inhibitor leads to apoptosis in glioblastoma cells. Several studies have reported the anti-cancer efficacy of forskolin in various tumour types, where forskolin-induced cAMP elevation leads to reduced proliferation, reduced migration, and increased epithelial morphology (Pattabiraman et al., 2016, Chen et al., 1998). Of particular interest, forskolin is able to induce differentiation in neuroblastoma and glioblastoma cell lines (Radha et al., 2008, Xing et al., 2017).

Both approaches used to analyse the RNAseq data in order to identify transcriptional changes that are relevant to BMOV activity in neuroblastoma cell lines, gene list filtering to identify BMOV effectors, and IPA network analysis, pointed to cAMP signalling. The above studies support the hypothesis that enhanced cAMP can lead to anti-cancer effects in various tumour models, and therefore give some confidence in cAMP signalling, both PKA dependent and independent, as a potential BMOV effector pathway in neuroblastoma. At this stage, the mechanism that drives this apparent link

between BMOV cytotoxicity and cAMP signalling is not at all clear. There have been some suggestions that treatment with vanadate leads to cAMP accumulation in renal and heart tissue; however, this has so far not been described in tumour cells, and a role for cAMP in the published anti-cancer effects of vanadium has not been described to my knowledge (Eiam-Ong et al., 2018, Krawietz et al., 1980, Hackbarth et al., 1980). PTP inhibition is one of the major consequences of oxidovanadium treatment and based on our current data is the most likely cause of BMOV-induced cytotoxicity in neuroblastoma cells (Clark et al., 2013, Clark et al., 2015). PKA is itself a serine/threonine rather than tyrosine kinase (Skalhegg and Tasken, 2000). However, there is cross talk between PKA signalling and canonical tyrosine kinase signalling pathways such as PI3K/AKT and MAPK/ERK (Gallo-Payet and Battista, 2014, Law et al., 2017). Law et al. (2017) reported that PKA signalling leads to inactivation of the dual specificity phosphatase 6 (DUSP6), which allows increased phosphorylation of ERK. Whilst PTP inhibition downstream of cAMP does not explain the apparent increase in cAMP concentration following BMOV treatment (**Figure 4.14C**), it may still play a role in BMOV-induced toxicity and could have contributed to the identification of the forskolin signalling network from the IPA analysis.

Increased cAMP signalling following treatment with BMOV may in part be due to BMOV-induced down regulation of PDE2A (**Figure 4.15**). Although *PDE2A* was not one of the genes that formed part of the forskolin networks reported from IPA (**Figure 4.13A+B**), it was significantly downregulated following BMOV treatment in KELLY, LAN5, SK-N-SH and to a lesser extent IMR32 cells (**Table 4.2** and **Figure 4.11B**). Furthermore, its knockdown using siRNAs led to reduced cell viability in BMOV-sensitive neuroblastoma cell lines (**Figure 4.9+4.10**). As mentioned above, there has been some interest in targeting PDEs in cancer. Specifically it was reported that PDE2A is mutated in malignant melanoma, and its inhibition using erythro-9-(2-hydroxy-3-nonyl) adenine (EHNA) hydrochloride led to reduced DNA synthesis and cell cycle arrest (Morita et al., 2013). Hiramoto et al. (2014) also reported that PDE2A inhibition using EHNA reduces growth and invasion of malignant melanoma cells. The same inhibitor was shown to be useful in the prevention and

treatment of UVB-induced skin cancer by inhibiting PDE2 (Bernard et al., 2014). Other PDE2 inhibitors, including BAY 60-7550 and Hcyb1 have been used to inhibit PDE2A in studies concerned with sympathetic hyperactivity, memory acquisition, and the treatment of depression and other cognitive impairments (Liu et al., 2018b, Liu et al., 2018a, Soares et al., 2017). If reduced PDE2A expression is important for the anti-neuroblastoma efficacy of BMOV, these inhibitors may induce BMOV-like cytotoxicity or differentiation in neuroblastoma cell lines, thus could prove to be novel therapeutic leads for the treatment of neuroblastoma and as well as other cancers. However, the possibility of side effects associated with these neurological functions of PDE2A would need to be considered.

In summary, I have presented some initial data that suggest a role of cAMP signalling, perhaps involving the reduced expression of PDE2A, in BMOV-induced cytotoxicity in neuroblastoma cells (**Figure 4.15**). In order to assess whether activation of cAMP signalling is required for BMOV activity, BMOV-induced cytotoxicity should be assessed in neuroblastoma cells where cAMP signalling has been inhibited. A reduction in BMOV-induced cytotoxicity in these cells would then suggest that cAMP signalling is an important BMOV effector pathway. Inactive cAMP analogues, such as Rp-cAMPS (Bell and McDermott, 1994), and specific inhibitors of signalling molecules associated with PKA-dependent and independent cAMP signalling should be used. These experiments may prove to be challenging, as broad inhibition of these major pathways, for example using Rp-cAMPS, may itself prove to be detrimental for neuroblastoma cells. However, if successful they could both confirm a positive role of cAMP signalling in BMOV-induced toxicity, and lead to a more advanced understanding of the specific molecules driving these events. This in turn could lead to the identification of novel therapeutic approaches for neuroblastoma.

Chapter 5. Delivery of hydrophobic oxidovanadium using liposomes

5.1. Introduction

Despite the abundant preclinical data in cell and animal models suggesting that oxidovanadium may be beneficial in cancer prevention and treatment, there are ongoing concerns regarding off-target toxicities, which have in part so far prevented clinical trials (Evangelou, 2002, Domingo, 2000, Bishayee et al., 2010). The development of a safer and more targeted delivery method may be critical if oxidovanadium were to be considered for use in humans. In recent years there has been great excitement surrounding the use of nanotechnology in medicine, including for the more effective delivery of drug molecules (Rizvi and Saleh, 2018). A wide range of nanoparticles have been, and continue to be, developed for drug delivery (**Figure 5.1**). These can involve attaching drug molecules to the surface of nanocarriers, covalently or by adsorption, or packaging them within carriers. The nanocarriers themselves can be composed of a variety of materials, including for example lipid, silicon, carbon and natural or synthetic polymers (Wilczewska et al., 2012, Conniot et al., 2014).

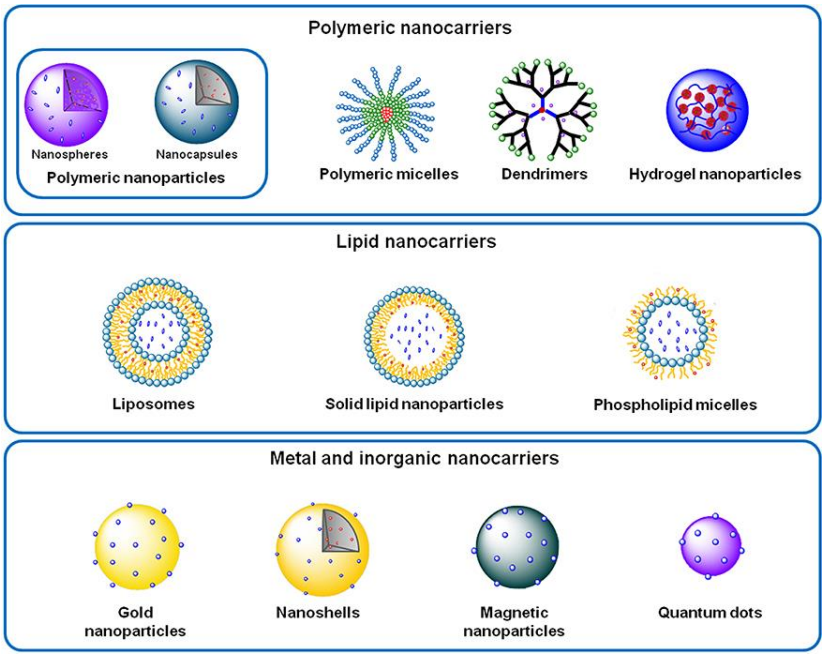

Figure 5.1 - Examples of nanoparticles used for drug delivery
Drug molecules can be encapsulated within nanocarriers or attached to their surface. Nanocarriers can be made of many materials, including but not limited to lipid, protein, silica, carbon and metals. Taken from Conniot et al. (2014).

There are several advantages associated with the use of nanoparticles for drug delivery. First, they can improve the efficiency of delivery to target tissue

meaning that lower doses can be administered to patients, therefore reducing dose-related adverse effects. The encapsulation of drug molecules, for example in the case of liposomes, can mean that degradation in circulation may be reduced, further concentrating the amount of active molecule reaching target tissues. This is particularly relevant for oxidovanadium compounds, which in many cases have been shown to undergo ligand exchange reactions in the gut and in circulation (Levina and Lay, 2017). Off-target effects associated with non-specific tissue delivery may also be reduced. The use of nanoparticles can also allow compounds that are water insoluble, true for many anti-cancer agents, to be more effectively delivered to target cells (Faraji and Wipf, 2009).

Nanoparticle delivery systems for therapeutics have already been approved for a range of human diseases, including but not limited to cardiovascular diseases, immune disorders, and degenerative disorders (Mekaru et al., 2015, Rizvi and Saleh, 2018). However, in a review of approved nanoparticle formulations and those in development, Etheridge et al. (2013) reported that the majority of formulations currently in development are for the treatment of cancer. Cancer is an appealing area for the use of nanoparticles due to the enhanced permeability and retention (EPR) effect, where nanoparticles are favourably delivered to and accumulate in solid tumour tissue due to its increased vasculature permeability (Matsumura and Maeda, 1986). This kind of delivery has been termed “passive targeting” and currently dominates the portfolio of approved nanoparticle delivery systems. One example of such a system is Abraxane®; an albumin bound paclitaxel formulation approved by the FDA for use in NSCLC, metastatic breast cancer and pancreatic cancer (Miele et al., 2009).

There are a small number of examples of vanadium nanoparticles in the literature. Nanocomposite carriers containing oxidovanadium and chitosan have been developed and have been shown to increase insulin sensitivity in mouse models of type 2 diabetes (Liu et al., 2015b, Lichawska et al., 2014). Chen et al. (2017) showed that polyethylene glycol (PEG) lipid micelles containing vanadium disulphide nanodots displayed high tumour uptake in

tumour-bearing mice. These micelles were developed to be used for image guided photo thermal cancer therapy; however, this study does demonstrate the principle that vanadium compounds could be packaged into nanocarriers and delivered to tumour cells.

My main objective in this chapter was to provide a proof-of-principle that cytotoxic oxidovanadium compounds can be packaged into liposomes and delivered to neuroblastoma tumour cells effectively and in an active form. To achieve this, we needed to identify suitable oxidovanadium compounds for nanocarrier delivery and demonstrate efficacy of delivery to cells. On searching the literature, nearly all oxidovanadium compounds with organic ligands proved to be reported as water soluble. However, our laboratory did locate a group of hydrophobic candidates from Finland (Hänninen et al., 2014). Our collaborator Dr. Ari Lehtonen (University of Turku, Finland) provided us with four such hydrophobic oxidovanadium derivatives to be used to explore the potential of packaging oxidovanadium into liposomes. These compounds will be referred to as AL1-4 hereafter.

Like BMOV, AL1-4 contain a centrally coordinated vanadium ion, but with much bulkier hydrocarbon chains acting as ligands (**Figure 5.2**). These hydrophobic oxidovanadium compounds were developed as industrial catalysts, rather than for use in biological systems, thus their use in cancer cells is entirely novel. In the first instance, we wanted to ask whether these compounds induce similar cytotoxicity, differentiation, and biochemical changes (phosphorylation of AKT and ERK) in neuroblastoma cells compared to BMOV. Based on the literature, we hypothesised that if they did have efficacy in neuroblastoma cells, it was likely that these larger hydrophobic oxidovanadium compounds would break down, either in media or once taken up by the cell, to release vanadium ions and free ligand, as is the case for BMOV (Peters et al., 2003, Levina and Lay, 2017, Caravan et al., 1995). Therefore, we expected that any biological activity associated with these compounds would be driven by similar mechanisms compared to BMOV. Following evaluation of the anti-cancer properties of these compounds, liposomal formulations of hydrophobic oxidovanadium were prepared to

assess whether this could present a viable method for delivery of oxidovanadium to neuroblastoma cells.

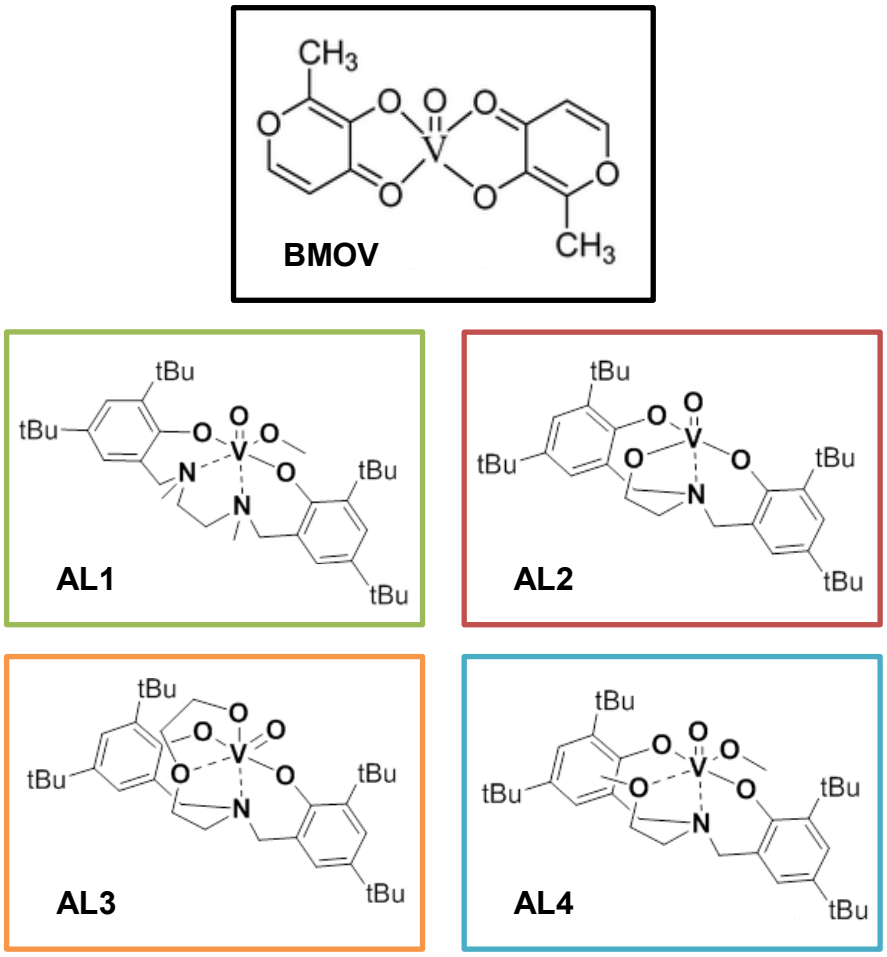

Figure 5.2 – Hydrophobic oxidovanadium compounds
AL1-4 contain centrally coordinated vanadium ions, similar to BMOV, but have much bulkier hydrocarbon ligands rendering them extremely hydrophobic.

5.2. Results

5.2.1. Hydrophobic oxidovanadium compounds

As mentioned previously, the hydrophobic oxidovanadium compounds (AL1-4) were obtained in order to explore the prospect of packaging oxidovanadium into liposomes for delivery to cells. However, before I began attempting to package them, it was important for me to assess the activity of these compounds compared to BMOV on cells. In order to do this they were first dissolved in ethanol. The highly hydrophobic nature of the compounds meant that some of them, in particular AL3, did not readily dissolve at high concentrations. However, after vortexing for a number of hours it was possible

to dissolve all 4 compounds at between 10 mM and 500 µM. The different compounds produced distinctly coloured solutions due to their transition metal chemistry, and these colours did not change in intensity or hue when stored for a week (**Figure 5.3**). This suggests that these compounds are likely to be stable in solution although, importantly, these are in ethanol and their stability in aqueous solution is still unknown.

Figure 5.3 – Hydrophobic oxidovanadium compounds produced coloured solutions in ethanol
Hydrophobic compounds (AL1-4) dissolved in ethanol at 500 µM and imaged immediately (top) and after 7 days (bottom).

For morphological assays, we routinely used 10 µM BMOV and intended to use the same molar concentration of the hydrophobic oxidovanadium compounds. Since the hydrophobic compounds were dissolved in ethanol, the final ethanol concentration had to be controlled in all assays. Unfortunately, AL3 could only be dissolved in ethanol at a maximum concentration of 500 µM, therefore the final ethanol concentration for cells treated with 10 µM AL3 would be 2%. This was deemed unacceptable as ethanol toxicity occurs at this concentration in neuroblastoma cell lines. As a result, AL3 could only be delivered at a maximum final concentration of 5 µM, whereas the other compounds were used at 10 µM in most of the experiments described below. A final concentration of 1% ethanol was used in all experiments to control for solvent, which was well tolerated by all cells used here.

5.2.2. Hydrophobic oxidovanadium compounds induced similar morphological and biochemical changes compared to BMOV

As described in **Chapter 4** and previous publications from our laboratory (Clark et al., 2013, Clark et al., 2015), BMOV induces cytotoxicity and/or differentiation, characterised by neurite outgrowth, in a subset of neuroblastoma cell lines. In the current study, a range of neuroblastoma and non-neuroblastoma cell lines were treated with BMOV and the hydrophobic oxidovanadium compounds. IMR32 cells treated for 3 days showed very clear signs of cytotoxicity, namely a rounded cell morphology and loss of adhesion that normally precedes apoptosis or necrosis, in response to all oxidovanadium compounds (**Figure 5.4A**). In fact, all of the hydrophobic oxidovanadium compounds induced higher levels of cytotoxicity compared to BMOV. AL3-treated cells experienced the highest degree of cytotoxicity even at 5 µM (compared to 10 µM for the other compounds). Very similar effects were observed in KELLY cells, where cells treated with the oxidovanadium compounds became very round and began to lose adhesion, indicative of cytotoxicity (**Figure 5.4B**).

To be more quantitative, IMR32, KELLY and HEK-293T cells were treated with a dosage range of each oxidovanadium compound for 3 days, after which cells were stained with Hoechst 33342 and the number of nuclei in representative fields of view were counted (**Figure 5.5**). The level of cytotoxicity observed in KELLY cells is underestimated in this assay, as these cells do not lose adherence as readily as IMR32 and therefore the nuclei are counted even though cells appear to be dying. As discussed in **Chapter 4** and **Appendix 3**, assaying viability in cells treated with oxidovanadium is challenging and the nuclei counting assay was deemed the most appropriate for these studies. Nonetheless, these data can still be used to make comparisons in the cellular responses between compounds. These dose response curves suggest that in all three cell lines, AL3 is 2-5 fold more potent than the other oxidovanadium compounds and the other compounds do not differ in their effects from BMOV.

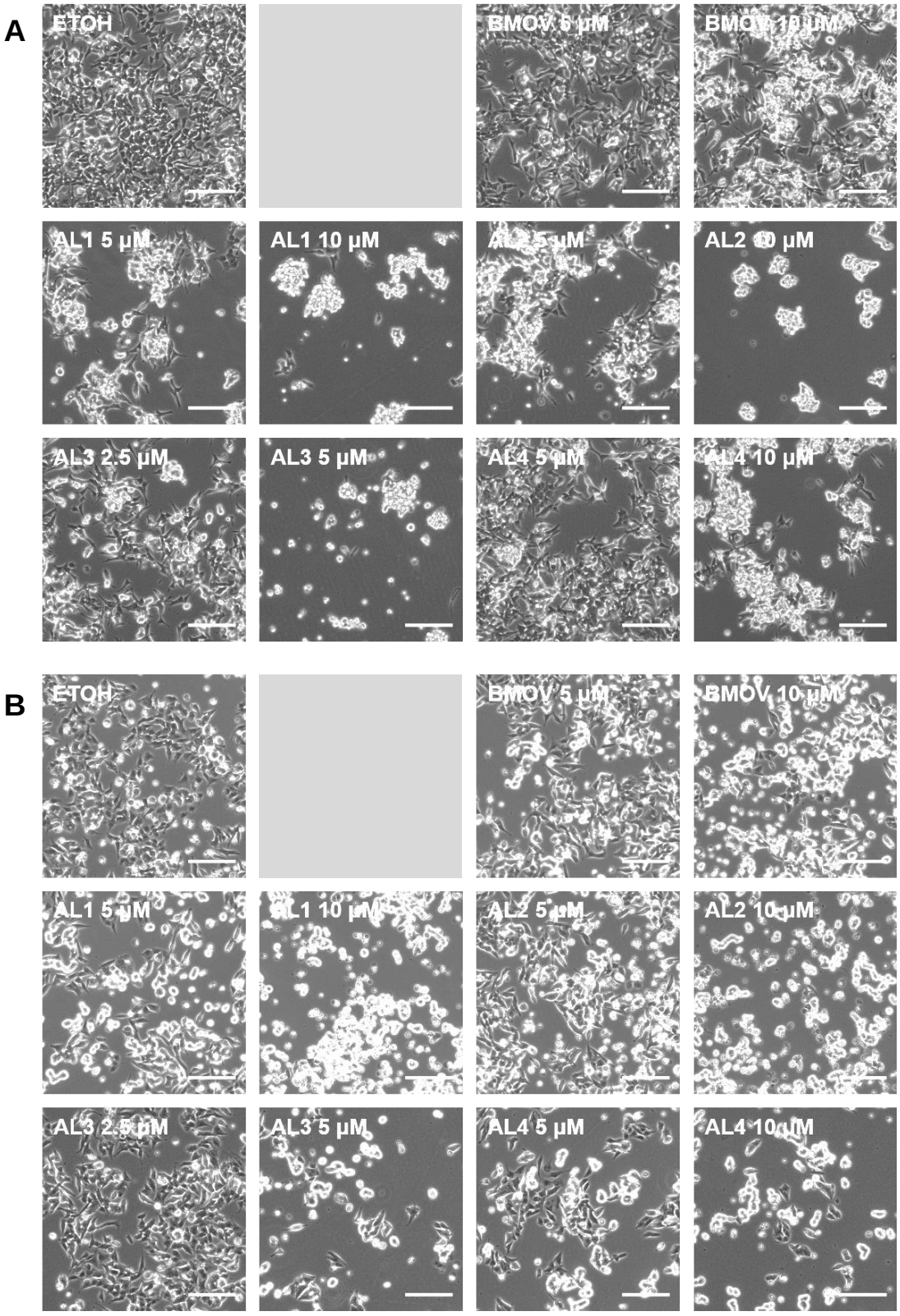

Figure 5.4 – Hydrophobic oxidovanadium compounds induced cytotoxicity in neuroblastoma cells

*IMR32 cells (**A**) and KELLY cells (**B**) treated with oxidovanadium compounds at 5 µM and 10 µM (2.5 µM and 5 µM for AL3) and imaged after 3 days. Treated cells have rounded cell bodies and have begun to lose adhesion, indicative of cytotoxicity. Scale bar = 150 µm.*

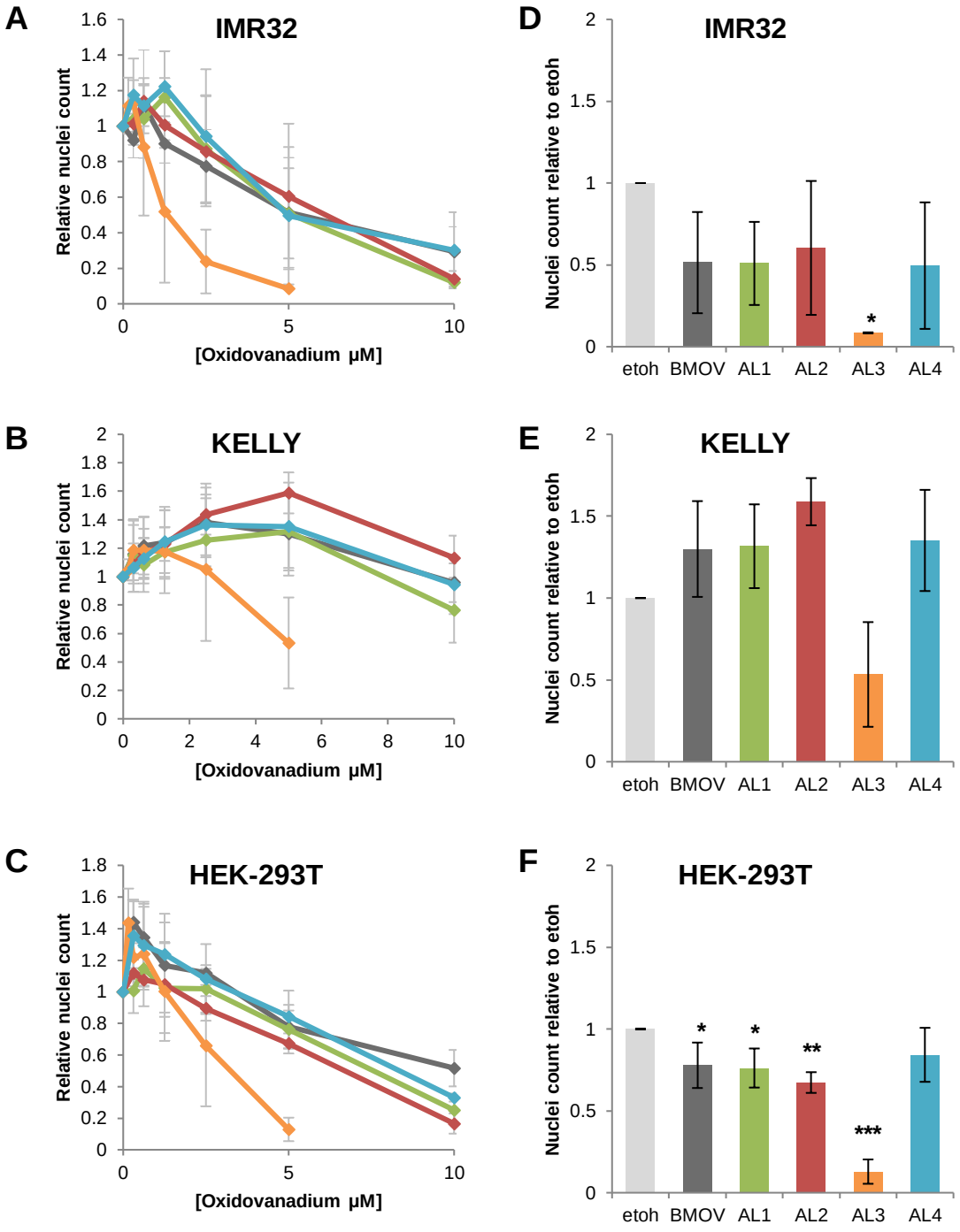

Figure 5.5 – AL3 induced stronger cytotoxicity compared to other hydrophobic oxidovanadium compounds and BMOV

A-C *- IMR32, KELLY and HEK-293T cells were treated with increasing concentrations of oxidovanadium up to 10 µM for BMOV and AL1,2,4 and 5 µM for AL3. After 3 days, cells were stained with Hoechst 33342 and nuclei were counted and normalised to ethanol only treated cells (ethanol concentration kept constant). Grey, BMOV; green, AL1; red, AL2; orange, AL3; blue, AL4 (n=3).* ***D-F*** *– Relative nuclei counts for IMR32, KELLY and HEK-293T cells treated with 5 µM oxidovanadium. ANOVA with Dunnett post hoc, * p<0.05, ** p<0.01, *** p<0.001 (n=3).*

As discussed in **Chapter 4**, previous publications by the laboratory have shown that the glutathione suppression using BSO greatly enhances BMOV-induced cytotoxicity in some neuroblastoma cells (Clark et al., 2015). KELLY and HEK-293T cells were treated with a dosage range of each hydrophobic oxidovanadium compound and 10 µM BSO to see whether glutathione suppression also enhances the activity of these alternative oxidovanadium compounds (**Figure 5.6**). As described above, the values obtained for KELLY cells do not fully reflect the cytotoxicity that can be observed when looking at the cell morphology. However, it is clear that in all cases BSO significantly enhances oxidovanadium-induced cytotoxicity in KELLY cells, except for AL3 for which the nuclei count is already very low, possibly masking the additive effects of BSO. The difference between oxidovanadium alone and in combination with BSO is less statistically significant in HEK-293T cells, perhaps suggesting a difference in the mechanisms driving cell death in these cells. However, this lack of statistical significance may also be due to a greater spread in the HEK-293T data. The effect of BSO is actually perhaps quite similar for AL2, AL3 and AL4 in KELLY and HEK-293T cells, but there does seem to be less of an additive effect for BMOV and AL1.

Loss of adhesion and cytotoxicity are common responses that are observed following treatment with a vast array of chemicals, therefore I assayed the effect of the hydrophobic oxidovanadium compounds on differentiation. BMOV induces neurite outgrowth in SK-N-SH cells (**Figure 4.3A+B** and Clark et al., 2013), possibly providing a more specific, positive read out of oxidovanadium activity. Although, it is possible that neurite outgrowth is part of a general stress response. To assess whether these hydrophobic oxidovanadium compounds could induce differentiation, SK-N-SH cells were treated for 5 days, after which high power images were taken and average neurite lengths were measured (**Figure 5.7**). All of the hydrophobic oxidovanadium compounds were able to induce differentiation, characterised by neurite outgrowth, to at least the same degree as BMOV. It was noted that whilst not entirely represented in the quantitation, cells treated with AL3 clearly had the longest neurites. However, these particular measurements were often underestimated due to these longer neurites extending beyond the field of view on the microscope.

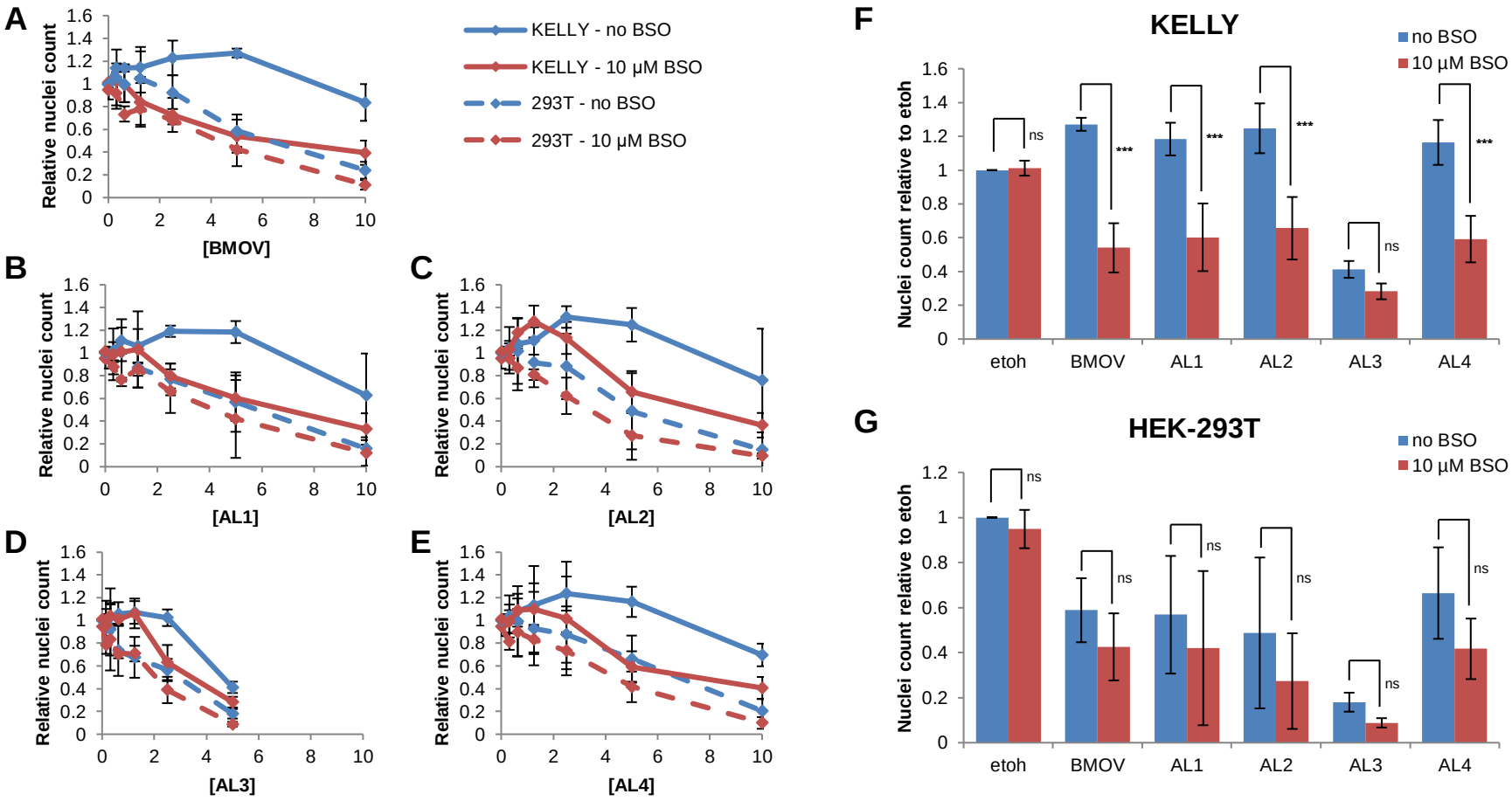

Figure 5.6 – BSO-mediated glutathione depletion enhanced hydrophobic oxidovanadium-induced cytotoxicity in neuroblastoma cells
A-E *– KELLY and HEK-293T cells were treated with increasing concentrations of oxidovanadium (up to 10 µM for BMOV and AL1,2,4 and 5 µM for AL3) +/- 10 µM BSO for 3 days, after which cells were Hoechst 33342-stained and nuclei were counted and normalised to ethanol only (n=3).* ***F+G*** *– Relative nuclei counts in KELLY (**F**) and HEK-293T (**G**) cells treated with 5 µM oxidovanadium +/- 10 µM BSO. ANOVA with Bonferroni post hoc, ns=not significant, *** p<0.001 (n=3).*

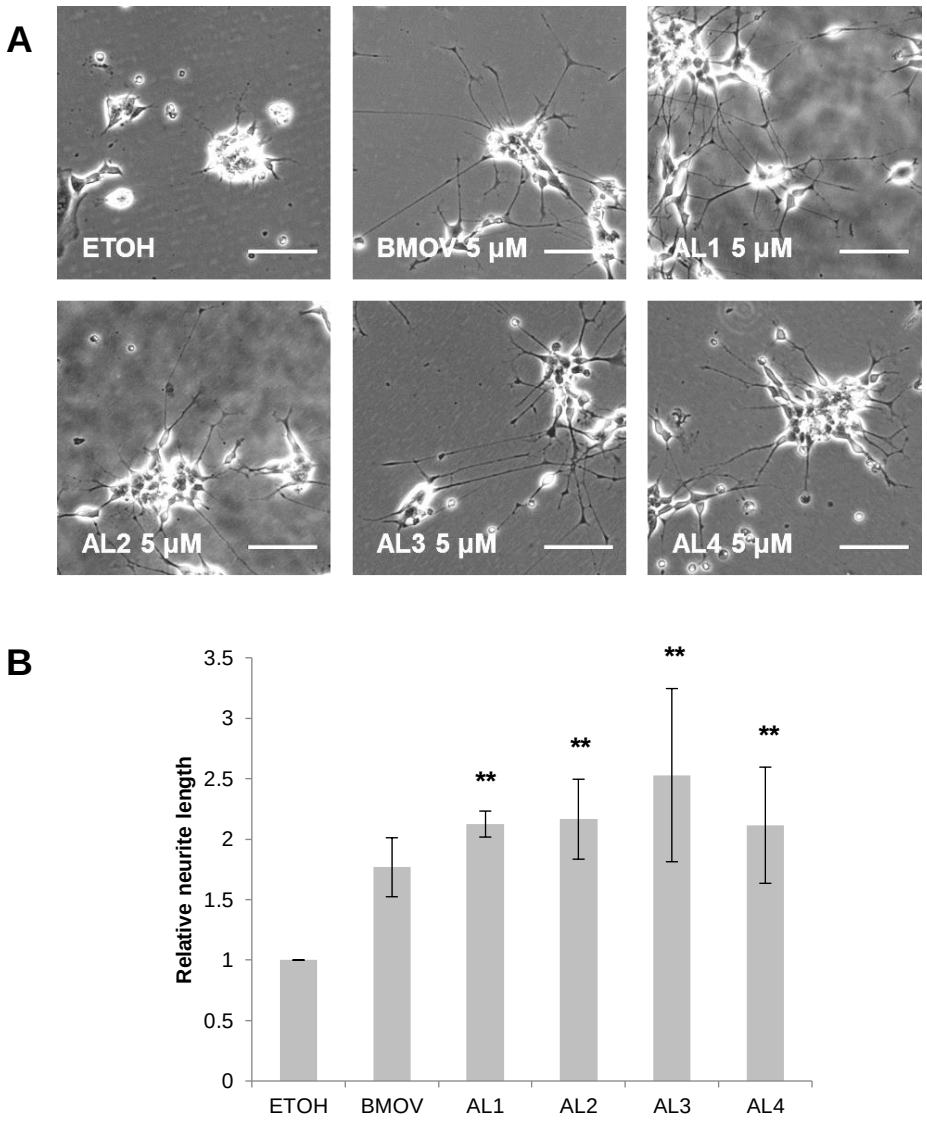

Figure 5.7 – Hydrophobic oxidovanadium compounds induced neurite outgrowth in SK-N-SH cells
SK-N-SH cells treated with 5 µM oxidovanadium compounds for 5 days. ***A*** *– Phase-contrast microscopy, scale bar = 100 µm.* ***B*** *– Relative neurite measurements. ** p<0.01 (n=3).*

When using small molecule inhibitors as potential anti-cancer therapeutic compounds, it is important to consider their specificity towards tumour cells. So far, I have shown that the hydrophobic oxidovanadium compounds induce cytotoxicity and differentiation similar to BMOV, however it is important to assess whether this activity, particularly the cytotoxicity, shows any specificity towards tumour cells. A range of neuroblastoma (IMR32, KELLY, SK-N-AS, SK-N-SH) and non-neuroblastoma (MEF, HEK-293T, COS7, IMDC3) cells were treated oxidovanadium compounds for 3 days, after which their effect on cell viability was qualitatively assessed by looking for rounding up of cell

bodies, loss of adhesion, and reduced cell density. Microscopy from these experiments can be found in **Figure 5.4** (for IMR32 and KELLY), and **Appendix 5** (other cell lines). **Figure 5.8** shows a summary of the sensitivities of each cell line to cytotoxicity induced by each of the oxidovanadium compounds. As with BMOV, there was no clear clustering showing sensitivity in neuroblastoma cells and resistance in non-neuroblastoma cells. Nonetheless, there are cell lines that do not display high levels of cell death in response to treatment with these compounds, namely IMCD3 and SK-N-AS. SK-N-SH cells were also largely resistant to the hydrophobic oxidovanadium compounds in terms of cell death. However, importantly they do differentiate in response to these chemicals, as is the case with BMOV (**Figure 5.7**). I also had access to a small panel of paediatric brain tumour cell lines, which I treated with BMOV, AL2 and AL3 (**Figure 5.9**). These tumour cells also showed very significant cytotoxicity when treated with the oxidovanadium compounds, suggesting that these kinds of chemicals may be useful in the treatment of other types of childhood cancer if targeted effectively. AL3 was again the most cytotoxic.

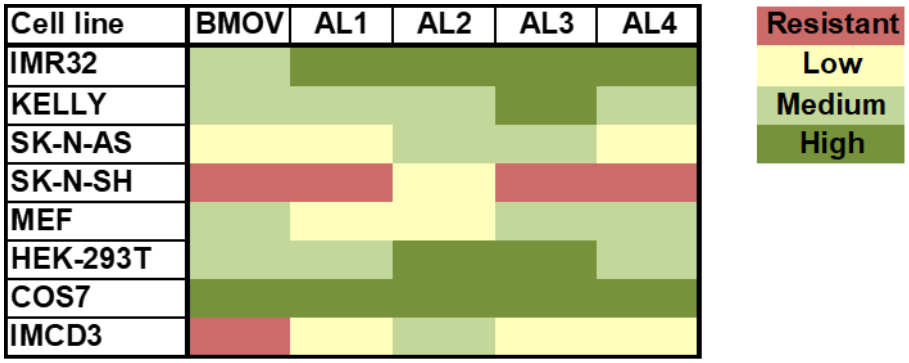

Figure 5.8 – Hydrophobic oxidovanadium sensitivity varied across cell lines
*IMR32, KELLY, SK-N-AS, SK-N-SH, MEF, HEK-293T, COS7 and IMCD3 cells were treated with oxidovanadium compounds at 5 µM and 10 µM (2.5 µM and 5 µM for AL3) for 3 days (5 days for SK-N-SH) and qualitatively assessed for differences in final cell density, cell body rounding and loss of adhesion, indicating reduced proliferation or loss of cell viability. Microscopy in **Appendix 5**. Note: This qualitative assessment was for cytotoxicity only, and does not reflect oxidovanadium-induced neurite outgrowth, which was observed in SK-N-SH cells (**Figure 5.7**).*

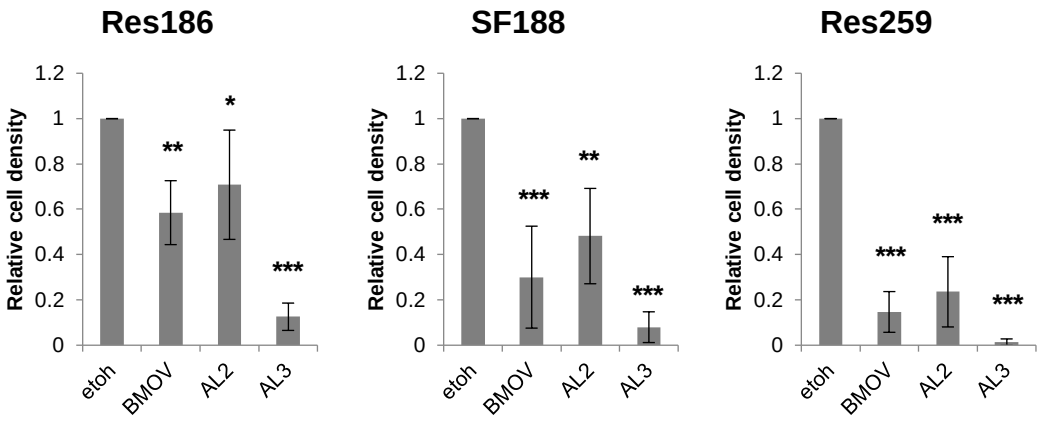

Figure 5.9 – BMOV and hydrophobic oxidovanadium compounds induced cytotoxicity in paediatric brain tumour cell lines
*Res186, SF188 and Res259 cells were treated with 5 µM BMOV, AL2 and AL3 for 6 days, after which cell viability was assessed using resazurin. ANOVA with Dunnett post hoc, * p<0.05, ** p<0.01, *** p<0.001 (n=3).*

Increased phosphorylation of AKT and ERK has been reported in neuroblastoma cells treated with BMOV (Clark et al., 2013, Clark et al., 2015). In order to assess whether the hydrophobic oxidovanadium compounds similarly enhance these signalling events, I performed western blotting using protein lysates from IMR32, KELLY and SK-N-SH cells treated with the oxidovanadium compounds. It should be noted that in all cases cells were treated with 10 µM BMOV, AL1, AL2 and AL4, but just 5 µM AL3. This was partly because 10 µM AL3 cannot be delivered to cells without introducing excessive ethanol toxicity, but also because the morphological data show that AL3 is at least 2-fold more active than the other oxidovanadium compounds (**Figure 5.5**). In IMR32 cells the signals for both phosphorylated AKT and ERK are very weak in some cases, however there is a clear trend showing that phosphorylation of AKT is enhanced by AL1, AL2 and AL4, and phosphorylation of ERK is enhanced most by AL1 and AL3 (**Figure 5.10D-F**). In KELLY cells phosphorylation of both AKT and ERK is enhanced by BMOV, AL1, AL2 and AL4, but much less by AL3 (**Figure 5.10D-F**). Similarly, in SK-N-SH cells, phosphorylation of AKT and ERK is enhanced by all oxidovanadium compounds, although to a much lesser extent by AL3 (**Figure 5.10A-C**). A qualitative summary of the average biochemical responses is presented in **Figure 5.10G**, although in some cases the quantitation could not be entirely representative of all three blots. It was expected that the level of

phosphorylation of these kinases would correlate with the level of morphological activity of the oxidovanadium compounds. This was not always the case. Although we have previously used phosphorylation of AKT and ERK as markers of BMOV activity, I have shown in **Chapter 4** that these signalling events are not essential for oxidovanadium-induced cytotoxicity; therefore, they will not necessarily track with activity. Even though it is the most cytotoxic, in these experiments AL3 has generally not induced such strong biochemical changes in AKT and ERK as the other compounds. This may be because of the reduced dose, where 5 µM is sufficient to drive very dramatic morphological changes, but not, the perhaps unrelated, biochemical changes in AKT and ERK. This cannot however explain the difference in AKT and ERK response in IMR32 cells, where for example treatment with AL3 induced high levels of ERK but not AKT phosphorylation. The fact that the biochemical responses to these compounds differed, specifically in a manner that did not correlate with efficacy, was interesting and suggests that the compounds do have distinct effects in cells. This was a surprising finding that will be discussed later.

In summary, ethanol solubilised hydrophobic oxidovanadium compounds have been used in various assays to compare their activity to BMOV. All four hydrophobic oxidovanadium compounds induce equivalent or stronger cytotoxicity and differentiation compared to BMOV in subsets of neuroblastoma cell lines, and they can be combined with glutathione suppression to enhance cytotoxicity. AL3 is the most active in terms of both cytotoxicity and differentiation. The hydrophobic oxidovanadium compounds induce in some cases very similar AKT and ERK signals compared to BMOV, but in others, including AL3 once again, some distinctly different signalling.

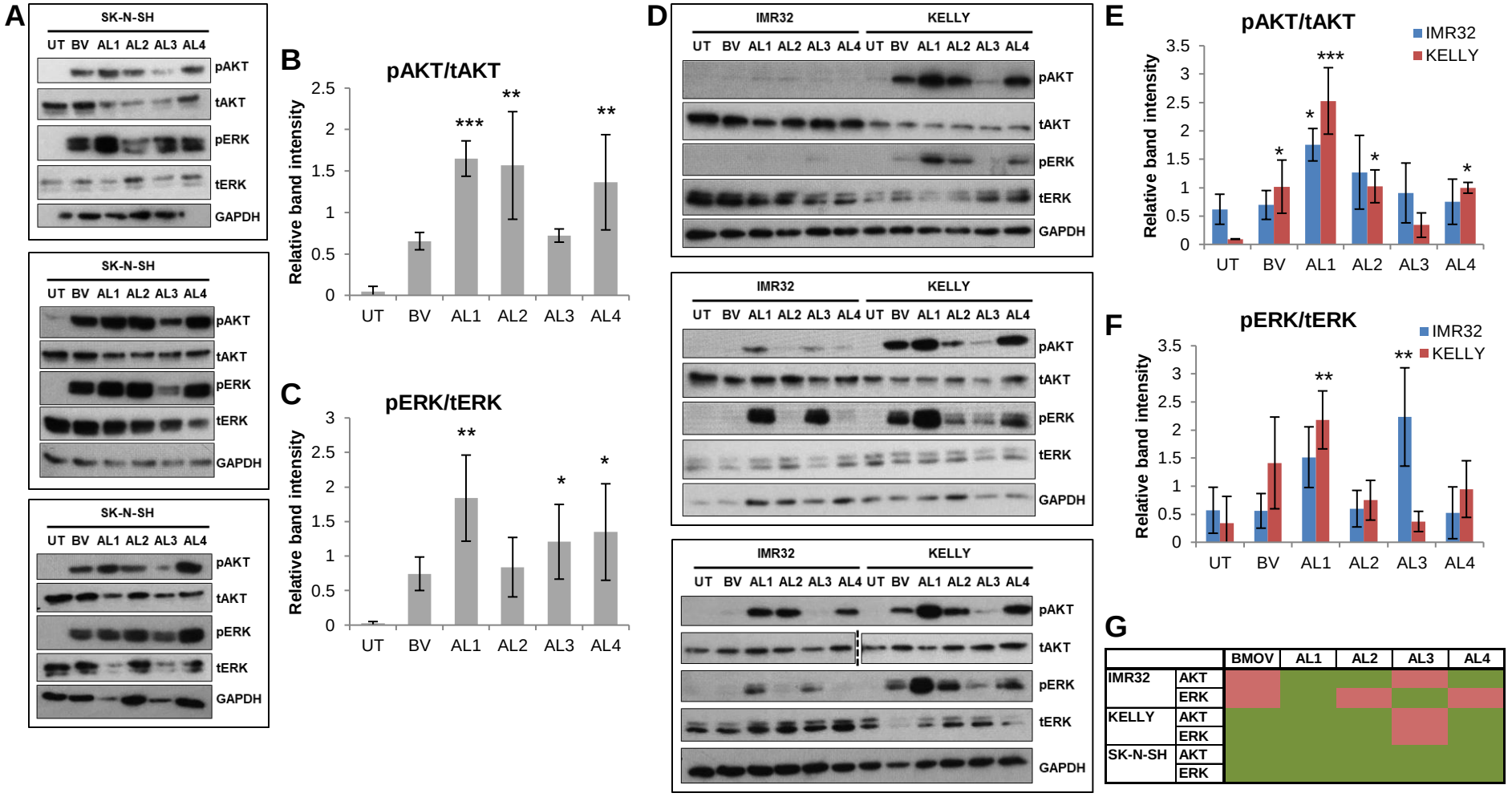
A
SK-N-SH
UT BV AL1 AL2 AL3 AL4
pAKT
tAKT
pERK
tERK
GAPDH
B
pAKT/tAKT
Relative band intensity
C
pERK/tERK
D
IMR32
KELLY
E
pAKT/tAKT
IMR32
KELLY
F
pERK/tERK
G
BMOV
AL1
AL2
AL3
AL4
IMR32
KELLY
SK-N-SH
AKT
ERK

Figure 5.10 – Hydrophobic oxidovanadium compounds induced some similar and some unique changes in phosphorylation of AKT and ERK compared to BMOV
***A** – SK-N-SH cells were treated with 10 µM BMOV and AL1,2,4 and 5 µM AL3 for 72 hours. Western blotting for phosphorylated and total AKT an ERK was performed (GAPDH loading control) (n=3, all repeats shown). **B+C** – Western blots from **A** were quantified and relative band intensities for phosphorylated proteins were normalised to total proteins. ANOVA with Dunnett post hoc, * p<0.05, ** p<0.01, *** p<0.001 (n=3). **D** – IMR32 and KELLY cells were treated with 10 µM BMOV and AL1,2,4 and 5 µM AL3 for 48 hours. Western blotting for phosphorylated and total AKT an ERK was performed, (GAPDH loading control) (n=3, all 3 repeats shown). **E+F** – Western blots from **D** were quantified and relative band intensities for phosphorylated proteins were normalised to total proteins. ANOVA with Dunnett post hoc for each cell line using untreated (UT) as the control, * p<0.05, ** p<0.01, *** p<0.001 (n=3). **G** – Phosphorylation of AKT and ERK following treatment with each of the oxidovanadium compounds in each cell line was qualitatively assessed. Green = increased phosphorylation, red = no change.*

5.2.3. Hydrophobic oxidovanadium compounds did not deplete glutathione

Having observed strong cytotoxicity in some neuroblastoma cells treated with the hydrophobic oxidovanadium compounds, particularly for AL3, we had some concerns surrounding the specificity of the compounds, in terms of both cell type specificity and the mechanism of activity. The cell panel experiments described above go some way to alleviate these concerns, as it has been shown that there are cell lines, both neuroblastoma and non-neuroblastoma, that can tolerate these compounds. However, it remains possible that these oxidovanadium compounds, including BMOV, are acting via non-specific toxicity, rather than by the specific actions of vanadate.

One of the most common forms of non-specific intracellular toxicity is oxidative stress caused by the excessive production of ROS (Sies and de Groot, 1992). This is particularly relevant to vanadium as it is known that the interconversion between vanadyl and vanadate produces cellular ROS (Nechay, 1984). Glutathione is the cell's major antioxidant defence; therefore, we reasoned that if cells were under significant oxidative stress following oxidovanadium treatment, then glutathione would be depleted. I used the MCB assay to measure intracellular reduced glutathione concentration following 24 hours oxidovanadium treatment, 10 µM BSO was used as a positive control for glutathione depletion (**Figure 5.11**). Glutathione levels were not significantly reduced in KELLY cells treated with any of the oxidovanadium compounds, and only very small reductions were observed in IMR32 cells treated with AL1

and AL3. This suggests that excessive generation of ROS is unlikely to be a major factor driving the observed oxidovanadium-induced cytotoxicity.

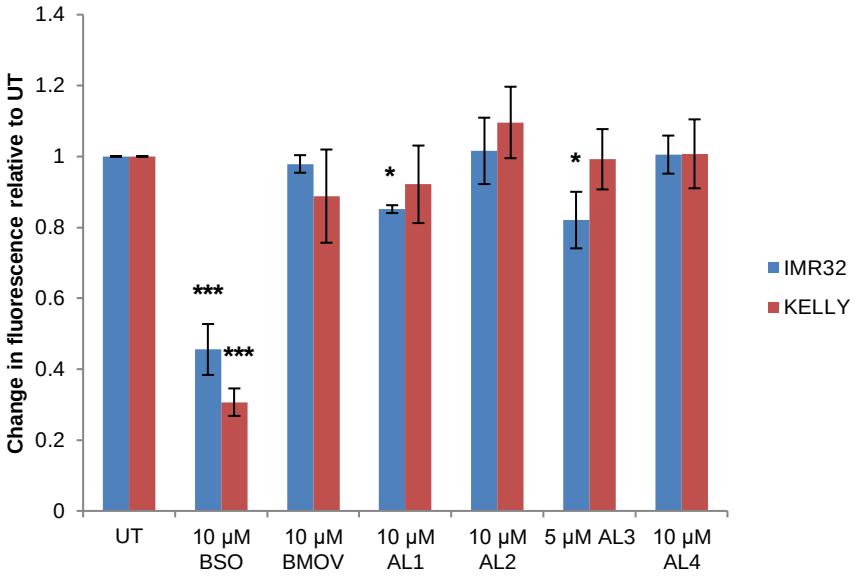

Figure 5.11 – Oxidovanadium did not cause dramatic reductions in reduced glutathione *IMR32 and KELLY cells were treated with 10 µM BSO, BMOV or AL1,2,4 or 5 µM AL3. After 24 hours, relative reduced glutathione levels were assessed using a monochlorobimane (MCB) fluorescence assay. ANOVA with Dunnett post hoc for each cell line using untreated (UT) as the control, * p<0.05, *** p<0.001 (n=3).*

5.2.4. AL1-4-induced morphological and biochemical responses are not driven by their organic ligands

As has been discussed previously, many different oxidovanadium compounds have been used in cancer disease models in the literature, each with different ligating molecules that vary in complexity (Irving and Stoker, 2017). There is an ongoing question as to whether these ligands themselves contribute to the anti-cancer properties of these molecules, particularly as there are increasing data that suggest that the majority of vanadium complexes are likely to dissociate in circulation, releasing vanadium and free ligand (Levina and Lay, 2017, Kremer et al., 2015). This question can be applied to the hydrophobic oxidovanadium compounds used here, in particular as both quantitative differences in potency and some qualitative differences in biochemical responses have been described.

In order to assess whether the ligands do contribute to the observed activity of these compounds, we first obtained two molybdenum-based compounds from Dr. Ari Lehtonen (University of Turku, Finland) with similar ligation to the

hydrophobic oxidovanadium compounds (**Figure 5.12A**). IMR32 cells were treated with these compounds and BMOV for 3 days and cell density was quantified using crystal violet (**Figure 5.12B**). IMR32 cells were sensitive to BMOV but not to either molybdenum compound. Similarly, SK-N-SH cells were treated with BMOV or the molybdenum compounds for 5 days after which phase-contrast microscopy images were taken (**Figure 5.12C**). There are clear signs of differentiation in BMOV-treated cells, characterised by neurite outgrowth, but not in cells treated with the molybdenum compounds. These data suggest that the ligating molecules in the oxidovanadium complexes do not contribute to the observed cytotoxicity or differentiation. However, very little is known about the stability of these molybdenum compounds compared to the oxidovanadium equivalents, therefore the ligand molecules may not have been released from the molybdenum complexes in the same form or at the same rate as for the oxidovanadium compounds.

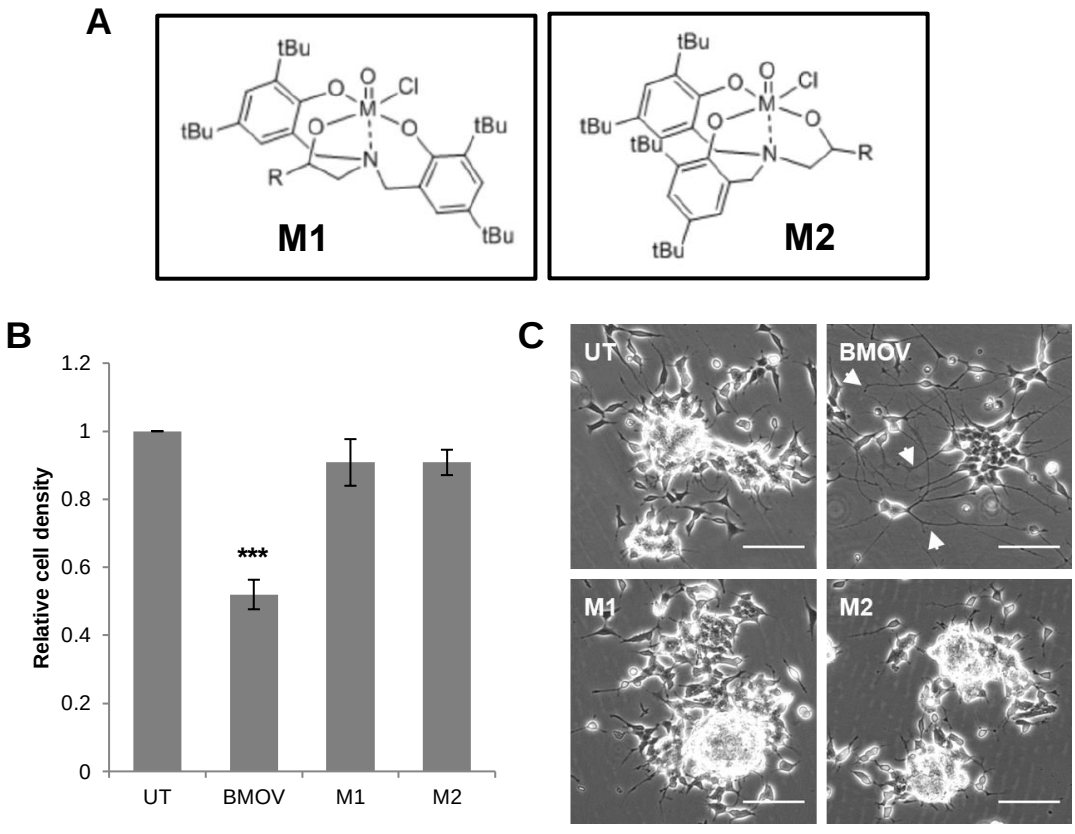

Figure 5.12 – Neuroblastoma cells were resistant to molybdenum compounds
A *– M1 and M2 are compounds with centrally co-ordinated molybdenum ions obtained from Dr. Ari Lehtonen (University of Turku, Finland).* ***B*** *– IMR32 cells were treated with 10 µM BMOV, M1 or M2 for 3 days. Cell viability was assessed using crystal violet staining and solubilisation. Reduced cell density was detected after BMOV, but not M1 or M2, treatment. ANOVA with Dunnett post hoc, *** p<0.001 (n=3).* ***C*** *– SK-N-SH cells were treated with 10 µM BMOV, M1 or M2 for 5 days. Representative images were taken showing that BMOV, but not M1 or M2, induced neurite outgrowth (white arrows). Scale bar = 100 µm.*

Fortunately, our collaborator (Dr. Ari Lehtonen, University of Turku, Finland) was later able to provide us with the free ligand molecules used to generate the AL1-4 oxidovanadium complexes (**Figure 5.13A**). These were dissolved in ethanol, and used to perform some morphological and biochemical analysis to assess their effect on neuroblastoma cells. First, IMR32 cells were treated with oxidovanadium or free ligand for 3 days, after which Hoechst 33342 staining and nuclei counting was performed (**Figure 5.13B**). All oxidovanadium compounds significantly reduced final cell number as reported previously, whereas the free ligand molecules had no effect. Similarly, when SK-N-SH cells were treated with oxidovanadium or free ligand for 6 days, significantly longer neurites were observed in oxidovanadium-treated cells, but no differences were seen for free ligands (**Figure 5.13C**). Protein lysates were also collected from SK-N-SH cells treated with oxidovanadium or free ligand for 6 days. Western blotting for phosphorylated and total AKT and ERK showed that whilst the oxidovanadium complexes enhanced phosphorylation of both kinases to varying degrees, the free ligands alone had no effect (**Figure 5.13D-F**). These data indicate that it is the vanadium within these oxidovanadium complexes, or the whole complex themselves, rather than the ligating molecules that induce the morphological and biochemical changes that have been described thus far.

Figure 5.13 – The ligands within hydrophobic oxidovanadium complexes had no effect on cell viability, differentiation, or phosphorylation of AKT or ERK
***A** – L1-4 are the ligands from the hydrophobic oxidovanadium complexes (AL1-4) (obtained from Dr. Ari Lehtonen, University of Turku, Finland). **B** – IMR32 cells were treated with 10 µM oxidovanadium or ligand only (5 µM for AL3 and L3) for 3 days. Nuclei counting was used to assess cell viability. ANOVA with Dunnet post hoc using untreated (UT) as the control, *** p<0.001 (n=3). **C** – SK-N-SH cells were treated with 5 µM oxidovanadium or ligand only for 6 days, after which relative neurite length was assessed. ANOVA with Dunnet post hoc using UT as the control, * p<0.05, ** p<0.01 (n=3). **D** - Western blotting for phosphorylated and total AKT and ERK was performed using protein lysates from **C** (GAPDH loading control). **E+F** - Western blots from **D** were quantified and relative band intensities for phosphorylated proteins were normalised to total proteins. ANOVA with Dunnett post hoc for each cell line using UT as the control, ** p<0.01, *** p<0.001 (n=3).*

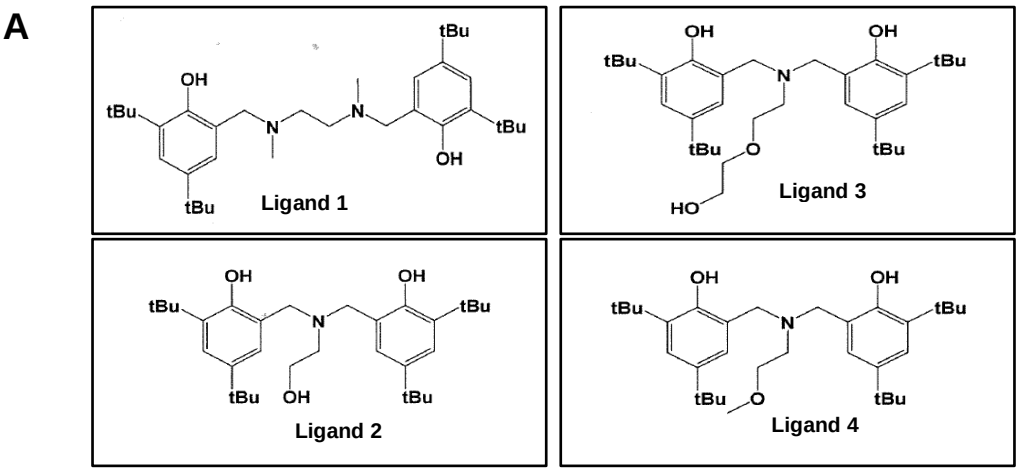
A
Ligand 1
Ligand 3
Ligand 2
Ligand 4

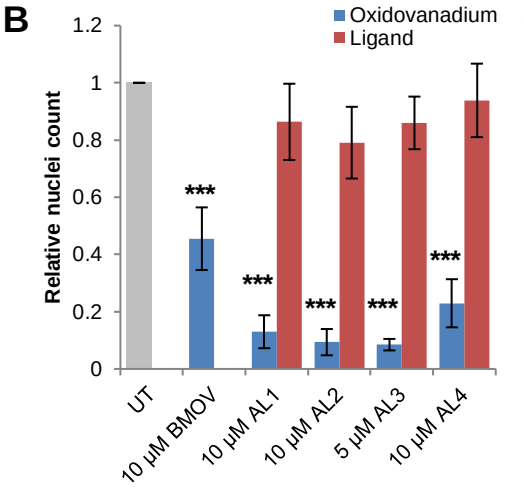
B
Oxidovanadium
Ligand
Relative nuclei count
UT
10 µM BMOV
10 µM AL1
10 µM AL2
5 µM AL3
10 µM AL4

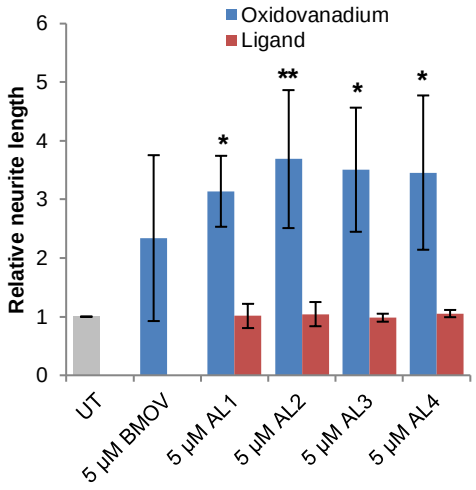
C
Oxidovanadium
Ligand
Relative neurite length
UT
5 µM BMOV
5 µM AL1
5 µM AL2
5 µM AL3
5 µM AL4

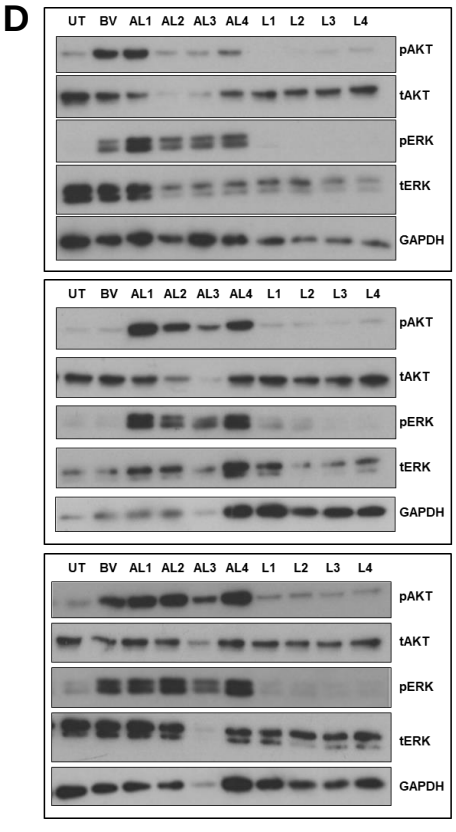
D
UT BV AL1 AL2 AL3 AL4 L1 L2 L3 L4
pAKT
tAKT
pERK
tERK
GAPDH

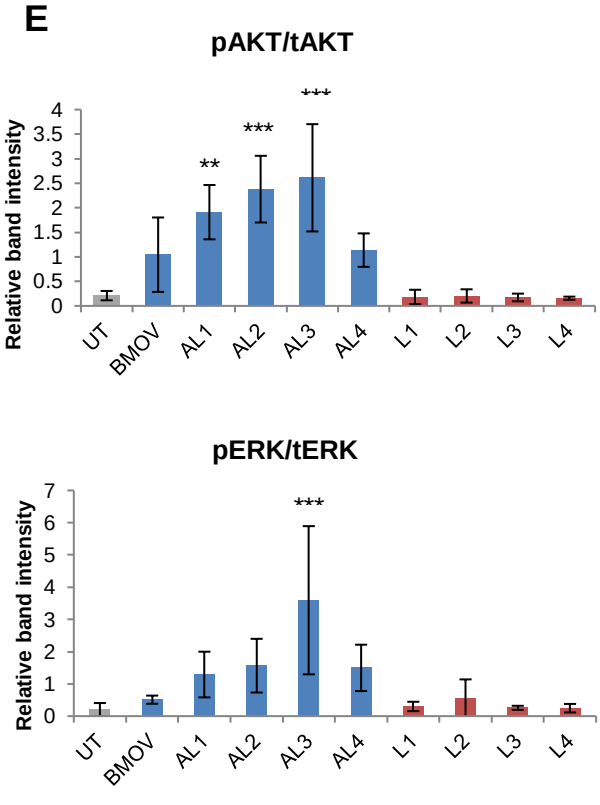
E
pAKT/tAKT
Relative band intensity
UT
BMOV
AL1
AL2
AL3
AL4
L1
L2
L3
L4
pERK/tERK
Relative band intensity

5.2.5. AL3 can be packaged into liposomes

Having shown that the hydrophobic oxidovanadium compounds display similar, or in many cases stronger, activity in neuroblastoma cells compared to BMOV, and that these effects are likely caused by vanadium itself, I next wanted to explore the important and novel question of whether these compounds could be delivered to cells using liposomal formulations. This may allow more efficient oxidovanadium delivery *in vivo* with potentially fewer off-target toxicities. AL3 was chosen for these liposomal packaging experiments as it had shown the most promising activity in the cytotoxicity and differentiation assays so far.

Our collaborators Aris Tagalakis and Ruhina Maeshima (ICH Genetics and Genomic Medicine, UCL) attempted to package AL3 into a liposomal formulation. Three lipids were used in this formulation; DOPC, a neutral lipid used to promote stable lamellar structures, cholesterol to increase stability of the liposomes, and DOTMA, a cationic lipid that improves uptake into mammalian cells. The liposomal formulations that were produced contained AL3 at a theoretical maximum concentration of 154 µM. Three batches of AL3 liposomes were synthesised and size and charge analysis was carried out on each of them (**Figure 5.14A+B**). The liposomes were cationic with an average charge of 64 mV. Their mean diameter was 159 nm.

The liposomal AL3 concentration stated above (154 µM) is based on theoretical maximum incorporation. However, in common with other reported studies of liposomal technologies, it is unlikely that all of the available AL3 was incorporated into liposomes (Edwards and Baeumner, 2006, Yamamoto et al., 2018). In order to quantify the precise concentration of AL3 in each liposomal formulation, we performed reverse-phase HPLC using 100% acetonitrile as the organic solvent (**Figure 5.14C-E**). This new assay was set up in collaboration with Dr. Simon Eaton (Stem cells and regenerative medicine, ICH, UCL). AL3 was found to elute from the column at around 20 minutes and absorption peaks were detected at 280 and 360 nm; example traces are shown in **Figure 5.14C**. 280 and 360 were the predicted absorption peaks for AL3 calculated using the Beer-Lambert law, confirming that we were indeed

detection AL3. A standard curve from the measurements at 360 nm was generated using known concentrations of ethanol-solubilised AL3, from which liposomal concentrations were extrapolated (**Figure 5.14D**). Although AL3 was detected in all three liposomal formulations, there was a high degree of variation in concentration ranging from 84 µM to 185 µM, with a mean concentration of 131 µM (**Figure 5.14E**). This variation is likely due to non-uniformity during liposomal preparation, nonetheless biological data using the three batches can be interpreted in light of these findings.

It was also important to consider that some of the AL3 measured in the HPLC described above may have actually not been packaged within liposomes, but free in the aqueous solution surrounding the liposomes. We thought this unlikely as the highly hydrophobic nature of AL3 renders it highly water insoluble. Nonetheless, I addressed this question using dialysis. Liposomal formulations were dialysed for 24 hours using dialysis chambers with a molecular weight cut-off of 10 000 Da. These should retain the liposomes but allow free AL3 in solution to pass through, thus separating encapsulated from non-encapsulated AL3. Dialysis was completed within 48 hours after liposome synthesis. After dialysis, size and charge analysis as well as HPLC to determine AL3 concentration was repeated (**Figure 5.14**). There were no significant changes in diameter or charge, suggesting that the biophysical properties of the liposomes had not been altered by dialysis (**Figure 5.14A+B)**. The average concentration of AL3 in the three batches of liposome was not significantly different following dialysis (**Figure 5.14E left**). The concentration of AL3 in batch 1 and 2 dropped slightly after dialysis, by 15% and 23% respectively (**Figure 5.14E right**). The concentration of batch 3 was reported as higher after dialysis, but this is likely experimental error, as it can be difficult to keep the volume of liquid within the dialysis chamber constant throughout dialysis. Overall, it was concluded that on average around 80% of the available AL3 is successfully packaged and retained in these liposomes.

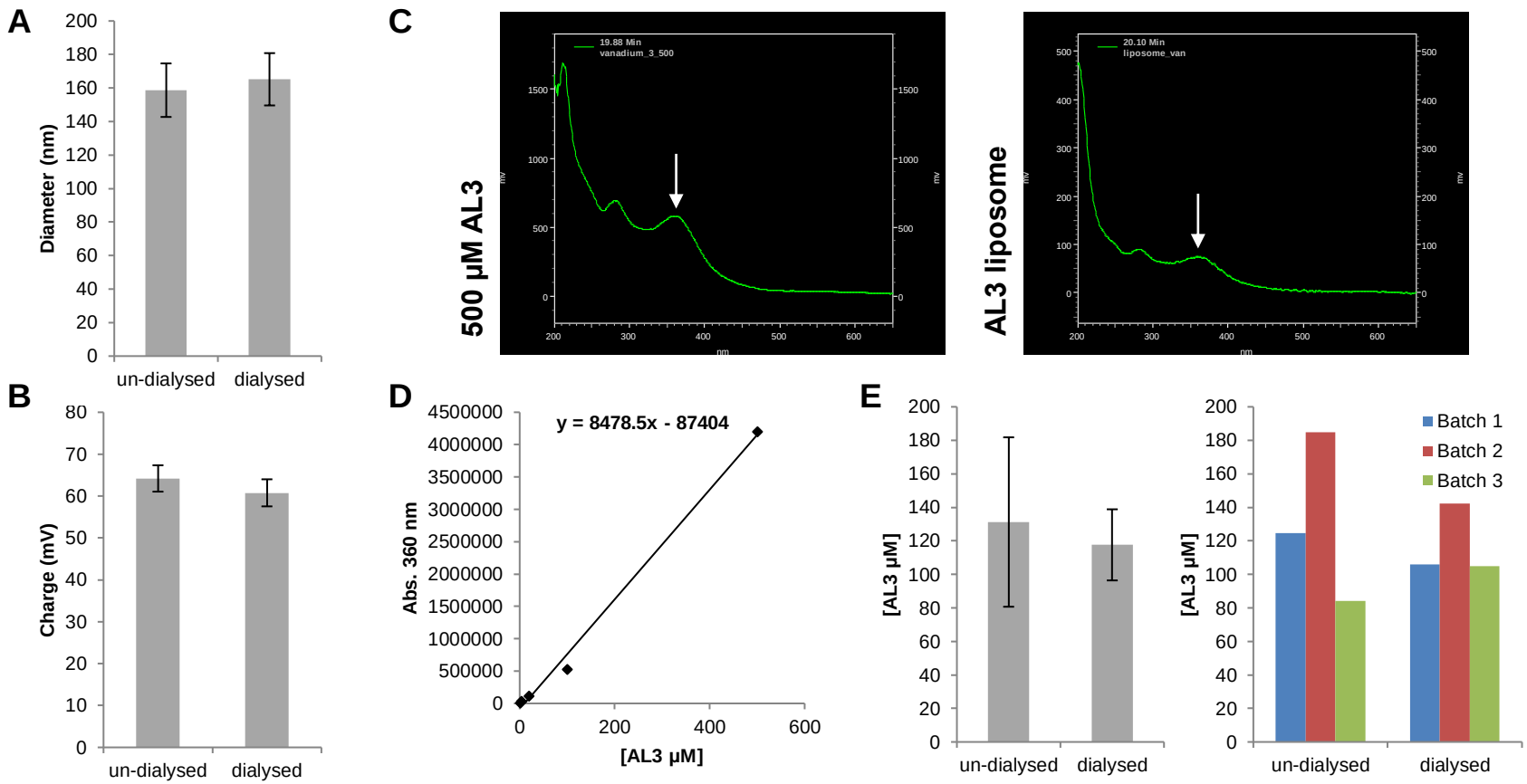

Figure 5.14 – AL3 liposome size, charge and oxidovanadium concentration was not significantly altered by dialysis
Three batches of AL3 liposomes were synthesised and dialysed. ***A+B*** *– Average liposome size (**A**) and charge (**B**) was measured pre- and post-dialysis for each batch using a Zetasizer Nano ZS (n=3).* ***C-E*** *– Reverse-phase HPLC was used to measure AL3 concentration.* ***C*** *– Example traces for ethanol solubilised AL3 (left) and liposomal AL3 formulations (right). AL3 concentration was assessed using absorbance at 360 nm (white arrows).* ***D*** *– A standard curve was generated using absorbance at 360 nm for ethanol solubilised AL3 at increasing concentrations.* ***E*** *– Liposomal AL3 concentration was calculated pre- and post-dialysis using absorbance at 360 nm and the standard curve (**D**). Mean concentrations for all 3 liposomal batches (left) and those of individual batches (right).*

5.2.6. AL3 liposomes induce similar morphological and biochemical changes compared to AL3 in ethanol

The formulation of the liposomes used in this study dictates the available molar ratios between its components including AL3. Therefore it was not possible to increase the concentration of oxidovanadium within the liposomes without altering the formulations themselves. Thus, the relatively low AL3 concentration in these liposomes only allowed a final concentration of 1 µM AL3 to be delivered to cells, any higher would have resulted in unacceptable levels of non-specific liposome toxicity. Initially all experiments were carried out in triplicate using the first batch of AL3 liposomes. I subsequently obtained the second and third batches, which were used to repeat some of the biological assays described below.

IMR32 cells were treated with (a) BMOV or AL3 in solution, (b) liposomal AL3 dialysed and non-dialysed (batch 1), or (c) an empty liposome (prepared using the same lipid formulations but with no oxidovanadium) dialysed and non-dialysed. After 3 days, cells were fixed and Hoechst 33342-stained to allow nuclei to be counted as a measure of cell viability (**Figure 5.15A**). BMOV and AL3 delivered in solution resulted in reduced cell viability as expected. However, it was not possible to assess the effect of AL3 packaged into liposomes due to the high levels of toxicity caused by the control, empty liposomes. It is however worth noting that there was no significant difference between dialysed and non-dialysed liposomes, again indicating that dialysis does not affect liposomal properties. In an attempt to circumvent this problem, IMR32 cells were subjected to lower doses of the same treatments for 6 days to see if the general liposome toxicity could be separated from specific oxidovanadium toxicity (**Figure 5.15B**). Use of these lower doses eliminated empty liposome toxicity, whilst retaining some loss of cell viability in cells treated with 0.25 µM liposomal AL3. Although this loss of viability did not reach statistical significance using an overall ANOVA test, it is very promising to see any effect with such a low concentration of AL3. Furthermore, pairwise comparison of 0.25 µM AL3 liposome and empty liposome-treated cells in individual experiments showed a small reduction in cell number in each case,

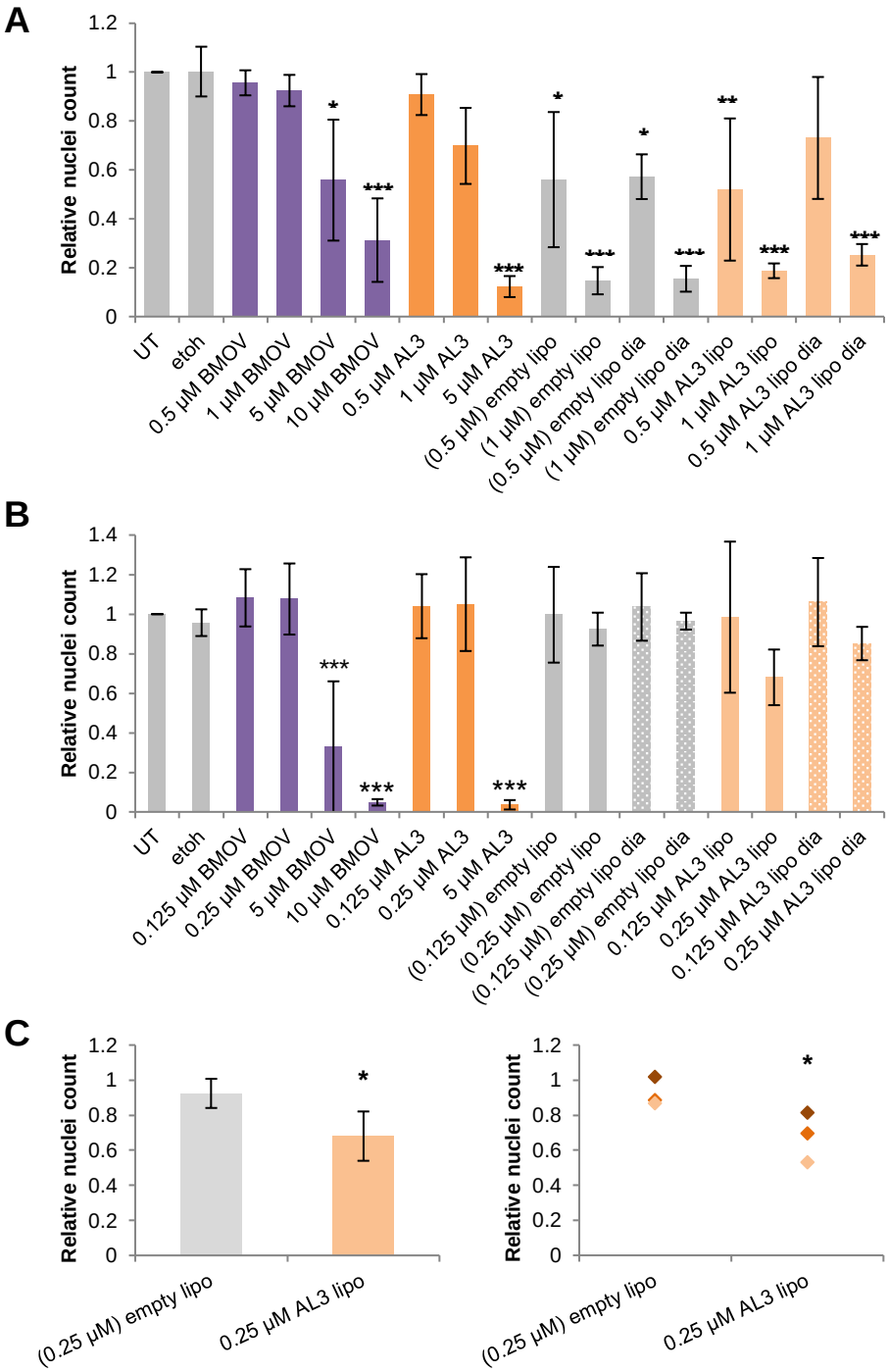

Figure 5.15 – Batch 1 AL3 liposomes were slightly more cytotoxic compared to empty liposomes in neuroblastoma cells.

A *- IMR32 cells were treated with BMOV or AL3 in solution, empty liposomes, or batch 1 AL3 liposomes (both dialysed and dialysed) for 3 days after which cell viability was assessed by nuclei counting. ANOVA with Dunnet post hoc using untreated (UT) as the control, * p<0.05, ** p<0.01, *** p<0.001 (n=3).* ***B*** *– Given that high levels of cytotoxicity were observed even with empty liposomes, IMR32 cells were treated with lower concentrations of BMOV or AL3 in solution, empty liposomes, or batch 1 AL3 liposomes (both dialysed and dialysed) for 6 days after which cell viability was assessed by nuclei counting. ANOVA with Dunnet post hoc using UT as the control, * p<0.05, ** p<0.01, *** p<0.001 (n=3).* ***C*** *– Nuclei counts for 0.25 µM empty liposome and AL3 liposome treated cells (from* ***B****) plotted as mean averages (left) and a dot plot showing data points from each repeat experiment. Statistical analysis for these conditions was repeated using a paired T-test, * p<0.05 (n=3) Note: These values are fold change nuclei counts relative to UT cells plotted in* ***B****.*

which was statistically significant using a paired T-test (**Figure 5.15C**). Ethanol solubilised AL3 at 0.25 µM does not induce any changes in cell viability, suggesting that liposomal delivery may be a much more efficient route for the delivery of AL3 to cells.

SK-N-SH cells, which normally differentiate in response to oxidovanadium, were treated with (a) BMOV or AL3 in solution, (b) liposomal AL3 dialysed and non-dialysed (batch 1), or (c) empty liposome dialysed and non-dialysed. Images were taken after 5 days and average neurite length was quantified (**Figure 5.16A+B**). As reported previously, BMOV and AL3 delivered in solution induced differentiation characterised by neurite outgrowth at a concentration of 5 µM. Empty liposomes as well as BMOV and AL3 in solution at concentrations below 5 µM had no effect on neurite length. Liposomal AL3, both dialysed and non-dialysed, significantly increased neurite length even at a low concentration of 0.5 µM. In fact 1 µM liposomal AL3 was sufficient to increase neurite length to the level seen with 5 µM AL3 in solution, suggesting a 5-fold increase in activity. There is a small, but not significant, difference in neurite length in cells treated with dialysed as opposed to non-dialysed AL3 liposomes, mirroring the difference in concentration of these formulations described above (**Figure 5.14E**). These neurite length assays were repeated for the second and third batches of AL3 liposomes (**Figure 5.16C+D**). The third batch had minimal effect on neurite length, although this was to be expected as the AL3 concentration in these liposomes was much lower (**Figure 5.14E**). The second batch however, gave very similar results to the original formulation.

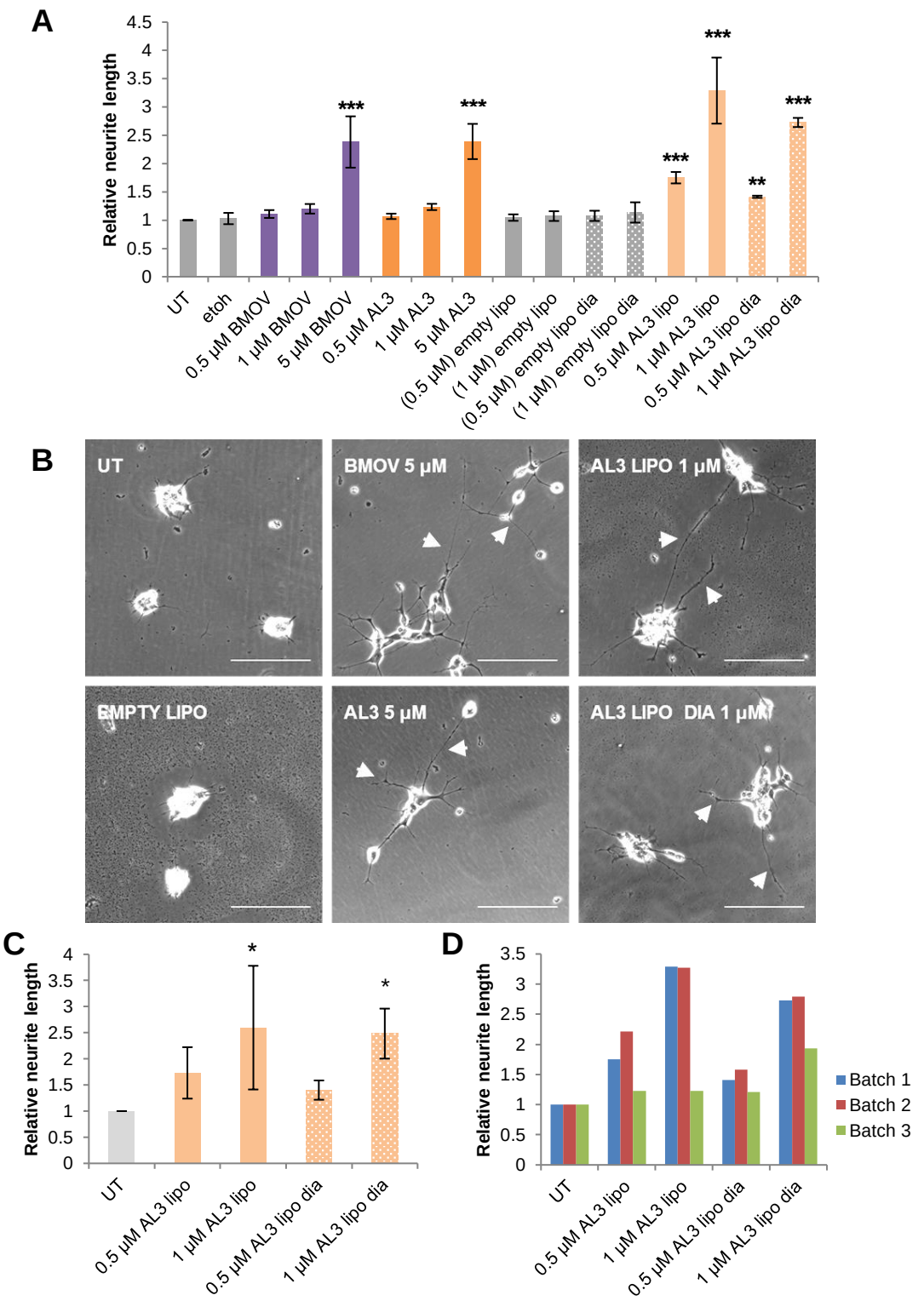

Figure 5.16 – Liposomal AL3 induced stronger differentiation than AL3 in solution
A+B *– SK-N-SH cells were treated with BMOV or AL3 in solution, empty liposomes, or batch 1 AL3 liposomes (both dialysed and non-dialysed) for 5 days after which neurite length was measured. ANOVA with Dunnett post hoc using untreated (UT) as the control ** p<0.01, *** p<0.001 (n=3) (**A**). Representative phase-contrast microscopy images showing neurite outgrowth (white arrows) (**B**).* ***C+D*** *– SK-N-SH cells were subsequently treated in the same way using batch 2 and 3 AL3 liposomes. Mean average effects on neurite length using all three batches were plotted (**C**) as well as the individual values for each batch (**D**). ANOVA with Dunnet post hoc using UT as the control, * p<0.05 (n=3 – three AL3 liposome batches).*

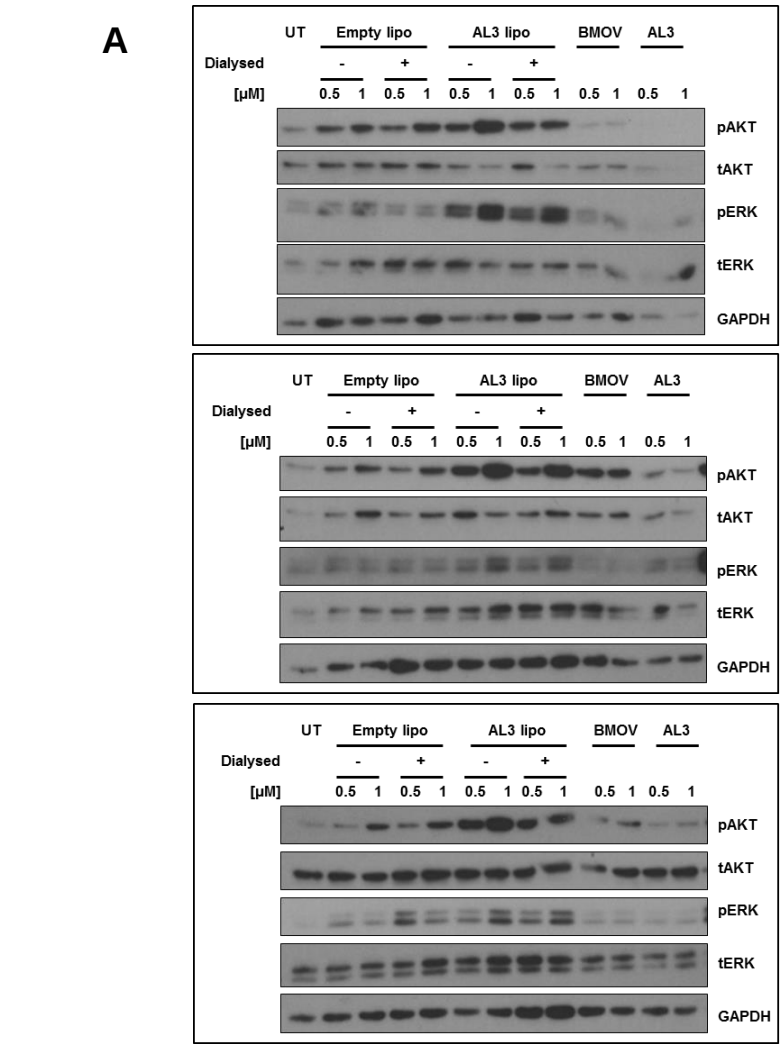
A
UT
Empty lipo
AL3 lipo
BMOV
AL3
Dialysed
[μM]
pAKT
tAKT
pERK
tERK
GAPDH

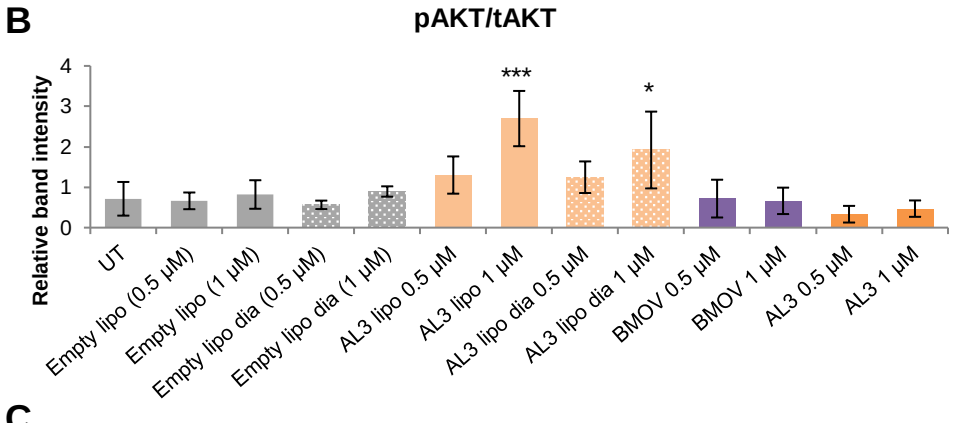
B
pAKT/tAKT
Relative band intensity
***
*
UT
Empty lipo (0.5 μM)
Empty lipo (1 μM)
Empty lipo dia (0.5 μM)
Empty lipo dia (1 μM)
AL3 lipo 0.5 μM
AL3 lipo 1 μM
AL3 lipo dia 0.5 μM
AL3 lipo dia 1 μM
BMOV 0.5 μM
BMOV 1 μM
AL3 0.5 μM
AL3 1 μM

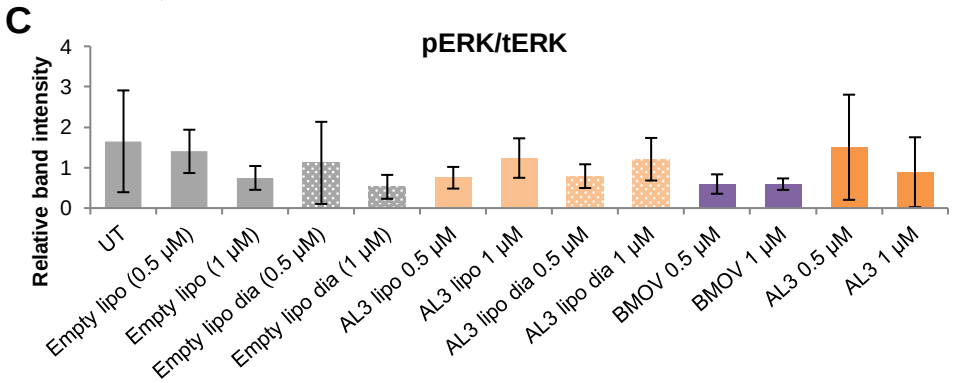
C
pERK/tERK
Relative band intensity
UT
Empty lipo (0.5 μM)
Empty lipo (1 μM)
Empty lipo dia (0.5 μM)
Empty lipo dia (1 μM)
AL3 lipo 0.5 μM
AL3 lipo 1 μM
AL3 lipo dia 0.5 μM
AL3 lipo dia 1 μM
BMOV 0.5 μM
BMOV 1 μM
AL3 0.5 μM
AL3 1 μM

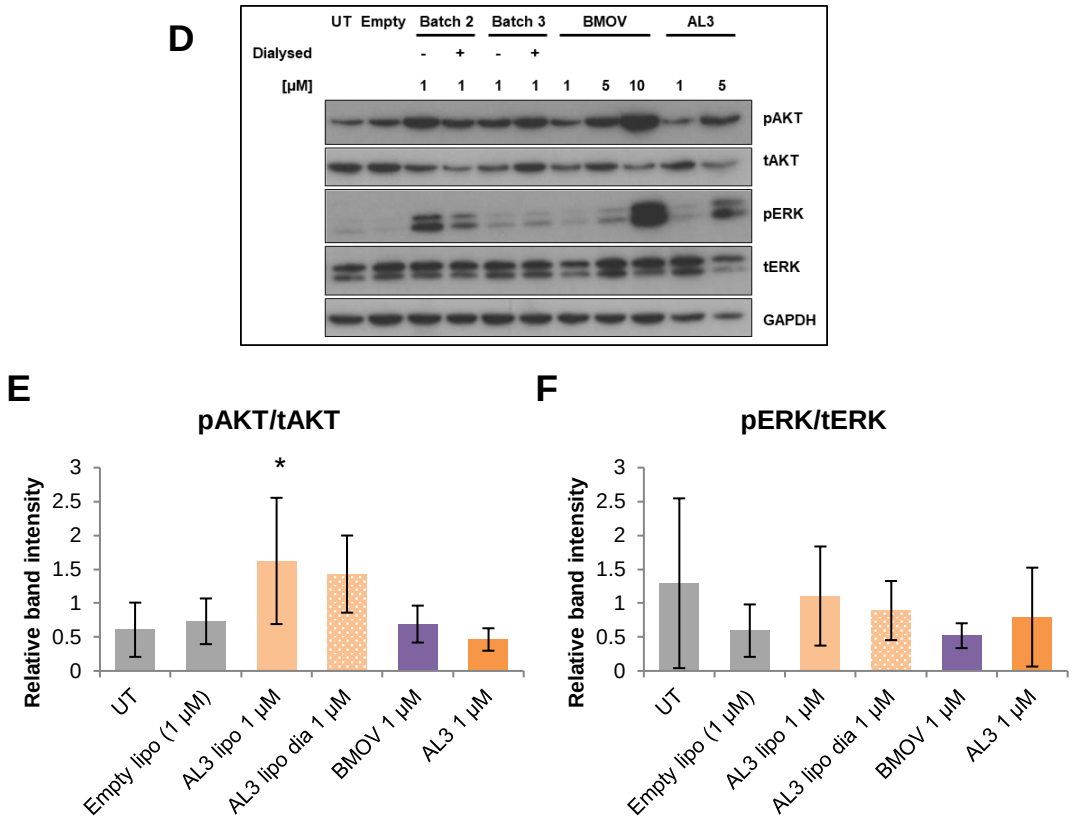

Figure 5.17 – Liposomal AL3 enhanced phosphorylation of AKT, and to an extent ERK, to a greater degree than AL3 in solution
A *(previous page) – SK-N-SH cells were treated with BMOV or AL3 in solution, empty liposomes, or batch 1 AL3 liposomes (both dialysed and dialysed) for 3 days. Western blotting for phosphorylated and total AKT and ERK was performed (GAPDH loading control) (n=3).* ***B+C*** *(previous page) - Western blots from* ***A*** *were quantified and relative band intensities for phosphorylated proteins were normalised to total proteins. ANOVA with Dunnett post hoc using untreated (UT) as the control, * p<0.05, *** p<0.001 (n=3).* ***D*** *– SK-N-SH were subsequently treated in the same way using batch 2 and 3 AL3 liposomes and western blotting was repeated (n=1).* ***E+F*** *– Western blot from* ***D*** *was quantified (as in* ***B+C****), and mean average effects on AKT and ERK phosphorylation using all three batches were plotted. ANOVA with Dunnet post hoc using UT as the control, * p<0.05 (n=3 – three AL3 liposome batches).*

Western blotting for AKT and ERK was performed using lysates from SK-N-SH cells treated for 3 days with (a) BMOV or AL3 in solution, (b) dialysed and non-dialysed AL3 (batch 1), or (c) dialysed and non-dialysed empty liposome (**Figure 5.17A-C**). Significant increases in phosphorylation of AKT were observed in cells treated with 1 μM liposomal AL3, both dialysed and non-dialysed. There does also appear to be an increase in phosphorylated ERK following treatment with the AL3 liposomes, however this has not been reflected in the quantitation of band intensity, likely due to inconsistencies in total ERK. This biochemical analysis was repeated using AL3 liposome batches 2 and 3 (**Figure 5.17D**). Very minimal changes in phosphorylation

were detected using the lower concentration batch 3 liposomes, however batch 2 liposomes caused greater increases in phosphorylation of both ERK and AKT. When the mean band intensities for all three batches of AL3 liposomes were calculated the inter-experimental error was high (**Figure 5.17E+F**). This was unsurprising given the differences in AL3 concentration measured by HPLC. Inconsistencies in total AKT and total ERK also likely contributed. There was however a significant increase in phosphorylation of AKT.

Taken together these data indicate that AL3 can be successfully packaged into liposomes and delivered to neuroblastoma cells in culture. These liposomal formulations are able to induce neurite outgrowth, enhance phosphorylation of AKT and ERK, and potentially reduce cell viability and are in fact more active than AL3 dissolved in ethanol across all of these parameters.

5.3. Discussion

The data presented here show that four hydrophobic oxidovanadium derivatives (AL1-4) are able to induce similar or, in the case of AL3, far superior cytotoxicity and/or differentiation compared to BMOV in a subset of neuroblastoma cell lines. Like BMOV, these compounds may prove to be useful in the treatment of neuroblastoma, but ongoing safety concerns surrounding the clinical use of oxidovanadium dictate that alternative delivery strategies should still be considered. Here one oxidovanadium compound, AL3, has been successfully packaged into liposomes and delivered to neuroblastoma cells. This liposomal formulation induced approximately 5-fold stronger differentiation compared to AL3 in solution, suggesting that liposomal delivery may be more effective even *in vitro*. This may in turn result in lower doses required for efficacy *in vivo* compared to unpackaged BMOV-like compounds, potentially reducing drug-associated toxicities. Encapsulation may also both protect AL3-like molecules from degradation in circulation and allow passive tumour targeting, further reducing the required dose and going some way to reducing off-target tissue toxicity. An important question that must be answered if oxovanadium compounds are to be considered for use in neuroblastoma treatment in humans is whether the oxidovanadium doses that

we have used *in vitro* would be achievable *in vivo*. Many of the preclinical animal studies that use vanadium-derived compounds in cancer models (**Table 1.3 and 1.4**) do not report the tumour or plasma vanadium concentrations that were achieved. In the BEOV human clinical trials, the maximum reported plasma concentration was just 493 nM, although this was sufficient to induce anti-diabetic efficacy (Thompson and Orvig, 2006). Whether it would be possible to achieve a higher plasma vanadium concentration using BMOV *in vivo*, that is tolerated, and produces anti-cancer efficacy, remains a significant question. However, the fact that AL3 is both more potent in solution compared to BMOV, and can be packaged into liposomes which appear to be an even more efficient delivery route for vanadate, will hopefully improve the likelihood that effective dosing can be achieved *in vivo*.

The four hydrophobic oxidovanadium compounds used in this study differ from one another based on the ligand molecules used to co-ordinate vanadium within them (**Figure 5.2**). Whilst they all induced cytotoxicity and differentiation, there were quantitative differences in their potencies, and some unexpected qualitative differences in the neuroblastoma cell biochemical responses (AKT and ERK phosphorylation). Some of these differences in AKT and ERK phosphorylation may be explained by the lower dose of AL3 that was administered in the experiments presented in **Figure 5.10**. However, given that AL3 has at least 2-fold higher activity in terms of cytotoxicity and differentiation compared to the other oxidovanadium compounds, we reasoned that induction of phosphorylation of AKT and ERK may also occur at lower doses. This was not found. Furthermore, there were dramatic differences in biochemical responses between the cell lines; for example, treatment with AL3 resulted in strong phosphorylation of ERK in IMR32 but not KELLY cells, despite both cell lines having a strong cytotoxic response to this compound, suggesting that specific cells line may lack critical signalling intermediates. This uncoupling of the morphological and biochemical responses to the oxidovanadium compounds was not foreseen, and suggests that these novel hydrophobic complexes play a more interesting role than simply delivering vanadate to neuroblastoma cells.

As discussed in **Chapter 1**, it is likely that for most oxidovanadium compounds, complexes dissociate in biological solutions to release vanadate and free ligand molecules (Levina and Lay, 2017, Kremer et al., 2015). It was therefore possible that the ligands associated with each of the hydrophobic oxidovanadium compounds accounted for some of these differences in potency and biochemical activity. However, when neuroblastoma cells were treated with the free ligand molecules without vanadium, there was no effect on cell viability, neurite outgrowth, or phosphorylation of AKT or ERK (**Figure 5.13**). Given that the free ligand molecules did not induce any cytotoxicity or differentiation, it is reasonable to conclude that vanadium itself is responsible for these morphological changes. The quantitative differences in efficacy may therefore be explained by the efficiency by which these complexes are able to deliver vanadate to the cell. Both the uptake of compounds into the cell, and the release of vanadate within or outside of the cell may be affected by the ligands present within these oxidovanadium complexes (**Figure 5.18**). These complexes appeared to be very stable in ethanol (**Figure 5.3**), but their stability in biological solutions has not been measured so far, partly because we have not been able to identify a feasible method to quantify vanadate within cells. However, it may be possible to use the reverse-phase HPLC method developed for measuring liposomal AL3 concentrations to assess the stability of these complexes. The absorbance peaks used to detect AL3 occur due to the carbon rings within the complex; the other hydrophobic oxidovanadium compounds will similarly have characteristic absorbance peaks. The carbon rings within the free ligand compounds should also have peaks of absorbance, but these will have slightly different wavelengths compared to those in the intact complexes. If the sensitivity of the HPLC assay is high enough, this shift in absorbance may allow the detection of free ligand, as opposed to intact complex, in solutions and possibly cell lysates containing oxidovanadium compounds, indicating that vanadium has been released. This may allow the relative stability of these complexes to be assessed. If the stability of the complexes were to correlate negatively with their biological activity, this would suggest that vanadium itself drives the observed cytotoxicity and differentiation, and differences in the effective release of vanadium confers the quantitative differences in efficacy of these compounds.

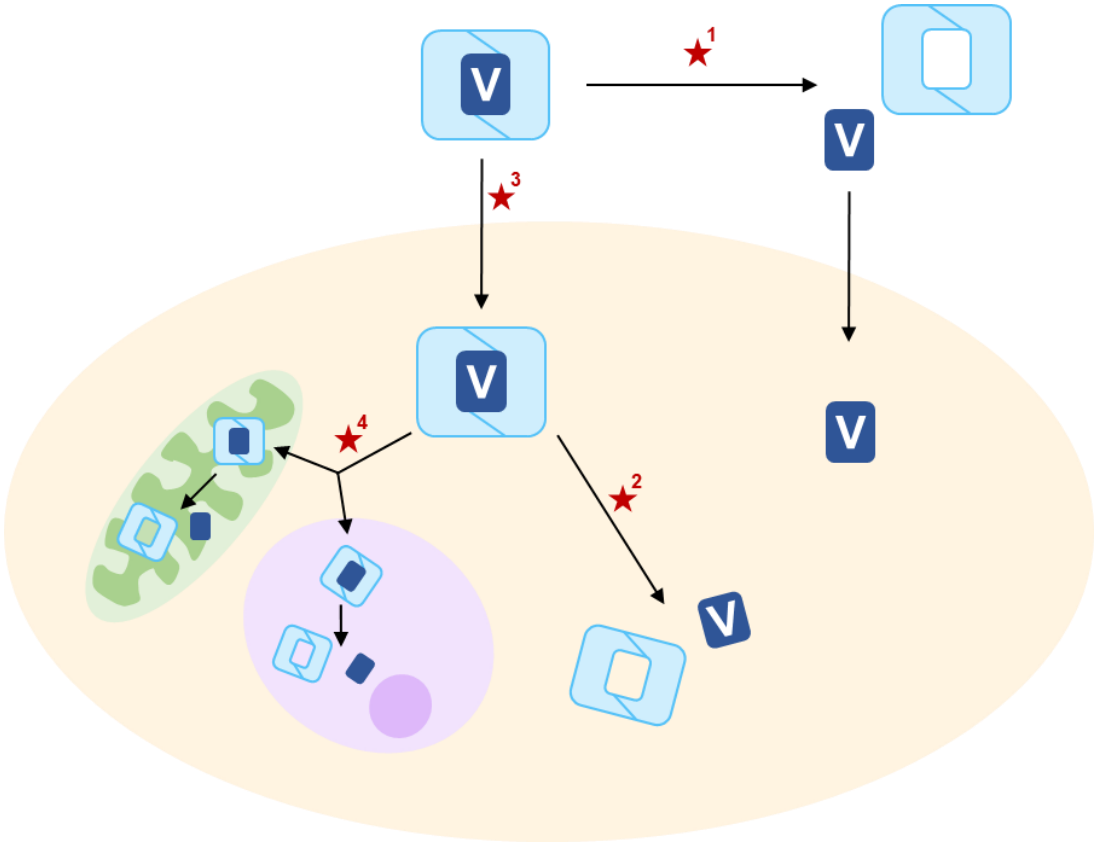

Figure 5.18 – Possible effects of ligands in hydrophobic oxidovanadium complexes
Red stars indicate ways by which hydrophobic ligands may affect oxidovanadium activity. Ligands may affect extra (1) or intracellular (2) dissociation of vanadate from complexes, cellular uptake of intact complexes (3), or intracellular localisation of oxidovanadium complexes (4).

If correct, this potential difference in the efficiency of vanadate release may go some way to explaining the quantitative difference in compound efficacy, but it does not address the qualitative differences in phosphorylation of AKT and ERK. The ligands used in these hydrophobic oxidovanadium complexes clearly exert distinct effects on the activity of the overall complex, but the ligands themselves do not account for the differences in biochemical activity (**Figure 5.13D-F**). One possibility is that the ligation leads to alternative compartmentalisation of the compounds within cells, where intact complexes are taken up by the cell and compartmentalised according to specific properties of the ligands (**Figure 5.18**). Indeed decavanadate has been reported to induce mitochondrial membrane depolarisation by localising specifically to mitochondria (Soares et al., 2007a, Aureliano and Crans, 2009, Aureliano and Ohlin, 2014). Once delivered, the hydrophobic oxidovanadium complexes may then degrade to release vanadate within these specific

subcellular organelles, which will contain distinct vanadate targets. For example, PTPs often contain localisation domains that target them to specific intracellular sites (Tonks and Neel, 2001, Ostman and Böhmer, 2001). There are examples of PTPs that are localised to the mitochondria, nucleus, endosomes and of course the entire receptor-type PTP sub-family that are plasma membrane associated (Radha et al., 1994, Zhang et al., 2011, Du and Grandis, 2015, Lorenzo et al., 2006). Thus the ligands used in AL1-4 may result in differential subcellular delivery, which may be cell type specific, causing distinct substrates to be targeted, which may then account for the qualitative differences in AKT and ERK phosphorylation. This might also account for some of the quantitative differences in potency. In order to assess whether these compounds are delivered to different subcellular compartments, oxidovanadium compounds could be modified with fluorescent labels. However, this could also confound their activity. Alternatively, subcellular compartments could be isolated following chemical treatment and assessed for vanadium content.

Although perhaps unlikely given the reported dissociation of other oxidovanadium complexes (Levina and Lay, 2017), a biological effect of the intact hydrophobic oxidovanadium complexes cannot be ruled out. It is unlikely that these intact compounds would be able to inhibit PTPs directly, given the spatial arrangement of their substrate-binding sites in catalytic domains (Peters et al., 2003). Furthermore, presumably vanadate-to-vanadyl cycling to produce ROS would also be limited by ligation in the intact complex. Nonetheless, until the stability of these compounds in biological solutions, and the dynamics of vanadate release in the cell can be understood, we must be open to a role of the intact oxidovanadium complexes in cytotoxicity and differentiation in neuroblastoma cells.

Whatever the cause of differences in activity, it is clear that we have identified an alternative oxidovanadium compound (AL3) that has high efficacy, both in terms of cytotoxicity and differentiation in neuroblastoma cells. *In vivo* testing in animals will be required to assess whether AL3 is likely to be tolerated in humans, and the off-target toxicities associated with this compound may well prove to be different, and even possibly more severe compared to BMOV.

However, given that we have also shown that AL3 can be packaged into liposomes and delivered to neuroblastoma cells in culture, these concerns may be alleviated by successful nanoparticle delivery.

In this study, encapsulation efficiency was assessed by using HPLC to measure the concentration of AL3 in the liposomal formulations following dialysis. Dialysis methods have been widely used in the nanoparticle field to assess encapsulation efficiency (Berger et al., 2001, Panwar et al., 2010, Wallace et al., 2012). Whilst these data indicate that AL3 was successfully packaged, it does not address the issue of liposome stability. Every effort was made to complete all biological assays using the liposomal formulations as soon after synthesis as possible. However, in some cases liposomes were stored at 4ºC for a number of weeks. It is possible that some AL3 leaked out of the liposomes and into the surrounding solution during this storage. AL3 is highly water insoluble, therefore it is likely that if a significant proportion had leaked out of the liposomes, it would have formed microcrystals that are unlikely to be taken up by cells. Nonetheless, it is possible that cells treated with stored liposomes will have received a dose of AL3 not entirely encapsulated within liposomes. In order to assess the stability of these oxidovanadium liposomes over time, dialysis followed by HPLC should be performed after increasing time intervals to measure the degree, if any, of AL3 leakage out of the liposomes. This would be important if these formulations were to be used for future *in vivo* preclinical evaluation. It should be noted that we have not identified a method to confirm that dialysis successfully removes all AL3 not encapsulated within liposomes. However, we do know that at least some is separated from the liposome solution, as we did detect a small reduction in AL3 concentration in batch 1 and 2 liposomes following dialysis (**Figure 5.14E**).

If used *in vivo,* the liposomal formulations used in this study would be an example of what is known as ‘passive targeting’. During passive targeting, formulations are introduced into the bloodstream and are absorbed by various tissues. The EPR effect causes them to be delivered to tumour cells with some favourability, but they will also reach other off-target tissues (Bae and Park, 2011). Whilst there has been success surrounding the use of passive

targeting, increasing attention is now being given to ‘actively targeted’ nano-formulations. Active targeting often involves specific targeting of nanoparticles to target tissue, for example by adding ligands to the surface of the particles that bind molecules that are expressed at the target site (Bazak et al., 2015). For example, denileukin diftitox fusion protein (Ontak®), approved for use in cutaneous T-cell lymphoma (CTCL), utilises specific binding to interleukin-2 (IL-2) receptors for targeted delivery of the diphtheria toxin (Olsen et al., 2001). More sophisticated active targeting systems are also in development. For example, ThermoDox® is a liposome based delivery system for doxorubicin that utilises a thermosensitive lipid such that the active drug is only released from the liposome when heat is applied, thus can be specifically targeted (Lindner et al., 2008). Disialoganglioside 2, or GD2, is an antigen that is abundantly expressed on the surface of neuroblastoma cells, for which monoclonal antibodies are approved for use in the treatment of neuroblastoma (Malone and Stegmaier, 2017). Importantly, GD2 is also expressed in some normal neural tissues, possibly accounting for significant side effects that have been reported in some anti-GD2 therapy trials (Tivnan et al., 2012). Despite this, GD2 has thus proven to be a very exciting target in immunotherapy, and it can also be used to target other therapeutic agents to neuroblastoma cells by active targeting (Rodríguez-Nogales et al., 2018). Bispecific antibodies or chimeric antigen receptor (CAR)-modified T cells can redirect cytotoxic T lymphocytes to GD2-expressing tumour cells, and radiolabelled GD2 antibodies can be used for tumour detection. Of particular relevance here, anti-GD2 antibodies can be incorporated onto the surface of nanoparticles loaded with drug molecules or other therapeutics to target them directly and specifically to tumour cells (Suzuki and Cheung, 2015). Di Paolo et al. (2011) demonstrated anti-cancer activity in a mouse xenograft model of neuroblastoma using GD2-targted liposomes containing ALK-targeting siRNA. Similarly, silica nanoparticles containing the pro-apoptotic microRNA-34a were targeted to neuroblastoma tumour cells in mice using an anti-GD2 antibody. These nanoparticles increased tumour cell apoptosis, and reduced tumour growth and vascularisation (Tivnan et al., 2012). Active targeting to direct nanoparticles, for example by using GD2 antibodies, could be used in an attempt to improve the specific delivery of oxidovanadium *in vivo*. Active

targeting may further enhance the efficiency of on-target tissue delivery of AL3 compared to passive targeting, and should further reduce the concern for off-target toxicities.

Here I have shown that the hydrophobic oxidovanadium compound AL3 induces cytotoxicity and differentiation with higher efficacy than BMOV in neuroblastoma cell lines. Some differences in AKT and ERK activation were detected in AL3-treated compared to BMOV-treated cells, which are not due to the hydrophobic ligands themselves in isolation. Although interesting, these biochemical differences are unlikely to be relevant in the mechanisms that drive cytotoxicity and differentiation, as AKT and ERK activation was found to be dispensable for BMOV activity (**Chapter 4**, Clark et al., 2013, Clark et al., 2015). In order to further investigate to what degree the cellular responses to BMOV and AL3 are similar, expression of PDE2A and cAMP concentrations following AL3 treatment could be assessed. If, like BMOV, AL3 treatment causes reduced PDE2A expression and/or increased cAMP concentration, this would give confidence to the hypothesis that cAMP signalling is involved in oxidovanadium-induced cytotoxicity (**Figure 4.15**). I have also shown here that AL3 can be successfully packaged into liposomes and delivered to neuroblastoma cells, where they have higher activity compared to AL3 delivered in solution. The use of these liposomal formulations, or of more advanced active targeting approaches described above, may allow safer delivery of oxidovanadium to tumour cells in neuroblastoma patients.

Chapter 6. Concluding remarks

6.1. Summary of key findings

This PhD project aimed to explore the therapeutic potential of targeting PTPs for the treatment of neuroblastoma. Neuroblastoma is a highly heterogeneous disease, representing a significant clinical challenge, with overall survival of the high-risk patient group remaining stubbornly below 50% despite aggressive, multimodal therapy (Whittle et al., 2017, Park et al., 2013). The identification and therapeutic inhibition of specific molecular targets that drive tumourigenesis and/or are required for tumour cell proliferation and survival may lead to improved outcomes for these patients. We hypothesise that PTPs, an enzyme family whose members are now being widely implicated as positive regulators of cancer (Elson, 2018, Frankson et al., 2017, Bollu et al., 2017), may be a useful source of such therapeutic targets for neuroblastoma, as could their effector pathways. Here I have presented data that support this hypothesis, using both genetic silencing of specific PTPs, and oxidovanadium-induced pan-PTP chemical inhibition.

In **Chapter 3**, siRNA-mediated gene knockdown was used to explore the effect of specific PTP gene suppression on neuroblastoma cell viability. PTPRN, CDC14B, MTMR12 and ACP1 had been identified as candidate growth and/or survival promoting PTPs based on a PTP family-wide shRNA dropout screen (A. Cichon and A. Stoker, unpublished), and the dual-specificity PTP CDC14B was taken through as a promising potential therapeutic target based on my own siRNA data. CRISPR/Cas9 was also used in an attempt to validate further the potential of CDC14B as a therapeutic target for neuroblastoma. I have so far not been able to show that genomic *CDC14B* editing leads to reduced proliferation or cell viability. Differences in the effect of gene knockdown versus knockout have been previously described for CDC14B as well as other, unrelated genes (El-Brolosy and Stainier, 2017, Mocciaro and Schiebel, 2010). However, based on my current data it is not possible to determine whether there is truly a difference between the response of neuroblastoma cells to shRNA/siRNA *CDC14B* gene silencing and CRISPR/Cas9 gene deletion, or whether there remains an underlying technical problem with one or both of these approaches.

The parallel studies presented in this thesis were concerned with the use of oxidovanadium compounds as pan-PTP inhibitors in neuroblastoma cells. Various vanadium-derived compounds have previously been used with success to induce net anti-cancer efficacy in a range of tumour models by our group and others (Evangelou, 2002, Rehder, 2012, Clark et al., 2013, Clark et al., 2015). However, there remains a lack of understanding concerning how these compounds actually work inside cells and there are also significant concerns regarding the safety of their use in humans (Domingo, 2000). I chose two directions to address these issues. One was to look at effector pathways as alternative targets and the other was to demonstrate an alternative cellular delivery route.

In **Chapter 4**, I explored the mechanisms that drive oxidovanadium activity in neuroblastoma cells. First, activation of the classical AKT and/or ERK pathways were ruled out as drivers of BMOV-induced cytotoxicity. Analysis of RNAseq data from four neuroblastoma cell lines treated with BMOV then revealed, not unexpectedly, that there is an extremely complex transcriptional response to oxidovanadium. Activation of forskolin-cAMP signalling, possibly involving reduced PDE2A expression, was identified as a candidate, critical BMOV effector pathway that could be targeted therapeutically, possibly with fewer off-target toxicities compared to oxidovanadium itself. Indeed, as discussed previously (Section 4.3.), several small molecule PDE2 inhibitors have been described in preclinical studies regarding cancer and other human diseases (Morita et al., 2013, Bernard et al., 2014, Liu et al., 2018a, Liu et al., 2018b, Soares et al., 2017). The transcriptomic analysis reported here was also used to ask how BSO-mediated glutathione suppression enhances oxidovanadium-induced cytotoxicity in neuroblastoma cells. It was concluded that BSO likely operates here largely by chemically enhancing BMOV-induced intracellular activity and therefore cytotoxicity. Co-administration of BSO with BMOV is likely to greatly enhance BMOV efficacy *in vivo* and this will be an important, next experiment in this research. Finally, in **Chapter 5** I present a proof of principle that the oxidovanadium derivative AL3 can be successfully packaged into liposomes and delivered to neuroblastoma cells in culture, resulting in increased phosphorylation of AKT and ERK, as has been reported

following treatment with BMOV in solution (Clark et al., 2013, Clark et al., 2015). Furthermore, these liposomal hydrophobic oxidovanadium formulations retain anti-cancer activity characterised by differentiation and cytotoxicity. In fact these AL3 liposomes were 5-fold more active compared to AL3 in solution, which in itself had much higher activity compared to BMOV. These liposomal formulations may allow safer and more efficient delivery of oxidovanadium to neuroblastoma tumour cells *in vivo*.

6.2. Final discussions

6.2.1. Targeting of specific PTPs

I used several methods in this project to inhibit the activity of specific PTPs, in order to assess their potential as therapeutic targets for neuroblastoma. Initially RNAi was used to silence PTP gene expression, and later CRISPR/Cas9 was used in an attempt to permanently knockout genomic *CDC14B*. These approaches utilise distinct biochemistry to abrogate gene function via different mechanisms. In the case of siRNA, gene expression is transiently silenced, although it is unlikely that 100% mRNA depletion is ever achieved. For CRISPR/Cas9, gene modification is permanent; however, depending on the specific editing that has occurred, some functional protein may persist, resulting from short, in frame deletions in non-essential domains for example. Both approaches allow effective *in vitro* target validation and, in particular when used in parallel, could provide strong evidence to support an oncogene-like role for specific PTPs in neuroblastoma. The data generated using these two approaches did not correlate in the case of CDC14B, although as discussed in **Section 3.3.**, this may have been partly due to technical challenges with one of or both of these methodologies, or a genuine difference in cellular response. Future target validation *in vivo*, perhaps for CDC14B as well as other candidate tumour-promoting PTPs being investigated by the laboratory, will involve inhibition of PTP activity in mouse xenograft models of neuroblastoma. The inducible CRISPR/Cas9 system developed by Dr. Vruti Patel, used in **Section 3.2.5,** can be used for this. Preliminary experiments carried out by Dr. Patel have shown that NOD scid gamma (NSG) mice develop tumours when injected with IMR32-derived Cas9-inducible 2E11 cells.

For target validation, NGS mice can be injected with 2E11 cells expressing PTP-targeting gRNAs, and Dr. Patel has shown that doxycycline can be administered in feed to induce Cas9 expression and successful indel formation *in vivo*. Evaluation of tumour burden in mice with and without doxycycline feed will allow us to evaluate the potential of specific PTPs as therapeutic targets in this *in vivo* setting.

As discussed previously, small molecule targeting of PTPs is challenging and to date there are no FDA-approved specific PTP inhibitors, thus genomic approaches have so far been favoured for target validation by us and others (Stanford and Bottini, 2017, Lazo et al., 2018) (**Section 1.2.5.**). However, recent advances using more creative approaches to target PTPs are beginning to yield potent small molecule PTP inhibitors with high specificity (Stanford and Bottini, 2017, Zhang, 2017). Professor Zhong-Yin Zhang's laboratory at Purdue University (Indiana, USA) have created a 'PTP-based drug discovery platform'. This platform utilises a fragment based approach for developing bidentate PTP inhibitors, targeting both the active site and less conserved peripheral pockets, allowing highly specific inhibitors to be developed (Zhang, 2017). For example, 11a-1 is a potent bidentate SHP2 inhibitor with 5-fold selectivity towards SHP2 compared to a panel of 20 mammalian PTPs, including a 7-fold preference for SHP2 compared to its close relative SHP1. 11a-1 was anti-proliferative in lung, breast and leukaemia cell lines, and demonstrated anti-cancer efficacy in a xenograft model of melanoma (Zeng et al., 2014, Zhang et al., 2016). Allosteric inhibition, involving non-competitive inhibition at sites distinct from the PTP active site is also beginning to yield promising therapeutic leads including SHP099, JMS-053 and trodusquemine, which target SHP2, PRL3 and PTP1B respectively (Chen et al., 2016, Sun et al., 2018b, McQueeney et al., 2018, Krishnan et al., 2014) (**Section 1.2.3.**). Specific PTP inhibitors will be critical for the translation of target validation into the development of useful PTP-inhibiting therapeutics to treat neuroblastoma in the clinic.

6.2.2. Utilising BMOV-induced cytotoxicity

We have shown here and in a previous publication that the oxidovanadium derivative BMOV has a net effect of cytotoxicity in a subset of neuroblastoma cell lines (Clark et al., 2015). Given the safety concerns associated with the use of vanadium-derived compounds as therapeutics, we have sought to identify specific molecular targets of BMOV that contribute to its overall anti-cancer efficacy, and could therefore be targeted independently. Therapeutic strategies that target specific molecules rather than those using broad acting chemicals such as BMOV are likely to be associated with fewer off-target toxicities, although these can still be significant (Baudino, 2015, Widakowich et al., 2007). We have begun to deconvolute the mechanisms driving BMOV-induced cytotoxicity using two large-scale screens (**Figure 6.1**). In one approach (**Figure 6.1*1**) we used a PTP family-wide shRNA dropout screen (A. Cichon and A. Stoker, unpublished), followed by my own siRNA validation, which led to the identification of CDC14B as a potential tumour-promoting PTP and therapeutic target. Although, as discussed previously, this was not yet validated using CRISPR/Cas9. In the other approach, we used RNAseq to define the transcriptional response to BMOV (**Figure 6.1*2**), and BMOV in combination with BSO-mediated glutathione suppression. We hypothesised this would lead to the identification of critical, oxidovanadium effector pathways, both PTP-related and non-PTP related. Here, activation of the forskolin-cAMP signalling network was identified as a possible BMOV-effector mechanism. Some early validation experiments provided some support for the hypothesis that targeting this pathway may be useful in the treatment of neuroblastoma. Combining these two strands to give a more complete picture of oxidovanadium-induced cytotoxicity will ideally involve characterising the substrates of specific cancer-promoting PTPs, and linking these to the gene expression changes observed in the RNAseq analysis (**Figure 6.1*3**).

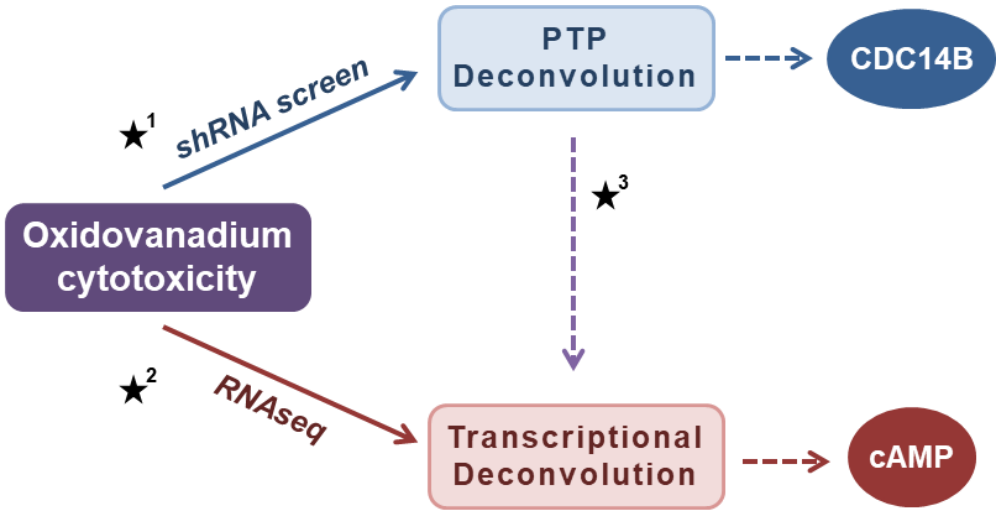

Figure 6.1 – Deconvolution of oxidovanadium-induced cytotoxicity
Pan-PTP inhibition using oxidovanadium-derived compounds induces cytotoxicity in a subset of neuroblastoma cell lines (Clark et al., 2015). Two reductionist approaches were used in an attempt to deconvolute the mechanisms driving this cytotoxicity. (1) A PTP family-wide shRNA screen was used to identify candidate pro-tumour PTPs. SiRNA-mediated gene knockdown provided some further support for a pro-neuroblastoma role of CDC14B. (2) RNAseq was used in an attempt to deconvolute the transcriptional response to oxidovanadium, revealing cAMP signalling as a potential critical effector pathway. (3) We hypothesise that the oxidovanadium-induced transcriptional response is driven at least in part by pan-PTP inhibition.

The use of both the RNAi and RNAseq screens described above attempted to identify specific, novel effectors that are critical for BMOV-induced anti-cancer activity, and could be targeted independently. These may be PTPs or other signalling proteins, however in either case their identification and specific targeting is a reductionist approach for harnessing oxidovanadium anti-cancer activity (**Figure 6.2**). As stated above, this kind of specific molecular targeting may be associated with fewer off-target toxicities compared to broad acting chemicals, and as such is currently a significant focus in the cancer research field. Indeed targeted therapy is being used with a great deal of success in many cases where tumour cells are dependent on specific molecular drivers, a phenomenon known as oncogene addiction (Weinstein, 2002, Weinstein and Joe, 2006). Targeted inhibition of these critical oncogenes can thus be very effective, for example EGFR inhibitors such as gefitinib and erlotinib are used in the treatment of EGFR driven NSCLC (Lynch et al., 2004, Shepherd et al., 2005). Similarly imatinib is used to inhibit the BCR/ABL fusion protein in CML, leading to improved patient outcomes (Hughes et al., 2003, O'Brien et al., 2003, O'Brien and Deininger, 2003), and BRAF mutant melanoma patients respond positively to treatment with vemurafenib (Bollag et al., 2010).

Although clearly the reductionistic targeting of specific tumour drivers has provided vital leaps forward in the treatment of some cancers, many have also been hindered by lack of efficacy, often caused by redundancy between signalling pathways, and importantly, high levels of acquired resistance (Rosenzweig, 2012, Barouch-Bentov and Sauer, 2011, Saijo, 2012). Tumour cells may become resistant to targeted therapies by altering the structure of drug binding sites through favourable mutations, such that inhibitors are no longer active, as has been described in some cases of imatinib and EGFR inhibitor resistance (Gorre et al., 2001, Kobayashi et al., 2005, Sequist et al., 2011, Yu et al., 2013). Other mechanisms of resistance include, but are not limited to, activating mutations or amplification of proteins downstream of the primary target, compensatory activation of redundant signalling pathways, and upregulation of drug efflux molecules (Lackner et al., 2012). In the case of oxidovanadium, although the reductionist approach may indeed be feasible, it may instead be that oxidovanadium's multiple effectors could be a benefit. Oxidovanadium compounds have been shown to induce several distinct anti-cancer effects in many tumour types, including reduced proliferation, cytotoxicity and reduced metastatic properties *in vitro* and *in vivo* (Evangelou, 2002, Bishayee et al., 2010, Irving and Stoker, 2017) (**Section 1.3.6.**). This suggests that several cellular signalling networks are at play, and multiple oxidovanadium targets may be critical for its anti-cancer activity. The very broad range of BMOV-associated gene expression changes observed in our RNAseq experiments indicates that this is indeed likely to be the case. This diverse intracellular activity is unsurprising given the range of biochemical activities of vanadium compounds in the cell, including inhibiting PTPs, but also potentially other phosphate binding enzymes, as well as producing ROS and direct DNA damage (Nechay, 1984, Rehder, 2012). Reducing BMOV's anti-cancer efficacy to the targeting of individual proteins may not therefore be the most effective way to harness its therapeutic potential for neuroblastoma. Pan-inhibition of all PTPs, as well as the other intracellular consequences of vanadium, may be essential for achieving net, high levels of anti-cancer efficacy. Hitting multiple cancer related intracellular signalling pathways, which contribute to several of Weinberg's Hallmarks of Cancer (Hanahan and Weinberg, 2000, Hanahan and Weinberg, 2011), may lead to higher initial

efficacy and even reduced emergence of resistance compared to molecular targeted therapies.

If we were therefore to propose the use of oxidovanadium itself *in vivo* as the preferred approach, there remain the on-going and well-founded safety concerns regarding its use in human patients (Domingo, 2000, Thompson and Orvig, 2006). However, advanced methods of drug delivery, including encapsulation within nanoparticles, may allow alternative and safer use of oxidovanadium-derived compounds (**Figure 6.2**). We have shown for the first time that organic, hydrophobic oxidovanadium complexes can indeed be successfully packaged into liposomes, potentially offering opportunities for reduced off-target toxicity whilst retaining wide ranging anti-cancer effects. The *in vivo* anti-cancer efficacy of these formulations, and potentially others with active targeting surface molecules, should now be validated using mouse xenograft models of neuroblastoma.

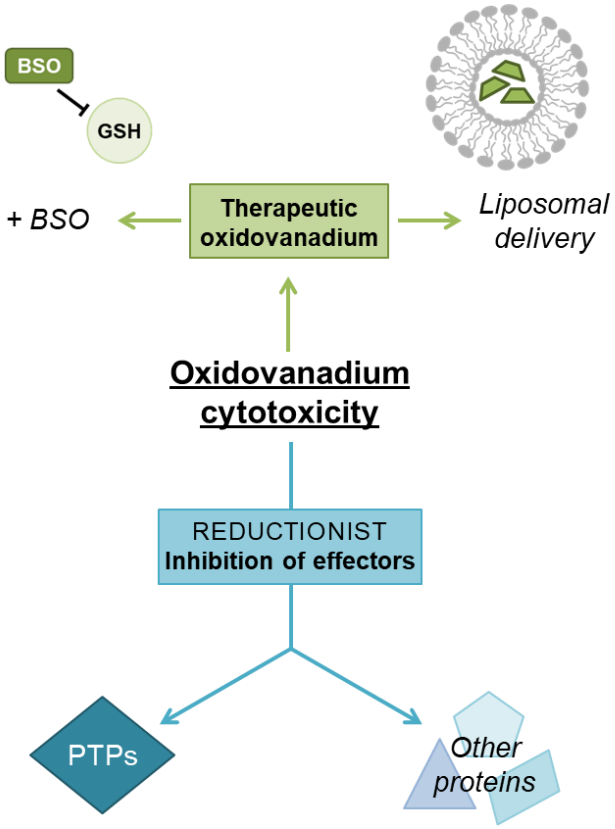

Figure 6.2 – Approaches to utilise oxidovanadium activity for neuroblastoma treatment *The net effect of oxidovanadium in a subset of neuroblastoma cell lines is cytotoxicity. In an attempt to translate this cytotoxicity into useful therapeutic strategies for neuroblastoma we have used several approaches. In a reductionist approach (blue), we have sought to identify specific oxidovanadium effectors, both PTPs and other proteins, which could be independently targeted. Alternatively, we suggest that oxidovanadium compounds themselves could be used as therapeutic leads (green), in particular when combined with BSO-mediated glutathione (GSH) suppression, and/or when delivered in liposomal formulations.*

6.2.3. PTP-inhibition beyond neuroblastoma

This project aimed to explore the therapeutic targeting of PTPs for neuroblastoma specifically. However, as discussed previously (**Section 1.2.3.**), tumour-promoting roles for specific PTPs have been described for many other human cancers (He et al., 2014, Elson, 2018). In some cases, specific PTP family members are drivers of tumourigenesis and/or cancer progression across multiple tumour types. For example SHP2 has been implicated in neuroblastoma, as well as leukaemias, melanoma and breast, lung, thyroid, liver, gastric and laryngeal tumours (Chan et al., 2008, Zhang et al., 2015, Bentires-Alj et al., 2004, Zhang, 2017, Zhou and Agazie, 2008, Hu et al., 2015, Xu et al., 2005). The role of CDC14B in tumours other than neuroblastoma has not been explored in this project. However, Sun et al. (2018a) reported that suppression of CDC14B correlated with reduced proliferation and increased apoptosis in laryngeal carcinoma cells. Thus therapeutic targeting of CDC14B could be useful in cancer treatment beyond neuroblastoma. Similarly, widespread anti-cancer activity of oxidovanadium-derived compounds across many tumour types has been reported in the literature and was discussed in **Section 1.3.6.** (Evangelou, 2002, Bishayee et al., 2010, Irving and Stoker, 2017). Indeed I have shown here that oxidovanadium induces loss of viability in a panel of paediatric brain tumour cell lines, as well as in neuroblastoma. It will be of significant interest to understand whether oxidovanadium acts via common mechanisms in these distinct cells and tissues. This may strengthen the case for either the more reductionist approach of targeting oxidovanadium effectors, both PTPs or other signalling proteins, or the clinical use of oxidovanadium complexes themselves (**Figure 6.2**).

Thus, with the knowledge of oxidovanadium effectors, the use of oxidovanadium complexes, the combination of oxidovanadium with BSO and our novel delivery of hydrophobic oxidovanadium using liposomes, we may provide new opportunities for exploring clinical efficacy both in neuroblastoma and in other paediatric and adult tumour types.

Appendices

Appendix 1 – PTP-targeting siRNA knockdown efficiency

Table A1 – PTP-targeting siRNA knockdown efficiency
Knockdown efficiency achieved in IMR32 cells using PTP-targeting siRNAs. Percentages indicate mRNA expression, assessed by qPCR, in siRNA-transfected cells compared to a non-targeting scrambled control siRNA (SCR) (n=1). Data provided by Dr. Jessica Pickles.

siRNA	% Expression compared to SCR	siRNA	% Expression compared to SCR
PTPRN_06	14	**MTMR12_09**	24
PTPRN_07	3	**MTMR12_10**	67
PTPRN_08	4	**MTMR12_11**	68
PTPRN_09	11	**MTMR12_12**	66
CDC14B_10	14	**ACP1_05**	8
CDC14B_11	21	**ACP1_06**	7
CDC14B_12	14	**ACP1_07**	9
CDC14B_13	10	**ACP1_08**	9

Appendix 2 – BMOV/BSO microscopy

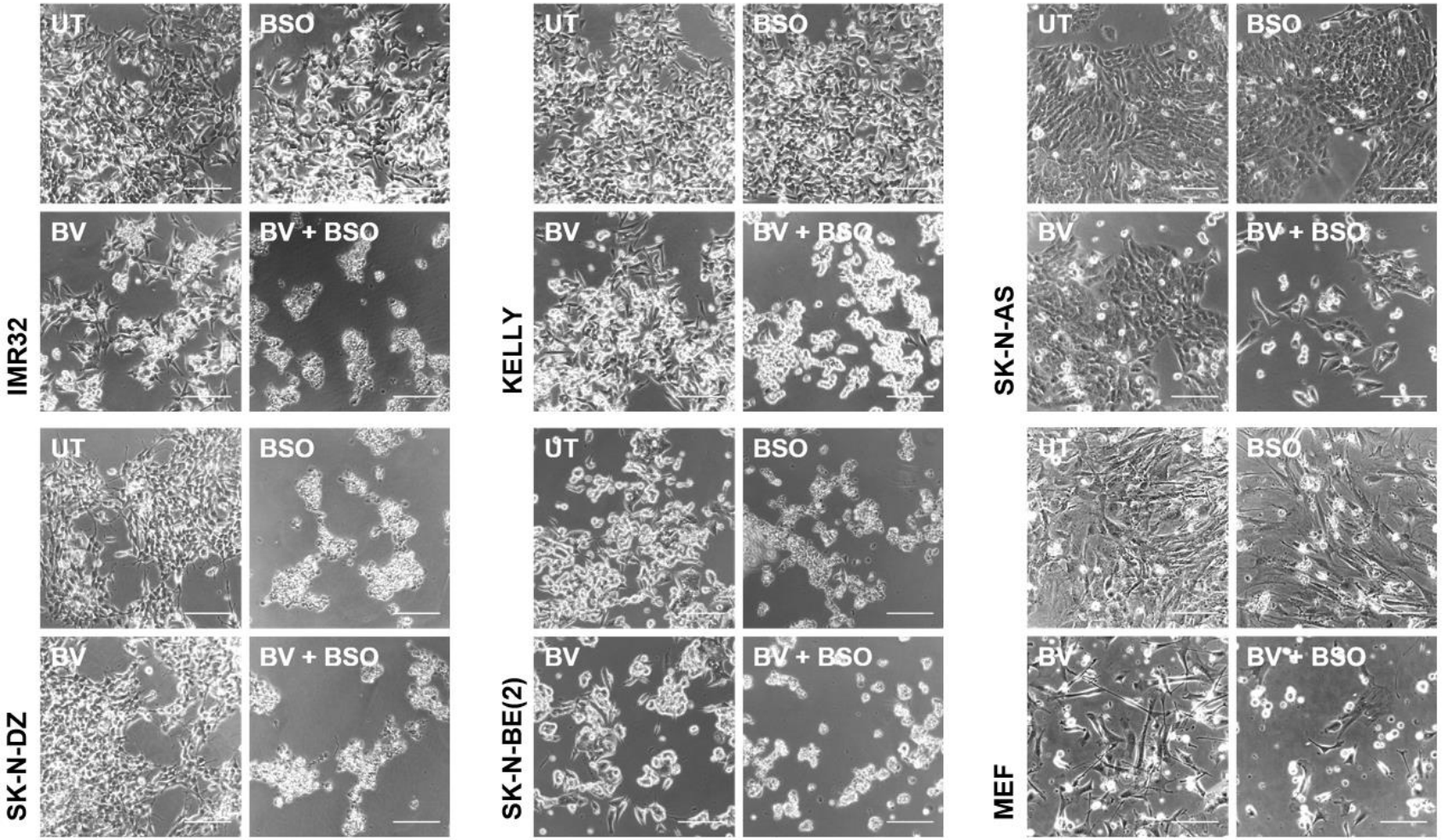

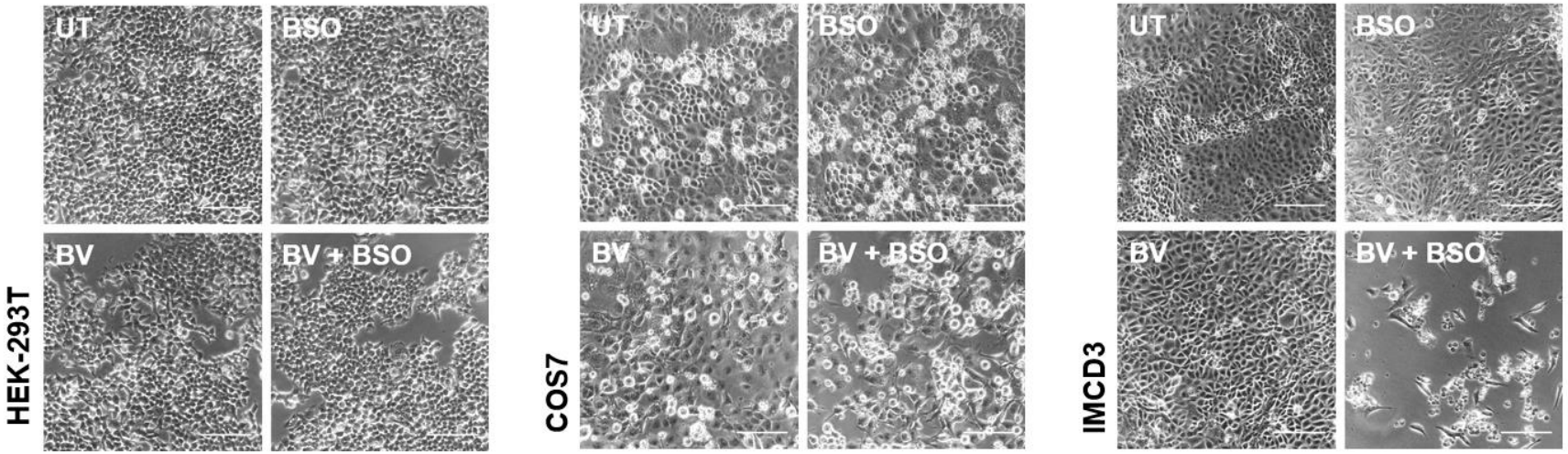

Figure A1 – BMOV/BSO cytotoxicity in neuroblastoma and non-neuroblastoma cell lines

IMR32, KELLY, SK-N-AS, SK-N-DZ, SK-N-BE(2), MEF, HEK-293T, COS7 and IMCD3 cells treated with 10 µM BMOV and 10 µM BSO for 3 days. Scale bar = 150 µm. Qualitatively assessed for cell viability in ***Figure 4.2A.*** *Note: At this stage of my project I did not have a reliable assay to quantitatively assess cell viability following oxidovanadium treatment (discussed in* ***Appendix 3****). Therefore, I qualitatively summarised relative cell viability effects, shown in* ***Figure 4.2A****.*

Appendix 3 – Cell viability assays

Many different methods can be used to assess the effect of an experimental condition, for example chemical treatment or under or overexpression of a specific gene, on cell viability. These methods vary in complexity, and can provide very different information about proliferation rates and mechanisms of cell death. Colourimetric or fluorescence-based cell viability assays that measure the relative metabolic activity of cell populations by utilising reduction by mitochondrial enzymes, are commonly used to quickly assess any cytotoxic effects. These are typically very straightforward assays that are performed in 96 well plates and can be automated, for example the very commonly used MTT assay, which was the first to be developed for high throughput screening (Mosmann, 1983). These assays rely on the assumption that the experimental readout will be relative to the number of viable cells. However, this may not always be true. If the experimental treatment directly affects the activity of the enzymes responsible for the experimental readout, in a way that does not entirely correlate with cell viability, these assays may not be suitable (Marshall et al., 1995). Many studies have described limitations of these viability assays, where specific chemicals can cause false positives and negatives based on their intracellular activity (van Tonder et al., 2015, Ganapathy-Kanniappan et al., 2010, Wang et al., 2011, Vistica et al., 1991, Gonzalez and Tarloff, 2001). Obtaining reliable quantitative data to assess neuroblastoma cell viability following treatment with oxidovanadium compounds has been a reoccurring challenge for our group. In light of the impending requirement for such assays in my project, I compared the suitability of a number of assays and this work is described below.

Initially the CCK-8 reagent from Sigma-Aldrich was used. This reagent contains a tetrazolium salt named WST-8, which is reduced by dehydrogenases in living cells, producing a yellow/orange formazan dye that absorbs light at 460nm (Ishiyama et al., 1993). Absorbance at 460nm is therefore proportional to the relative number of viable cells. However, it very quickly became clear that the resulting values were not always reliable in quantifying the effect of oxidovanadium treatment on cell viability. A very intense orange colour corresponding to very high absorbance values was

observed when high concentrations of oxidovanadium were applied (**Figure A2A**). Phase-contrast microscopy images indicate that there were fewer viable cells in BMOV-treated compared to untreated cells (**Figure A2B)**. Furthermore, our group have previously reported that BMOV induces apoptosis in these cells using subG1 analysis and caspase cleavage assays (Clark et al., 2015). This phenomenon of over-estimating BMOV-treated cells may be due to a direct interaction between the reagent and oxidovanadium, or more likely the effect of oxidovanadium on the activity or cellular levels of dehydrogenases. If treating cells with oxidovanadium increases dehydrogenase activity, a high absorbance could be observed even from fewer live cells.

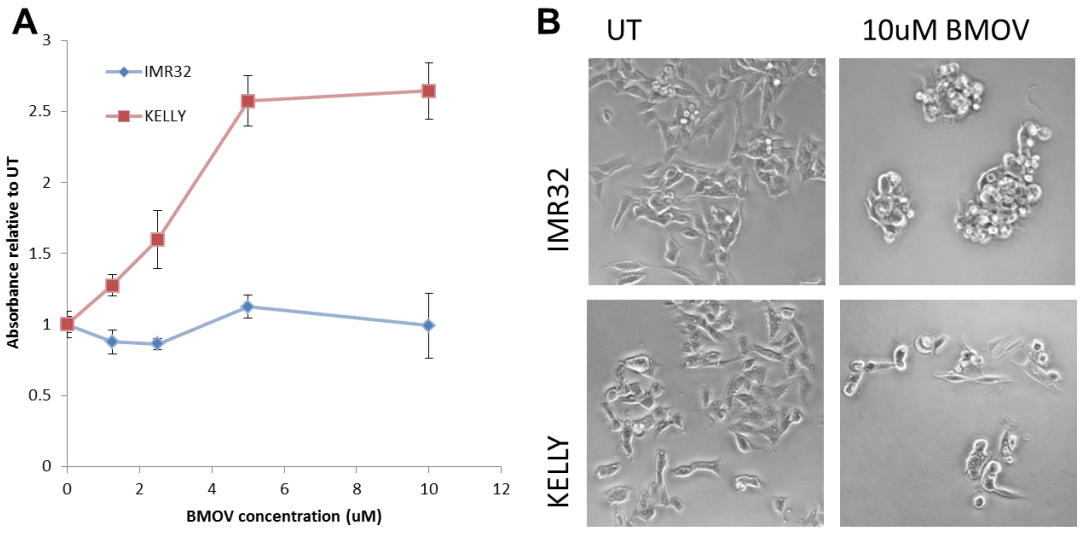

Figure A2 - CCK8 quantified cell viability does not always agree with observed BMOV-induced cytotoxicity
A *- IMR32 (blue) and KELLY (red) cells were treated with a BMOV dosage range for 3 days, after which cell viability was quantified using a CCK-8 cell viability assay (n=1).* ***B*** *- Untreated cells and cells treated with 10 μM BMOV for 3 days were imaged using phase-contrast microscopy, showing clear rounding of BMOV-treated cells, indicative of cytotoxicity.*

Having concluded that the CCK-8 assay was not entirely suitable for use with oxidovanadium, alternative cell viability assays were sought, including resazurin, from R&D Systems (Minnesota, USA), and ATPlite 1step, from PerkinElmer (Massachusetts, USA). Resazurin is another redox sensitive dye that changes colour and fluoresces when it is reduced to resorufin by dehydrogenases (O'Brien et al., 2000). Absorbance at 570nm or fluorescence (544nm excitation and 590nm emission) is proportional to aerobic respiration and therefore the number of viable cells. The ATPlite system indicates the

number of metabolically active cells by assessing ATP levels (Cree and Andreotti, 1997). The reagent contains D-Luciferin and luciferase, ATP reacts with D-Luciferin producing light. Thus relative luminescence can be used as a measure of cell viability. In order to test the suitability of these assays for assessing the effect of oxidovanadium compounds on cell viability, a range of neuroblastoma cell densities were plated and treated with 10 µM BMOV for 3 days. The data obtained using the resazurin assay suggest that there were very minor differences in cell density when BMOV was added (**Figure A3A**). As shown previously, this is not reflective of what can be observed by looking at cell morphology (**Figure A2B**). The ATPlite 1step reagent did show a reduction in BMOV-treated IMR32 cell density compared to untreated cells (**Figure A3B**). This was perhaps not as great a difference as was observed by microscopy, although morphological assessments are subjective, hence the requirement for quantitative cell viability assays. However, the data obtained using this kit did not reflect the reduction in cell density that is observed in KELLY cells.

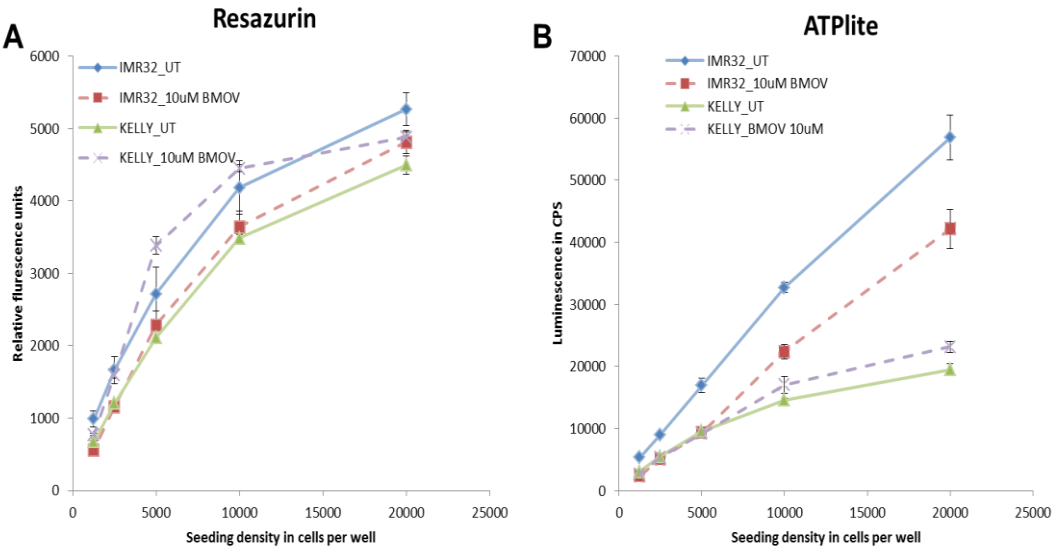

Figure A3 – Resazurin and ATPlite 1 Step assays in BMOV-treated neuroblastoma cells *IMR32 and KELLY cells were seeded at a range of densities +/- 10 µM BMOV. Cell viability was measured after 3 days using resazurin **(A)** and ATPlite 1 Step **(B)** (n=1).*

Crystal violet staining and solubilisation is another method that can be used to quantify cell numbers following chemical treatment. Crystal violet is a triarylmethane dye with a deep purple colour; it stains DNA and protein and therefore can be used to stain fixed cells (Feoktistova et al., 2016). Post-

staining, the dye can be solubilised and absorbance at 595 nm can be used as a measure of cell number. There are several caveats associated with the use of crystal violet staining and solubilisation as a cell viability assay. The dye will stain dead cells if they have remained adhered to the plastic. Conversely, live cells that have begun to lose adhesion, as is often the case in BMOV-treated cells, may be removed during the wash steps required for this assay. It is really a measure of loss of adhesion, which typically occurs during cell death, rather than of loss of viability itself. I have also observed a change in hue of the dye when BMOV is present, particularly in KELLY cells, which is likely to affect quantitation. Nonetheless, viability data obtained using this method in IMR32 cells was reflective of the observed cytotoxicity (**Figure A4**). Crystal violet staining and solubilisation was therefore deemed to be a reasonably suitable assay for assessing differences in cell viability caused by oxidovanadium treatment.

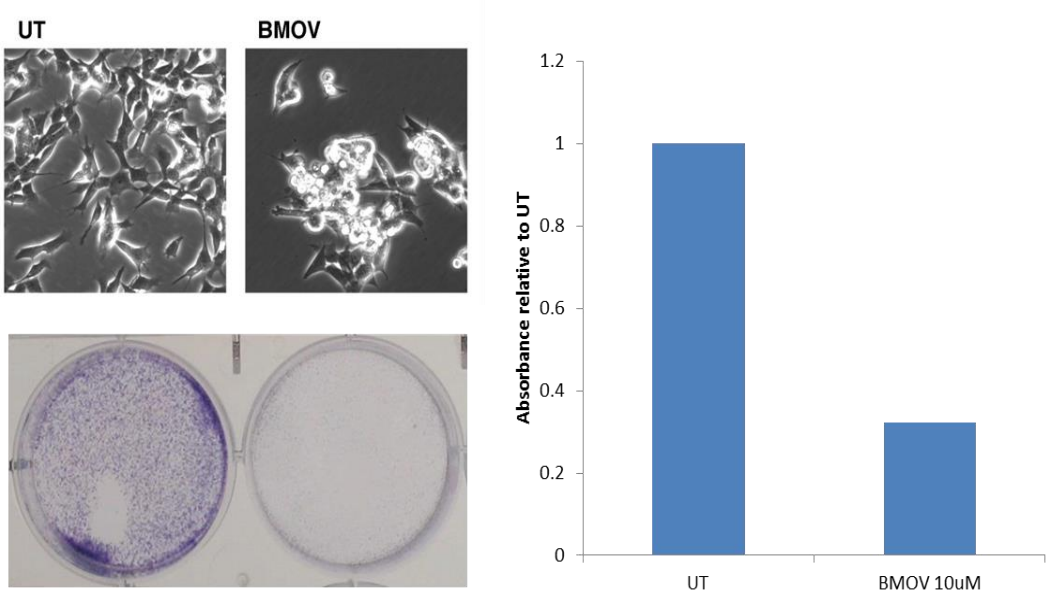

Figure A4 - Crystal violet staining and solubilisation can be used to quantify BMOV-induced cytotoxicity
IMR32 cells were treated with 10 μM BMOV for 3 days (left top). Cells were stained with crystal violet solution and images were taken (left bottom). Crystal violet was solubilised and absorbance at 595 nm was measured (right) (n=1).

Crystal violet staining and solubilisation was successfully used for a number of the experiments involving oxidovanadium treatment in this thesis. However, in later experiments a nuclei counting assay was also developed and used, as this was found to give the most reliable quantitation with less variability between repeat experiments. In this assay, Hoechst 33342 is used to stain the

nuclei of cells following chemical treatment. This allows visualisation of nuclei using fluorescence microscopy, as Hoechst 33342 emits blue fluorescent light when bound to DNA (Latt and Stetten, 1976). The number of nuclei can then be counted from representative images using automated counting on ImageJ, allowing relative cell numbers to be quantified. When compared to the resazurin assay, nuclei counting is more labour-intensive, but gives a more representative quantitation of BMOV-induced cytotoxicity in both IMR32 and KELLY cells (**Figure A5**). There are however still limitations with this technique. As with crystal violet staining, this method will detect dead cells if they are still adhered to tissue culture plastic. Therefore, it may partially underestimate BMOV-induced cytotoxicity. This was found to be particularly true for KELLY cells, which round up following BMOV treatment, but do not lose adhesion as readily as IMR32 cells. Although these cells are still viable at this point, they are clearly unhealthy, and previous experiments in the laboratory have shown that they eventually undergo apoptosis (Clark et al., 2015).

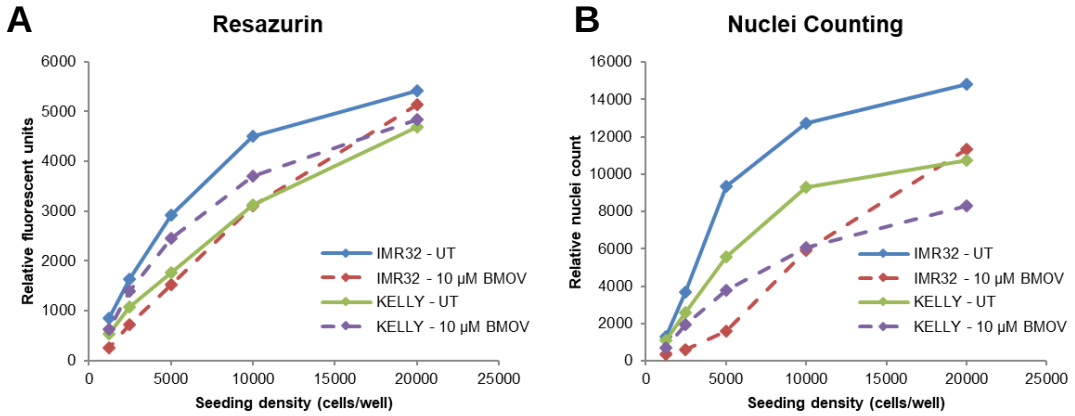

Figure A5 – Nuclei counting can be used to assess cell viability following BMOV treatment
*IMR32 and KELLY cells were seeded at a range of densities +/- 10 µM BMOV. Cell viability was measured after 3 days using resazurin **(A)** and the nuclei counting assay **(B)** (n=1).*

In conclusion, it is clear that routine cell viability assays are problematic when using oxidovanadium, probably due to their effects on cell metabolism (Gullapalli et al., 1989). In fact this may be of interest from a scientific standpoint as these effects may be relevant to the anti-cancer activities of vanadium-derived compounds. Based on the experiments described here, the most appropriate cell viability assays for use with oxidovanadium are crystal violet staining and nuclei counting.

Appendix 4 – Differentially expressed genes in BMOV-treated cells

Genes that were significantly differentially expressed in response to BMOV in IMR32, KELLY, SK-N-SH and LAN5 cells. Significant differential expression is defined as having a log2 fold change greater than 0.3 or less than -0.3, and an adjusted p value less than 0.05 (0.1 for SK-N-SH).

C2orf48	*DNHD1*	*LPCAT3*	*RUNDC3A*
C9orf172	*DPP7*	*LTBP2*	*SGSH*
CCDC28B	*DUOXA1*	*MROH6*	*SSU72*
CCDC33	*ECD*	*MUC20*	*TCTE1*
CDK12	*ECI1*	*MYH3*	*VPS51*
CLDN15	*EEF1A2*	*PPIL6*	*ZFAND2B*
CLIP3	*FPGS*	*PPP1R10*	
DCTN1	*GCAT*	*PTGES2*	
DGAT1	*ITFG2*	*ROGDI*	

Genes that were significantly differentially expressed in response to BMOV in IMR32, KELLY and LAN5, but not SK-N-SH cells. Significant differential expression is defined as having a log2 fold change greater than 0.3 or less than -0.3, and an adjusted p value less than 0.05 (0.1 for SK-N-SH).

AARS	*APOLD1*	*CASKIN1*	*CNRIP1*
ABCC10	*ASPRV1*	*CCDC9*	*COQ9*
AGBL5	*ATG2A*	*CD151*	*COX20*
ALDOC	*BCL7C*	*CDC42EP2*	*CPT2*
ALKBH7	*BRD9*	*CDKL3*	*CSTF3*
ANKRD39	*C1S*	*CEACAM19*	*CYB561A3*
AOC2	*C21orf58*	*CHMP2A*	*CYP27B1*
AOC3	*C8orf31*	*CINP*	*DALRD3*
APOE	*CAPN5*	*CISD3*	*DDB2*

DERA
DNAH1
DNLZ
DYRK1B
EML3
ENDOV
EVC
FAM163B
FAM173B
FLOT2
G6PC3
GAMT
GCDH
GGPS1
GGT1
GMIP
GMPPA
GOSR2
GUCA1B
HRSP12
IAH1
IL17RC
ISLR2
KPTN
KRCC1
LNP1
LRRC37A3
LRRC41
LRRC66
LTB4R
LYRM1
LYSMD1
MAP3K12
MAP4K2
MECR
MORN4
MPDU1
MRPL30
MYH15
MYRF
NCKIPSD
NDUFAF4
NEU3
NME3
NT5M
NTRK1
OPN3
P4HTM
PBXIP1
PCF11
PCGF1
PEX6
PFKL
PMAIP1
POU6F1
PROSC
RABEP2
RABL2A
RBFA
RHBDF2
RNF31
SAMD14
SARS2
SEPW1
SHISA4
SIPA1
SLC2A4RG
SLC6A2
SLIT3
SNX21
SPATA2L
SPIB
SUMF2
SYN2
SYNPO
TANGO6
TCEA2
TDRKH
TERF2
TLCD1
TLX2
TMEM5
TOP1MT
TSPAN11
TTLL1
TUBGCP6
TXNIP
UBL7
USP4
VAT1
VEZF1
VIPAS39
WBP1L
WDR78
XRCC1
YPEL3
ZNF226
ZNF251
ZNF425
ZNF606
ZNF862

Appendix 5 – Hydrophobic oxidovanadium microscopy

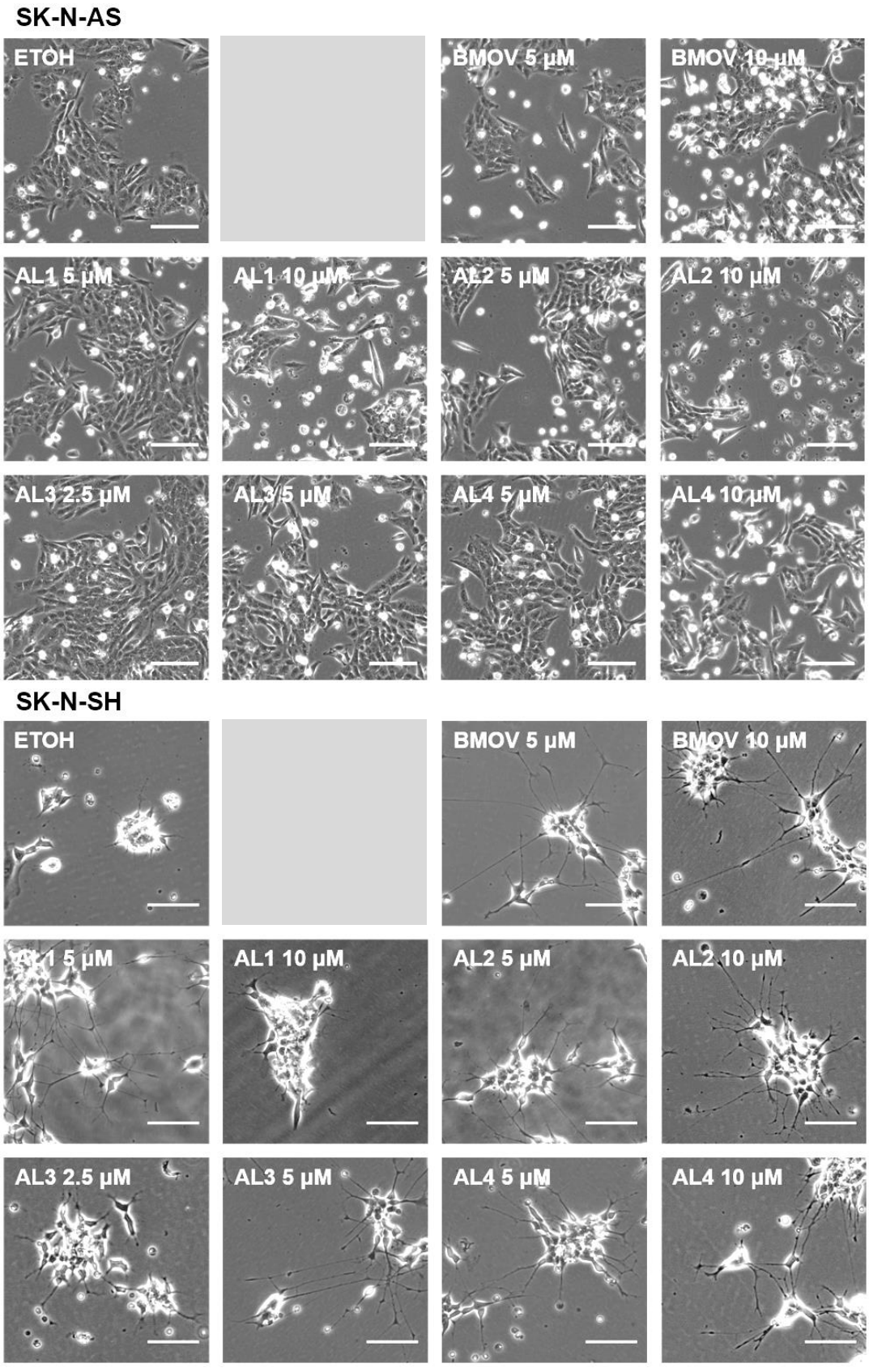

MEF

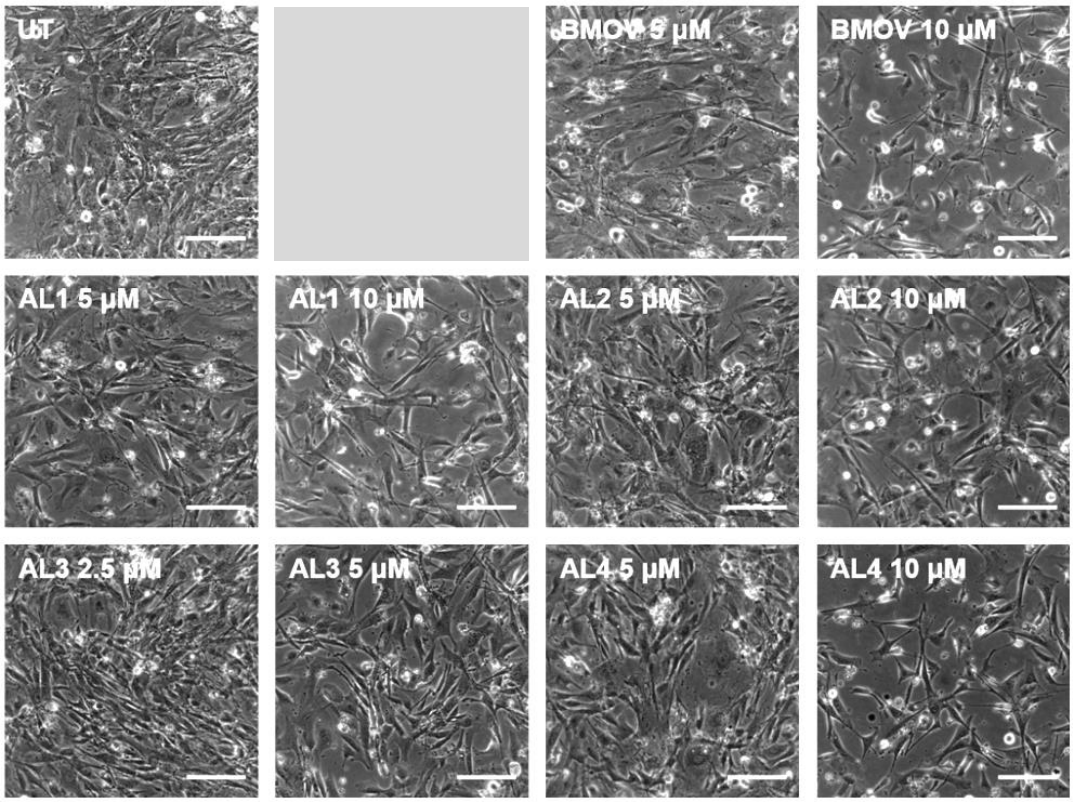
UT
BMOV 5 µM
BMOV 10 µM
AL1 5 µM
AL1 10 µM
AL2 5 µM
AL2 10 µM
AL3 2.5 µM
AL3 5 µM
AL4 5 µM
AL4 10 µM

HEK-293T

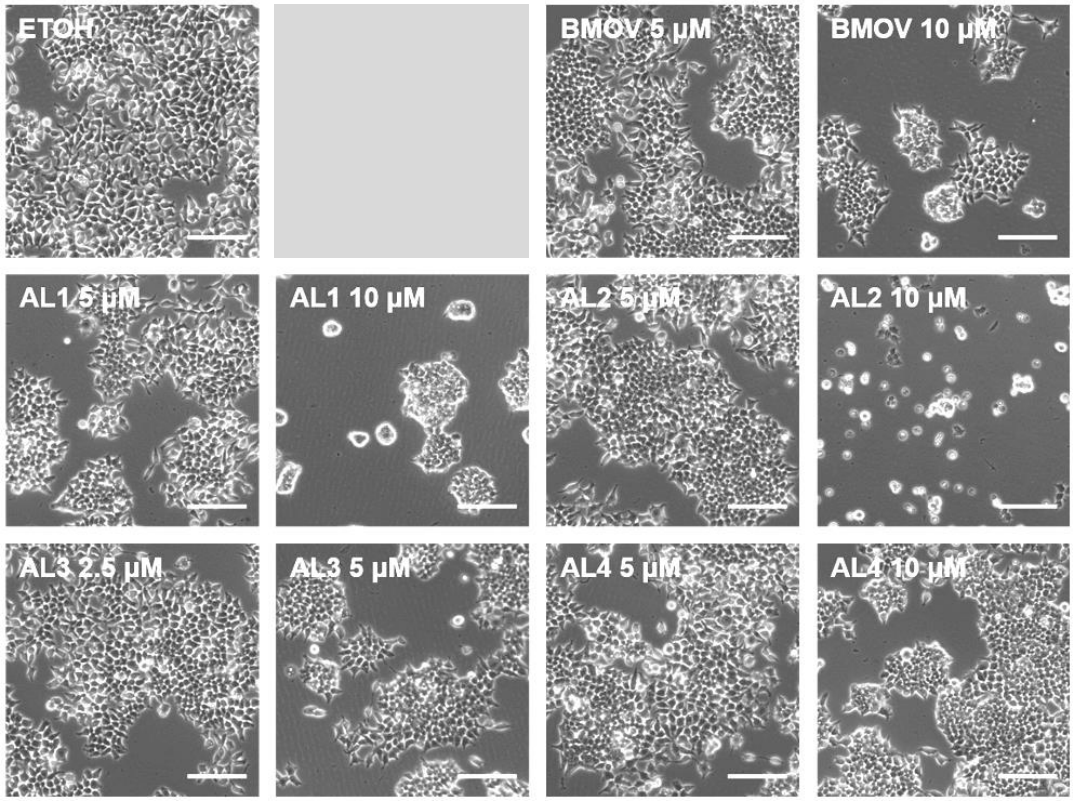
ETOH
BMOV 5 µM
BMOV 10 µM
AL1 5 µM
AL1 10 µM
AL2 5 µM
AL2 10 µM
AL3 2.5 µM
AL3 5 µM
AL4 5 µM
AL4 10 µM

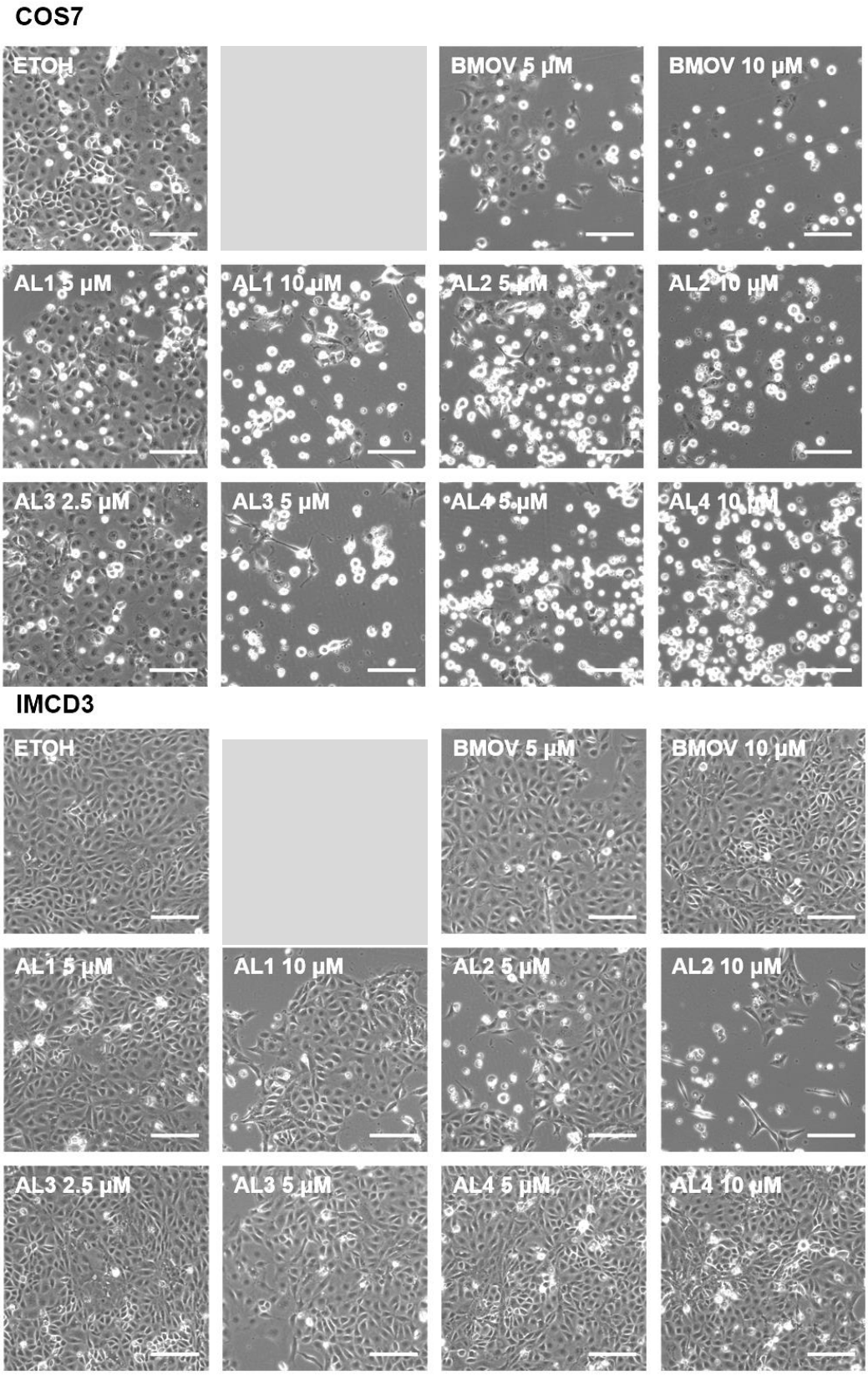

Figure A6 - Oxidovanadium cytotoxicity in neuroblastoma and non-neuroblastoma cells *SK-N-AS, SK-N-SH, MEF, HEK-293T, COS7 and IMCD3 cells treated with 5 µM and 10 µM BMOV, AL1, AL2 and AL4, and 2.5 µM and 5 µM AL3 for 3 days. Scale bar = 150 µm. (5 days treatment and 100 µm scale bar for SK-N-SH cells). Note: At this stage of my project I did not have a reliable assay to quantitatively assess cell viability following oxidovanadium treatment (discussed in* ***Appendix 3****). Therefore, I qualitatively summarised relative cell viability effects, shown in* ***Figure 5.8****.*

References

ADHIKARY, S. & EILERS, M. 2005. Transcriptional regulation and transformation by Myc proteins. *Nat Rev Mol Cell Biol,* 6**,** 635-45.

AJEAWUNG, N. F., FAURE, R., JONES, C. & KAMNASARAN, D. 2013. Preclinical evaluation of dipotassium bisperoxo (picolinato) oxovanadate V for the treatment of pediatric low-grade gliomas. *Future Oncol,* 9**,** 1215-29.

ALHO, I., COSTA, L., BICHO, M. & COELHO, C. 2013. The role of low-molecular-weight protein tyrosine phosphatase (LMW-PTP ACP1) in oncogenesis. *Tumour Biol,* 34**,** 1979-89.

ALONSO, A., NUNES-XAVIER, C. E., BAYÓN, Y. & PULIDO, R. 2016. The Extended Family of Protein Tyrosine Phosphatases. *Methods Mol Biol,* 1447**,** 1-23.

ALONSO, A., SASIN, J., BOTTINI, N., FRIEDBERG, I., OSTERMAN, A., GODZIK, A., HUNTER, T., DIXON, J. & MUSTELIN, T. 2004. Protein tyrosine phosphatases in the human genome. *Cell,* 117**,** 699-711.

ANDERS, S., PYL, P. T. & HUBER, W. 2015. HTSeq--a Python framework to work with high-throughput sequencing data. *Bioinformatics,* 31**,** 166-9.

ANDERSON, C. P. & REYNOLDS, C. P. 2002. Synergistic cytotoxicity of buthionine sulfoximine (BSO) and intensive melphalan (L-PAM) for neuroblastoma cell lines established at relapse after myeloablative therapy. *Bone Marrow Transplant,* 30**,** 135-40.

ANDERSON, C. P., SEEGER, R. C., SATAKE, N., MONFORTE-MUNOZ, H. L., KESHELAVA, N., BAILEY, H. H. & REYNOLDS, C. P. 2001. Buthionine sulfoximine and myeloablative concentrations of melphalan overcome resistance in a melphalan-resistant neuroblastoma cell line. *J Pediatr Hematol Oncol,* 23**,** 500-5.

ANDERSON, C. P., TSAI, J., CHAN, W., PARK, C. K., TIAN, L., LUI, R. M., FORMAN, H. J. & REYNOLDS, C. P. 1997. Buthionine sulphoximine alone and in combination with melphalan (L-PAM) is highly cytotoxic for human neuroblastoma cell lines. *Eur J Cancer,* 33**,** 2016-9.

ATTIYEH, E. F., LONDON, W. B., MOSSÉ, Y. P., WANG, Q., WINTER, C., KHAZI, D., MCGRADY, P. W., SEEGER, R. C., LOOK, A. T., SHIMADA, H., BRODEUR, G. M., COHN, S. L., MATTHAY, K. K., MARIS, J. M. & GROUP, C. S. O. 2005. Chromosome 1p and 11q deletions and outcome in neuroblastoma. *N Engl J Med,* 353**,** 2243-53.

AURELIANO, M. 2016. Decavanadate Toxicology and Pharmacological Activities: V10 or V1, Both or None? *Oxid Med Cell Longev,* 2016**,** 6103457.

AURELIANO, M. & CRANS, D. C. 2009. Decavanadate (V10 O28 6-) and oxovanadates: oxometalates with many biological activities. *J Inorg Biochem,* 103**,** 536-46.

AURELIANO, M. & GANDARA, R. M. 2005. Decavanadate effects in biological systems. *J Inorg Biochem,* 99**,** 979-85.

AURELIANO, M. & OHLIN, C. A. 2014. Decavanadate in vitro and in vivo effects: facts and opinions. *J Inorg Biochem,* 137**,** 123-30.

AYLON, Y. & OREN, M. 2016. The Hippo pathway, p53 and cholesterol. *Cell Cycle,* 15**,** 2248-55.

BAE, Y. H. & PARK, K. 2011. Targeted drug delivery to tumors: myths, reality and possibility. *J Control Release,* 153**,** 198-205.

BAILEY, H. H., MULCAHY, R. T., TUTSCH, K. D., ARZOOMANIAN, R. Z., ALBERTI, D., TOMBES, M. B., WILDING, G., POMPLUN, M. & SPRIGGS, D. R. 1994. Phase I clinical trial of intravenous L-buthionine sulfoximine and melphalan: an attempt at modulation of glutathione. *J Clin Oncol,* 12**,** 194-205.

BANTING, F. G., BEST, C. H., COLLIP, J. B., CAMPBELL, W. R. & FLETCHER, A. A. 1922. Pancreatic Extracts in the Treatment of Diabetes Mellitus. *Can Med Assoc J,* 12**,** 141-6.

BARFORD, D. 2004. The role of cysteine residues as redox-sensitive regulatory switches. *Curr Opin Struct Biol,* 14**,** 679-86.

BARFORD, D., DAS, A. K. & EGLOFF, M. P. 1998. The structure and mechanism of protein phosphatases: insights into catalysis and regulation. Annu Rev Biophys Biomol Struct, 27, 133-64.

BARONE, G., ANDERSON, J., PEARSON, A. D., PETRIE, K. & CHESLER, L. 2013. New strategies in neuroblastoma: Therapeutic targeting of MYCN and ALK. *Clin Cancer Res,* 19**,** 5814-21.

BAROUCH-BENTOV, R. & SAUER, K. 2011. Mechanisms of drug resistance in kinases. *Expert Opin Investig Drugs,* 20**,** 153-208.

BARRETINA, J., CAPONIGRO, G., STRANSKY, N., VENKATESAN, K., MARGOLIN, A. A., KIM, S., WILSON, C. J., LEHÁR, J., KRYUKOV, G. V., SONKIN, D., REDDY, A., LIU, M., MURRAY, L., BERGER, M. F., MONAHAN, J. E., MORAIS, P., MELTZER, J., KOREJWA, A., JANÉ-VALBUENA, J., MAPA, F. A., THIBAULT, J., BRIC-FURLONG, E., RAMAN, P., SHIPWAY, A., ENGELS, I. H., CHENG, J., YU, G. K., YU, J., ASPESI, P. JR., DE SILVA, M., JAGTAP, K., JONES, M. D., WANG, L., HATTON, C., PALESCANDOLO, E., GUPTA, S., MAHAN, S., SOUGNEZ, C., ONOFRIO, R. C., LIEFELD, T., MACCONAILL, L., WINCKLER, W., REICH, M., LI, N., MESIROV, J. P., GABRIEL, S. B., GETZ, G., ARDLIE, K., CHAN, V., MYER, V. E., WEBER, B. L., PORTER, J., WARMUTH, M., FINAN, P., HARRIS, J. L., MEYERSON, M., GOLUB, T. R., MORRISSEY, M. P., SELLERS, W. R., SCHLEGEL, R. & GARRAWAY, L. A. 2012. The Cancer Cell Line Encyclopedia enables predictive modelling of anticancer drug sensitivity. *Nature,* 483**,** 603-7.

BARRIO, D. A. & ETCHEVERRY, S. B. 2010. Potential use of vanadium compounds in therapeutics. *Curr Med Chem,* 17**,** 3632-42.

BASSERMANN, F., FRESCAS, D., GUARDAVACCARO, D., BUSINO, L., PESCHIAROLI, A. & PAGANO, M. 2008. The Cdc14B-Cdh1-Plk1 axis controls the G2 DNA-damage-response checkpoint. *Cell,* 134**,** 256-67.

BAUDINO, T. A. 2015. Targeted Cancer Therapy: The Next Generation of Cancer Treatment. *Curr Drug Discov Technol,* 12**,** 3-20.

BAYLISS, R., BURGESS, S. G., LEEN, E. & RICHARDS, M. W. 2017. A moving target: structure and disorder in pursuit of Myc inhibitors. *Biochem Soc Trans,* 45**,** 709-717.

BAZAK, R., HOURI, M., EL ACHY, S., KAMEL, S. & REFAAT, T. 2015. Cancer active targeting by nanoparticles: a comprehensive review of literature. *J Cancer Res Clin Oncol,* 141**,** 769-84.

BEAVO, J. A., HARDMAN, J. G. & SUTHERLAND, E. W. 1971. Stimulation of adenosine 3',5'-monophosphate hydrolysis by guanosine 3',5'-monophosphate. *J Biol Chem,* 246**,** 3841-6.

BELL, D. & MCDERMOTT, B. J. 1994. Use of the cyclic AMP antagonist, Rp-cAMPS, to distinguish between cyclic AMP-dependent and cyclic AMP-independent contractile responses in rat ventricular cardiomyocytes. *J Mol Cell Cardiol,* 26**,** 1439-48.

BELL, E., PREMKUMAR, R., CARR, J., LU, X., LOVAT, P. E., KEES, U. R., LUNEC, J. & TWEDDLE, D. A. 2006. The role of MYCN in the failure of MYCN amplified neuroblastoma cell lines to G1 arrest after DNA damage. *Cell Cycle,* 5**,** 2639-47.

BENTIRES-ALJ, M. & NEEL, B. G. 2007. Protein-tyrosine phosphatase 1B is required for HER2/Neu-induced breast cancer. *Cancer Res,* 67**,** 2420-4.

BENTIRES-ALJ, M., PAEZ, J. G., DAVID, F. S., KEILHACK, H., HALMOS, B., NAOKI, K., MARIS, J. M., RICHARDSON, A., BARDELLI, A., SUGARBAKER, D. J., RICHARDS, W. G., DU, J., GIRARD, L., MINNA, J. D., LOH, M. L., FISHER, D. E., VELCULESCU, V. E., VOGELSTEIN, B., MEYERSON, M., SELLERS, W. R. & NEEL, B. G. 2004. Activating mutations of the noonan syndrome-associated SHP2/PTPN11 gene in human solid tumors and adult acute myelogenous leukemia. *Cancer Res,* 64**,** 8816-20.

BERDOUGO, E., NACHURY, M. V., JACKSON, P. K. & JALLEPALLI, P. V. 2008. The nucleolar phosphatase Cdc14B is dispensable for chromosome segregation and mitotic exit in human cells. *Cell Cycle,* 7**,** 1184-90.

BERGER, N., SACHSE, A., BENDER, J., SCHUBERT, R. & BRANDL, M. 2001. Filter extrusion of liposomes using different devices: comparison of liposome size, encapsulation efficiency, and process characteristics. *Int J Pharm,* 223**,** 55-68.

BERNARD, J. J., LOU, Y. R., PENG, Q. Y., LI, T. & LU, Y. P. 2014. PDE2 is a novel target for attenuating tumor formation in a mouse model of UVB-induced skin carcinogenesis. *PLoS One,* 9**,** e109862.

BESSETTE, D. C., QIU, D. & PALLEN, C. J. 2008. PRL PTPs: mediators and markers of cancer progression. *Cancer Metastasis Rev,* 27**,** 231-52.

BEVAN, A., DRAKE, P., YALE, J., SHAVER, A. & POSNER, B. 1995. Peroxovanadium compounds: Biological actions and mechanism of insulin-mimesis. *Molecular and Cellular Biochemistry,* 153**,** 49-58.

BHULLAR, K. S., LAGARÓN, N. O., MCGOWAN, E. M., PARMAR, I., JHA, A., HUBBARD, B. P. & RUPASINGHE, H. P. V. 2018. Kinase-targeted cancer therapies: progress, challenges and future directions. *Mol Cancer,* 17**,** 48.

BIEL, M. 2009. Cyclic nucleotide-regulated cation channels. *J Biol Chem,* 284**,** 9017-21.

BIRNBOIM, H. C. 1983. A rapid alkaline extraction method for the isolation of plasmid DNA. *Methods Enzymol,* 100**,** 243-55.

BIRNBOIM, H. C. & DOLY, J. 1979. A rapid alkaline extraction procedure for screening recombinant plasmid DNA. *Nucleic Acids Res,* 7**,** 1513-23.
BISHAYEE, A., OINAM, S., BASU, M. & CHATTERJEE, M. 2000. Vanadium chemoprevention of 7,12-dimethylbenz(a)anthracene-induced rat mammary carcinogenesis: probable involvement of representative hepatic phase I and II xenobiotic metabolizing enzymes. *Breast Cancer Res Treat,* 63**,** 133-45.
BISHAYEE, A., ROY, S. & CHATTERJEE, M. 1999. Characterization of selective induction and alteration of xenobiotic biotransforming enzymes by vanadium during diethylnitrosamine-induced chemical rat liver carcinogenesis. *Oncol Res,* 11**,** 41-53.
BISHAYEE, A., WAGHRAY, A., PATEL, M. A. & CHATTERJEE, M. 2010. Vanadium in the detection, prevention and treatment of cancer: the in vivo evidence. *Cancer Lett,* 294**,** 1-12.
BLANC, E., GOLDSCHNEIDER, D., DOUC-RASY, S., BÉNARD, J. & RAGUÉNEZ, G. 2005. Wnt-5a gene expression in malignant human neuroblasts. *Cancer Lett,* 228**,** 117-23.
BLONDEL, O., BAILBE, D. & PORTHA, B. 1989. In vivo insulin resistance in streptozotocin-diabetic rats--evidence for reversal following oral vanadate treatment. *Diabetologia,* 32**,** 185-90.
BLUME-JENSEN, P. & HUNTER, T. 2001. Oncogenic kinase signalling. *Nature,* 411**,** 355-65.
BODEN, G., CHEN, X., RUIZ, J., VAN ROSSUM, G. D. & TURCO, S. 1996. Effects of vanadyl sulfate on carbohydrate and lipid metabolism in patients with non-insulin-dependent diabetes mellitus. *Metabolism,* 45**,** 1130-5.
BOLLAG, G., HIRTH, P., TSAI, J., ZHANG, J., IBRAHIM, P. N., CHO, H., SPEVAK, W., ZHANG, C., ZHANG, Y., HABETS, G., BURTON, E. A., WONG, B., TSANG, G., WEST, B. L., POWELL, B., SHELLOOE, R., MARIMUTHU, A., NGUYEN, H., ZHANG, K. Y., ARTIS, D. R., SCHLESSINGER, J., SU, F., HIGGINS, B., IYER, R., D'ANDREA, K., KOEHLER, A., STUMM, M., LIN, P. S., LEE, R. J., GRIPPO, J., PUZANOV, I., KIM, K. B., RIBAS, A., MCARTHUR, G. A., SOSMAN, J. A., CHAPMAN, P. B., FLAHERTY, K. T., XU, X., NATHANSON, K. L. & NOLOP, K. 2010. Clinical efficacy of a RAF inhibitor needs broad target blockade in BRAF-mutant melanoma. *Nature,* 467**,** 596-9.
BOLLU, L. R., MAZUMDAR, A., SAVAGE, M. I. & BROWN, P. H. 2017. Molecular Pathways: Targeting Protein Tyrosine Phosphatases in Cancer. *Clin Cancer Res*.
BOUTROS, R., LOBJOIS, V. & DUCOMMUN, B. 2007. CDC25 phosphatases in cancer cells: key players? Good targets? *Nat Rev Cancer,* 7**,** 495-507.
BRANDÃO, T. A., HENGGE, A. C. & JOHNSON, S. J. 2010. Insights into the reaction of protein-tyrosine phosphatase 1B: crystal structures for transition state analogs of both catalytic steps. *J Biol Chem,* 285**,** 15874-83.
BRAUNE, E. B. & LENDAHL, U. 2016. Notch -- a goldilocks signaling pathway in disease and cancer therapy. *Discov Med,* 21**,** 189-96.
BRESLER, S. C., WOOD, A. C., HAGLUND, E. A., COURTRIGHT, J., BELCASTRO, L. T., PLEGARIA, J. S., COLE, K., TOPOROVSKAYA, Y., ZHAO, H., CARPENTER, E. L., CHRISTENSEN, J. G., MARIS, J. M., LEMMON, M. A. & MOSSÉ, Y. P. 2011. Differential inhibitor sensitivity of anaplastic lymphoma kinase variants found in neuroblastoma. *Sci Transl Med,* 3**,** 108ra114.
BRICHARD, S. M. 1995. Effects of vanadate on the expression of genes involved in fuel homeostasis in animal models of Type I and Type II diabetes. *Mol Cell Biochem,* 153**,** 121-4.
BRODEUR, G. & BAGATELL, R. 2014. Mechanisms of neuroblastoma regression. *Nature Reviews Clinical Oncology,* 11**,** 704-713.
BRODEUR, G. M. 2003. Neuroblastoma: biological insights into a clinical enigma. *Nat Rev Cancer,* 3**,** 203-16.
BRODEUR, G. M., PRITCHARD, J., BERTHOLD, F., CARLSEN, N. L., CASTEL, V., CASTELBERRY, R. P., DE BERNARDI, B., EVANS, A. E., FAVROT, M. & HEDBORG, F. 1993. Revisions of the international criteria for neuroblastoma diagnosis, staging, and response to treatment. *J Clin Oncol,* 11**,** 1466-77.
BRODEUR, G. M., SEEGER, R. C., BARRETT, A., BERTHOLD, F., CASTLEBERRY, R. P., D'ANGIO, G., DE BERNARDI, B., EVANS, A. E., FAVROT, M. & FREEMAN, A. I. 1988. International criteria for diagnosis, staging, and response to treatment in patients with neuroblastoma. *J Clin Oncol,* 6**,** 1874-81.

BRODEUR, G. M., SEEGER, R. C., SCHWAB, M., VARMUS, H. E. & BISHOP, J. M. 1984. Amplification of N-myc in untreated human neuroblastomas correlates with advanced disease stage. *Science,* 224**,** 1121-4.

BRONNER, M. 2012. Formation and migration of neural crest cells in the vertebrate embryo. *Histochemistry and Cell Biology,* 138**,** 179-186.

BURDYGA, A., CONANT, A., HAYNES, L., ZHANG, J., JALINK, K., SUTTON, R., NEOPTOLEMOS, J., COSTELLO, E. & TEPIKIN, A. 2013. cAMP inhibits migration, ruffling and paxillin accumulation in focal adhesions of pancreatic ductal adenocarcinoma cells: effects of PKA and EPAC. *Biochim Biophys Acta,* 1833**,** 2664-2672.

CAGNOL, S. & CHAMBARD, J. C. 2010. ERK and cell death: mechanisms of ERK-induced cell death--apoptosis, autophagy and senescence. *FEBS J,* 277**,** 2-21.

CALERO, O., BULLIDO, M. J., CLARIMÓN, J., HORTIGÜELA, R., FRANK-GARCÍA, A., MARTÍNEZ-MARTÍN, P., LLEÓ, A., REY, M. J., SASTRE, I., RÁBANO, A., DE PEDRO-CUESTA, J., FERRER, I. & CALERO, M. 2012. Genetic variability of the gene cluster CALHM 1-3 in sporadic Creutzfeldt-Jakob disease. *Prion,* 6**,** 407-12.

CAMPBELL, A. M. & ZHANG, Z. Y. 2014. Phosphatase of regenerating liver: a novel target for cancer therapy. *Expert Opin Ther Targets,* 18**,** 555-69.

CANTLEY, L. C., JOSEPHSON, L., WARNER, R., YANAGISAWA, M., LECHENE, C. & GUIDOTTI, G. 1977. Vanadate is a potent (Na,K)-ATPase inhibitor found in ATP derived from muscle. *J Biol Chem,* 252**,** 7421-3.

CARAVAN, P., GELMINI, L., GLOVER, N., HERRING, F., LI, H., MCNEILL, J., RETTIG, S., SETYAWATI, I., SHUTER, E., SUN, Y., TRACEY, A., YUEN, V. & ORVIG, C. 1995. Reaction chemistry of BMOV, bis(maltolato)oxovanadium(IV) - A potent insulin mimetic agent. *Journal of the American Chemical Society,* 117**,** 12759-12770.

CARETTA, A. & MUCIGNAT-CARETTA, C. 2011. Protein kinase a in cancer. *Cancers (Basel),* 3**,** 913-26.

CARR-WILKINSON, J., O'TOOLE, K., WOOD, K. M., CHALLEN, C. C., BAKER, A. G., BOARD, J. R., EVANS, L., COLE, M., CHEUNG, N. K., BOOS, J., KÖHLER, G., LEUSCHNER, I., PEARSON, A. D., LUNEC, J. & TWEDDLE, D. A. 2010. High Frequency of p53/MDM2/p14ARF Pathway Abnormalities in Relapsed Neuroblastoma. *Clin Cancer Res,* 16**,** 1108-18.

CARR, J., BELL, E., PEARSON, A. D., KEES, U. R., BERIS, H., LUNEC, J. & TWEDDLE, D. A. 2006. Increased frequency of aberrations in the p53/MDM2/p14(ARF) pathway in neuroblastoma cell lines established at relapse. *Cancer Res,* 66**,** 2138-45.

CERAMI, E., GAO, J., DOGRUSOZ, U., GROSS, B. E., SUMER, S. O., AKSOY, B. A., JACOBSEN, A., BYRNE, C. J., HEUER, M. L., LARSSON, E., ANTIPIN, Y., REVA, B., GOLDBERG, A. P., SANDER, C. & SCHULTZ, N. 2012. The cBio cancer genomics portal: an open platform for exploring multidimensional cancer genomics data. *Cancer Discov,* 2**,** 401-4.

CHAKRABORTY, T., CHATTERJEE, A., DHACHINAMOORTHI, D., SRIVASTAWA, S., PANAYAPPAN, L. & CHATTERJEE, M. 2006a. Vanadium limits the expression of proliferating cell nuclear antigen and inhibits early DNA damage during diethylnitrosamine-induced hepatocellular preneoplasia in rats. *Environ Mol Mutagen,* 47**,** 603-15.

CHAKRABORTY, T., CHATTERJEE, A., RANA, A., DHACHINAMOORTHI, D., KUMAR P, A. & CHATTERJEE, M. 2007a. Carcinogen-induced early molecular events and its implication in the initiation of chemical hepatocarcinogenesis in rats: chemopreventive role of vanadium on this process. *Biochim Biophys Acta,* 1772**,** 48-59.

CHAKRABORTY, T., CHATTERJEE, A., RANA, A., RANA, B., PALANISAMY, A., MADHAPPAN, R. & CHATTERJEE, M. 2007b. Suppression of early stages of neoplastic transformation in a two-stage chemical hepatocarcinogenesis model: supplementation of vanadium, a dietary micronutrient, limits cell proliferation and inhibits the formations of 8-hydroxy-2'-deoxyguanosines and DNA strand-breaks in the liver of sprague-dawley rats. *Nutr Cancer,* 59**,** 228-47.

CHAKRABORTY, T., CHATTERJEE, A., SARALAYA, M. G. & CHATTERJEE, M. 2006b. Chemopreventive effect of vanadium in a rodent model of chemical hepatocarcinogenesis: reflections in oxidative DNA damage, energy-dispersive X-ray fluorescence profile and metallothionein expression. *J Biol Inorg Chem,* 11**,** 855-66.

CHAKRABORTY, T., GHOSH, S., DATTA, S., CHAKRABORTY, P. & CHATTERJEE, M. 2003. Vanadium suppresses sister-chromatid exchange and DNA-protein crosslink formation and restores antioxidant status and hepatocellular architecture during 2-

acetylaminofluorene-induced experimental rat hepatocarcinogenesis. *J Exp Ther Oncol,* 3**,** 346-62.
CHAKRABORTY, T., PANDEY, N., CHATTERJEE, A., GHOSH, B., RANA, B. & CHATTERJEE, M. 2006c. Molecular basis of anticlastogenic potential of vanadium in vivo during the early stages of diethylnitrosamine-induced hepatocarcinogenesis in rats. *Mutat Res,* 609**,** 117-28.
CHAKRABORTY, T., SAMANTA, S., GHOSH, B., THIRUMOORTHY, N. & CHATTERJEE, M. 2005. Vanadium induces apoptosis and modulates the expressions of metallothionein, Ki-67 nuclear antigen, and p53 during 2-acetylaminofluorene-induced rat liver preneoplasia. *J Cell Biochem,* 94**,** 744-62.
CHAKRABORTY, T., SWAMY, A. H., CHATTERJEE, A., RANA, B., SHYAMSUNDAR, A. & CHATTERJEE, M. 2007c. Molecular basis of vanadium-mediated inhibition of hepatocellular preneoplasia during experimental hepatocarcinogenesis in rats. *J Cell Biochem,* 101**,** 244-58.
CHAN, G., KALAITZIDIS, D. & NEEL, B. G. 2008. The tyrosine phosphatase Shp2 (PTPN11) in cancer. *Cancer Metastasis Rev,* 27**,** 179-92.
CHAN, R. J. & FENG, G. S. 2007. PTPN11 is the first identified proto-oncogene that encodes a tyrosine phosphatase. *Blood,* 109**,** 862-7.
CHEN, J., MENG, Y., ZHOU, J., ZHUO, M., LING, F., ZHANG, Y., DU, H. & WANG, X. 2013. Identifying candidate genes for Type 2 Diabetes Mellitus and obesity through gene expression profiling in multiple tissues or cells. *J Diabetes Res,* 2013**,** 970435.
CHEN, T. C., HINTON, D. R., ZIDOVETZKI, R. & HOFMAN, F. M. 1998. Up-regulation of the cAMP/PKA pathway inhibits proliferation, induces differentiation, and leads to apoptosis in malignant gliomas. *Lab Invest,* 78**,** 165-74.
CHEN, T. C., WADSTEN, P., SU, S., RAWLINSON, N., HOFMAN, F. M., HILL, C. K. & SCHÖNTHAL, A. H. 2002. The type IV phosphodiesterase inhibitor rolipram induces expression of the cell cycle inhibitors p21(Cip1) and p27(Kip1), resulting in growth inhibition, increased differentiation, and subsequent apoptosis of malignant A-172 glioma cells. *Cancer Biol Ther,* 1**,** 268-76.
CHEN, Y., CHENG, L., DONG, Z., CHAO, Y., LEI, H., ZHAO, H., WANG, J. & LIU, Z. 2017. Degradable Vanadium Disulfide Nanostructures with Unique Optical and Magnetic Functions for Cancer Theranostics. *Angew Chem Int Ed Engl,* 56**,** 12991-12996.
CHEN, Y., TAKITA, J., CHOI, Y. L., KATO, M., OHIRA, M., SANADA, M., WANG, L., SODA, M., KIKUCHI, A., IGARASHI, T., NAKAGAWARA, A., HAYASHI, Y., MANO, H. & OGAWA, S. 2008. Oncogenic mutations of ALK kinase in neuroblastoma. *Nature,* 455**,** 971-4.
CHEN, Y. N., LAMARCHE, M. J., CHAN, H. M., FEKKES, P., GARCIA-FORTANET, J., ACKER, M. G., ANTONAKOS, B., CHEN, C. H., CHEN, Z., COOKE, V. G., DOBSON, J. R., DENG, Z., FEI, F., FIRESTONE, B., FODOR, M., FRIDRICH, C., GAO, H., GRUNENFELDER, D., HAO, H. X., JACOB, J., HO, S., HSIAO, K., KANG, Z. B., KARKI, R., KATO, M., LARROW, J., LA BONTE, L. R., LENOIR, F., LIU, G., LIU, S., MAJUMDAR, D., MEYER, M. J., PALERMO, M., PEREZ, L., PU, M., PRICE, E., QUINN, C., SHAKYA, S., SHULTZ, M. D., SLISZ, J., VENKATESAN, K., WANG, P., WARMUTH, M., WILLIAMS, S., YANG, G., YUAN, J., ZHANG, J. H., ZHU, P., RAMSEY, T., KEEN, N. J., SELLERS, W. R., STAMS, T. & FORTIN, P. D. 2016. Allosteric inhibition of SHP2 phosphatase inhibits cancers driven by receptor tyrosine kinases. *Nature,* 535**,** 148-52.
CHEUNG, N. K., ZHANG, J., LU, C., PARKER, M., BAHRAMI, A., TICKOO, S. K., HEGUY, A., PAPPO, A. S., FEDERICO, S., DALTON, J., CHEUNG, I. Y., DING, L., FULTON, R., WANG, J., CHEN, X., BECKSFORT, J., WU, J., BILLUPS, C. A., ELLISON, D., MARDIS, E. R., WILSON, R. K., DOWNING, J. R., DYER, M. A. & PROJECT, S. J. C. S. R. H. W. U. P. C. G. 2012. Association of age at diagnosis and genetic mutations in patients with neuroblastoma. *JAMA,* 307**,** 1062-71.
CHIARUGI, P., TADDEI, M. L., SCHIAVONE, N., PAPUCCI, L., GIANNONI, E., FIASCHI, T., CAPACCIOLI, S., RAUGEI, G. & RAMPONI, G. 2004. LMW-PTP is a positive regulator of tumor onset and growth. *Oncogene,* 23**,** 3905-14.
CHIESA, M., GUILLAMOT, M., BUENO, M. J. & MALUMBRES, M. 2011. The Cdc14B phosphatase displays oncogenic activity mediated by the Ras-Mek signaling pathway. *Cell Cycle,* 10**,** 1607-17.
CHUBAK, J., BOUDREAU, D. M., RULYAK, S. J. & MANDELSON, M. T. 2011. Colorectal cancer risk in relation to antidepressant medication use. *Int J Cancer,* 128**,** 227-32.

CLARK, O., DAGA, S. & STOKER, A. W. 2013. Tyrosine phosphatase inhibitors combined with retinoic acid can enhance differentiation of neuroblastoma cells and trigger ERK- and AKT-dependent, p53-independent senescence. *Cancer Lett,* 328**,** 44-54.

CLARK, O., PARK, I., DI FLORIO, A., CICHON, A. C., RUSTIN, S., JUGOV, R., MAESHIMA, R. & STOKER, A. W. 2015. Oxovanadium-based inhibitors can drive redox-sensitive cytotoxicity in neuroblastoma cells and synergise strongly with buthionine sulfoximine. *Cancer Lett,* 357**,** 316-27.

COHEN, J. N., YEH, I., JORDAN, R. C., WOLSKY, R. J., HORVAI, A. E., MCCALMONT, T. H. & LEBOIT, P. E. 2018. Cutaneous Non-Neural Granular Cell Tumors Harbor Recurrent ALK Gene Fusions. *Am J Surg Pathol,* 42**,** 1133-1142.

COHEN, N., HALBERSTAM, M., SHLIMOVICH, P., CHANG, C. J., SHAMOON, H. & ROSSETTI, L. 1995. Oral vanadyl sulfate improves hepatic and peripheral insulin sensitivity in patients with non-insulin-dependent diabetes mellitus. *J Clin Invest,* 95**,** 2501-9.

COHN, S., PEARSON, A., LONDON, W., MONCLAIR, T., AMBROS, P., BRODEUR, G., FALDUM, A., HERO, B., IEHARA, T., MACHIN, D., MOSSERI, V., SIMON, T., GARAVENTA, A., CASTEL, V. & MATTHAY, K. 2009. The International Neuroblastoma Risk Group (INRG) Classification System: An INRG Task Force Report. *Journal of Clinical Oncology,* 27**,** 289-297.

COHN, S. L. & TWEDDLE, D. A. 2004. MYCN amplification remains prognostically strong 20 years after its "clinical debut". *Eur J Cancer,* 40**,** 2639-42.

COLLAUTO, A., MISHRA, S., LITVINOV, A., MCHAOURAB, H. S. & GOLDFARB, D. 2017. Direct Spectroscopic Detection of ATP Turnover Reveals Mechanistic Divergence of ABC Exporters. *Structure,* 25**,** 1264-1274.e3.

CONNIOT, J., SILVA, J. M., FERNANDES, J. G., SILVA, L. C., GASPAR, R., BROCCHINI, S., FLORINDO, H. F. & BARATA, T. S. 2014. Cancer immunotherapy: nanodelivery approaches for immune cell targeting and tracking. *Front Chem,* 2**,** 105.

COYLE, B., KINSELLA, P., MCCANN, M., DEVEREUX, M., O'CONNOR, R., CLYNES, M. & KAVANAGH, K. 2004. Induction of apoptosis in yeast and mammalian cells by exposure to 1,10-phenanthroline metal complexes. *Toxicol In Vitro,* 18**,** 63-70.

CRANS, D. C. 2015. Antidiabetic, Chemical, and Physical Properties of Organic Vanadates as Presumed Transition-State Inhibitors for Phosphatases. *J Org Chem,* 80**,** 11899-915.

CRANS, D. C., SMEE, J. J., GAIDAMAUSKAS, E. & YANG, L. 2004. The chemistry and biochemistry of vanadium and the biological activities exerted by vanadium compounds. *Chem Rev,* 104**,** 849-902.

CRANS, D. C., YANG, L., HAASE, A. & YANG, X. 2018. Health Benefits of Vanadium and Its Potential as an Anticancer Agent. *Met Ions Life Sci,* 18.

CREE, I. A. & ANDREOTTI, P. E. 1997. Measurement of cytotoxicity by ATP-based luminescence assay in primary cell cultures and cell lines. *Toxicol In Vitro,* 11**,** 553-6.

CUSI, K., CUKIER, S., DEFRONZO, R. A., TORRES, M., PUCHULU, F. M. & REDONDO, J. C. 2001. Vanadyl sulfate improves hepatic and muscle insulin sensitivity in type 2 diabetes. *J Clin Endocrinol Metab,* 86**,** 1410-7.

D'CRUZ, O. J. & UCKUN, F. M. 2002. Metvan: a novel oxovanadium(IV) complex with broad spectrum anticancer activity. *Expert Opin Investig Drugs,* 11**,** 1829-36.

DA SILVA, J. S. & DOTTI, C. G. 2002. Breaking the neuronal sphere: regulation of the actin cytoskeleton in neuritogenesis. *Nat Rev Neurosci,* 3**,** 694-704.

DĄBROŚ, W., ADAMCZYK, A., CIURKOT, K. & KORDOWIAK, A. M. 2011. Vanadium compounds affect growth and morphology of human rhabdomyosarcoma cell line. *Pol J Pathol,* 62**,** 262-8.

DAHL, S. G., SYLTE, I. & RAVNA, A. W. 2004. Structures and models of transporter proteins. *J Pharmacol Exp Ther,* 309**,** 853-60.

DAI, Z., SHERIDAN, J. M., GEARING, L. J., MOORE, D. L., SU, S., WORMALD, S., WILCOX, S., O'CONNOR, L., DICKINS, R. A., BLEWITT, M. E. & RITCHIE, M. E. 2014. edgeR: a versatile tool for the analysis of shRNA-seq and CRISPR-Cas9 genetic screens. *F1000Res,* 3**,** 95.

DANIEL, P. M., FILIZ, G. & MANTAMADIOTIS, T. 2016. Sensitivity of GBM cells to cAMP agonist-mediated apoptosis correlates with CD44 expression and agonist resistance with MAPK signaling. *Cell Death Dis,* 7**,** e2494.

DASSONVILLE, O., BOZEC, A., FISCHEL, J. L. & MILANO, G. 2007. EGFR targeting therapies: monoclonal antibodies versus tyrosine kinase inhibitors. Similarities and differences. *Crit Rev Oncol Hematol,* 62**,** 53-61.

DATLER, C. & GRIMM, S. 2013. Reconstitution of CKMT1 expression fails to rescue cells from mitochondrial membrane potential dissipation: implications for controlling RNAi experiments. *Biochim Biophys Acta,* 1833**,** 2844-2855.

DE, A. 2011. Wnt/Ca2+ signaling pathway: a brief overview. *Acta Biochim Biophys Sin (Shanghai),* 43**,** 745-56.

DE BROUWER, S., DE PRETER, K., KUMPS, C., ZABROCKI, P., PORCU, M., WESTERHOUT, E. M., LAKEMAN, A., VANDESOMPELE, J., HOEBEECK, J., VAN MAERKEN, T., DE PAEPE, A., LAUREYS, G., SCHULTE, J. H., SCHRAMM, A., VAN DEN BROECKE, C., VERMEULEN, J., VAN ROY, N., BEISKE, K., RENARD, M., NOGUERA, R., DELATTRE, O., JANOUEIX-LEROSEY, I., KOGNER, P., MARTINSSON, T., NAKAGAWARA, A., OHIRA, M., CARON, H., EGGERT, A., COOLS, J., VERSTEEG, R. & SPELEMAN, F. 2010. Meta-analysis of neuroblastomas reveals a skewed ALK mutation spectrum in tumors with MYCN amplification. *Clin Cancer Res,* 16**,** 4353-62.

DE ROOIJ, J., ZWARTKRUIS, F. J., VERHEIJEN, M. H., COOL, R. H., NIJMAN, S. M., WITTINGHOFER, A. & BOS, J. L. 1998. Epac is a Rap1 guanine-nucleotide-exchange factor directly activated by cyclic AMP. *Nature,* 396**,** 474-7.

DE THÉ, H. 2018. Differentiation therapy revisited. *Nat Rev Cancer,* 18**,** 117-127.

DELPLANQUE, J., DEVOS, D., HUIN, V., GENET, A., SAND, O., MOREAU, C., GOIZET, C., CHARLES, P., ANHEIM, M., MONIN, M. L., BUÉE, L., DESTÉE, A., GROLEZ, G., DELMAIRE, C., DUJARDIN, K., DELLACHERIE, D., BRICE, A., STEVANIN, G., STRUBI-VUILLAUME, I., DÜRR, A. & SABLONNIÈRE, B. 2014. TMEM240 mutations cause spinocerebellar ataxia 21 with mental retardation and severe cognitive impairment. *Brain,* 137**,** 2657-63.

DEN HERTOG, J., GROEN, A. & VAN DER WIJK, T. 2005. Redox regulation of protein-tyrosine phosphatases. *Arch Biochem Biophys,* 434**,** 11-5.

DI PAOLO, D., BRIGNOLE, C., PASTORINO, F., CAROSIO, R., ZORZOLI, A., ROSSI, M., LOI, M., PAGNAN, G., EMIONITE, L., CILLI, M., BRUNO, S., CHIARLE, R., ALLEN, T. M., PONZONI, M. & PERRI, P. 2011. Neuroblastoma-targeted nanoparticles entrapping siRNA specifically knockdown ALK. *Mol Ther,* 19**,** 1131-40.

DOMINGO, J. L. 2000. Vanadium and diabetes. What about vanadium toxicity? *Mol Cell Biochem,* 203**,** 185-7.

DOMINGO, J. L. & GÓMEZ, M. 2016. Vanadium compounds for the treatment of human diabetes mellitus: A scientific curiosity? A review of thirty years of research. *Food Chem Toxicol,* 95**,** 137-41.

DONG, H., CLAFFEY, K. P., BROCKE, S. & EPSTEIN, P. M. 2015. Inhibition of breast cancer cell migration by activation of cAMP signaling. *Breast Cancer Res Treat,* 152**,** 17-28.

DONG, Y., NARLA, R. K., SUDBECK, E. & UCKUN, F. M. 2000. Synthesis, X-ray structure, and anti-leukemic activity of oxovanadium(IV) complexes. *J Inorg Biochem,* 78**,** 321-30.

DU, Y. & GRANDIS, J. R. 2015. Receptor-type protein tyrosine phosphatases in cancer. *Chin J Cancer,* 34**,** 61-9.

DUBOIS, S., KALIKA, Y., LUKENS, J., BRODEUR, G., SEEGER, R., ATKINSON, J., HAASE, G., BLACK, C., PEREZ, C., SHIMADA, H., GERBING, R., STRAM, D. & MATTHAY, K. 1999. Metastatic sites in stage IV and IVS neuroblastoma correlate with age, tumor biology, and survival. *Journal of Pediatric Hematology Oncology,* 21**,** 181-189.

DUBOIS, S. G., MARACHELIAN, A., FOX, E., KUDGUS, R. A., REID, J. M., GROSHEN, S., MALVAR, J., BAGATELL, R., WAGNER, L., MARIS, J. M., HAWKINS, R., COURTIER, J., LAI, H., GOODARZIAN, F., SHIMADA, H., CZARNECKI, S., TSAO-WEI, D., MATTHAY, K. K. & MOSSE, Y. P. 2016. Phase I Study of the Aurora A Kinase Inhibitor Alisertib in Combination With Irinotecan and Temozolomide for Patients With Relapsed or Refractory Neuroblastoma: A NANT (New Approaches to Neuroblastoma Therapy) Trial. *J Clin Oncol,* 34**,** 1368-75.

DUKHANDE, V. V., KAWIKOVA, I., BOTHWELL, A. L. & LAI, J. C. 2013. Neuroprotection against neuroblastoma cell death induced by depletion of mitochondrial glutathione. *Apoptosis,* 18**,** 702-12.

DURAND, R. E. & OLIVE, P. L. 1983. Flow cytometry techniques for studying cellular thiols. *Radiat Res,* 95**,** 456-70.

ECKFORD, P. D. & SHAROM, F. J. 2009. ABC efflux pump-based resistance to chemotherapy drugs. *Chem Rev,* 109**,** 2989-3011.
EDWARDS, K. A. & BAEUMNER, A. J. 2006. Analysis of liposomes. *Talanta,* 68**,** 1432-41.
EIAM-ONG, S., NAKCHUI, Y. & CHAIPIPAT, M. 2018. Vanadate-Induced Renal cAMP and Malondialdehyde Accumulation Suppresses Alpha 1 Sodium Potassium Adenosine Triphosphatase Protein Levels. *Toxicol Res,* 34**,** 143-150.
EL-BROLOSY, M. A. & STAINIER, D. Y. R. 2017. Genetic compensation: A phenomenon in search of mechanisms. *PLoS Genet,* 13**,** e1006780.
ELCHEBLY, M., PAYETTE, P., MICHALISZYN, E., CROMLISH, W., COLLINS, S., LOY, A. L., NORMANDIN, D., CHENG, A., HIMMS-HAGEN, J., CHAN, C. C., RAMACHANDRAN, C., GRESSER, M. J., TREMBLAY, M. L. & KENNEDY, B. P. 1999. Increased insulin sensitivity and obesity resistance in mice lacking the protein tyrosine phosphatase-1B gene. *Science,* 283**,** 1544-8.
ELEVELD, T. F., OLDRIDGE, D. A., BERNARD, V., KOSTER, J., COLMET DAAGE, L., DISKIN, S. J., SCHILD, L., BENTAHAR, N. B., BELLINI, A., CHICARD, M., LAPOUBLE, E., COMBARET, V., LEGOIX-NÉ, P., MICHON, J., PUGH, T. J., HART, L. S., RADER, J., ATTIYEH, E. F., WEI, J. S., ZHANG, S., NARANJO, A., GASTIER-FOSTER, J. M., HOGARTY, M. D., ASGHARZADEH, S., SMITH, M. A., GUIDRY AUVIL, J. M., WATKINS, T. B., ZWIJNENBURG, D. A., EBUS, M. E., VAN SLUIS, P., HAKKERT, A., VAN WEZEL, E., VAN DER SCHOOT, C. E., WESTERHOUT, E. M., SCHULTE, J. H., TYTGAT, G. A., DOLMAN, M. E., JANOUEIX-LEROSEY, I., GERHARD, D. S., CARON, H. N., DELATTRE, O., KHAN, J., VERSTEEG, R., SCHLEIERMACHER, G., MOLENAAR, J. J. & MARIS, J. M. 2015. Relapsed neuroblastomas show frequent RAS-MAPK pathway mutations. *Nat Genet,* 47**,** 864-71.
ELSON, A. 2018. Stepping out of the shadows: Oncogenic and tumor-promoting protein tyrosine phosphatases. *Int J Biochem Cell Biol,* 96**,** 135-147.
ENGEL, R. H. & EVENS, A. M. 2006. Oxidative stress and apoptosis: a new treatment paradigm in cancer. *Front Biosci,* 11**,** 300-12.
ESCHENBRENNER, J., WINSEL, S., HAMMER, S., SOMMER, A., MITTELSTAEDT, K., DROSCH, M., KLAR, U., SACHSE, C., HANNUS, M., SEIDEL, M., WEISS, B., MERZ, C., SIEMEISTER, G. & HOFFMANN, J. 2011. Evaluation of activity and combination strategies with the microtubule-targeting drug sagopilone in breast cancer cell lines. *Front Oncol,* 1**,** 44.
ETHERIDGE, M. L., CAMPBELL, S. A., ERDMAN, A. G., HAYNES, C. L., WOLF, S. M. & MCCULLOUGH, J. 2013. The big picture on nanomedicine: the state of investigational and approved nanomedicine products. *Nanomedicine,* 9**,** 1-14.
EVANGELOU, A. M. 2002. Vanadium in cancer treatment. *Crit Rev Oncol Hematol,* 42**,** 249-65.
FACCHINI, D. M., YUEN, V. G., BATTELL, M. L., MCNEILL, J. H. & GRYNPAS, M. D. 2006. The effects of vanadium treatment on bone in diabetic and non-diabetic rats. *Bone,* 38**,** 368-77.
FANG, J., NAKAMURA, H. & IYER, A. K. 2007. Tumor-targeted induction of oxystress for cancer therapy. *J Drug Target,* 15**,** 475-86.
FARAJI, A. H. & WIPF, P. 2009. Nanoparticles in cellular drug delivery. *Bioorg Med Chem,* 17**,** 2950-62.
FAUMAN, E. B., COGSWELL, J. P., LOVEJOY, B., ROCQUE, W. J., HOLMES, W., MONTANA, V. G., PIWNICA-WORMS, H., RINK, M. J. & SAPER, M. A. 1998. Crystal structure of the catalytic domain of the human cell cycle control phosphatase, Cdc25A. *Cell,* 93**,** 617-25.
FAVATA, M. F., HORIUCHI, K. Y., MANOS, E. J., DAULERIO, A. J., STRADLEY, D. A., FEESER, W. S., VAN DYK, D. E., PITTS, W. J., EARL, R. A., HOBBS, F., COPELAND, R. A., MAGOLDA, R. L., SCHERLE, P. A. & TRZASKOS, J. M. 1998. Identification of a novel inhibitor of mitogen-activated protein kinase kinase. *J Biol Chem,* 273**,** 18623-32.
FEOKTISTOVA, M., GESERICK, P. & LEVERKUS, M. 2016. Crystal Violet Assay for Determining Viability of Cultured Cells. *Cold Spring Harb Protoc,* 2016**,** pdb.prot087379.
FERNÁNDEZ-CHECA, J. C. & KAPLOWITZ, N. 1990. The use of monochlorobimane to determine hepatic GSH levels and synthesis. *Anal Biochem,* 190**,** 212-9.
FERTIG, B. A. & BAILLIE, G. S. 2018. PDE4-Mediated cAMP Signalling. *J Cardiovasc Dev Dis,* 5.
FINKEL, T. 2000. Redox-dependent signal transduction. *FEBS Lett,* 476**,** 52-4.

FOLLIN-ARBELET, V., MISUND, K., NADERI, E. H., UGLAND, H., SUNDAN, A. & BLOMHOFF, H. K. 2015. The natural compound forskolin synergizes with dexamethasone to induce cell death in myeloma cells via BIM. *Sci Rep,* 5**,** 13001.

FOTSIS, T., BREIT, S., LUTZ, W., RÖSSLER, J., HATZI, E., SCHWAB, M. & SCHWEIGERER, L. 1999. Down-regulation of endothelial cell growth inhibitors by enhanced MYCN oncogene expression in human neuroblastoma cells. *Eur J Biochem,* 263**,** 757-64.

FRANKSON, R., YU, Z. H., BAI, Y., LI, Q., ZHANG, R. Y. & ZHANG, Z. Y. 2017. Therapeutic Targeting of Oncogenic Tyrosine Phosphatases. *Cancer Res,* 77**,** 5701-5705.

FRAQUEZA, G., BATISTA DE CARVALHO, L. A., MARQUES, M. P., MAIA, L., OHLIN, C. A., CASEY, W. H. & AURELIANO, M. 2012. Decavanadate, decaniobate, tungstate and molybdate interactions with sarcoplasmic reticulum Ca(2+)-ATPase: quercetin prevents cysteine oxidation by vanadate but does not reverse ATPase inhibition. *Dalton Trans,* 41**,** 12749-58.

FRENCH, R. J. & JONES, P. J. 1993. Role of vanadium in nutrition: metabolism, essentiality and dietary considerations. *Life Sci,* 52**,** 339-46.

FUKUI, K., FUJISAWA, Y., OHYANISHIGUCHI, H., KAMADA, H. & SAKURAI, H. 1999. In vivo coordination structural changes of a potent insulin-mimetic agent, bis(picolinato)oxovanadium(IV), studied by electron spin-echo envelope modulation spectroscopy. *J Inorg Biochem,* 77**,** 215-24.

GALLO-PAYET, N. & BATTISTA, M. C. 2014. Steroidogenesis-adrenal cell signal transduction. *Compr Physiol,* 4**,** 889-964.

GANAPATHY-KANNIAPPAN, S., GESCHWIND, J. F., KUNJITHAPATHAM, R., BUIJS, M., SYED, L. H., RAO, P. P., OTA, S. & VALI, M. 2010. The pyruvic acid analog 3-bromopyruvate interferes with the tetrazolium reagent MTS in the evaluation of cytotoxicity. *Assay Drug Dev Technol,* 8**,** 258-62.

GAO, J., AKSOY, B. A., DOGRUSOZ, U., DRESDNER, G., GROSS, B., SUMER, S. O., SUN, Y., JACOBSEN, A., SINHA, R., LARSSON, E., CERAMI, E., SANDER, C. & SCHULTZ, N. 2013. Integrative analysis of complex cancer genomics and clinical profiles using the cBioPortal. *Sci Signal,* 6**,** pl1.

GEORGE, R. E., SANDA, T., HANNA, M., FRÖHLING, S., LUTHER, W., ZHANG, J., AHN, Y., ZHOU, W., LONDON, W. B., MCGRADY, P., XUE, L., ZOZULYA, S., GREGOR, V. E., WEBB, T. R., GRAY, N. S., GILLILAND, D. G., DILLER, L., GREULICH, H., MORRIS, S. W., MEYERSON, M. & LOOK, A. T. 2008. Activating mutations in ALK provide a therapeutic target in neuroblastoma. *Nature,* 455**,** 975-8.

GHOSH, P., D'CRUZ, O. J., NARLA, R. K. & UCKUN, F. M. 2000. Apoptosis-inducing vanadocene compounds against human testicular cancer. *Clin Cancer Res,* 6**,** 1536-45.

GILBERT, L. A., HORLBECK, M. A., ADAMSON, B., VILLALTA, J. E., CHEN, Y., WHITEHEAD, E. H., GUIMARAES, C., PANNING, B., PLOEGH, H. L., BASSIK, M. C., QI, L. S., KAMPMANN, M. & WEISSMAN, J. S. 2014. Genome-Scale CRISPR-Mediated Control of Gene Repression and Activation. *Cell,* 159**,** 647-61.

GOLDFINE, A. B., PATTI, M. E., ZUBERI, L., GOLDSTEIN, B. J., LEBLANC, R., LANDAKER, E. J., JIANG, Z. Y., WILLSKY, G. R. & KAHN, C. R. 2000. Metabolic effects of vanadyl sulfate in humans with non-insulin-dependent diabetes mellitus: in vivo and in vitro studies. *Metabolism,* 49**,** 400-10.

GOLDFINE, A. B., SIMONSON, D. C., FOLLI, F., PATTI, M. E. & KAHN, C. R. 1995. Metabolic effects of sodium metavanadate in humans with insulin-dependent and noninsulin-dependent diabetes mellitus in vivo and in vitro studies. *J Clin Endocrinol Metab,* 80**,** 3311-20.

GONZALEZ, R. J. & TARLOFF, J. B. 2001. Evaluation of hepatic subcellular fractions for Alamar blue and MTT reductase activity. *Toxicol In Vitro,* 15**,** 257-9.

GOODMAN, L. A., LIU, B. C., THIELE, C. J., SCHMIDT, M. L., COHN, S. L., YAMASHIRO, J. M., PAI, D. S., IKEGAKI, N. & WADA, R. K. 1997. Modulation of N-myc expression alters the invasiveness of neuroblastoma. *Clin Exp Metastasis,* 15**,** 130-9.

GORDON, J. A. 1991. Use of vanadate as protein-phosphotyrosine phosphatase inhibitor. *Methods Enzymol,* 201**,** 477-82.

GORRE, M. E., MOHAMMED, M., ELLWOOD, K., HSU, N., PAQUETTE, R., RAO, P. N. & SAWYERS, C. L. 2001. Clinical resistance to STI-571 cancer therapy caused by BCR-ABL gene mutation or amplification. *Science,* 293**,** 876-80.

GRAY, C. H., GOOD, V. M., TONKS, N. K. & BARFORD, D. 2003. The structure of the cell cycle protein Cdc14 reveals a proline-directed protein phosphatase. *EMBO J,* 22**,** 3524-35.
GREENGARD, E. G. 2018. Molecularly Targeted Therapy for Neuroblastoma. *Children (Basel),* 5.
GRIFFITH, O. W. & MEISTER, A. 1979. Potent and specific inhibition of glutathione synthesis by buthionine sulfoximine (S-n-butyl homocysteine sulfoximine). *J Biol Chem,* 254**,** 7558-60.
GROEN, A., LEMEER, S., VAN DER WIJK, T., OVERVOORDE, J., HECK, A. J., OSTMAN, A., BARFORD, D., SLIJPER, M. & DEN HERTOG, J. 2005. Differential oxidation of protein-tyrosine phosphatases. *J Biol Chem,* 280**,** 10298-304.
GUAN, K. L. & DIXON, J. E. 1991. Evidence for protein-tyrosine-phosphatase catalysis proceeding via a cysteine-phosphate intermediate. *J Biol Chem,* 266**,** 17026-30.
GUILLAMOT, M., MANCHADO, E., CHIESA, M., GÓMEZ-LÓPEZ, G., PISANO, D. G., SACRISTÁN, M. P. & MALUMBRES, M. 2011. Cdc14b regulates mammalian RNA polymerase II and represses cell cycle transcription. *Sci Rep,* 1**,** 189.
GULATI, P., KLÖHN, P. C., KRUG, H., GÖTTLICHER, M., MARKOVA, B., BÖHMER, F. D. & HERRLICH, P. 2001. Redox regulation in mammalian signal transduction. *IUBMB Life,* 52**,** 25-8.
GULLAPALLI, S., SHIVASWAMY, V., RAMASARMA, T. & KURUP, C. K. 1989. Increase in alpha-glycerophosphate dehydrogenase and other oxidoreductase activities of hepatic mitochondria on administration of vanadate to the rat. *Indian J Biochem Biophys,* 26**,** 227-33.
GUM, R. J., GAEDE, L. L., KOTERSKI, S. L., HEINDEL, M., CLAMPIT, J. E., ZINKER, B. A., TREVILLYAN, J. M., ULRICH, R. G., JIROUSEK, M. R. & RONDINONE, C. M. 2003. Reduction of protein tyrosine phosphatase 1B increases insulin-dependent signaling in ob/ob mice. *Diabetes,* 52**,** 21-8.
HACKBARTH, I., SCHMITZ, W., SCHOLZ, H., WETZEL, E., ERDMANN, E., KRAWIETZ, W. & PHILIPP, G. 1980. Stimulatory effect of vanadate on cyclic AMP levels in cat papillary muscle. *Biochem Pharmacol,* 29**,** 1429-32.
HALBERSTAM, M., COHEN, N., SHLIMOVICH, P., ROSSETTI, L. & SHAMOON, H. 1996. Oral vanadyl sulfate improves insulin sensitivity in NIDDM but not in obese nondiabetic subjects. *Diabetes,* 45**,** 659-66.
HALLIWELL, B. 2007. Oxidative stress and cancer: have we moved forward? *Biochem J,* 401**,** 1-11.
HAMILTON, B., HOYERT, D., MARTIN, J., STROBINO, D. & GUYER, B. 2013. Annual Summary of Vital Statistics: 2010-2011. *Pediatrics,* 131**,** 548-558.
HANAHAN, D. & WEINBERG, R. A. 2000. The hallmarks of cancer. *Cell,* 100**,** 57-70.
HANAHAN, D. & WEINBERG, R. A. 2011. Hallmarks of cancer: the next generation. *Cell,* 144**,** 646-74.
HÄNNINEN, M. M., PEURONEN, A., DAMLIN, P., TYYSTJÄRVI, V., KIVELÄ, H. & LEHTONEN, A. 2014. Vanadium complexes with multidentate amine bisphenols. *Dalton Trans,* 43**,** 14022-8.
HARDING, M. M. & MOKDSI, G. 2000. Antitumour metallocenes: structure-activity studies and interactions with biomolecules. *Curr Med Chem,* 7**,** 1289-303.
HARLAND, B. F. & HARDEN-WILLIAMS, B. A. 1994. Is vanadium of human nutritional importance yet? *J Am Diet Assoc,* 94**,** 891-4.
HARTWELL, L. H., MORTIMER, R. K., CULOTTI, J. & CULOTTI, M. 1973. Genetic Control of the Cell Division Cycle in Yeast: V. Genetic Analysis of cdc Mutants. *Genetics,* 74**,** 267-86.
HAWKES, W. C. & ALKAN, Z. 2011. Delayed cell cycle progression from SEPW1 depletion is p53- and p21-dependent in MCF-7 breast cancer cells. *Biochem Biophys Res Commun,* 413**,** 36-40.
HE, R. J., YU, Z. H., ZHANG, R. Y. & ZHANG, Z. Y. 2014. Protein tyrosine phosphatases as potential therapeutic targets. *Acta Pharmacol Sin,* 35**,** 1227-46.
HE, X. P., DENG, Q., GAO, L. X., LI, C., ZHANG, W., ZHOU, Y. B., TANG, Y., SHI, X. X., XIE, J., LI, J., CHEN, G. R. & CHEN, K. 2011. Facile fabrication of promising protein tyrosine phosphatase (PTP) inhibitor entities based on 'clicked' serine/threonine-monosaccharide hybrids. *Bioorg Med Chem,* 19**,** 3892-900.
HECHT, M., BROMBERG, Y. & ROST, B. 2015. Better prediction of functional effects for sequence variants. *BMC Genomics,* 16 Suppl 8**,** S1.

HELDIN, C. H. 1995. Dimerization of cell surface receptors in signal transduction. *Cell,* 80**,** 213-23.
HENEBERG, P. 2009. Use of protein tyrosine phosphatase inhibitors as promising targeted therapeutic drugs. *Curr Med Chem,* 16**,** 706-33.
HENNESSY, B. T., SMITH, D. L., RAM, P. T., LU, Y. & MILLS, G. B. 2005. Exploiting the PI3K/AKT pathway for cancer drug discovery. *Nat Rev Drug Discov,* 4**,** 988-1004.
HERRLICH, P. & BÖHMER, F. D. 2000. Redox regulation of signal transduction in mammalian cells. *Biochem Pharmacol,* 59**,** 35-41.
HEYLIGER, C. E., TAHILIANI, A. G. & MCNEILL, J. H. 1985. Effect of vanadate on elevated blood glucose and depressed cardiac performance of diabetic rats. *Science,* 227**,** 1474-7.
HIRAI, H., SOOTOME, H., NAKATSURU, Y., MIYAMA, K., TAGUCHI, S., TSUJIOKA, K., UENO, Y., HATCH, H., MAJUMDER, P. K., PAN, B. S. & KOTANI, H. 2010. MK-2206, an allosteric Akt inhibitor, enhances antitumor efficacy by standard chemotherapeutic agents or molecular targeted drugs in vitro and in vivo. *Mol Cancer Ther,* 9**,** 1956-67.
HIRAMOTO, K., MURATA, T., SHIMIZU, K., MORITA, H., INUI, M., MANGANIELLO, V. C., TAGAWA, T. & ARAI, N. 2014. Role of phosphodiesterase 2 in growth and invasion of human malignant melanoma cells. *Cell Signal,* 26**,** 1807-17.
HNIA, K., VACCARI, I., BOLINO, A. & LAPORTE, J. 2012. Myotubularin phosphoinositide phosphatases: cellular functions and disease pathophysiology. *Trends Mol Med,* 18**,** 317-27.
HOEHNER, J., GESTBLOM, C., HEDBORG, F., SANDSTEDT, B., OLSEN, L. & PAHLMAN, S. 1996. A developmental model of neuroblastoma: Differentiating stroma-poor tumors' progress along an extra-adrenal chromaffin lineage. *Laboratory Investigation,* 75**,** 659-675.
HOEKSTRA, E., DAS, A. M., SWETS, M., CAO, W., VAN DER WOUDE, C. J., BRUNO, M. J., PEPPELENBOSCH, M. P., KUPPEN, P. J., TEN HAGEN, T. L. & FUHLER, G. M. 2016. Increased PTP1B expression and phosphatase activity in colorectal cancer results in a more invasive phenotype and worse patient outcome. *Oncotarget,* 7**,** 21922-38.
HOLLANDER, M. C., BLUMENTHAL, G. M. & DENNIS, P. A. 2011. PTEN loss in the continuum of common cancers, rare syndromes and mouse models. *Nat Rev Cancer,* 11**,** 289-301.
HU, Z. Q., MA, R., ZHANG, C. M., LI, J., LI, L., HU, Z. T., GAO, Q. I. & LI, W. M. 2015. Expression and clinical significance of tyrosine phosphatase SHP2 in thyroid carcinoma. *Oncol Lett,* 10**,** 1507-1512.
HUANG, C., ZHANG, Z., DING, M., LI, J., YE, J., LEONARD, S. S., SHEN, H. M., BUTTERWORTH, L., LU, Y., COSTA, M., ROJANASAKUL, Y., CASTRANOVA, V., VALLYATHAN, V. & SHI, X. 2000a. Vanadate induces p53 transactivation through hydrogen peroxide and causes apoptosis. *J Biol Chem,* 275**,** 32516-22.
HUANG, M. & WEISS, W. A. 2013. Neuroblastoma and MYCN. *Cold Spring Harb Perspect Med,* 3**,** a014415.
HUANG, P., FENG, L., OLDHAM, E. A., KEATING, M. J. & PLUNKETT, W. 2000b. Superoxide dismutase as a target for the selective killing of cancer cells. *Nature,* 407**,** 390-5.
HUANG, W. Q., LIN, Q., ZHUANG, X., CAI, L. L., RUAN, R. S., LU, Z. X. & TZENG, C. M. 2014. Structure, function, and pathogenesis of SHP2 in developmental disorders and tumorigenesis. *Curr Cancer Drug Targets,* 14**,** 567-88.
HUBBARD, S. R. 1999. Structural analysis of receptor tyrosine kinases. *Prog Biophys Mol Biol,* 71**,** 343-58.
HUBBARD, S. R. & MILLER, W. T. 2007. Receptor tyrosine kinases: mechanisms of activation and signaling. *Curr Opin Cell Biol,* 19**,** 117-23.
HUGHES, T. P., KAEDA, J., BRANFORD, S., RUDZKI, Z., HOCHHAUS, A., HENSLEY, M. L., GATHMANN, I., BOLTON, A. E., VAN HOOMISSEN, I. C., GOLDMAN, J. M., RADICH, J. P. & GROUP, I. R. S. O. I. V. S. I. S. 2003. Frequency of major molecular responses to imatinib or interferon alfa plus cytarabine in newly diagnosed chronic myeloid leukemia. *N Engl J Med,* 349**,** 1423-32.
HUNTER, T. 1998. The Croonian Lecture 1997. The phosphorylation of proteins on tyrosine: its role in cell growth and disease. *Philos Trans R Soc Lond B Biol Sci,* 353**,** 583-605.
HUYER, G., LIU, S., KELLY, J., MOFFAT, J., PAYETTE, P., KENNEDY, B., TSAPRAILIS, G., GRESSER, M. J. & RAMACHANDRAN, C. 1997. Mechanism of inhibition of protein-tyrosine phosphatases by vanadate and pervanadate. *J Biol Chem,* 272**,** 843-51.

HWANG, S. H., KIM, E. J., HONG, Y. B., JOO, J., KIM, S. M., NAM, S. H., HONG, H. D., KIM, S. H., OH, K., LIM, J. G., CHO, J. H., CHUNG, K. W. & CHOI, B. O. 2016. Distal hereditary motor neuropathy type 7B with Dynactin 1 mutation. *Mol Med Rep,* 14**,** 3362-8.

INSEL, P. A., ZHANG, L., MURRAY, F., YOKOUCHI, H. & ZAMBON, A. C. 2012. Cyclic AMP is both a pro-apoptotic and anti-apoptotic second messenger. *Acta Physiol (Oxf),* 204**,** 277-87.

IRVING, E. & STOKER, A. W. 2017. Vanadium Compounds as PTP Inhibitors. *Molecules,* 22.

ISHIYAMA, M., SHIGA, M., SASAMOTO, K., MIZOGUCHI, M. & HE, P. 1993. A new sulfonated tetrazolium salt that produces a highly water-soluble formazan dye. *Chemical & Pharmaceutical Bulletin,* 41**,** 1118-1122.

IWAHARA, T., FUJIMOTO, J., WEN, D., CUPPLES, R., BUCAY, N., ARAKAWA, T., MORI, S., RATZKIN, B. & YAMAMOTO, T. 1997. Molecular characterization of ALK, a receptor tyrosine kinase expressed specifically in the nervous system. *Oncogene,* 14**,** 439-49.

IZYCKA-SWIESZEWSKA, E., BRZESKWINIEWICZ, M., WOZNIAK, A., DROZYNSKA, E., GRAJKOWSKA, W., PEREK, D., BALCERSKA, A., KLEPACKA, T. & LIMON, J. 2010. EGFR, PIK3CA and PTEN gene status and their protein product expression in neuroblastic tumours. *Folia Neuropathol,* 48**,** 238-45.

JACKSON, A. L., BURCHARD, J., LEAKE, D., REYNOLDS, A., SCHELTER, J., GUO, J., JOHNSON, J. M., LIM, L., KARPILOW, J., NICHOLS, K., MARSHALL, W., KHVOROVA, A. & LINSLEY, P. S. 2006. Position-specific chemical modification of siRNAs reduces "off-target" transcript silencing. *RNA,* 12**,** 1197-205.

JACKSON, A. L. & LINSLEY, P. S. 2010. Recognizing and avoiding siRNA off-target effects for target identification and therapeutic application. *Nat Rev Drug Discov,* 9**,** 57-67.

JANOUEIX-LEROSEY, I., LEQUIN, D., BRUGIÈRES, L., RIBEIRO, A., DE PONTUAL, L., COMBARET, V., RAYNAL, V., PUISIEUX, A., SCHLEIERMACHER, G., PIERRON, G., VALTEAU-COUANET, D., FREBOURG, T., MICHON, J., LYONNET, S., AMIEL, J. & DELATTRE, O. 2008. Somatic and germline activating mutations of the ALK kinase receptor in neuroblastoma. *Nature,* 455**,** 967-70.

JANOUEIX-LEROSEY, I., SCHLEIERMACHER, G. & DELATTRE, O. 2010. Molecular pathogenesis of peripheral neuroblastic tumors. *Oncogene,* 29**,** 1566-1579.

JIANG, M., STANKE, J., LAHTI, J. & DYER, M. 2011. The connections between neural crest development and neuroblastoma. *Cancer and Development,* 94**,** 77-127.

JIN, Q., REN, Y., WANG, M., SURANENI, P. K., LI, D., CRISPINO, J. D., FAN, J. & HUANG, Z. 2016. Novel function of FAXDC2 in megakaryopoiesis. *Blood Cancer J,* 6**,** e478.

JULIEN, S. G., DUBÉ, N., READ, M., PENNEY, J., PAQUET, M., HAN, Y., KENNEDY, B. P., MULLER, W. J. & TREMBLAY, M. L. 2007. Protein tyrosine phosphatase 1B deficiency or inhibition delays ErbB2-induced mammary tumorigenesis and protects from lung metastasis. *Nat Genet,* 39**,** 338-46.

JUNG, S. K., JEONG, D. G., CHUNG, S. J., KIM, J. H., PARK, B. C., TONKS, N. K., RYU, S. E. & KIM, S. J. 2010. Crystal structure of ED-Eya2: insight into dual roles as a protein tyrosine phosphatase and a transcription factor. *FASEB J,* 24**,** 560-9.

KANNA, P. S., MAHENDRAKUMAR, C. B., INDIRA, B. N., SRIVASTAWA, S., KALAISELVI, K., ELAYARAJA, T. & CHATTERJEE, M. 2004. Chemopreventive effects of vanadium toward 1,2-dimethylhydrazine-induced genotoxicity and preneoplastic lesions in rat colon. *Environ Mol Mutagen,* 44**,** 113-8.

KANNE, H., BURTE, N. P., PRASANNA, V. & GUJJULA, R. 2015. Extraction and elemental analysis of Coleus forskohlii extract. *Pharmacognosy Res,* 7**,** 237-41.

KARAKAS, B., WEERARATNA, A. T., ABUKHDEIR, A. M., KONISHI, H., GUSTIN, J. P., VITOLO, M. I., BACHMAN, K. E. & PARK, B. H. 2007. P21 gene knock down does not identify genetic effectors seen with gene knock out. *Cancer Biol Ther,* 6**,** 1025-30.

KATO, H., SEMBA, S., MISKAD, U. A., SEO, Y., KASUGA, M. & YOKOZAKI, H. 2004. High expression of PRL-3 promotes cancer cell motility and liver metastasis in human colorectal cancer: a predictive molecular marker of metachronous liver and lung metastases. *Clin Cancer Res,* 10**,** 7318-28.

KE, J., YANG, Y., CHE, Q., JIANG, F., WANG, H., CHEN, Z., ZHU, M., TONG, H., ZHANG, H., YAN, X., WANG, X., WANG, F., LIU, Y., DAI, C. & WAN, X. 2016. Prostaglandin E2 (PGE2) promotes proliferation and invasion by enhancing SUMO-1 activity via EP4 receptor in endometrial cancer. *Tumour Biol,* 37**,** 12203-12211.

KIELER, J., GROMEK, A. & NISSEN, N. I. 1965. Studies on the antineoplastic effect of vanadium salts. *Acta Chir Scand Suppl,* 343**,** 154-64.

KIM, D., PERTEA, G., TRAPNELL, C., PIMENTEL, H., KELLEY, R. & SALZBERG, S. L. 2013. TopHat2: accurate alignment of transcriptomes in the presence of insertions, deletions and gene fusions. *Genome Biol,* 14**,** R36.
KIM, D. H. & LERNER, A. 1998. Type 4 cyclic adenosine monophosphate phosphodiesterase as a therapeutic target in chronic lymphocytic leukemia. *Blood,* 92**,** 2484-94.
KIM, S. J. & RYU, S. E. 2012. Structure and catalytic mechanism of human protein tyrosine phosphatome. *BMB Rep,* 45**,** 693-9.
KIM, Y., CHOI, J. W., LEE, J. H. & KIM, Y. S. 2014. Loss of CDC14B expression in clear cell renal cell carcinoma: meta-analysis of microarray data sets. *Am J Clin Pathol,* 141**,** 551-8.
KLEIBLOVA, P., SHALTIEL, I., BENADA, J., ŠEVČÍK, J., PECHÁČKOVÁ, S., POHLREICH, P., VOEST, E. E., DUNDR, P., BARTEK, J., KLEIBL, Z., MEDEMA, R. H. & MACUREK, L. 2013. Gain-of-function mutations of PPM1D/Wip1 impair the p53-dependent G1 checkpoint. *J Cell Biol,* 201(4)**,** 511-21.
KNIJNENBURG, T. A., WANG, L., ZIMMERMANN, M. T., CHAMBWE, N., GAO, G. F., CHERNIACK, A. D., FAN, H., SHEN, H., WAY, G. P., GREENE, C. S., LIU, Y., AKBANI, R., FENG, B., DONEHOWER, L. A., MILLER, C., SHEN, Y., KARIMI, M., CHEN, H., KIM, P., JIA, P., SHINBROT, E., ZHANG, S., LIU, J., HU, H., BAILEY, M. H., YAU, C., WOLF, D., ZHAO, Z., WEINSTEIN, J. N., LI, L., DING, L., MILLS, G. B., LAIRD, P. W., WHEELER, D. A., SHMULEVICH, I., MONNAT, R. J., XIAO, Y., WANG, C. & NETWORK, C. G. A. R. 2018. Genomic and Molecular Landscape of DNA Damage Repair Deficiency across The Cancer Genome Atlas. *Cell Rep,* 23**,** 239-254.e6.
KOBAYASHI, S., BOGGON, T. J., DAYARAM, T., JÄNNE, P. A., KOCHER, O., MEYERSON, M., JOHNSON, B. E., ECK, M. J., TENEN, D. G. & HALMOS, B. 2005. EGFR mutation and resistance of non-small-cell lung cancer to gefitinib. *N Engl J Med,* 352**,** 786-92.
KÖPF-MAIER, P., WAGNER, W., HESSE, B. & KÖPF, H. 1981. Tumor inhibition by metallocenes: activity against leukemias and detection of the systemic effect. *Eur J Cancer,* 17**,** 665-9.
KÖPF-MAIER, P., WAGNER, W. & LISS, E. 1983. Induction of cell arrest at G1/S and in G2 after treatment of Ehrlich ascites tumor cells with metallocene dichlorides and cis-platinum in vitro. *J Cancer Res Clin Oncol,* 106**,** 44-52.
KORBECKI, J., BARANOWSKA-BOSIACKA, I., GUTOWSKA, I. & CHLUBEK, D. 2015. Vanadium Compounds as Pro-Inflammatory Agents: Effects on Cyclooxygenases. *Int J Mol Sci,* 16**,** 12648-68.
KOWALSKI, S., HAĆ, S., WYRZYKOWSKI, D., ZAUSZKIEWICZ-PAWLAK, A. & INKIELEWICZ-STĘPNIAK, I. 2017. Selective cytotoxicity of vanadium complexes on human pancreatic ductal adenocarcinoma cell line by inducing necroptosis, apoptosis and mitotic catastrophe process. *Oncotarget,* 8**,** 60324-60341.
KRAWIETZ, W., WERDAN, K. & ERDMANN, E. 1980. Stimulation of human cardiac adenylate cyclase by vanadate. *Basic Res Cardiol,* 75**,** 433-7.
KREMER, L. E., MCLEOD, A. I., AITKEN, J. B., LEVINA, A. & LAY, P. A. 2015. Vanadium(V) and -(IV) complexes of anionic polysaccharides: Controlled release pharmaceutical formulations and models of vanadium biotransformation products. *J Inorg Biochem,* 147**,** 227-34.
KRISHNAN, N., KOVEAL, D., MILLER, D. H., XUE, B., AKSHINTHALA, S. D., KRAGELJ, J., JENSEN, M. R., GAUSS, C. M., PAGE, R., BLACKLEDGE, M., MUTHUSWAMY, S. K., PETI, W. & TONKS, N. K. 2014. Targeting the disordered C terminus of PTP1B with an allosteric inhibitor. *Nat Chem Biol,* 10**,** 558-66.
KUMARI, S., BADANA, A. K., G, M. M., G, S. & MALLA, R. 2018. Reactive Oxygen Species: A Key Constituent in Cancer Survival. *Biomark Insights,* 13**,** 1177271918755391.
LABBÉ, D. P., HARDY, S. & TREMBLAY, M. L. 2012. Protein tyrosine phosphatases in cancer: friends and foes! *Prog Mol Biol Transl Sci,* 106**,** 253-306.
LACKNER, M. R., WILSON, T. R. & SETTLEMAN, J. 2012. Mechanisms of acquired resistance to targeted cancer therapies. *Future Oncol,* 8**,** 999-1014.
LACZMANSKA, I. & SASIADEK, M. M. 2011. Tyrosine phosphatases as a superfamily of tumor suppressors in colorectal cancer. *Acta Biochim Pol,* 58**,** 467-70.
LATT, S. A. & STETTEN, G. 1976. Spectral studies on 33258 Hoechst and related bisbenzimidazole dyes useful for fluorescent detection of deoxyribonucleic acid synthesis. *J Histochem Cytochem,* 24**,** 24-33.
LAU, A. A., KING, B. M., THORSEN, C. L., HASSIOTIS, S., BEARD, H., TRIM, P. J., WHYTE, L. S., TAMANG, S. J., DUPLOCK, S. K., SNEL, M. F., HOPWOOD, J. J. & HEMSLEY, K.

M. 2017. A novel conditional Sgsh knockout mouse model recapitulates phenotypic and neuropathic deficits of Sanfilippo syndrome. *J Inherit Metab Dis,* 40**,** 715-724.
LAW, N. C., DONAUBAUER, E. M., ZELEZNIK, A. J. & HUNZICKER-DUNN, M. 2017. How Protein Kinase A Activates Canonical Tyrosine Kinase Signaling Pathways To Promote Granulosa Cell Differentiation. *Endocrinology,* 158**,** 2043-2051.
LAZO, J. S., MCQUEENEY, K. E., BURNETT, J. C., WIPF, P. & SHARLOW, E. R. 2018. Small molecule targeting of PTPs in cancer. *Int J Biochem Cell Biol,* 96**,** 171-181.
LE, M., RATHJE, O., LEVINA, A. & LAY, P. A. 2017. High cytotoxicity of vanadium(IV) complexes with 1,10-phenanthroline and related ligands is due to decomposition in cell culture medium. *J Biol Inorg Chem,* 22**,** 663-672.
LEON, I. E., DI VIRGILIO, A. L., PORRO, V., MUGLIA, C. I., NASO, L. G., WILLIAMS, P. A., BOLLATI-FOGOLIN, M. & ETCHEVERRY, S. B. 2013. Antitumor properties of a vanadyl(IV) complex with the flavonoid chrysin [VO(chrysin)2EtOH]2 in a human osteosarcoma model: the role of oxidative stress and apoptosis. *Dalton Trans,* 42**,** 11868-80.
LEON, I. E., PORRO, V., DI VIRGILIO, A. L., NASO, L. G., WILLIAMS, P. A., BOLLATI-FOGOLÍN, M. & ETCHEVERRY, S. B. 2014. Antiproliferative and apoptosis-inducing activity of an oxidovanadium(IV) complex with the flavonoid silibinin against osteosarcoma cells. *J Biol Inorg Chem,* 19**,** 59-74.
LESSARD, L., STUIBLE, M. & TREMBLAY, M. L. 2010. The two faces of PTP1B in cancer. *Biochim Biophys Acta,* 1804**,** 613-9.
LEVINA, A. & LAY, P. A. 2017. Stabilities and Biological Activities of Vanadium Drugs: What is the Nature of the Active Species? *Chem Asian J,* 12**,** 1692-1699.
LEVINA, A., MCLEOD, A. I., KREMER, L. E., AITKEN, J. B., GLOVER, C. J., JOHANNESSEN, B. & LAY, P. A. 2014. Reactivity-activity relationships of oral anti-diabetic vanadium complexes in gastrointestinal media: an X-ray absorption spectroscopic study. *Metallomics,* 6**,** 1880-8.
LI, S., CROOKS, P. A., WEI, X. & DE LEON, J. 2004. Toxicity of dipyridyl compounds and related compounds. *Crit Rev Toxicol,* 34**,** 447-60.
LI, Z. R., WANG, Z., ZHU, B. H., HE, Y. L., PENG, J. S., CAI, S. R., MA, J. P. & ZHAN, W. H. 2007. Association of tyrosine PRL-3 phosphatase protein expression with peritoneal metastasis of gastric carcinoma and prognosis. *Surg Today,* 37**,** 646-51.
LICHAWSKA, M. E., BODEK, K. H., JEZIERSKA, J. & KUFELNICKI, A. 2014. Coordinative interaction of microcrystalline chitosan with oxovanadium (IV) ions in aqueous solution. *Chem Cent J,* 8**,** 50.
LIM, S. M., HWANG, J. W., AHN, J. B., BAE, S. K., PARK, C. H., KIM, K. Y., RHA, S. Y., CHUNG, H. C., ROH, J. K. & SHIN, S. J. 2013. Combination of CYP inhibitor with MEK/ERK inhibitor enhances the inhibitory effect on ERK in BRAF mutant colon cancer cells. *Anticancer Res,* 33**,** 2499-508.
LIN, H., HA, K., LU, G., FANG, X., CHENG, R., ZUO, Q. & ZHANG, P. 2015. Cdc14A and Cdc14B Redundantly Regulate DNA Double-Strand Break Repair. *Mol Cell Biol,* 35**,** 3657-68.
LINDNER, L. H., HOSSANN, M., VOGESER, M., TEICHERT, N., WACHHOLZ, K., EIBL, H., HIDDEMANN, W. & ISSELS, R. D. 2008. Dual role of hexadecylphosphocholine (miltefosine) in thermosensitive liposomes: active ingredient and mediator of drug release. *J Control Release,* 125**,** 112-20.
LIOU, G. Y. & STORZ, P. 2010. Reactive oxygen species in cancer. *Free Radic Res,* 44**,** 479-96.
LIU, H., WU, Y., ZHU, S., LIANG, W., WANG, Z., WANG, Y., LV, T., YAO, Y., YUAN, D. & SONG, Y. 2015a. PTP1B promotes cell proliferation and metastasis through activating src and ERK1/2 in non-small cell lung cancer. *Cancer Lett,* 359**,** 218-25.
LIU, K., LI, D., HAO, G., MCCAFFARY, D., NEELY, O., WOODWARD, L., IOANNIDES, D., LU, C. J., BRESCIA, M., ZACCOLO, M., TANDRI, H., AJIJOLA, O. A., ARDELL, J. L., SHIVKUMAR, K. & PATERSON, D. J. 2018a. Phosphodiesterase 2A as a therapeutic target to restore cardiac neurotransmission during sympathetic hyperactivity. *JCI Insight,* 3.
LIU, L., ZHENG, J., HUANG, X. F., ZHU, X., DING, S. M., KE, H. M., O'DONNELL, J. M., ZHANG, H. T., SONG, G. Q. & XU, Y. 2018b. The neuroprotective and antidepressant-like effects of Hcyb1, a novel selective PDE2 inhibitor. *CNS Neurosci Ther,* 24**,** 652-660.

LIU, T. T., LIU, Y. J., WANG, Q., YANG, X. G. & WANG, K. 2012. Reactive-oxygen-species-mediated Cdc25C degradation results in differential antiproliferative activities of vanadate, tungstate, and molybdate in the PC-3 human prostate cancer cell line. *J Biol Inorg Chem,* 17**,** 311-20.

LIU, X., CHEN, Q., HU, X. G., ZHANG, X. C., FU, T. W., LIU, Q., LIANG, Y., ZHAO, X. L., ZHANG, X., PING, Y. F. & BIAN, X. W. 2016. PTP1B promotes aggressiveness of breast cancer cells by regulating PTEN but not EMT. *Tumour Biol,* 37**,** 13479-13487.

LIU, Y., JIE, X., GUO, Y., ZHANG, X., WANG, J. & XUE, C. 2015b. Green Synthesis of Oxovanadium(IV)/chitosan Nanocomposites and Its Ameliorative Effect on Hyperglycemia, Insulin Resistance, and Oxidative Stress. *Biol Trace Elem Res*.

LIVAK, K. J. & SCHMITTGEN, T. D. 2001. Analysis of relative gene expression data using real-time quantitative PCR and the 2(-Delta Delta C(T)) Method. *Methods,* 25**,** 402-8.

LLAVERIAS, G., DANILO, C., MERCIER, I., DAUMER, K., CAPOZZA, F., WILLIAMS, T. M., SOTGIA, F., LISANTI, M. P. & FRANK, P. G. 2011. Role of cholesterol in the development and progression of breast cancer. *Am J Pathol,* 178**,** 402-12.

LOEW, R., HEINZ, N., HAMPF, M., BUJARD, H. & GOSSEN, M. 2010. Improved Tet-responsive promoters with minimized background expression. *BMC Biotechnol,* 10**,** 81.

LONDON, W., CASTLEBERRY, R., MATTHAY, K., LOOK, A., SEEGER, R., SHIMADA, H., THORNER, P., BRODEUR, G., MARIS, J., REYNOLDS, C. & COHN, S. 2005. Evidence for an age cutoff greater than 365 days for neuroblastoma risk group stratification in the Children's Oncology Group. *Journal of Clinical Oncology,* 23**,** 6459-6465.

LOO, T. W. & CLARKE, D. M. 2002. Vanadate trapping of nucleotide at the ATP-binding sites of human multidrug resistance P-glycoprotein exposes different residues to the drug-binding site. *Proc Natl Acad Sci U S A,* 99**,** 3511-6.

LÓPEZ-CARBALLO, G., MORENO, L., MASIÁ, S., PÉREZ, P. & BARETTINO, D. 2002. Activation of the phosphatidylinositol 3-kinase/Akt signaling pathway by retinoic acid is required for neural differentiation of SH-SY5Y human neuroblastoma cells. *J Biol Chem,* 277**,** 25297-304.

LORENZO, O., URBÉ, S. & CLAGUE, M. J. 2006. Systematic analysis of myotubularins: heteromeric interactions, subcellular localisation and endosome related functions. *J Cell Sci,* 119**,** 2953-9.

LOS, M., MADDIKA, S., ERB, B. & SCHULZE-OSTHOFF, K. 2009. Switching Akt: from survival signaling to deadly response. *Bioessays,* 31**,** 492-5.

LOUIS, C., SHOHET, J. & CASKEY, C. 2015. Neuroblastoma: Molecular Pathogenesis and Therapy. *Annual Review of Medicine, Vol 66,* 66**,** 49-63.

LOVE, M. I., HUBER, W. & ANDERS, S. 2014. Moderated estimation of fold change and dispersion for RNA-seq data with DESeq2. *Genome Biol,* 15**,** 550.

LUGO, M. R. & SHAROM, F. J. 2014. Kinetic validation of the models for P-glycoprotein ATP hydrolysis and vanadate-induced trapping. Proposal for additional steps. *PLoS One,* 9**,** e98804.

LYNCH, T. J., BELL, D. W., SORDELLA, R., GURUBHAGAVATULA, S., OKIMOTO, R. A., BRANNIGAN, B. W., HARRIS, P. L., HASERLAT, S. M., SUPKO, J. G., HALUSKA, F. G., LOUIS, D. N., CHRISTIANI, D. C., SETTLEMAN, J. & HABER, D. A. 2004. Activating mutations in the epidermal growth factor receptor underlying responsiveness of non-small-cell lung cancer to gefitinib. *N Engl J Med,* 350**,** 2129-39.

MA, H. T., ON, K. F., TSANG, Y. H. & POON, R. Y. 2007. An inducible system for expression and validation of the specificity of short hairpin RNA in mammalian cells. *Nucleic Acids Res,* 35**,** e22.

MACARA, I. G., KUSTIN, K. & CANTLEY, L. C. 1980. Glutathione reduces cytoplasmic vanadate. Mechanism and physiological implications. *Biochim Biophys Acta,* 629**,** 95-106.

MACKEIGAN, J. P., MURPHY, L. O. & BLENIS, J. 2005. Sensitized RNAi screen of human kinases and phosphatases identifies new regulators of apoptosis and chemoresistance. *Nat Cell Biol,* 7**,** 591-600.

MALENTACCHI, F., MARZOCCHINI, R., GELMINI, S., ORLANDO, C., SERIO, M., RAMPONI, G. & RAUGEI, G. 2005. Up-regulated expression of low molecular weight protein tyrosine phosphatases in different human cancers. *Biochem Biophys Res Commun,* 334**,** 875-83.

MALONE, C. F. & STEGMAIER, K. 2017. Scratching the Surface of Immunotherapeutic Targets in Neuroblastoma. *Cancer Cell,* 32**,** 271-273.

MANNA, S., DAS, S., CHATTERJEE, M. & JANARTHAN, M. 2011. Combined supplementation of vanadium and fish oil suppresses tumor growth, cell proliferation and induces apoptosis in DMBA-induced rat mammary carcinogenesis. *J Cell Biochem,* 112**,** 2327-39.

MARAMPON, F., BOSSI, G., CICCARELLI, C., DI ROCCO, A., SACCHI, A., PESTELL, R. G. & ZANI, B. M. 2009. MEK/ERK inhibitor U0126 affects in vitro and in vivo growth of embryonal rhabdomyosarcoma. *Mol Cancer Ther,* 8**,** 543-51.

MARENGO, B., DE CIUCIS, C., VERZOLA, D., PISTOIA, V., RAFFAGHELLO, L., PATRIARCA, S., BALBIS, E., TRAVERSO, N., COTTALASSO, D., PRONZATO, M. A., MARINARI, U. M. & DOMENICOTTI, C. 2008. Mechanisms of BSO (L-buthionine-S,R-sulfoximine)-induced cytotoxic effects in neuroblastoma. *Free Radic Biol Med,* 44**,** 474-82.

MARIS, J. M. 2010. Recent advances in neuroblastoma. *N Engl J Med,* 362**,** 2202-11.

MARSHALL, N. J., GOODWIN, C. J. & HOLT, S. J. 1995. A critical assessment of the use of microculture tetrazolium assays to measure cell growth and function. *Growth Regul,* 5**,** 69-84.

MARTIN, C., BERRIDGE, G., MISTRY, P., HIGGINS, C., CHARLTON, P. & CALLAGHAN, R. 2000. Drug binding sites on P-glycoprotein are altered by ATP binding prior to nucleotide hydrolysis. *Biochemistry,* 39**,** 11901-6.

MARTIN, C. A., AHMAD, I., KLINGSEISEN, A., HUSSAIN, M. S., BICKNELL, L. S., LEITCH, A., NÜRNBERG, G., TOLIAT, M. R., MURRAY, J. E., HUNT, D., KHAN, F., ALI, Z., TINSCHERT, S., DING, J., KEITH, C., HARLEY, M. E., HEYN, P., MÜLLER, R., HOFFMANN, I., CORMIER-DAIRE, V., DOLLFUS, H., DUPUIS, L., BASHAMBOO, A., MCELREAVEY, K., KARIMINEJAD, A., MENDOZA-LONDONO, R., MOORE, A. T., SAGGAR, A., SCHLECHTER, C., WELEBER, R., THIELE, H., ALTMÜLLER, J., HÖHNE, W., HURLES, M. E., NOEGEL, A. A., BAIG, S. M., NÜRNBERG, P. & JACKSON, A. P. 2014. Mutations in PLK4, encoding a master regulator of centriole biogenesis, cause microcephaly, growth failure and retinopathy. *Nat Genet,* 46**,** 1283-1292.

MARTINEZ, S. E., WU, A. Y., GLAVAS, N. A., TANG, X. B., TURLEY, S., HOL, W. G. & BEAVO, J. A. 2002. The two GAF domains in phosphodiesterase 2A have distinct roles in dimerization and in cGMP binding. *Proc Natl Acad Sci U S A,* 99**,** 13260-5.

MARTINS, T. J., MUMBY, M. C. & BEAVO, J. A. 1982. Purification and characterization of a cyclic GMP-stimulated cyclic nucleotide phosphodiesterase from bovine tissues. *J Biol Chem,* 257**,** 1973-9.

MATOZAKI, T., MURATA, Y., SAITO, Y., OKAZAWA, H. & OHNISHI, H. 2009. Protein tyrosine phosphatase SHP-2: a proto-oncogene product that promotes Ras activation. *Cancer Sci,* 100**,** 1786-93.

MATSUMURA, Y. & MAEDA, H. 1986. A new concept for macromolecular therapeutics in cancer chemotherapy: mechanism of tumoritropic accumulation of proteins and the antitumor agent smancs. *Cancer Res,* 46**,** 6387-92.

MATTHAY, K. K., MARIS, J. M., SCHLEIERMACHER, G., NAKAGAWARA, A., MACKALL, C. L., DILLER, L. & WEISS, W. A. 2016. Neuroblastoma. *Nat Rev Dis Primers,* 2**,** 16078.

MCCUBREY, J. A., STEELMAN, L. S., CHAPPELL, W. H., ABRAMS, S. L., WONG, E. W., CHANG, F., LEHMANN, B., TERRIAN, D. M., MILELLA, M., TAFURI, A., STIVALA, F., LIBRA, M., BASECKE, J., EVANGELISTI, C., MARTELLI, A. M. & FRANKLIN, R. A. 2007. Roles of the Raf/MEK/ERK pathway in cell growth, malignant transformation and drug resistance. *Biochim Biophys Acta,* 1773**,** 1263-84.

MCNEILL, J. H., YUEN, V. G., HOVEYDA, H. R. & ORVIG, C. 1992. Bis(maltolato)oxovanadium(IV) is a potent insulin mimic. *J Med Chem,* 35**,** 1489-91.

MCQUEENEY, K. E., SALAMOUN, J. M., BURNETT, J. C., BARABUTIS, N., PEKIC, P., LEWANDOWSKI, S. L., LLANEZA, D. C., CORNELISON, R., BAI, Y., ZHANG, Z. Y., CATRAVAS, J. D., LANDEN, C. N., WIPF, P., LAZO, J. S. & SHARLOW, E. R. 2018. Targeting ovarian cancer and endothelium with an allosteric PTP4A3 phosphatase inhibitor. *Oncotarget,* 9**,** 8223-8240.

MEHDI, M. Z., PANDEY, S. K., THÉBERGE, J. F. & SRIVASTAVA, A. K. 2006. Insulin signal mimicry as a mechanism for the insulin-like effects of vanadium. *Cell Biochem Biophys,* 44**,** 73-81.

MEIJERING, E., JACOB, M., SARRIA, J. C., STEINER, P., HIRLING, H. & UNSER, M. 2004. Design and validation of a tool for neurite tracing and analysis in fluorescence microscopy images. *Cytometry A,* 58**,** 167-76.

MEKARU, H., LU, J. & TAMANOI, F. 2015. Development of mesoporous silica-based nanoparticles with controlled release capability for cancer therapy. *Adv Drug Deliv Rev,* 95**,** 40-9.
MESHKINI, A. & YAZDANPARAST, R. 2010. Chemosensitization of human leukemia K562 cells to taxol by a Vanadium-salen complex. *Exp Mol Pathol,* 89**,** 334-42.
MEYEROVITCH, J., FARFEL, Z., SACK, J. & SHECHTER, Y. 1987. Oral administration of vanadate normalizes blood glucose levels in streptozotocin-treated rats. Characterization and mode of action. *J Biol Chem,* 262**,** 6658-62.
MIELE, E., SPINELLI, G. P., TOMAO, F. & TOMAO, S. 2009. Albumin-bound formulation of paclitaxel (Abraxane ABI-007) in the treatment of breast cancer. *Int J Nanomedicine,* 4**,** 99-105.
MILLER, R. W., YOUNG, J. L. & NOVAKOVIC, B. 1995. Childhood cancer. *Cancer,* 75**,** 395-405.
MISKAD, U. A., SEMBA, S., KATO, H., MATSUKAWA, Y., KODAMA, Y., MIZUUCHI, E., MAEDA, N., YANAGIHARA, K. & YOKOZAKI, H. 2007. High PRL-3 expression in human gastric cancer is a marker of metastasis and grades of malignancies: an in situ hybridization study. *Virchows Arch,* 450**,** 303-10.
MISKAD, U. A., SEMBA, S., KATO, H. & YOKOZAKI, H. 2004. Expression of PRL-3 phosphatase in human gastric carcinomas: close correlation with invasion and metastasis. *Pathobiology,* 71**,** 176-84.
MITRA, A., KALAYARASAN, S., GUPTA, V. & RADHA, V. 2011. TC-PTP dephosphorylates the guanine nucleotide exchange factor C3G (RapGEF1) and negatively regulates differentiation of human neuroblastoma cells. *PLoS One,* 6**,** e23681.
MOCCIARO, A., BERDOUGO, E., ZENG, K., BLACK, E., VAGNARELLI, P., EARNSHAW, W., GILLESPIE, D., JALLEPALLI, P. & SCHIEBEL, E. 2010. Vertebrate cells genetically deficient for Cdc14A or Cdc14B retain DNA damage checkpoint proficiency but are impaired in DNA repair. *J Cell Biol,* 189**,** 631-9.
MOCCIARO, A. & SCHIEBEL, E. 2010. Cdc14: a highly conserved family of phosphatases with non-conserved functions? *J Cell Sci,* 123**,** 2867-76.
MOHAMMAD, A., WANG, J. & MCNEILL, J. H. 2002. Bis(maltolato)oxovanadium(IV) inhibits the activity of PTP1B in Zucker rat skeletal muscle in vivo. *Mol Cell Biochem,* 229**,** 125-8.
MOLINUEVO, M. S., CORTIZO, A. M. & ETCHEVERRY, S. B. 2008. Vanadium(IV) complexes inhibit adhesion, migration and colony formation of UMR106 osteosarcoma cells. *Cancer Chemother Pharmacol,* 61**,** 767-73.
MONCLAIR, T., BRODEUR, G., AMBROS, P., BRISSE, H., CECCHETTO, G., HOLMES, K., KANEKO, M., LONDON, W., MATTHAY, K., NUCHTERN, J., VON SCHWEINITZ, D., SIMON, T., COHN, S. & PEARSON, A. 2009. The International Neuroblastoma Risk Group (INRG) Staging System: An INRG Task Force Report. *Journal of Clinical Oncology,* 27**,** 298-303.
MONTOR, W. R., SALAS, A. R. O. S. & MELO, F. H. M. 2018. Receptor tyrosine kinases and downstream pathways as druggable targets for cancer treatment: the current arsenal of inhibitors. *Mol Cancer,* 17**,** 55.
MORGENS, D. W., DEANS, R. M., LI, A. & BASSIK, M. C. 2016. Systematic comparison of CRISPR/Cas9 and RNAi screens for essential genes. *Nat Biotechnol,* 34**,** 634-6.
MORITA, H., MURATA, T., SHIMIZU, K., OKUMURA, K., INUI, M. & TAGAWA, T. 2013. Characterization of phosphodiesterase 2A in human malignant melanoma PMP cells. *Oncol Rep,* 29**,** 1275-84.
MORITAKE, H., HORII, Y., KURODA, H. & SUGIMOTO, T. 2001. Analysis of PTEN/MMAC1 alteration in neuroblastoma. *Cancer Genet Cytogenet,* 125**,** 151-5.
MOSMANN, T. 1983. Rapid colorimetric assay for cellular growth and survival: application to proliferation and cytotoxicity assays. *J Immunol Methods,* 65**,** 55-63.
MOSSE, Y., LAUDENSLAGER, M., LONGO, L., COLE, K., WOOD, A., ATTIYEH, E., LAQUAGLIA, M., SENNETT, R., LYNCH, J., PERRI, P., LAUREYS, G., SPELEMAN, F., KIM, C., HOU, C., HAKONARSON, H., TORKAMANI, A., SCHORK, N., BRODEUR, G., TONINI, G., RAPPAPORT, E., DEVOTO, M. & MARIS, J. 2008. Identification of ALK as a major familial neuroblastoma predisposition gene. *Nature,* 455**,** 930-U22.
MOSSÉ, Y. P., LIM, M. S., VOSS, S. D., WILNER, K., RUFFNER, K., LALIBERTE, J., ROLLAND, D., BALIS, F. M., MARIS, J. M., WEIGEL, B. J., INGLE, A. M., AHERN, C., ADAMSON, P. C. & BLANEY, S. M. 2013. Safety and activity of crizotinib for paediatric

patients with refractory solid tumours or anaplastic large-cell lymphoma: a Children's Oncology Group phase 1 consortium study. *Lancet Oncol,* 14**,** 472-80.
MOSSÉ, Y. P., LIPSITZ, E., FOX, E., TEACHEY, D. T., MARIS, J. M., WEIGEL, B., ADAMSON, P. C., INGLE, M. A., AHERN, C. H. & BLANEY, S. M. 2012. Pediatric phase I trial and pharmacokinetic study of MLN8237, an investigational oral selective small-molecule inhibitor of Aurora kinase A: a Children's Oncology Group Phase I Consortium study. *Clin Cancer Res,* 18**,** 6058-64.
MOTIWALA, T. & JACOB, S. T. 2006. Role of protein tyrosine phosphatases in cancer. *Prog Nucleic Acid Res Mol Biol,* 81**,** 297-329.
MUÑOZ, J., LÁZCOZ, P., INDA, M. M., NISTAL, M., PESTAÑA, A., ENCÍO, I. J. & CASTRESANA, J. S. 2004. Homozygous deletion and expression of PTEN and DMBT1 in human primary neuroblastoma and cell lines. *Int J Cancer,* 109**,** 673-9.
MURATA, K., SUDO, T., KAMEYAMA, M., FUKUOKA, H., MUKA, M., DOKI, Y., SASAKI, Y., ISHIKAWA, O., KIMURA, Y. & IMAOKA, S. 2000. Cyclic AMP specific phosphodiesterase activity and colon cancer cell motility. *Clin Exp Metastasis,* 18**,** 599-604.
NAIR, R. S., KURIAKOSE, M., SOMASUNDARAM, V., SHENOI, V., KURUP, M. R. & SRINIVAS, P. 2014. The molecular response of vanadium complexes of nicotinoyl hydrazone in cervical cancers--a possible interference with HPV oncogenic markers. *Life Sci,* 116**,** 90-7.
NANDURKAR, H. H., CALDWELL, K. K., WHISSTOCK, J. C., LAYTON, M. J., GAUDET, E. A., NORRIS, F. A., MAJERUS, P. W. & MITCHELL, C. A. 2001. Characterization of an adapter subunit to a phosphatidylinositol (3)P 3-phosphatase: identification of a myotubularin-related protein lacking catalytic activity. *Proc Natl Acad Sci U S A,* 98**,** 9499-504.
NANDURKAR, H. H., LAYTON, M., LAPORTE, J., SELAN, C., CORCORAN, L., CALDWELL, K. K., MOCHIZUKI, Y., MAJERUS, P. W. & MITCHELL, C. A. 2003. Identification of myotubularin as the lipid phosphatase catalytic subunit associated with the 3-phosphatase adapter protein, 3-PAP. *Proc Natl Acad Sci U S A,* 100**,** 8660-5.
NARAYAN, R. S., FEDRIGO, C. A., BRANDS, E., DIK, R., STALPERS, L. J., BAUMERT, B. G., SLOTMAN, B. J., WESTERMAN, B. A., PETERS, G. J. & SMINIA, P. 2017. The allosteric AKT inhibitor MK2206 shows a synergistic interaction with chemotherapy and radiotherapy in glioblastoma spheroid cultures. *BMC Cancer,* 17**,** 204.
NARLA, R. K., CHEN, C. L., DONG, Y. & UCKUN, F. M. 2001. In vivo antitumor activity of bis(4,7-dimethyl-1,10-phenanthroline) sulfatooxovanadium(IV) (METVAN [VO(SO4)(Me2-Phen)2]). *Clin Cancer Res,* 7**,** 2124-33.
NAVARA, C. S., BENYUMOV, A., VASSILEV, A., NARLA, R. K., GHOSH, P. & UCKUN, F. M. 2001. Vanadocenes as potent anti-proliferative agents disrupting mitotic spindle formation in cancer cells. *Anticancer Drugs,* 12**,** 369-76.
NAVIGLIO, S., DI GESTO, D., ILLIANO, F., CHIOSI, E., GIORDANO, A., ILLIANO, G. & SPINA, A. 2010. Leptin potentiates antiproliferative action of cAMP elevation via protein kinase A down-regulation in breast cancer cells. *J Cell Physiol,* 225**,** 801-9.
NECHAY, B. R. 1984. Mechanisms of action of vanadium. *Annu Rev Pharmacol Toxicol,* 24**,** 501-24.
NESSET, C. K., KONG, X. Y., DAMME, M., SCHJALM, C., ROOS, N., LØBERG, E. M. & ESKILD, W. 2016. Age-dependent development of liver fibrosis in Glmp (gt/gt) mice. *Fibrogenesis Tissue Repair,* 9**,** 5.
NOGUEIRA, V., PARK, Y., CHEN, C. C., XU, P. Z., CHEN, M. L., TONIC, I., UNTERMAN, T. & HAY, N. 2008. Akt determines replicative senescence and oxidative or oncogenic premature senescence and sensitizes cells to oxidative apoptosis. *Cancer Cell,* 14**,** 458-70.
NOTARANGELO, L. D., SAVOLDI, G., CAVAGNINI, S., BENNATO, V., VASILE, S., PILOTTA, A., PLEBANI, A. & PORTA, F. 2014. Severe congenital neutropenia due to G6PC3 deficiency: early and delayed phenotype in two patients with two novel mutations. *Ital J Pediatr,* 40**,** 80.
O'BRIEN, J., WILSON, I., ORTON, T. & POGNAN, F. 2000. Investigation of the Alamar Blue (resazurin) fluorescent dye for the assessment of mammalian cell cytotoxicity. *Eur J Biochem,* 267**,** 5421-6.
O'BRIEN, S. G. & DEININGER, M. W. 2003. Imatinib in patients with newly diagnosed chronic-phase chronic myeloid leukemia. *Semin Hematol,* 40**,** 26-30.

O'BRIEN, S. G., GUILHOT, F., LARSON, R. A., GATHMANN, I., BACCARANI, M., CERVANTES, F., CORNELISSEN, J. J., FISCHER, T., HOCHHAUS, A., HUGHES, T., LECHNER, K., NIELSEN, J. L., ROUSSELOT, P., REIFFERS, J., SAGLIO, G., SHEPHERD, J., SIMONSSON, B., GRATWOHL, A., GOLDMAN, J. M., KANTARJIAN, H., TAYLOR, K., VERHOEF, G., BOLTON, A. E., CAPDEVILLE, R., DRUKER, B. J. & INVESTIGATORS, I. 2003. Imatinib compared with interferon and low-dose cytarabine for newly diagnosed chronic-phase chronic myeloid leukemia. *N Engl J Med,* 348**,** 994-1004.

O'CONNOR, M. J. 2015. Targeting the DNA Damage Response in Cancer. *Mol Cell,* 60**,** 547-60.

OGAWA, S., TAKITA, J., SANADA, M. & HAYASHI, Y. 2011. Oncogenic mutations of ALK in neuroblastoma. *Cancer Sci,* 102**,** 302-8.

OGHABI BAKHSHAIESH, T., MAJIDZADEH-A, K. & ESMAEILI R. 2017. Wip1: A candidate phosphatase for cancer diagnosis and treatment. *DNA Repair (Amst),* 54**,** 63-66.

OLSEN, E., DUVIC, M., FRANKEL, A., KIM, Y., MARTIN, A., VONDERHEID, E., JEGASOTHY, B., WOOD, G., GORDON, M., HEALD, P., OSEROFF, A., PINTER-BROWN, L., BOWEN, G., KUZEL, T., FIVENSON, D., FOSS, F., GLODE, M., MOLINA, A., KNOBLER, E., STEWART, S., COOPER, K., STEVENS, S., CRAIG, F., REUBEN, J., BACHA, P. & NICHOLS, J. 2001. Pivotal phase III trial of two dose levels of denileukin diftitox for the treatment of cutaneous T-cell lymphoma. *J Clin Oncol,* 19**,** 376-88.

OMEROVIC, J., CLAGUE, M. J. & PRIOR, I. A. 2010. Phosphatome profiling reveals PTPN2, PTPRJ and PTEN as potent negative regulators of PKB/Akt activation in Ras-mutated cancer cells. *Biochem J,* 426**,** 65-72.

OSTMAN, A. & BÖHMER, F. D. 2001. Regulation of receptor tyrosine kinase signaling by protein tyrosine phosphatases. *Trends Cell Biol,* 11**,** 258-66.

OSTMAN, A., FRIJHOFF, J., SANDIN, A. & BÖHMER, F. D. 2011. Regulation of protein tyrosine phosphatases by reversible oxidation. *J Biochem,* 150**,** 345-56.

OSTMAN, A., HELLBERG, C. & BÖHMER, F. D. 2006. Protein-tyrosine phosphatases and cancer. *Nat Rev Cancer,* 6**,** 307-20.

OTTO, T., HORN, S., BROCKMANN, M., EILERS, U., SCHÜTTRUMPF, L., POPOV, N., KENNEY, A. M., SCHULTE, J. H., BEIJERSBERGEN, R., CHRISTIANSEN, H., BERWANGER, B. & EILERS, M. 2009. Stabilization of N-Myc is a critical function of Aurora A in human neuroblastoma. *Cancer Cell,* 15**,** 67-78.

PANWAR, P., PANDEY, B., LAKHERA, P. C. & SINGH, K. P. 2010. Preparation, characterization, and in vitro release study of albendazole-encapsulated nanosize liposomes. *Int J Nanomedicine,* 5**,** 101-8.

PARK, J., BAGATELL, R., LONDON, W., MARIS, J., COHN, S., MATTAY, K., HOGARTY, M., COMM, C. N. & COMM, C. N. 2013. Children's Oncology Group's 2013 blueprint for research: Neuroblastoma. *Pediatric Blood & Cancer,* 60**,** 985-993.

PARKER, R. D., SHARMA, R. P. & OBERG, S. G. 1980. Distribution and accumulation of vanadium in mice tissues. *Arch Environ Contam Toxicol,* 9**,** 393-403.

PATTABIRAMAN, D. R., BIERIE, B., KOBER, K. I., THIRU, P., KRALL, J. A., ZILL, C., REINHARDT, F., TAM, W. L. & WEINBERG, R. A. 2016. Activation of PKA leads to mesenchymal-to-epithelial transition and loss of tumor-initiating ability. *Science,* 351**,** aad3680.

PATTERSON, K. I., BRUMMER, T., O'BRIEN, P. M. & DALY, R. J. 2009. Dual-specificity phosphatases: critical regulators with diverse cellular targets. *Biochem J,* 418**,** 475-89.

PEDDIBHOTLA, S., WEI, Z., PAPINENI, R., LAM, M. H., ROSEN, J. M. & ZHANG, P. 2011. The DNA damage effector Chk1 kinase regulates Cdc14B nucleolar shuttling during cell cycle progression. *Cell Cycle,* 10**,** 671-9.

PEREZ, D. R., SMAGLEY, Y., GARCIA, M., CARTER, M. B., EVANGELISTI, A., MATLAWSKA-WASOWSKA, K., WINTER, S. S., SKLAR, L. A. & CHIGAEV, A. 2016. Cyclic AMP efflux inhibitors as potential therapeutic agents for leukemia. *Oncotarget,* 7**,** 33960-82.

PETANIDIS, S., KIOSEOGLOU, E., DOMVRI, K., ZAROGOULIDIS, P., CARTHY, J. M., ANESTAKIS, D., MOUSTAKAS, A. & SALIFOGLOU, A. 2016. In vitro and ex vivo vanadium antitumor activity in (TGF-β)-induced EMT. Synergistic activity with carboplatin and correlation with tumor metastasis in cancer patients. *Int J Biochem Cell Biol,* 74**,** 121-34.

PETANIDIS, S., KIOSEOGLOU, E., HADZOPOULOU-CLADARAS, M. & SALIFOGLOU, A. 2013. Novel ternary vanadium-betaine-peroxido species suppresses H-ras and matrix

metalloproteinase-2 expression by increasing reactive oxygen species-mediated apoptosis in cancer cells. *Cancer Lett,* 335**,** 387-96.

PETERS, K. G., DAVIS, M. G., HOWARD, B. W., POKROSS, M., RASTOGI, V., DIVEN, C., GREIS, K. D., EBY-WILKENS, E., MAIER, M., EVDOKIMOV, A., SOPER, S. & GENBAUFFE, F. 2003. Mechanism of insulin sensitization by BMOV (bis maltolato oxo vanadium); unliganded vanadium (VO4) as the active component. *J Inorg Biochem,* 96**,** 321-30.

PEZZA, R. J., VILLARREAL, M. A., MONTICH, G. G. & ARGARAÑA, C. E. 2002. Vanadate inhibits the ATPase activity and DNA binding capability of bacterial MutS. A structural model for the vanadate-MutS interaction at the Walker A motif. *Nucleic Acids Res,* 30**,** 4700-8.

PHORNPHUTKUL, C., ANIKSTER, Y., HUIZING, M., BRAUN, P., BRODIE, C., CHOU, J. Y. & GAHL, W. A. 2001. The promoter of a lysosomal membrane transporter gene, CTNS, binds Sp-1, shares sequences with the promoter of an adjacent gene, CARKL, and causes cystinosis if mutated in a critical region. *Am J Hum Genet,* 69**,** 712-21.

PINTO, N., APPLEBAUM, M., VOLCHENBOUM, S., MATTHAY, K., LONDON, W., AMBROS, P., NAKAGAWARA, A., BERTHOLD, F., SCHLEIERMACHER, G., PARK, J., VALTEAU-COUANET, D., PEARSON, A. & COHN, S. 2015. Advances in Risk Classification and Treatment Strategies for Neuroblastoma. *Journal of Clinical Oncology,* 33**,** 3008-U105.

PLOTKIN, J. B. & KUDLA, G. 2011. Synonymous but not the same: the causes and consequences of codon bias. *Nat Rev Genet,* 12**,** 32-42.

POUCHERET, P., VERMA, S., GRYNPAS, M. D. & MCNEILL, J. H. 1998. Vanadium and diabetes. *Mol Cell Biochem,* 188**,** 73-80.

PUGH, T. J., MOROZOVA, O., ATTIYEH, E. F., ASGHARZADEH, S., WEI, J. S., AUCLAIR, D., CARTER, S. L., CIBULSKIS, K., HANNA, M., KIEZUN, A., KIM, J., LAWRENCE, M. S., LICHENSTEIN, L., MCKENNA, A., PEDAMALLU, C. S., RAMOS, A. H., SHEFLER, E., SIVACHENKO, A., SOUGNEZ, C., STEWART, C., ALLY, A., BIROL, I., CHIU, R., CORBETT, R. D., HIRST, M., JACKMAN, S. D., KAMOH, B., KHODABAKSHI, A. H., KRZYWINSKI, M., LO, A., MOORE, R. A., MUNGALL, K. L., QIAN, J., TAM, A., THIESSEN, N., ZHAO, Y., COLE, K. A., DIAMOND, M., DISKIN, S. J., MOSSE, Y. P., WOOD, A. C., JI, L., SPOSTO, R., BADGETT, T., LONDON, W. B., MOYER, Y., GASTIER-FOSTER, J. M., SMITH, M. A., GUIDRY AUVIL, J. M., GERHARD, D. S., HOGARTY, M. D., JONES, S. J., LANDER, E. S., GABRIEL, S. B., GETZ, G., SEEGER, R. C., KHAN, J., MARRA, M. A., MEYERSON, M. & MARIS, J. M. 2013. The genetic landscape of high-risk neuroblastoma. *Nat Genet,* 45**,** 279-84.

PUISSANT, A., FRUMM, S. M., ALEXE, G., BASSIL, C. F., QI, J., CHANTHERY, Y. H., NEKRITZ, E. A., ZEID, R., GUSTAFSON, W. C., GRENINGER, P., GARNETT, M. J., MCDERMOTT, U., BENES, C. H., KUNG, A. L., WEISS, W. A., BRADNER, J. E. & STEGMAIER, K. 2013. Targeting MYCN in neuroblastoma by BET bromodomain inhibition. *Cancer Discov,* 3**,** 308-23.

PULIDO, R. & HOOFT VAN HUIJSDUIJNEN, R. 2008. Protein tyrosine phosphatases: dual-specificity phosphatases in health and disease. *FEBS J,* 275**,** 848-66.

RADHA, V., NAMBIRAJAN, S. & SWARUP, G. 1994. Subcellular localization of a protein-tyrosine phosphatase: evidence for association with chromatin. *Biochem J,* 299 (Pt 1)**,** 41-7.

RADHA, V., RAJANNA, A., GUPTA, R. K., DAYMA, K. & RAMAN, T. 2008. The guanine nucleotide exchange factor, C3G regulates differentiation and survival of human neuroblastoma cells. *J Neurochem,* 107**,** 1424-35.

RADKE, I., GÖTTE, M., KERSTING, C., MATTSSON, B., KIESEL, L. & WÜLFING, P. 2006. Expression and prognostic impact of the protein tyrosine phosphatases PRL-1, PRL-2, and PRL-3 in breast cancer. *Br J Cancer,* 95**,** 347-54.

RAESS, M. A., FRIANT, S., COWLING, B. S. & LAPORTE, J. 2017. WANTED - Dead or alive: Myotubularins, a large disease-associated protein family. *Adv Biol Regul,* 63**,** 49-58.

RAJ, L., IDE, T., GURKAR, A. U., FOLEY, M., SCHENONE, M., LI, X., TOLLIDAY, N. J., GOLUB, T. R., CARR, S. A., SHAMJI, A. F., STERN, A. M., MANDINOVA, A., SCHREIBER, S. L. & LEE, S. W. 2011. Selective killing of cancer cells by a small molecule targeting the stress response to ROS. *Nature,* 475**,** 231-4.

RALL, T. W. & SUTHERLAND, E. W. 1958. Formation of a cyclic adenine ribonucleotide by tissue particles. *J Biol Chem,* 232**,** 1065-76.

RAMOS-NINO, M. E., TIMBLIN, C. R. & MOSSMAN, B. T. 2002. Mesothelial cell transformation requires increased AP-1 binding activity and ERK-dependent Fra-1 expression. *Cancer Res,* 62**,** 6065-9.
RAN, F. A., HSU, P. D., WRIGHT, J., AGARWALA, V., SCOTT, D. A. & ZHANG, F. 2013. Genome engineering using the CRISPR-Cas9 system. *Nat Protoc,* 8**,** 2281-2308.
RAUGEI, G., RAMPONI, G. & CHIARUGI, P. 2002. Low molecular weight protein tyrosine phosphatases: small, but smart. *Cell Mol Life Sci,* 59**,** 941-9.
RAY, R. S., BASU, M., GHOSH, B., SAMANTA, K. & CHATTERJEE, M. 2005. Vanadium, a versatile biochemical effector in chemical rat mammary carcinogenesis. *Nutr Cancer,* 51**,** 184-96.
RAY, R. S., GHOSH, B., RANA, A. & CHATTERJEE, M. 2007. Suppression of cell proliferation, induction of apoptosis and cell cycle arrest: chemopreventive activity of vanadium in vivo and in vitro. *Int J Cancer,* 120**,** 13-23.
RAYAPUREDDI, J. P., KATTAMURI, C., STEINMETZ, B. D., FRANKFORT, B. J., OSTRIN, E. J., MARDON, G. & HEGDE, R. S. 2003. Eyes absent represents a class of protein tyrosine phosphatases. *Nature,* 426**,** 295-8.
REHDER, D. 2012. The potentiality of vanadium in medicinal applications. *Future Med Chem,* 4**,** 1823-37.
REHDER, D. 2013. Vanadium. Its role for humans. *Met Ions Life Sci,* 13**,** 139-69.
REINHARDT, H. C. & SCHUMACHER, B. 2012. The p53 network: cellular and systemic DNA damage responses in aging and cancer. *Trends Genet,* 28**,** 128-36.
RESS, N. B., CHOU, B. J., RENNE, R. A., DILL, J. A., MILLER, R. A., ROYCROFT, J. H., HAILEY, J. R., HASEMAN, J. K. & BUCHER, J. R. 2003. Carcinogenicity of inhaled vanadium pentoxide in F344/N rats and B6C3F1 mice. *Toxicol Sci,* 74**,** 287-96.
REYTMAN, L., BRAITBARD, O., HOCHMAN, J. & TSHUVA, E. Y. 2016. Highly Effective and Hydrolytically Stable Vanadium(V) Amino Phenolato Antitumor Agents. *Inorg Chem,* 55**,** 610-8.
RICHARDS, M. W., BURGESS, S. G., POON, E., CARSTENSEN, A., EILERS, M., CHESLER, L. & BAYLISS, R. 2016. Structural basis of N-Myc binding by Aurora-A and its destabilization by kinase inhibitors. *Proc Natl Acad Sci U S A,* 113**,** 13726-13731.
RIVERA, H., MARTÍN-HERNÁNDEZ, E., DELMIRO, A., GARCÍA-SILVA, M. T., QUIJADA-FRAILE, P., MULEY, R., ARENAS, J., MARTÍN, M. A. & MARTÍNEZ-AZORÍN, F. 2013. A new mutation in the gene encoding mitochondrial seryl-tRNA synthetase as a cause of HUPRA syndrome. *BMC Nephrol,* 14**,** 195.
RIZVI, S. A. A. & SALEH, A. M. 2018. Applications of nanoparticle systems in drug delivery technology. *Saudi Pharm J,* 26**,** 64-70.
ROBINSON, D. R., WU, Y. M. & LIN, S. F. 2000. The protein tyrosine kinase family of the human genome. *Oncogene,* 19**,** 5548-57.
ROBINSON, M. D., MCCARTHY, D. J. & SMYTH, G. K. 2010. edgeR: a Bioconductor package for differential expression analysis of digital gene expression data. *Bioinformatics,* 26**,** 139-40.
RODRÍGUEZ-NOGALES, C., GONZÁLEZ-FERNÁNDEZ, Y., ALDAZ, A., COUVREUR, P. & BLANCO-PRIETO, M. J. 2018. Nanomedicines for Pediatric Cancers. *ACS Nano,* 12**,** 7482-7496.
ROGERS, M. V., BUENSUCESO, C., MONTAGUE, F. & MAHADEVAN, L. 1994. Vanadate stimulates differentiation and neurite outgrowth in rat pheochromocytoma PC12 cells and neurite extension in human neuroblastoma SH-SY5Y cells. *Neuroscience,* 60**,** 479-94.
ROSENZWEIG, S. A. 2012. Acquired resistance to drugs targeting receptor tyrosine kinases. *Biochem Pharmacol,* 83**,** 1041-8.
ROSSI, A., KONTARAKIS, Z., GERRI, C., NOLTE, H., HÖLPER, S., KRÜGER, M. & STAINIER, D. Y. 2015. Genetic compensation induced by deleterious mutations but not gene knockdowns. *Nature,* 524**,** 230-3.
ROZZO, C., SANNA, D., GARRIBBA, E., SERRA, M., CANTARA, A., PALMIERI, G. & PISANO, M. 2017. Antitumoral effect of vanadium compounds in malignant melanoma cell lines. *J Inorg Biochem,* 174**,** 14-24.
RUSSWURM, C., ZOIDL, G., KOESLING, D. & RUSSWURM, M. 2009. Dual acylation of PDE2A splice variant 3: targeting to synaptic membranes. *J Biol Chem,* 284**,** 25782-90.
SAHA, S., BARDELLI, A., BUCKHAULTS, P., VELCULESCU, V. E., RAGO, C., ST CROIX, B., ROMANS, K. E., CHOTI, M. A., LENGAUER, C., KINZLER, K. W. & VOGELSTEIN, B.

2001. A phosphatase associated with metastasis of colorectal cancer. *Science,* 294**,** 1343-6.
SAIJO, N. 2012. Present status and problems on molecular targeted therapy of cancer. *Cancer Res Treat,* 44**,** 1-10.
SAKURAI, H., SHIMOMURA, S., FUKUZAWA, K. & ISHIZU, K. 1980. Detection of oxovanadium (IV) and characterization of its ligand environment in subcellular fractions of the liver of rats treated with pentavalent vanadium(V). *Biochem Biophys Res Commun,* 96**,** 293-8.
SÁLICE, V. C., CORTIZO, A. M., GÓMEZ DUMM, C. L. & ETCHEVERRY, S. B. 1999. Tyrosine phosphorylation and morphological transformation induced by four vanadium compounds on MC3T3E1 cells. *Mol Cell Biochem,* 198**,** 119-28.
SALMEEN, A., ANDERSEN, J. N., MYERS, M. P., MENG, T. C., HINKS, J. A., TONKS, N. K. & BARFORD, D. 2003. Redox regulation of protein tyrosine phosphatase 1B involves a sulphenyl-amide intermediate. *Nature,* 423**,** 769-73.
SALMEEN, A., ANDERSEN, J. N., MYERS, M. P., TONKS, N. K. & BARFORD, D. 2000. Molecular basis for the dephosphorylation of the activation segment of the insulin receptor by protein tyrosine phosphatase 1B. *Mol Cell,* 6**,** 1401-12.
SALOMON, D. S., BRANDT, R., CIARDIELLO, F. & NORMANNO, N. 1995. Epidermal growth factor-related peptides and their receptors in human malignancies. *Crit Rev Oncol Hematol,* 19**,** 183-232.
SAMANTA, S., CHATTERJEE, M., GHOSH, B., RAJKUMAR, M. & RANA, A. 2008a. Vanadium and 1, 25 (OH)2 vitamin D3 combination in inhibitions of 1,2, dimethylhydrazine-induced rat colon carcinogenesis. *Biochim Biophys Acta,* 1780**,** 1106-14.
SAMANTA, S., SWAMY, V., SURESH, D., RAJKUMAR, M., RANA, B., RANA, A. & CHATTERJEE, M. 2008b. Protective effects of vanadium against DMH-induced genotoxicity and carcinogenesis in rat colon: removal of O(6)-methylguanine DNA adducts, p53 expression, inducible nitric oxide synthase downregulation and apoptotic induction. *Mutat Res,* 650**,** 123-31.
SÁNCHEZ-LOMBARDO, I., ALVAREZ, S., MCLAUCHLAN, C. C. & CRANS, D. C. 2015. Evaluating transition state structures of vanadium-phosphatase protein complexes using shape analysis. *J Inorg Biochem,* 147**,** 153-64.
SANKAR RAY, R., ROY, S., GHOSH, S., KUMAR, M. & CHATTERJEE, M. 2004. Suppression of cell proliferation, DNA protein cross-links, and induction of apoptosis by vanadium in chemical rat mammary carcinogenesis. *Biochim Biophys Acta,* 1675**,** 165-73.
SANKAR RAY, R., ROY, S., SAMANTA, S., MAITRA, D. & CHATTERJEE, M. 2005. Protective role of vanadium on the early process of rat mammary carcinogenesis by influencing expression of metallothionein, GGT-positive foci and DNA fragmentation. *Cell Biochem Funct,* 23**,** 447-56.
SANNA, D., UGONE, V., MICERA, G., BUGLYÓ, P., BÍRÓ, L. & GARRIBBA, E. 2017. Speciation in human blood of Metvan, a vanadium based potential anti-tumor drug. *Dalton Trans,* 46**,** 8950-8967.
SANTARPIA, L., LIPPMAN, S. M. & EL-NAGGAR, A. K. 2012. Targeting the MAPK-RAS-RAF signaling pathway in cancer therapy. *Expert Opin Ther Targets,* 16**,** 103-19.
SAPIO, L., GALLO, M., ILLIANO, M., CHIOSI, E., NAVIGLIO, D., SPINA, A. & NAVIGLIO, S. 2017. The Natural cAMP Elevating Compound Forskolin in Cancer Therapy: Is It Time? *J Cell Physiol,* 232**,** 922-927.
SCALESE, G., MOSQUILLO, M. F., ROSTÁN, S., CASTIGLIONI, J., ALHO, I., PÉREZ, L., CORREIA, I., MARQUES, F., COSTA PESSOA, J. & GAMBINO, D. 2017. Heteroleptic oxidovanadium(IV) complexes of 2-hydroxynaphtylaldimine and polypyridyl ligands against Trypanosoma cruzi and prostate cancer cells. *J Inorg Biochem,* 175**,** 154-166.
SCHINDELIN, J., ARGANDA-CARRERAS, I., FRISE, E., KAYNIG, V., LONGAIR, M., PIETZSCH, T., PREIBISCH, S., RUEDEN, C., SAALFELD, S., SCHMID, B., TINEVEZ, J. Y., WHITE, D. J., HARTENSTEIN, V., ELICEIRI, K., TOMANCAK, P. & CARDONA, A. 2012. Fiji: an open-source platform for biological-image analysis. *Nat Methods,* 9**,** 676-82.
SCHINDELIN, J., RUEDEN, C. T., HINER, M. C. & ELICEIRI, K. W. 2015. The ImageJ ecosystem: An open platform for biomedical image analysis. *Mol Reprod Dev,* 82**,** 518-29.
SCHNEIDER, C. A., RASBAND, W. S. & ELICEIRI, K. W. 2012. NIH Image to ImageJ: 25 years of image analysis. *Nat Methods,* 9**,** 671-5.

SCHROEDER, A., MUELLER, O., STOCKER, S., SALOWSKY, R., LEIBER, M., GASSMANN, M., LIGHTFOOT, S., MENZEL, W., GRANZOW, M. & RAGG, T. 2006. The RIN: an RNA integrity number for assigning integrity values to RNA measurements. *BMC Mol Biol,* 7**,** 3.
SCHROEDER, H. A., BALASSA, J. J. & TIPTON, I. H. 1963. Abnormal Trace Metals in Man -- Vanadium. *J Chronic Dis,* 16**,** 1047-71.
SCHWAB, M., ALITALO, K., KLEMPNAUER, K. H., VARMUS, H. E., BISHOP, J. M., GILBERT, F., BRODEUR, G., GOLDSTEIN, M. & TRENT, J. 1983. Amplified DNA with limited homology to myc cellular oncogene is shared by human neuroblastoma cell lines and a neuroblastoma tumour. *Nature,* 305**,** 245-8.
SCHWEIGERER, L., BREIT, S., WENZEL, A., TSUNAMOTO, K., LUDWIG, R. & SCHWAB, M. 1990. Augmented MYCN expression advances the malignant phenotype of human neuroblastoma cells: evidence for induction of autocrine growth factor activity. *Cancer Res,* 50**,** 4411-6.
SCIOR, T., GUEVARA-GARCIA, J. A., DO, Q. T., BERNARD, P. & LAUFER, S. 2016. Why Antidiabetic Vanadium Complexes are Not in the Pipeline of "Big Pharma" Drug Research? A Critical Review. *Curr Med Chem,* 23**,** 2874-2891.
SCRIVENS, P. J., ALAOUI-JAMALI, M. A., GIANNINI, G., WANG, T., LOIGNON, M., BATIST, G. & SANDOR, V. A. 2003. Cdc25A-inhibitory properties and antineoplastic activity of bisperoxovanadium analogues. *Mol Cancer Ther,* 2**,** 1053-9.
SEAMON, K. B., PADGETT, W. & DALY, J. W. 1981. Forskolin: unique diterpene activator of adenylate cyclase in membranes and in intact cells. *Proc Natl Acad Sci U S A,* 78**,** 3363-7.
SEEGER, R. C., BRODEUR, G. M., SATHER, H., DALTON, A., SIEGEL, S. E., WONG, K. Y. & HAMMOND, D. 1985. Association of multiple copies of the N-myc oncogene with rapid progression of neuroblastomas. *N Engl J Med,* 313**,** 1111-6.
SEELY, B. L., STAUBS, P. A., REICHART, D. R., BERHANU, P., MILARSKI, K. L., SALTIEL, A. R., KUSARI, J. & OLEFSKY, J. M. 1996. Protein tyrosine phosphatase 1B interacts with the activated insulin receptor. *Diabetes,* 45**,** 1379-85.
SEFTON, E. C., QIANG, W., SERNA, V., KURITA, T., WEI, J. J., CHAKRAVARTI, D. & KIM, J. J. 2013. MK-2206, an AKT inhibitor, promotes caspase-independent cell death and inhibits leiomyoma growth. *Endocrinology,* 154**,** 4046-57.
SEKIMIZU, M., OSUMI, T., FUKANO, R., KOGA, Y., KADA, A., SAITO, A. M. & MORI, T. 2018. A Phase I/II Study of Crizotinib for Recurrent or Refractory Anaplastic Lymphoma Kinase-Positive Anaplastic Large Cell Lymphoma and a Phase I Study of Crizotinib for Recurrent or Refractory Neuroblastoma : Study Protocol for a Multicenter Single-arm Open-label Trial. *Acta Med Okayama,* 72**,** 431-436.
SEQUIST, L. V., WALTMAN, B. A., DIAS-SANTAGATA, D., DIGUMARTHY, S., TURKE, A. B., FIDIAS, P., BERGETHON, K., SHAW, A. T., GETTINGER, S., COSPER, A. K., AKHAVANFARD, S., HEIST, R. S., TEMEL, J., CHRISTENSEN, J. G., WAIN, J. C., LYNCH, T. J., VERNOVSKY, K., MARK, E. J., LANUTI, M., IAFRATE, A. J., MINO-KENUDSON, M. & ENGELMAN, J. A. 2011. Genotypic and histological evolution of lung cancers acquiring resistance to EGFR inhibitors. *Sci Transl Med,* 3**,** 75ra26.
SESHACHARYULU, P., PONNUSAMY, M. P., HARIDAS, D., JAIN, M., GANTI, A. K. & BATRA, S. K. 2012. Targeting the EGFR signaling pathway in cancer therapy. *Expert Opin Ther Targets,* 16**,** 15-31.
SETYAWATI, I. A., THOMPSON, K. H., YUEN, V. G., SUN, Y., BATTELL, M., LYSTER, D. M., VO, C., RUTH, T. J., ZEISLER, S., MCNEILL, J. H. & ORVIG, C. 1998. Kinetic analysis and comparison of uptake, distribution, and excretion of 48V-labeled compounds in rats. *J Appl Physiol (1985),* 84**,** 569-75.
SEVER, R. & BRUGGE, J. S. 2015. Signal transduction in cancer. *Cold Spring Harb Perspect Med,* 5.
SHANG, X., VASUDEVAN, S. A., YU, Y., GE, N., LUDWIG, A. D., WESSON, C. L., WANG, K., BURLINGAME, S. M., ZHAO, Y. J., RAO, P. H., LU, X., RUSSELL, H. V., OKCU, M. F., HICKS, M. J., SHOHET, J. M., DONEHOWER, L. A., NUCHTERN, J. G. & YANG, J. 2010. Dual-specificity phosphatase 26 is a novel p53 phosphatase and inhibits p53 tumor suppressor functions in human neuroblastoma. *Oncogene,* 29**,** 4938-46.
SHARMA, S. & DAVIDSON, A. L. 2000. Vanadate-induced trapping of nucleotides by purified maltose transport complex requires ATP hydrolysis. *J Bacteriol,* 182**,** 6570-6.
SHAROM, F. J. 2011. The P-glycoprotein multidrug transporter. *Essays Biochem,* 50**,** 161-78.

SHEPARD, R. L., WINTER, M. A., HSAIO, S. C., PEARCE, H. L., BECK, W. T. & DANTZIG, A. H. 1998. Effect of modulators on the ATPase activity and vanadate nucleotide trapping of human P-glycoprotein. *Biochem Pharmacol,* 56**,** 719-27.

SHEPHERD, F. A., RODRIGUES PEREIRA, J., CIULEANU, T., TAN, E. H., HIRSH, V., THONGPRASERT, S., CAMPOS, D., MAOLEEKOONPIROJ, S., SMYLIE, M., MARTINS, R., VAN KOOTEN, M., DEDIU, M., FINDLAY, B., TU, D., JOHNSTON, D., BEZJAK, A., CLARK, G., SANTABÁRBARA, P., SEYMOUR, L. & GROUP, N. C. I. O. C. C. T. 2005. Erlotinib in previously treated non-small-cell lung cancer. *N Engl J Med,* 353**,** 123-32.

SHERGALIS, A., BANKHEAD, A., LUESAKUL, U., MUANGSIN, N. & NEAMATI, N. 2018. Current Challenges and Opportunities in Treating Glioblastoma. *Pharmacol Rev,* 70**,** 412-445.

SHI, J. & VAKOC, C. R. 2014. The mechanisms behind the therapeutic activity of BET bromodomain inhibition. *Mol Cell,* 54**,** 728-36.

SHI, Y. 2009. Serine/threonine phosphatases: mechanism through structure. Cell, 139, 468-84.

SHI, Y., MA, I. T., PATEL, R. H., SHANG, X., CHEN, Z., ZHAO, Y., CHENG, J., FAN, Y., ROJAS, Y., BARBIERI, E., YU, Y., JIN, J., KIM, E. S., SHOHET, J. M., VASUDEVAN, S. A. & YANG, J. 2015. NSC-87877 inhibits DUSP26 function in neuroblastoma resulting in p53-mediated apoptosis. *Cell Death Dis,* 6**,** e1841.

SHIBATA, N., KUERBAN, B., KOMATSU, M., OHNUMA, T., BABA, H. & ARAI, H. 2010. Genetic association between CALHM1, 2, and 3 polymorphisms and Alzheimer's disease in a Japanese population. *J Alzheimers Dis,* 20**,** 417-21.

SHOJAEI-BROSSEAU, T., CHOMPRET, A., ABEL, A., DE VATHAIRE, F., RAQUIN, M., BRUGIERES, L., FEUNTEUN, J., HARTMANN, O. & BONAITI-PELLIE, C. 2004. Genetic epidemiology of neuroblastoma: A study of 426 cases at the Institut Gustave-Roussy in France. *Pediatric Blood & Cancer,* 42**,** 99-105.

SIES, H. & DE GROOT, H. 1992. Role of reactive oxygen species in cell toxicity. *Toxicol Lett,* 64-65 Spec No**,** 547-51.

SIMONS, T. J. 1979. Vanadate--a new tool for biologists. *Nature,* 281**,** 337-8.

SIMS, D., MENDES-PEREIRA, A. M., FRANKUM, J., BURGESS, D., CERONE, M. A., LOMBARDELLI, C., MITSOPOULOS, C., HAKAS, J., MURUGAESU, N., ISACKE, C. M., FENWICK, K., ASSIOTIS, I., KOZAREWA, I., ZVELEBIL, M., ASHWORTH, A. & LORD, C. J. 2011. High-throughput RNA interference screening using pooled shRNA libraries and next generation sequencing. *Genome Biol,* 12**,** R104.

SINGH, U. S., PAN, J., KAO, Y. L., JOSHI, S., YOUNG, K. L. & BAKER, K. M. 2003. Tissue transglutaminase mediates activation of RhoA and MAP kinase pathways during retinoic acid-induced neuronal differentiation of SH-SY5Y cells. *J Biol Chem,* 278**,** 391-9.

SINHA, A., BANERJEE, K., BANERJEE, A., SARKAR, A., AHIR, M., ADHIKARY, A., CHATTERJEE, M. & CHOUDHURI, S. K. 2017. Induction of apoptosis in human colorectal cancer cell line, HCT-116 by a vanadium- Schiff base complex. *Biomed Pharmacother,* 92**,** 509-518.

SKALHEGG, B. S. & TASKEN, K. 2000. Specificity in the cAMP/PKA signaling pathway. Differential expression,regulation, and subcellular localization of subunits of PKA. *Front Biosci,* 5**,** D678-93.

SMITH, C. A. & RAYMENT, I. 1996. X-ray structure of the magnesium(II).ADP.vanadate complex of the Dictyostelium discoideum myosin motor domain to 1.9 A resolution. *Biochemistry,* 35**,** 5404-17.

SMITH, D. M., PICKERING, R. M. & LEWITH, G. T. 2008. A systematic review of vanadium oral supplements for glycaemic control in type 2 diabetes mellitus. *QJM,* 101**,** 351-8.

SOARES, L. M., MEYER, E., MILANI, H., STEINBUSCH, H. W., PRICKAERTS, J. & DE OLIVEIRA, R. M. 2017. The phosphodiesterase type 2 inhibitor BAY 60-7550 reverses functional impairments induced by brain ischemia by decreasing hippocampal neurodegeneration and enhancing hippocampal neuronal plasticity. *Eur J Neurosci,* 45**,** 510-520.

SOARES, S. S., GUTIERREZ-MERINO, C. & AURELIANO, M. 2007a. Decavanadate induces mitochondrial membrane depolarization and inhibits oxygen consumption. *J Inorg Biochem,* 101**,** 789-96.

SOARES, S. S., GUTIERREZ-MERINO, C. & AURELIANO, M. 2007b. Mitochondria as a target for decavanadate toxicity in Sparus aurata heart. *Aquat Toxicol,* 83**,** 1-9.

SOARES, S. S., GUTIÉRREZ-MERINO, C. & AURELIANO, M. 2007c. Decavanadate induces mitochondrial membrane depolarization and inhibits oxygen consumption. *J Inorg Biochem,* 101**,** 789-96.
SOMERVILLE, J. & DAVIES, B. 1962. Effect of vanadium on serum cholesterol. *Am Heart J,* 64**,** 54-6.
SONDALLE, S. B. & BASERGA, S. J. 2014. Human diseases of the SSU processome. *Biochim Biophys Acta,* 1842**,** 758-64.
SONG, L., ARA, T., WU, H. W., WOO, C. W., REYNOLDS, C. P., SEEGER, R. C., DECLERCK, Y. A., THIELE, C. J., SPOSTO, R. & METELITSA, L. S. 2007. Oncogene MYCN regulates localization of NKT cells to the site of disease in neuroblastoma. *J Clin Invest,* 117**,** 2702-12.
SONG, M. S., SALMENA, L. & PANDOLFI, P. P. 2012. The functions and regulation of the PTEN tumour suppressor. *Nat Rev Mol Cell Biol,* 13**,** 283-96.
SOROKIN, A. V., NAIR, B. C., WEI, Y., AZIZ, K. E., EVDOKIMOVA, V., HUNG, M. C. & CHEN, J. 2015. Aberrant Expression of proPTPRN2 in Cancer Cells Confers Resistance to Apoptosis. *Cancer Res,* 75**,** 1846-58.
SOSA, L., TORKKO, J. M., PRIMO, M. E., LLOVERA, R. E., TOLEDO, P. L., RIOS, A. S., FLECHA, F. L., TRABUCCHI, A., VALDEZ, S. N., POSKUS, E., SOLIMENA, M. & ERMÁCORA, M. R. 2016. Biochemical, biophysical, and functional properties of ICA512/IA-2 RESP18 homology domain. *Biochim Biophys Acta,* 1864**,** 511-22.
STANFORD, S. M. & BOTTINI, N. 2017. Targeting Tyrosine Phosphatases: Time to End the Stigma. *Trends Pharmacol Sci,* 38**,** 524-540.
STRIANESE, M., BASILE, A., MAZZONE, A., MORELLO, S., TURCO, M. C. & PELLECCHIA, C. 2013. Therapeutic potential of a pyridoxal-based vanadium(IV) complex showing selective cytotoxicity for cancer versus healthy cells. *J Cell Physiol,* 228**,** 2202-9.
SUGIHARA, E., KANAI, M., MATSUI, A., ONODERA, M., SCHWAB, M. & MIWA, M. 2004. Enhanced expression of MYCN leads to centrosome hyperamplification after DNA damage in neuroblastoma cells. *Oncogene,* 23**,** 1005-9.
SUN, P., ZHANG, D., HUANG, H., YU, Y., YANG, Z., NIU, Y. & LIU, J. 2018a. MicroRNA-1225-5p acts as a tumor-suppressor in laryngeal cancer via targeting CDC14B. *Biol Chem*.
SUN, X., REN, Y., GUNAWAN, S., TENG, P., CHEN, Z., LAWRENCE, H. R., CAI, J., LAWRENCE, N. J. & WU, J. 2018b. Selective inhibition of leukemia-associated SHP2. *Leukemia,* 32**,** 1246-1249.
SUZUKI, M. & CHEUNG, N. K. 2015. Disialoganglioside GD2 as a therapeutic target for human diseases. *Expert Opin Ther Targets,* 19**,** 349-62.
SWARUP, G., COHEN, S. & GARBERS, D. L. 1982. Inhibition of membrane phosphotyrosyl-protein phosphatase activity by vanadate. *Biochem Biophys Res Commun,* 107**,** 1104-9.
SZKLARCZYK, R., WANSCHERS, B. F., NIJTMANS, L. G., RODENBURG, R. J., ZSCHOCKE, J., DIKOW, N., VAN DEN BRAND, M. A., HENDRIKS-FRANSSEN, M. G., GILISSEN, C., VELTMAN, J. A., NOOTEBOOM, M., KOOPMAN, W. J., WILLEMS, P. H., SMEITINK, J. A., HUYNEN, M. A. & VAN DEN HEUVEL, L. P. 2013. A mutation in the FAM36A gene, the human ortholog of COX20, impairs cytochrome c oxidase assembly and is associated with ataxia and muscle hypotonia. *Hum Mol Genet,* 22**,** 656-67.
TABERNERO, J. 2007. The role of VEGF and EGFR inhibition: implications for combining anti-VEGF and anti-EGFR agents. *Mol Cancer Res,* 5**,** 203-20.
TAI, W. T., CHEN, Y. L., CHU, P. Y., CHEN, L. J., HUNG, M. H., SHIAU, C. W., HUANG, J. W., TSAI, M. H. & CHEN, K. F. 2016. Protein tyrosine phosphatase 1B dephosphorylates PITX1 and regulates p120RasGAP in hepatocellular carcinoma. *Hepatology,* 63**,** 1528-43.
TARTAGLIA, M., MEHLER, E. L., GOLDBERG, R., ZAMPINO, G., BRUNNER, H. G., KREMER, H., VAN DER BURGT, I., CROSBY, A. H., ION, A., JEFFERY, S., KALIDAS, K., PATTON, M. A., KUCHERLAPATI, R. S. & GELB, B. D. 2001. Mutations in PTPN11, encoding the protein tyrosine phosphatase SHP-2, cause Noonan syndrome. *Nat Genet,* 29**,** 465-8.
TARTAGLIA, M., NIEMEYER, C. M., FRAGALE, A., SONG, X., BUECHNER, J., JUNG, A., HÄHLEN, K., HASLE, H., LICHT, J. D. & GELB, B. D. 2003. Somatic mutations in PTPN11 in juvenile myelomonocytic leukemia, myelodysplastic syndromes and acute myeloid leukemia. *Nat Genet,* 34**,** 148-50.
TENG, H. W., HUNG, M. H., CHEN, L. J., CHANG, M. J., HSIEH, F. S., TSAI, M. H., HUANG, J. W., LIN, C. L., TSENG, H. W., KUO, Z. K., JIANG, J. K., YANG, S. H., SHIAU, C. W. &

CHEN, K. F. 2016. Protein tyrosine phosphatase 1B targets PITX1/p120RasGAP thus showing therapeutic potential in colorectal carcinoma. *Sci Rep,* 6**,** 35308.
THIELE, C. 1998. Neuroblastoma Cell Lines. *In (Ed.) Masters, J. Human Cell Culture.* Lancaster, UK: Kluwer Academic Publishers.
THOMPSON, D., MORRICE, N., GRANT, L., LE SOMMER, S., LEES, E. K., MODY, N., WILSON, H. M. & DELIBEGOVIC, M. 2017. Pharmacological inhibition of protein tyrosine phosphatase 1B protects against atherosclerotic plaque formation in the LDLR-/- mouse model of atherosclerosis. *Clin Sci (Lond),* 131**,** 2489-2501.
THOMPSON, H. J., CHASTEEN, N. D. & MEEKER, L. D. 1984. Dietary vanadyl(IV) sulfate inhibits chemically-induced mammary carcinogenesis. *Carcinogenesis,* 5**,** 849-51.
THOMPSON, K. H., LICHTER, J., LEBEL, C., SCAIFE, M. C., MCNEILL, J. H. & ORVIG, C. 2009. Vanadium treatment of type 2 diabetes: a view to the future. *J Inorg Biochem,* 103**,** 554-8.
THOMPSON, K. H. & ORVIG, C. 2006. Vanadium in diabetes: 100 years from Phase 0 to Phase I. *J Inorg Biochem,* 100**,** 1925-35.
TIAGO, T., MARTEL, P., GUTIERREZ-MERINO, C. & AURELIANO, M. 2007. Binding modes of decavanadate to myosin and inhibition of the actomyosin ATPase activity. *Biochim Biophys Acta,* 1774**,** 474-80.
TIVNAN, A., ORR, W. S., GUBALA, V., NOONEY, R., WILLIAMS, D. E., MCDONAGH, C., PRENTER, S., HARVEY, H., DOMINGO-FERNÁNDEZ, R., BRAY, I. M., PISKAREVA, O., NG, C. Y., LODE, H. N., DAVIDOFF, A. M. & STALLINGS, R. L. 2012. Inhibition of neuroblastoma tumor growth by targeted delivery of microRNA-34a using anti-disialoganglioside GD2 coated nanoparticles. *PLoS One,* 7**,** e38129.
TOLBERT, V. P. & MATTHAY, K. K. 2018. Neuroblastoma: clinical and biological approach to risk stratification and treatment. *Cell Tissue Res*.
TONKS, N. K. 2006. Protein tyrosine phosphatases: from genes, to function, to disease. *Nat Rev Mol Cell Biol,* 7**,** 833-46.
TONKS, N. K. 2013. Protein tyrosine phosphatases--from housekeeping enzymes to master regulators of signal transduction. *FEBS J,* 280**,** 346-78.
TONKS, N. K. & NEEL, B. G. 2001. Combinatorial control of the specificity of protein tyrosine phosphatases. *Curr Opin Cell Biol,* 13**,** 182-95.
TRACHOOTHAM, D., LU, W., OGASAWARA, M. A., NILSA, R. D. & HUANG, P. 2008. Redox regulation of cell survival. *Antioxid Redox Signal,* 10**,** 1343-74.
TREVIÑO, S., DÍAZ, A., SÁNCHEZ-LARA, E., SANCHEZ-GAYTAN, B. L., PEREZ-AGUILAR, J. M. & GONZÁLEZ-VERGARA, E. 2018. Vanadium in Biological Action: Chemical, Pharmacological Aspects, and Metabolic Implications in Diabetes Mellitus. *Biol Trace Elem Res*.
TRIGG, R. M. & TURNER, S. D. 2018. ALK in Neuroblastoma: Biological and Therapeutic Implications. *Cancers (Basel),* 10.
TUMURBAATAR, I., CIZMECIOGLU, O., HOFFMANN, I., GRUMMT, I. & VOIT, R. 2011. Human Cdc14B promotes progression through mitosis by dephosphorylating Cdc25 and regulating Cdk1/cyclin B activity. *PLoS One,* 6**,** e14711.
TWEDDLE, D. A., MALCOLM, A. J., BOWN, N., PEARSON, A. D. & LUNEC, J. 2001. Evidence for the development of p53 mutations after cytotoxic therapy in a neuroblastoma cell line. *Cancer Res,* 61**,** 8-13.
TWEDDLE, D. A., PEARSON, A. D., HABER, M., NORRIS, M. D., XUE, C., FLEMMING, C. & LUNEC, J. 2003. The p53 pathway and its inactivation in neuroblastoma. *Cancer Lett,* 197**,** 93-8.
URBATSCH, I. L., SANKARAN, B., WEBER, J. & SENIOR, A. E. 1995. P-glycoprotein is stably inhibited by vanadate-induced trapping of nucleotide at a single catalytic site. *J Biol Chem,* 270**,** 19383-90.
VAN TONDER, A., JOUBERT, A. M. & CROMARTY, A. D. 2015. Limitations of the 3-(4,5-dimethylthiazol-2-yl)-2,5-diphenyl-2H-tetrazolium bromide (MTT) assay when compared to three commonly used cell enumeration assays. *BMC Res Notes,* 8**,** 47.
VEAS-PEREZ DE TUDELA, M., DELGADO-ESTEBAN, M., CUENDE, J., BOLAÑOS, J. P. & ALMEIDA, A. 2010. Human neuroblastoma cells with MYCN amplification are selectively resistant to oxidative stress by transcriptionally up-regulating glutamate cysteine ligase. *J Neurochem,* 113**,** 819-25.

VERNERSSON, E., KHOO, N. K., HENRIKSSON, M. L., ROOS, G., PALMER, R. H. & HALLBERG, B. 2006. Characterization of the expression of the ALK receptor tyrosine kinase in mice. *Gene Expr Patterns,* 6**,** 448-61.

VISTICA, D. T., SKEHAN, P., SCUDIERO, D., MONKS, A., PITTMAN, A. & BOYD, M. R. 1991. Tetrazolium-based assays for cellular viability: a critical examination of selected parameters affecting formazan production. *Cancer Res,* 51**,** 2515-20.

WALLACE, S. J., LI, J., NATION, R. L. & BOYD, B. J. 2012. Drug release from nanomedicines: Selection of appropriate encapsulation and release methodology. *Drug Deliv Transl Res,* 2**,** 284-92.

WALSH, D. A., PERKINS, J. P. & KREBS, E. G. 1968. An adenosine 3',5'-monophosphate-dependant protein kinase from rabbit skeletal muscle. *J Biol Chem,* 243**,** 3763-5.

WANG, B., RONG, X., PALLADINO, E. N. D., WANG, J., FOGELMAN, A. M., MARTÍN, M. G., ALREFAI, W. A., FORD, D. A. & TONTONOZ, P. 2018. Phospholipid Remodeling and Cholesterol Availability Regulate Intestinal Stemness and Tumorigenesis. *Cell Stem Cell,* 22**,** 206-220.e4.

WANG, L., PENG, L., DONG, B., KONG, L., MENG, L., YAN, L., XIE, Y. & SHOU, C. 2006. Overexpression of phosphatase of regenerating liver-3 in breast cancer: association with a poor clinical outcome. *Ann Oncol,* 17**,** 1517-22.

WANG, N., SHE, J., LIU, W., SHI, J., YANG, Q., SHI, B. & HOU, P. 2015. Frequent amplification of PTP1B is associated with poor survival of gastric cancer patients. *Cell Cycle,* 14**,** 732-43.

WANG, P., ZHOU, Z., HU, A., PONTE DE ALBUQUERQUE, C., ZHOU, Y., HONG, L., SIERECKI, E., AJIRO, M., KRUHLAK, M., HARRIS, C., GUAN, K. L., ZHENG, Z. M., NEWTON, A. C., SUN, P., ZHOU, H. & FU, X. D. 2014. Both decreased and increased SRPK1 levels promote cancer by interfering with PHLPP-mediated dephosphorylation of Akt. *Mol Cell,* 54**,** 378-91.

WANG, S., YU, H. & WICKLIFFE, J. K. 2011. Limitation of the MTT and XTT assays for measuring cell viability due to superoxide formation induced by nano-scale TiO2. *Toxicol In Vitro,* 25**,** 2147-51.

WANG, Z., SHEN, D., PARSONS, D. W., BARDELLI, A., SAGER, J., SZABO, S., PTAK, J., SILLIMAN, N., PETERS, B. A., VAN DER HEIJDEN, M. S., PARMIGIANI, G., YAN, H., WANG, T. L., RIGGINS, G., POWELL, S. M., WILLSON, J. K., MARKOWITZ, S., KINZLER, K. W., VOGELSTEIN, B. & VELCULESCU, V. E. 2004. Mutational analysis of the tyrosine phosphatome in colorectal cancers. *Science,* 304**,** 1164-6.

WEI, M., KOROTKOV, K. V. & BLACKBURN, J. S. 2018. Targeting phosphatases of regenerating liver (PRLs) in cancer. *Pharmacol Ther,* 190**,** 128-138.

WEI, Z., PEDDIBHOTLA, S., LIN, H., FANG, X., LI, M., ROSEN, J. M. & ZHANG, P. 2011. Early-onset aging and defective DNA damage response in Cdc14b-deficient mice. *Mol Cell Biol,* 31**,** 1470-7.

WEI, Z. & ZHANG, P. 2011. A phosphatase turns aggressive: the oncogenicity of Cdc14B. *Cell Cycle,* 10**,** 2414.

WEIDNER, P., SÖHN, M., GUTTING, T., FRIEDRICH, T., GAISER, T., MAGDEBURG, J., KIENLE, P., RUH, H., HOPF, C., BEHRENS, H. M., RÖCKEN, C., HANOCH, T., SEGER, R., EBERT, M. P. & BURGERMEISTER, E. 2016. Myotubularin-related protein 7 inhibits insulin signaling in colorectal cancer. *Oncotarget,* 7**,** 50490-50506.

WEINSTEIN, I. B. 2002. Cancer. Addiction to oncogenes--the Achilles heal of cancer. *Science,* 297**,** 63-4.

WEINSTEIN, I. B. & JOE, A. K. 2006. Mechanisms of disease: Oncogene addiction--a rationale for molecular targeting in cancer therapy. *Nat Clin Pract Oncol,* 3**,** 448-57.

WEISS, W. A., ALDAPE, K., MOHAPATRA, G., FEUERSTEIN, B. G. & BISHOP, J. M. 1997. Targeted expression of MYCN causes neuroblastoma in transgenic mice. *EMBO J,* 16**,** 2985-95.

WHITTLE, S. B., SMITH, V., DOHERTY, E., ZHAO, S., MCCARTY, S. & ZAGE, P. E. 2017. Overview and recent advances in the treatment of neuroblastoma. *Expert Rev Anticancer Ther*.

WIDAKOWICH, C., DE CASTRO, G., DE AZAMBUJA, E., DINH, P. & AWADA, A. 2007. Review: side effects of approved molecular targeted therapies in solid cancers. *Oncologist,* 12**,** 1443-55.

WILCZEWSKA, A. Z., NIEMIROWICZ, K., MARKIEWICZ, K. H. & CAR, H. 2012. Nanoparticles as drug delivery systems. *Pharmacol Rep,* 64**,** 1020-37.

WILLSKY, G. R., WHITE, D. A. & MCCABE, B. C. 1984. Metabolism of added orthovanadate to vanadyl and high-molecular-weight vanadates by Saccharomyces cerevisiae. *J Biol Chem,* 259**,** 13273-81.
WOLFSON, R. L., CHANTRANUPONG, L., WYANT, G. A., GU, X., OROZCO, J. M., SHEN, K., CONDON, K. J., PETRI, S., KEDIR, J., SCARIA, S. M., ABU-REMAILEH, M., FRANKEL, W. N. & SABATINI, D. M. 2017. KICSTOR recruits GATOR1 to the lysosome and is necessary for nutrients to regulate mTORC1. *Nature,* 543**,** 438-442.
WU, J. X., HONG, Y. H. & YANG, X. G. 2016a. Bis(acetylacetonato)-oxidovanadium(IV) and sodium metavanadate inhibit cell proliferation via ROS-induced sustained MAPK/ERK activation but with elevated AKT activity in human pancreatic cancer AsPC-1 cells. *J Biol Inorg Chem,* 21**,** 919-929.
WU, P., NIELSEN, T. E. & CLAUSEN, M. H. 2016b. Small-molecule kinase inhibitors: an analysis of FDA-approved drugs. *Drug Discov Today,* 21**,** 5-10.
WU, Y., MA, Y., XU, Z., WANG, D., ZHAO, B., PAN, H., WANG, J., XU, D., ZHAO, X., PAN, S., LIU, L., DAI, W. & JIANG, H. 2014. Sodium orthovanadate inhibits growth of human hepatocellular carcinoma cells in vitro and in an orthotopic model in vivo. *Cancer Lett,* 351**,** 108-16.
WYKOSKY, J., FENTON, T., FURNARI, F. & CAVENEE, W. K. 2011. Therapeutic targeting of epidermal growth factor receptor in human cancer: successes and limitations. *Chin J Cancer,* 30**,** 5-12.
XIANG, K., NAGAIKE, T., XIANG, S., KILIC, T., BEH, M. M., MANLEY, J. L. & TONG, L. 2010. Crystal structure of the human symplekin-Ssu72-CTD phosphopeptide complex. *Nature,* 467**,** 729-33.
XIE, H., NOTKINS, A. L. & LAN, M. S. 1996. IA-2, a transmembrane protein tyrosine phosphatase, is expressed in human lung cancer cell lines with neuroendocrine phenotype. *Cancer Res,* 56**,** 2742-4.
XING, F., LUAN, Y., CAI, J., WU, S., MAI, J., GU, J., ZHANG, H., LI, K., LIN, Y., XIAO, X., LIANG, J., LI, Y., CHEN, W., TAN, Y., SHENG, L., LU, B., LU, W., GAO, M., QIU, P., SU, X., YIN, W., HU, J., CHEN, Z., SAI, K., WANG, J., CHEN, F., CHEN, Y., ZHU, S., LIU, D., CHENG, S., XIE, Z., ZHU, W. & YAN, G. 2017. The Anti-Warburg Effect Elicited by the cAMP-PGC1α Pathway Drives Differentiation of Glioblastoma Cells into Astrocytes. *Cell Rep,* 18**,** 468-481.
XU, H., CAI, T., CARMONA, G. N., ABUHATZIRA, L. & NOTKINS, A. L. 2016. Small cell lung cancer growth is inhibited by miR-342 through its effect of the target gene IA-2. *J Transl Med,* 14**,** 278.
XU, R., YU, Y., ZHENG, S., ZHAO, X., DONG, Q., HE, Z., LIANG, Y., LU, Q., FANG, Y., GAN, X., XU, X., ZHANG, S., ZHANG, X. & FENG, G. S. 2005. Overexpression of Shp2 tyrosine phosphatase is implicated in leukemogenesis in adult human leukemia. *Blood,* 106**,** 3142-9.
YAMAMOTO, E., MIYAZAKI, S., AOYAMA, C. & KATO, M. 2018. A simple and rapid measurement method of encapsulation efficiency of doxorubicin loaded liposomes by direct injection of the liposomal suspension to liquid chromatography. *Int J Pharm,* 536**,** 21-28.
YANG, X., WANG, K., LU, J. & CRANS, D. 2003. Membrane transport of vanadium compounds and the interaction with the erythrocyte membrane. *Coordination Chemistry Reviews,* 237**,** 103-111.
YOU, Z., DONG, Y., KONG, X., ZHANG, Y., VESSELLA, R. L. & MELAMED, J. 2007. Differential expression of IL-17RC isoforms in androgen-dependent and androgen-independent prostate cancers. *Neoplasia,* 9**,** 464-70.
YOUNG, R. M., POLSKY, A. & REFAELI, Y. 2009. TC-PTP is required for the maintenance of MYC-driven B-cell lymphomas. *Blood,* 114**,** 5016-23.
YU, H. A., ARCILA, M. E., REKHTMAN, N., SIMA, C. S., ZAKOWSKI, M. F., PAO, W., KRIS, M. G., MILLER, V. A., LADANYI, M. & RIELY, G. J. 2013. Analysis of tumor specimens at the time of acquired resistance to EGFR-TKI therapy in 155 patients with EGFR-mutant lung cancers. *Clin Cancer Res,* 19**,** 2240-7.
ZENG, L. F., ZHANG, R. Y., YU, Z. H., LI, S., WU, L., GUNAWAN, A. M., LANE, B. S., MALI, R. S., LI, X., CHAN, R. J., KAPUR, R., WELLS, C. D. & ZHANG, Z. Y. 2014. Therapeutic potential of targeting the oncogenic SHP2 phosphatase. *J Med Chem,* 57**,** 6594-609.
ZERDOUMI, Y., KASPER, E., SOUBIGOU, F., ADRIOUCH, S., BOUGEARD, G., FREBOURG, T. & FLAMAN, J. M. 2015. A new genotoxicity assay based on p53 target gene induction. *Mutat Res Genet Toxicol Environ Mutagen,* 789-790**,** 28-35.

ZHANG, J., GUAN, Z., MURPHY, A. N., WILEY, S. E., PERKINS, G. A., WORBY, C. A., ENGEL, J. L., HEACOCK, P., NGUYEN, O. K., WANG, J. H., RAETZ, C. R., DOWHAN, W. & DIXON, J. E. 2011. Mitochondrial phosphatase PTPMT1 is essential for cardiolipin biosynthesis. *Cell Metab,* 13**,** 690-700.

ZHANG, J., ZHANG, F. & NIU, R. 2015. Functions of Shp2 in cancer. *J Cell Mol Med,* 19**,** 2075-83.

ZHANG, R. Y., YU, Z. H., ZENG, L., ZHANG, S., BAI, Y., MIAO, J., CHEN, L., XIE, J. & ZHANG, Z. Y. 2016. SHP2 phosphatase as a novel therapeutic target for melanoma treatment. *Oncotarget,* 7**,** 73817-73829.

ZHANG, X., DONG, Z., ZHANG, C., UNG, C. Y., HE, S., TAO, T., OLIVEIRA, A. M., MEVES, A., JI, B., LOOK, A. T., LI, H., NEEL, B. G. & ZHU, S. 2017. Critical Role for GAB2 in Neuroblastoma Pathogenesis through the Promotion of SHP2/MYCN Cooperation. *Cell Rep,* 18**,** 2932-2942.

ZHANG, Z. Y. 2017. Drugging the Undruggable: Therapeutic Potential of Targeting Protein Tyrosine Phosphatases. *Acc Chem Res,* 50**,** 122-129.

ZHONG, Y., ZOU, L., WANG, Z., PAN, Y., DAI, Z., LIU, X., CUI, L. & ZUO, C. 2016. Lrrc75b is a novel negative regulator of C2C12 myogenic differentiation. *Int J Mol Med,* 38**,** 1411-1418.

ZHOU, X., COAD, J., DUCATMAN, B. & AGAZIE, Y. M. 2008. SHP2 is up-regulated in breast cancer cells and in infiltrating ductal carcinoma of the breast, implying its involvement in breast oncogenesis. *Histopathology,* 53**,** 389-402.

ZHOU, X. D. & AGAZIE, Y. M. 2008. Inhibition of SHP2 leads to mesenchymal to epithelial transition in breast cancer cells. *Cell Death Differ,* 15**,** 988-96.

ZHU, S., LEE, J. S., GUO, F., SHIN, J., PEREZ-ATAYDE, A. R., KUTOK, J. L., RODIG, S. J., NEUBERG, D. S., HELMAN, D., FENG, H., STEWART, R. A., WANG, W., GEORGE, R. E., KANKI, J. P. & LOOK, A. T. 2012. Activated ALK collaborates with MYCN in neuroblastoma pathogenesis. *Cancer Cell,* 21**,** 362-73.

ZWICK, E., BANGE, J. & ULLRICH, A. 2001. Receptor tyrosine kinase signalling as a target for cancer intervention strategies. *Endocr Relat Cancer,* 8**,** 161-73.